

Mathematical Modeling and Numerical Simulation of Sisko Fluid Flow over a Stretching Surface



By

Latif Ahmad

Department of Mathematics

Quaid-i-Azam University

Islamabad, Pakistan

2019

**Mathematical Modeling and Numerical Simulation of
Sisko Fluid Flow over a Stretching Surface**



By
Latif Ahmad

Supervised By
Professor Dr. Masood Khan

Department of Mathematics
Quaid-i-Azam University
Islamabad, Pakistan

2019

Mathematical Modeling and Numerical Simulation of Sisko Fluid Flow over a Stretching Surface



By
Latif Ahmad

A DISSERTATION SUBMITTED IN THE PARTIAL FULFILLMENT OF THE REQUIREMENT
FOR THE DEGREE OF
DOCTOR OF PHILOSOPHY

IN

MATHEMATICS

Supervised By
Professor Dr. Masood Khan

Department of Mathematics

Quaid-i-Azam University

Islamabad, Pakistan

2019

Author's Declaration

I, **Latif Ahmad** hereby state that my PhD thesis titled “**Mathematical Modeling and Numerical Simulation of Sisko Fluid Flow over a Stretching Surface**” is my own work and has not been submitted previously by me for taking any degree from the Quaid-i-Azam University Islamabad, Pakistan or anywhere else in the country/world.

At any time if my statement is found to be incorrect even after my graduate the university has the right to withdraw my PhD degree.



Name of Student: **Latif Ahmad**

Date: **12-07-2019**

Plagiarism Undertaking

I solemnly declare that research work presented in the thesis titled “**Mathematical Modeling and Numerical Simulation of Sisko Fluid Flow over a Stretching Surface**” is solely my research work with no significant contribution from any other person. Small contribution/help wherever taken has been duly acknowledged and that complete thesis has been written by me.

I understand the zero tolerance policy of the HEC and **Quaid-i-Azam University, Islamabad** towards plagiarism. Therefore, I as an Author of the above titled thesis declare that no portion of my thesis has been plagiarized and any material used as reference is properly referred/cited.

I undertake that if I am found guilty of any formal plagiarism in the above titled thesis even afterward of PhD degree, the University reserves the rights to withdraw/revoke my PhD degree and that HEC and the University has the right to publish my name on the HEC/University Website on which names of students are placed who submitted plagiarized thesis.

Student/Author Signature: _____




Name: **Latif Ahmad**

Certificate of Approval

This is to certify that the research work presented in this thesis entitled **Mathematical Modeling and Numerical Simulation of Sisko Fluid Flow over a Stretching Surface** was conducted by Mr. **Latif Ahmad** under the kind supervision of **Prof. Dr. Masood Khan**. No part of this thesis has been submitted anywhere else for any other degree. This thesis is submitted to the Department of Mathematics, Quaid-i-Azam University, Islamabad in partial fulfillment of the requirements for the degree of Doctor of Philosophy in field of Mathematics from Department of Mathematics, Quaid-i-Azam University Islamabad, Pakistan.

Student Name: **Latif Ahmad**

Signature: 

External committee:

a) **External Examiner 1:**

Signature: 

Name: **Dr. Rahmat Ellahi**

Designation: Associate Professor

Office Address: Department of Mathematics & Statistics, Faculty of Basics Applied Sciences International Islamic University, Islamabad.

b) **External Examiner 2:**

Signature: 

Name: **Dr. Muhammad Mushtaq**

Designation: Assistant Professor

Office Address: Department of Mathematics, COMSATS University Park road Chak Shahzad, Islamabad.

c) **Internal Examiner**

Signature: 

Name: **Dr. Masood Khan**

Designation: Professor

Office Address: Department of Mathematics, QAU Islamabad.

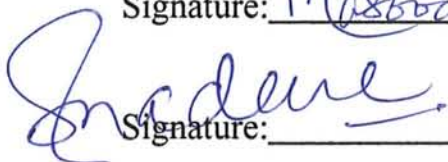
Supervisor Name:

Prof. Dr. Masood Khan

Signature: 

Name of Dean/ HOD

Prof. Dr. Sohail Nadeem

Signature: 

Mathematical Modeling and Numerical Simulation of Sisko Fluid Flow over a Stretching Surface


By

Latif Ahmad


CERTIFICATE

A DISSERTATION SUBMITTED IN THE PARTIAL FULFILLMENT OF THE
REQUIREMENTS FOR THE DEGREE OF THE DOCTOR OF
PHILOSOPHY

We accept this dissertation as conforming to the required standard

1. 

Prof. Dr. Sohail Nadeem
(Chairman)


2. 

Prof. Dr. Masood Khan
(Supervisor)

3. 

Dr. Rehmat Ellahi

Department of Mathematics & Statistics
International Islamic University, Sector H-10
Islamabad

4. 

Dr. Muhammad Mushtaq
Department of Mathematics
COMSATS University
Park Road Chak Shahzad,
Islamabad

Department of Mathematics
Quaid-I-Azam University
Islamabad, Pakistan
2019

Dedicated to

My beloved parents and my wife

Acknowledgement

In the name of **ALLAH**, the Most Glorious and the Most Merciful Lord, the creator and all praises to **ALLAH** who guide me in darkness, helps me in troubles and empowers me to view tentative blocks as stepping stones to the stars to reach the eventual stage with courage. I am nothing without my **ALLAH** but I can achieve everything with assistance. All of my reverence and commitment goes to our **Prophet Hazrat Muhammad SAWW** the source of humanity, kindness and guidance for the whole creatures and who declared it an obligatory duty of every Muslim to seek and procure knowledge. My **ALLAH** shower His countless blessings upon **Muhammad** His family and companions. First and foremost I would like to express my special appreciation and thanks to my supervisor **Professor Dr. Masood Khan**, you have been a tremendous mentor for me. I would like to thank you for encouraging my research and for allowing me to grow as a research scientist. Your advice on both research as well as on my career have been invaluable. In short, your tireless work, unique way of research and devotion to your profession cannot be expressed in words.

Nobody has been more important to me in the pursuit of this achievement than the members of my family. I would like to thank my parents (**mother and father (late)**) whose love, prayers and guidance are with me in whatever I pursue. They are the ultimate role models. I am very thankful to my loving parents (**mother and father (late)**) for their guidance, support and encouragement. I owe my heartiest gratitude for their assistance and never ending prayers for success. I highly commend the cooperative behavior of my brothers (**Nazir Muhammad, Nisar Muhammad and Mohsin Ali**) who endeavored for my edification and betterment. Most importantly, I wish to thank my loving supportive wife **Sumaira** and my two wonderful children's **Zayam Ahmad** and **Adan Fatima**, who provide unending inspiration.

I gratefully acknowledge the Department of Mathematics for this wonderful facilitation sources that made my Ph.D. work possible. In this regard, I would also thanks to chairman Department of Mathematics **Professor Dr. Sohail Nadeem**, you are the one who

motivates me for this milestone achievement. Many thanks also to **Professor Dr. Tasawar Hayat** who convinced me during our many discussions that I should pursue my doctoral degree and who made it possible for me to obtain this precious degree successfully. I am also grateful to **Mr. Zahoor Jan, Mr. Sheraz, Mr. Sajid Mehmood and Mr. Safdar** for their support every time.

My time at Quaid-i-Azam University was made enjoyable in large part due to the many friends and groups that became a part of my life. I am grateful for time spent with roommates and friends, for my backpacking buddies and our memorable trips into many places with very enjoyment as I finished up my degree, and for many other people and memories. My time at Quaid-i-Azam University was also enriched by the graduates and fellows **Dr. Waqar Azeem Khan, Dr. Rabia Malik, Dr. Hashim, Dr. Masood Ur Rahman, Dr. Muhammad Azam, Dr. Muhammad Waqas, Dr. Shahid Farooq, Jawad Ahmed, Aamir Muhammad, Muhammad Irfan, Kaleem Iqbal, Humara Sardar, Muhammad Ijaz Khan, Ikram Ullah, Naeem Ullah and Faisal Shah.**

In the end I would like to thank to all my research fellows and to those people who directly and indirectly helped me during my research work.

Best Regards

Latif Ahmad

Contents

Abstract	xv
List of Symbols	xvii
1 Introduction	1
1.1 Motivation	1
1.2 Context and Scope of the Study	3
1.3 Numerical Methods	13
1.3.1 Runge-Kutta-Fehlberg Method	14
1.3.2 Bvp4c Built in Solver	16
1.3.3 BVP Traprich Method (Richardson's Extrapolations)	18
1.4 Basic Physical Laws	19
1.4.1 Conservation of Mass	20
1.4.2 Conservation of Momentum	20
1.4.3 Conservation of Energy	22
1.4.4 Conservation of Concentration	23
1.4.5 Curvilinear Coordinates	24
1.4.6 Continuity Equation for Curved Surface	26
1.4.7 Momentum Equation for Curved Surface	26
1.4.8 Boundary Layer Equations for Curved Surface	28
1.4.9 Energy Equation for Curved Surface	29
1.4.10 Concentration Equation for Curved Surface	29

1.5	The Sisko Rheological Model	29
1.6	Research Objectives	31
1.7	Contribution in Thesis	31
2	Numerical Computations of Generalized Fourier's and Fick's Laws for Sisko Fluid Flow	36
2.1	Flow Geometry	37
2.2	Constitutive Equations and Mathematical Formulation	37
2.3	Numerical Method	40
2.4	Pictorial Interpretation and Discussion	41
3	Numerical Study of Non-linear Radiative Flow of Magneto Nanoparticles for 3D Sisko Fluid	47
3.1	Pictorial Interpretation of the Problem	48
3.2	Problem Formulation	48
3.3	Graphical Results and Discussion	51
4	A 3D Study of Sisko Liquid Flow with non-Fourier's Heat Flux Model and Heterogeneous-Homogeneous Reactions	61
4.1	Problem Formulation	62
4.2	Numerical Results and Discussion	64
5	Numerical Computations of Unsteady Generalized Newtonian Fluid Flow with Convective Heat Transfer	70
5.1	Formulation of the Flow Problem	71
5.2	Numerical Scheme	74
5.3	Testing of Method	75
5.4	Computational Results and Discussion	75
6	Thermophoresis and Brownian Motion Applications to the Flow of Un-	

steady 3D Magneto-Sisko Liquid: A Numerical Study	86
6.1 Mathematical Construction of the Model	87
6.2 Engineering Quantities	89
6.3 Authentication of Numerical Outcomes	89
6.4 Description of the Results	90
7 Unsteady 3D Sisko Nano-magnetic Liquid Flow with Heat Absorption and Temperature Dependent Thermal Conductivity	107
7.1 Flow Analysis	108
7.2 Physical Quantities	110
7.3 Validation of Code	111
7.4 Results Description	111
7.5 Velocity Profiles	112
7.6 Temperature Profiles	112
7.7 Concentration Profiles	114
8 Chemically reactive Flow of MHD Transient 3D Sisko Liquid with Ther- mal Radiation	124
8.1 Problem Description	125
8.2 Physical Quantities	127
8.3 Validation of Scheme	128
8.4 Computational Results and Discussion	128
8.4.1 Drag Forces and Heat Transfer Rate	128
8.4.2 Velocity Profiles	129
8.4.3 Temperature Profiles	129
8.4.4 Concentration Profiles	131
9 Modeling and Computations of Sisko Liquid Flow with Transfer of Heat over a Curved Boundary	139

9.1	Governing Equations	140
9.2	Model Development	144
9.3	Testing of Code	147
9.4	Numerical Outcomes and Discussion	148
10	Numerical Computations for MHD Flow of Sisko-nanoliquid over a Moving Curved Boundary	157
10.1	Configuration of the Problem	158
10.2	Results Validation	161
10.3	Physical Interpretation of Results	162
10.3.1	Flow Pattern	162
10.3.2	Velocity Profiles	163
10.3.3	Pressure Profiles	163
10.3.4	Temperature Profiles	164
10.3.5	Concentration Profiles	165
10.3.6	Drag Forces, Heat and Mass Transfer Rates	165
11	Conclusions and Further Research	179
11.1	General Overview	179
11.2	Conclusions	180
11.3	Flow Analysis	180
11.4	Heat Transfer Analysis	181
11.5	Mass Transfer Analysis	182
11.6	Pressure Analysis	182
11.7	Future Research	183
	Bibliography	184

Abstract

Flow behavior of several complex fluids is characterized by viscosity dependency on the rate of deformation. Such type of viscosity dependency is one of the basic category of non-Newtonian fluids rather than Newtonian fluids. Appropriate prediction of rheological characteristics such as shear stress and shear strain are forcible in useful applications. For instance, protein formulations/injections, inkjet printing and food/beverage manufacturing and so forth. Such engineering importance insured that the modeling and in-depth study of non-Newtonian fluids is one of the need of the day. The contributions in this thesis push further the mathematical modeling and analysis of generalized Newtonian Sisko fluid which is declared a subclass of non-Newtonian fluids. This thesis consists of two main parts: One presenting mathematical modeling of Sisko fluid and the other one describing and analyzing the results for flow, heat and mass transfer. In current thesis, we present a contribution to the mathematical formulations for 2D as well as 3D steady and unsteady Sisko fluid flows with heat and mass transfer. The modeled governing PDEs are transformed through some dimensionless variables into ordinary differential equations (ODEs). The whole computational work is carried out with the help of well known numerical approaches namely RKF with shooting technique, built in boundary value problem (BVP) solver `bvp4c` and Richardson extrapolation with built in command `BVP traprich`. A meaningful physical interpretation in the form of computational analysis is performed to characterize the behavior of velocity, pressure, temperature and concentration of Sisko fluid.

The major observations associated to the flows of pseudo-plastic as well as dilatant fluids which are the subcases of Sisko fluid are highlighted with the important enhancement behavior of the velocity and associated momentum boundary layer thickness(MBLT) with higher material and curvature parameters. This study is more important in the context where the magnitude of pressure inside the boundary layer(BL) is observed in the growing conduct for weaker values of the curvature parameter and outside of the BL the magnitude becomes zero. However, this study reported a very significant de

ing trend in the temperature and concentration as well as related thermal boundary layer thickness(TBLT) and concentration boundary layer thickness(CBLT) with enhancing material and curvature parameters. Ultimately, the research work presented in this thesis will aid in the understanding and analyzing the diverse rheological characteristics of the generalized Newtonian Sisko fluid.

List of Symbols

A_1^*	Chemical species
a_1	Chemical species of A_1^*
A_1	First Rivlin-Erickson tensor
a	Physical quantities (viscosity at high shear rate)
a^*	Acceleration
a_0	Uniform concentration
B_0	Applied magnetic field
B_1^*	Chemical species
b_1	Chemical species of B_1^*
b	Physical quantity of Sisko fluid (consistency index)
C_∞	Ambient concentration
C	Concentration of the fluid
C_w	Concentration at the wall
c, c_1, C^*	Stretching rates constants
C^1	Continuous solution
c_f	Specific heat of fluid
c_p	Specific heat via constant pressure
d, d_1	Constants
D_B	Brownian diffusion coefficients
dS	Vector normal to a small patch to the surface
$\frac{d}{dt}$	Material derivatives

D	Molecular diffusivity of concentration species
D_T	Thermophoresis diffusion coefficient
Δ	Dell Operator
E	Desired quantity
e, e^*	Positive constants
e_{ij}	Resultant unit vector
$E(h)$	An approximation
E_1	Improved approximations
f_1	The local force
f_2	Continuous function
f	Dimensionless stream function
F	The flux of Φ in the absence of fluid transport
f'	Dimensionless velocity
g	Dimensionless stream function
g_2	Continuous function
g'	Dimensionless velocity
h	Step size
$(h_1, h_2 < h_3)$	Scale factors for boundary layer flows
i	ith component
I	Identity tensor
J	Normal mass flux
\bar{J}	Jacobian
(j_1, j_2, j_3)	Three scalar point functions
(k_1^*, k_2^*)	Rates of chemical species constants

k_{∞}	Thermal conductivity at infinite distance
k	Thermal conductivity of the fluid
k^*	Stefan–Boltzmann constant
$k(T)$	Variable thermal conductivity of the fluid
K_1, K_1', K_1''	Unknown constants
L	The typical characteristics length
l	Known constant
m	Mass of a quantity
m_1	Scalar quantity
n	Power law index
n_1	Advection/convection component
O	Origin
p	Pressure of the fluid
P	Dimensionless pressure
p_1	Unknown parameter
P_2	A point in space
Q_0	Heat generation/absorption coefficient
q	Normal heat flux
q_r	Radiative heat flux
r	Curvilinear coordinate in vertical direction
r_1	Represents sink/source
r^*	Dimensionless curvilinear coordinate in vertical direction
r_1^*	Residual error
R	Radius of curvature

s_1	Nonlinear stretching parameter
s	Curvilinear coordinate in axial direction
s^*	Dimensionless curvilinear coordinate in axial direction
s_1^*	Functional values
t	Time
T	Temperature of fluid
T_∞	Ambient temperature
T^*	Transpose of matrix
u	Velocity in x -direction
u^*	Dimensionless velocity
U_w	Stretching speed in x -direction
\mathbf{V}	Velocity vector
v	Velocity component
v_i	Cell volume
V_1	Volume
V_w	Stretching speed in y -direction
v^*	Dimensionless velocity
x	Horizontal cartesian coordinate
x^*	Dimensionless horizontal coordinate
x_0	Initial value
y	Vertical Cartesian coordinate
y^*	Dimensionless vertical coordinate
y_0	Boundary value
z	Vertical Cartesian coordinate perpendicular to (x, y) plane

GREEK SYMBOLS

α	Stretching ratio parameter
α_1	Thermal diffusivity of fluid
β	Time constant
δ	Boundary layer thickness
ρ_f	Fluid density
ν_f	Kinematic viscosity
η	Dimensionless variable
μ_f	Dynamic viscosity
σ	Electrical conductivity
$\gamma, \gamma_1, \gamma_2$	Generalized Biot numbers
τ^*	Ratio of effective heat capacity
τ_w	Shear stress at the wall
τ_{xz}	Shear stress along x -axis
τ_{yz}	Shear stress along y -axis
τ_{rs}	Shear stress along s -axis
λ	Heat generation/absorption parameter
θ	Dimensionless temperature
ϕ	Dimensionless concentration
ψ	Stream function
δ_E	Relaxation times of heat flux
δ_C	Relaxation times of mass flux

λ_E	Relaxation time parameter for temperature
λ_C	Relaxation time parameter for concentration
σ^*	Stefan-Boltzmann constant
ε	Variable thermal conductivity of the fluid

DIMENSIONLESS GROUPS

A	Material parameter
α	Stretching ratio parameter
Cf	Skin-friction coefficient
Cf_x	Skin-friction referred to x -axis
Cf_y	Skin-friction referred to y -axis
Nu_x	Local Nusselt number along x -axis
Sh_x	Local Sherwood number x -axis
Nu_s	Local Nusselt number along s -axis
Sh_s	Local Sherwood number along s -axis
K	Dimensionless curvature parameter
k_1	Measure the reaction strength of homogeneous parameter
k_2	Measure the reaction strength of heterogeneous parameter
Le	Lewis number
M	Magnetic parameter
N_b	Brownian motion parameter

N_t	Thermophoresis parameter
Pr	Generalized Prandtl number
R_d	Radiation parameter
(Re_a, Re_b)	Local Reynolds numbers
S	Unsteadiness parameter
Sc	The generalized Schmidt number
$(\gamma, \gamma_1, \gamma_2)$	Generalized Biot numbers
λ	Heat generation/absorption parameter
λ_E	Time relaxation heat flux parameter
λ_C	Time relaxation mass flux parameter
θ_w	Temperature ratio parameter

ACRONYMS

RVE	Representative volume element
CV	Control volume
BL	Boundary layer
BVP	Boundary value problem
BLT	Boundary layer thickness
CBLT	Concentration boundary layer thickness
ODE	Ordinary differential equation
PDE	Partial differential equation

2D	Two dimensional
3D	Three dimensional
MHD	Magnetohydrodynamics
BLF	Boundary layer flow
MBLT	Momentum boundary layer thickness
TBLT	Thermal boundary layer thickness
RKF	Runge-Kutta Fehlberg

Chapter 1

Introduction

The motivation for the present study is introduced in this chapter. Moreover, the scop of the study, basic physical laws, numerical methods and research objectives are introduced. Lastly, the contribution of the thesis is highlighted briefly.

1.1 Motivation

Fluid flow is one of the most important principle in the process of respiration. Because air and water are those flowing materials which are nominated as life charging materials. It is about the basics need for any living things which are further scientifically assumed as Newtonian fluids for useful calculations under usual circumstances. The Newtonian fluid was first introduced by a illustrious British scientist, Sir Isaac Newton in 1687, who first postulated the correlation between shear stress and shear strain rate for such fluids in the form of differential equation (DE). This research of Newton was published in the form of Newton's law of viscosity. These are the simplest mathematical models of liquids that justification for viscosity. In other words, the flow of those liquids which holds the Newton's law of viscosity are acknowledged as Newtonian liquids. Many attempts have been made to investigate the flow, mass and energy balance of Newtonian fluids in complicated flow geometries. Onward from 19th century, it is very clear that the

fluids like materials which having non-linear correspondence between rate of strain and shear stress cannot be categorized as Newtonian liquids. An increasing applications urges to expand this phenomenon to the flow of non-Newtonian fluids with energy and mass balances. Actually, there would be no amplification in maxim that non-Newtonian fluids conduct is so extensive in an atmosphere that the Newtonian fluid trend textures as an exclusion rather than the rule. A large number of examples of such fluids contain greases, foams, paints, emulsions, blood at low shear rate, dispersions and suspensions, certain oils, mud and polymer melt etc. Rapidly varying technologies are the features of the current century and this development is an encouragement toward the area of fluid flows. In current century systematic attention has been given to the philosophies of fluid mechanics and how to apply them to several applied problems. Biomedical, aeronautical, marine, civil and mechanical engineers as well as meteorologists, astrophysicist, space researchers, physicists, physical oceanographers, geophysicists and mathematicians have used this knowledge to hold an assembly of intricate flow phenomena. The usual complex flows confront by these researchers often comprise of two or more junctures in which the correspondence between them plays a principal role in monitoring transport process such as the exchange of heat and mass and reaction kinetics. A computable study concluded a proper theory is vital to realize the physics of the complex flow conduct and also to obtain priceless scale-up knowledge for industrial uses. In view of above applications, the analysis of non-Newtonian fluids flow gained extensive attention in the modern world. For better working, the empirically derived from the Newton's law of viscosity is a first step toward the variation of viscosity with shear stress (or with shear rate). In this regard, generalized Newtonian fluids(GNF) is the classification of non-Newtonian fluids and described by Bird *et al.* [1]. For GNF, the constitutive relation is

$$\tau = \eta(\dot{\gamma})A_1. \tag{1.1}$$

A number of empirical relationships for $\eta(\dot{\gamma})$ have been available from raw data. It is more suitable and beneficial to make usage of analytical terms of $\eta(\dot{\gamma})$ that have been established to 'fit' the experimental data with enough exactness. Thus GNF model is frequently used for particular fluids of significance in industry. It may be highlighted that it does have severe restrictions. This fluid model cannot provide justification for phenomena including visco-elastics unsteady effects, normal forces, or flows that are not controlled by steady shear. However, the development of the GNF was existing as an addition of the Newtonian fluids sustained by experimental data, a dispute based on continuum mechanics indicates that $\eta(\dot{\gamma})$ is a general first term expression for time-independent state for shear flows as presented in [1]. Where the normal stresses in such flows are the related details provided by higher order terms. Although the origin of GNF model is the empirical data and attained an appropriate basis from recent theories in continuum mechanics. The Sisko liquid model is one of the GNF model which overcomes the deficiencies in the power-law fluid and which describes the flow behavior in the power-law as well as in upper Newtonian regions. Firstly this model was used to demonstrate the flow behavior of greases which indicates regions of higher shear rate.

1.2 Context and Scope of the Study

Fluid flow with the transfer of mass and heat analysis have been the subject of considerable interest, owing primarily to the applicability of this information to the field of science and technology. In particular, mathematical modeling and numerical simulation of non-Newtonian fluids flow due to stretching surfaces have increased huge desirability because of their massive applications related to engineering and industries. For instance, oil recoveries, fuel slurries, glass blowing, food processing melts, sheet processing, refrigeration equipment, design of heat-exchangers and turbo-machinery. Specially, this description is a motivation towards the enhancement of non-Newtonian fluids flow consideration with different moving surfaces and physical effects. However, due to special importance in this

direction some work related to non-Newtonian fluids and their mathematical modeling can be found in Bird *et al.* [1]. Major models related to fluid mechanics with non-Newtonian properties like, Bingham plastic, Power-law, Cross, Ellis, Carreau and Sisko etc. Many of these models show a variation of viscosity with shear rate and also predict the pseudo-plastic ($0 < n < 1$) as well as dilatant ($n > 1$) properties of the fluids. Meanwhile, the simple power-law model for small shear rates has a zero-effective value of the apparent viscosity. From rheological point of view, the behavior of non-Newtonian fluids will be characterizing by stresses relations with rate of change of strain or strain rates by considering least number of functions. Moreover, a large number of fluids possess a finite region of viscosity, i.e., where the velocity shear is very small and negligible away from the boundary layer flow (BLF). Hence, the behavior of a real fluid for which the viscosity model gives a constant or although small values of apparent viscosity for the shear rate near zero. Thus, the shear rate dependency of apparent viscosity classifies to the non-Newtonian fluids into numerous types. In this regard, Power-law model is the most simplest and a common GNF model but cannot predict the flow features in lower or upper Newtonian regions. However, an enough interest has not been compensated to model the flow of such GNF and which leads to overcome the gap corresponding to related applications of industry and chemical engineering. In a simple way there is no single model of non-Newtonian liquids which predict all behaviors of the liquids, whereas some attempts are made to discuss the development of some useful relationships amongst the types of non-Newtonian fluids.

A three parameters liquid model namely Sisko liquid is one of the most considerable non-linear material which possesses the imperious scope of shear rates. This experimental three parameters model is more applicable in the region of upper Newtonian and power-law fluid flows. Enlightening about the results of this liquid model demonstrated in terms of pseudo-plastic (shear-thinning) and dilatant (shear-thickening) liquids characteristics. Particularly, the pseudo-plastic liquids are those for which the viscosity rises while reducing the shear rate. This remarkability guarantee about the stress of the study of rheology

and an attention towards the rheological conduct of many liquids, likely the ketchup, blood and whipped cream etc. Specifically, biorheology demonstrated about the analysis practiced by the flow and falsification of biological structures and ingredients got from active life customs. To relate the rheological features of materials/frameworks to their cell, molecular and supporting properties is an indication towards the significance of biorheology. Blood rheology is strongly essential for both scholarly and miserable to practical determinations. The flow features of blood directly influenced human well-being from hemolysis or stenosis up to cardiovascular medical process. From the rheological outlook, blood is fundamentally an intricate liquid context, shape changeable particles (commonly red cells) deferred in plasma. The analysis of flow behavior of blood emphasizes principally on the existing joining between its micro physical fluctuations and rheology. During the blood flow and being a pseudo plastic (shear-thinning) fluid, the features of Sisko liquid model can be deliberated. For the cause of their admirable collective diminishing and scattering nature, Sisko [2] presented this liquid model in 1958 for the first time. The investigation of such liquids has increased enthusiasm among researchers in latest years as a result of their plenteous innovative and modern applications. Such liquids are as frequently assigned to as nonlinear materials (non-Newtonian liquids). Classic non-Newtonian liquids characteristics incorporates pseudo-plastic as well as dilatant viscoelasticity etc. For the flow of nonlinear materials there is definitely not a lonely model that depicts most of their properties as is proficient for the Newtonian liquid. Thus, most of the properties of flow of such liquids can be described with by considering a power-law model. Although, Siddiqui *et al.* [3] demonstrated the problem firstly while using the integer values of power- index. In this study a free surface condition, i.e., at $x = d$ is used by them, where d is assumed to be the film thickness. Asghar *et al.* [4] illustrated the analytically the same problem for the non-integer values with correct free surface condition. Wang *et al.* [5] used the lubrication methodology, while studied the electrically conducting numerical elucidations. Abelman *et al.* [6] investigated the time dependent Sisko liquid flow with sudden moved plate. The transversely attached magnetic field in

the flow of one dimensional time dependent Sisko liquid was elucidated by Molati *et al.* [7]. Hayat *et al.* [8] elaborated the flow of Sisko liquid on the porous surface. The basic BLF equations produced by a velocity due stretching while considering this nonlinear materials in order to analyze different features. In this regard, Khan and Shahzad [9] was made a first attempt to formulate the flow such materials in Cartesian geometry. Munir *et al.* [10] investigated the impact of non-linear moving surface on forced convective heat energy balance in BLF of Sisko fluid. Same materials flows were later on characterized with non-linear moving sheet and convective boundary conditions(BCs) by Malik *et al.* [11]. Munir *et al.* [12] elucidated the features of the said materials in 3D geometry with convective heat transfer mechanism over a moving boundary.

The study of combined heat and mass transfer is a widespread phenomenon and have received spectacular engrossment by the research community due to their considerably applications in metallurgy process, engineering and industry. Fourier's law of heat conduction and Fick's law of diffusion are utilized adequately for understanding the phenomena of heat and mass transfer. The phenomenon of heat exchange has, no matter how you look at it present day and biomedical uses, for example, electronic cooling contraptions, nuclear cooling of reactor, control period, heat conduction inside tissues and various others. The heat flux pattern anticipated by Fourier [13] has been the preeminent show for perception of the heat balance instrument in different conditions. One of the confinements of this rheological model is that it consistently stimulates to a descriptive imperativeness condition which shows that starting agitating impact is immediately experienced with the medium beneath idea. Both the scholar and innovative enthusiasm of heat exchange at the atomic stage is discerning. Really, a limited time is incorporated into transfer of heat through solids, which occurs through effects between essentials carrier's free phonons, electrons, moreover, by scattering of these conveys at limits and material deformities. The limited speed of heat exchange was seen by many, containing Chester [14], Joseph and Preziosi [15] on heat waves are their fundamental work. The free electrons are overwhelming transporters in metals, and where the phonons are preeminent heat bearers for separators and

semi-conductors as exhibited in [16]. The key downside of the Fourier's law is that it creates illustrative vitality condition which demonstrates that the entire medium is in a split second influenced by the underlying aggravation. To overwhelmed this complication, Cattaneo [17] proposed a non-Fourier's law by incorporating relaxation of thermal distinctive time duration to escape the absurdity of heat conduction. It is also anticipated that this amendment yields a hyperbolic energy balance and enables the exchange of heat due the dissemination of thermal waves with constrained speed. Moreover, these finite waves have various applications in areas such as nanofluids and skin burns. Christov [18] further introduced the derivative with respect to time in the Maxwell-Cattaneo model in the presence of Oldroyd upper-convected derivative which successfully preserves the material-invariant formulation. The structural constancy and distinctiveness of the elucidations for heat flux equation of Cattaneo-Christov have been substantiated by Ciarletta and Straughan [19]. Hayat *et al.* [20] investigated the impacts of heterogeneous-homogeneous reactions on Oldroyd-B liquid in counting of Cattaneo-Christov heat flux model. They determined that the temperature field reduces for uplifting values for the time of thermal relaxation. Khan and Khan [21] illustrated the effect of heat flux model namely Cattaneo-Christov for 3D flow of Burgers liquids over a bidirectional moving surface. They established that the temperature field is remarkably affected by the time of thermal relaxation variation. Waqas *et al.* [22] scrutinized the features of heat flux model, Cattaneo-Christov model in the flow of generalized Burgers liquid with the additional effect of inconstant thermal conductivity. Sui *et al.* [23] examined the impact of Cattaneo-Christov heat and mass flux models of upper-convected Maxwell nano-liquid flow over a moving boundary in the conjunction with slip velocity. The features of Cattaneo-Christov heat flux model on MHD viscoelastic flow and balance of heat past an erect moving boundary is explored by Liu *et al.* [24]. Newly, the effect of chemical practices on flow of 3D Burgers liquid with application of Cattaneo-Christov phenomenon has been studied by Khan *et al.* [25].

With the swift worldwide developments in science and technology such as elevated power outputs, high operating speeds, miniaturization of devices and enhancing the efficiency

of energy transfer and saving energy are posing new challenges and thus became as the top priority in numerous industrial applications. Nowadays, cooling technologies such as enhancing the surface area by fins, dual-phase heat transfer and micro-channel cooling techniques have reached their technological limits due to the poor intrinsic thermal conductivity of common coolants. As a result, this has led researchers and engineers to search new innovative cooling liquids with superior thermo physical properties that will be able to empty the substantial heat created to preserve the temperature of electrical apparatuses less than a definite suggested level. Developments in nanotechnology has led to a new class of cooling liquids referred as nano-fluids which has become a hotly debated topic in the domain of heat transfer. Nano-fluids have unbounded thermal management advantages than their base fluids and are far more stable than millimeter or micrometer sized solid-liquid suspensions. In 1995, Choi [26] was the first name who introduced fluid with nano-particles. Much research work has been carried out with this new phenomenon. Additionally, balance of heat utilization due to nano-liquids as coolant medium and has appeared as one of the operating procedures in order to complete high heat degeneracy. This holds prospective uses in boundaries like squeezing heated exchanges and heat pipes etc.

Buongiorno [27] revealed that the solo phase model creates clash with the experimental discernment and unalloyed liquid associations, (for instance, Dittus–Boelter's) to foresee the nano-liquid coefficient of heat exchange. At that point a replacement of model that streaks out the insufficiencies of the scattering or solo phase models (DPM models) was formed. He believed about seven slip apparatuses, at that point recognized that limited thermophoresis and Brownian diffusion are the prodigious slip appliances in nano-liquids. With these outcomes as a foundation, he anticipated a non-homogeneous two phase model of equilibrium for convective exchange in nano-liquids. One of the key erections of this innovative model is that the influence of the comparative velocity amongst nano-particles and base liquid is illustrated more systematically than in the models of scattering. Kuznetsov and Nield [28] explored the impact of nanoparticles on natural

convective BLF over a vertical plate. They perceived that the reduced Nusselt number declines for each incremented value of the N_b and N_t . Turkyilmazoglu [29] described the impact of MHD slip flow for heat and mass balance utilizing the nano-particles. Nadeem *et al.* [30] illustrated the effects of nano-particle on the Oldroyd-B over a moving surface. Kuznetsov and Nield [31] explored the characteristics of nano-particles for natural convective BLF past a moving sheet. Khan *et al.* [32] analytically framed the effect of generation/absorption on flow of 3D Oldroyd-B in the presence of nano-particles. However, many research works [33,34] are carried out to explain the nanofluid flow conducts. Rehman *et al.* [35] investigated the characteristics of entropy generation and new mass flux conditions for non-Newtonian fluid over a moving boundary. Hayat *et al.* [36] illustrated the impact of magneto nano-particles for the Burgers fluid with convective BCs. The process of synergies between two or more chemicals to produce one or more new chemical compound is known as a chemical reaction. An essential bit of development, of culture, and an unavoidable truth itself is the strong association with chemical reactions. Blasting fills, refining iron, stoneware and making glass, mixing blend, and manufacturing of wine are among various instances of activities solidifying chemical reactions and used for the next some year in many numbers as well. The modification in physical sense is totally recognized from compound response. Physical variations join change of state, for instance, ice liquefying to water and water disseminating to vapor. If a physical amendment occurs, the physical characteristics of a material will change, anyway its compound character will proceed as previously. As needs be, investigation and speculation, the two establishments of concoction science in the present world, laidback described the possibility of chemical reaction. The chemical reaction is additionally delegated heterogeneous-homogeneous reactions. Homogeneous reaction is one the chemical reaction, where the reactants and items are in a comparable stage, however, the heterogeneous reaction is one where the reactants are in no less than two phases. Reaction that happen on the surface of a stimulus of a substitute stage are furthermore heterogeneous. The joint efforts between the heterogeneous-homogeneous reactions are incredibly, amazingly troublesome and have be-

come expanded thought, yet it is as yet uncertain.

Based on physical structure (i.e. length, weight, architectural pattern, color, temperature, size, shape, distribution, language, disease, appearance, radioactivity, income etc.) the objects in such a reaction are described through heterogeneous and homogeneous reactions. Chemical reaction can appear on catalyst surface, i.e., (heterogeneous situation of reactions) as well as in bulk i.e. (homogeneous situation of reactions). Since reactant product relies merely on the type of reactant species therefore, homogeneous processes are more simple than heterogeneous processes. However, heterogeneous processes sustain practical significance as it communicates dependency of the product on type of distinct reactant species. Corrosion phenomenon, electrolytic cells and batteries involve such reactions. The models regarding heterogeneous and homogeneous situation of reactions with same/unequal diffusivities are suggested by Chaudhary and Merkin [37, 38]. Pizza *et al.* [39, 40] demonstrated the capacity of chemically covered dividers in directing trademark fire dangers of meso/littler scale channels. Wang *et al.* [41] revealed about the response power among synergist and non-reactant combustors. It has been demonstrated that these affiliations consolidate the progression of homogeneous reaction since of artificially impelled exothermicity and the controller of heterogeneous reaction on the homogeneous reaction generally realized by contention of empowers, in addition, oxidizers related to heterogeneous reaction against homogeneous reaction is outlined by Li *et al.* [42]. The results exhibited that the synergist combustor demonstrated a high security and feeble response power. Nandkeolyar *et al.* [43] reported the importance of heterogeneous and homogeneous situation of reactions in stretchable flow of convective viscous liquid subject to viscous dissipation. Impact of non-Fourier theory in Williamson liquid flow through heterogeneous and homogeneous situation of reactions is addressed by Ramzan *et al.* [44]. Qayyum *et al.* [45] explored melting heat and inclined MHD aspects in chemically reacting hyperbolic-tangent liquid towards nonlinear moving surface.

Thermal radiation has an extensive role in high temperature practices. It has a large number of uses in different construct trades for the intention of nuclear power plants.

This concept is also prevalent in boilers, furnaces, cooling process of engine and many others. Further, the thermal radiation depict has considerable role in aircraft, space vehicles, gas turbines, nuclear plants and for satellites devices etc. Rahman *et al.* [46] examined the thermally radiative and effect of heat transport to modified second grade liquid. Kothandapani and Prakash [47] discussed the effects on MHD radiative flow of Williamson nanoliquid in a asymmetric channel. Seddeek and Abdel [48] reported thermally radiative flow over a moving surface and variable heat flux transfer with impact of thermal diffusivity. Khan *et al.* [49] presented the radiative flow of magneto-Burgers nanofluid with gyrotactic microorganisms. Additionally, Khan *et al.* [50] reported the convective heating MHD 3D flow of Eyring-Powell nanofluid with nonlinear thermal radiation.

The consideration of BLF problem needs the BCs which are both specified at surface heat flux or specified at simple surfaces. But some of the fluid flow problems, where the transfer of heat is treated in the form of surface dependent temperature are considered. The situation with Newtonian heating accruing and is acknowledged as conjugate convective flow. The formation of Newtonian heating arises in numerous significant engineering devices. The requirement of high temperature in the process of many chemical, engineering and so many other fields has broad applications. For example, gas turbine, storage of chemical energy and nuclear plants, etc. Further, it is justified that there are many applications of convective conditions like in the field of engineering and industries. For example, transpiration of cooling procedure, material aeration and so forth. This importance has convinced researchers to focus such types of heat transfer. No attempts were made to examine the nano-fluid flows with convective surfaces conditions. Recently BLF problems with the convective BCs was explored by Aziz [51]. Natural convective BLF over a convectively vertical heated surface is described by Aziz and Khan [52]. Hayat *et al.* [53] reported the heat exchange of an upper convected Maxwell liquid over a moving sheet with convective BCs. Moreover, the convective flow conditions on both transfer of mass and heat is utilized by Imtiaz *et al.* [54] in their recent work of flow of mixed

convection regarding Casson nano-liquid over a moving cylinder with convective BCs. Recently, Khan *et al.* [55] discussed the flow of unsteady with convective surfaces conditions and they concluded that whenever the values of Biot numbers increases both the profiles (temperature and concentration) show uplifting behavior. Additionally, Waqas *et al.* [56] addressed the convective heat transfer with micropolar liquid and mixed convection MHD flow because of the nonlinear stretching surface.

The flow pattern appearing in the presence of time dependency is more effective as compared with steady flow. A significant time-dependent BL problem was deliberated by Todd [57] for a constant velocity free stream passing through a fixed semi-infinite flat plate. The illustration reported by Ishak *et al.* [58] demonstrates the time dependent stretching sheet with given wall temperature. Analytical examination of unsteady with the heat exchange mechanism of an Oldroyd-B nanofluid over an unsteady stretching sheet was ended by Zhang *et al.* [59]. Recently the transient flow along with transfer of heat in power-law liquid is inspected by Ahmed *et al.* [60] where the flow is due to radially stretching surface. As of late Zhang *et al.* [61] displayed the time dependent flow and heat exchange of power-law nanoliquid film over an extending sheet with power-law speed slip and inconstant magnetic field impacts.

Many mechanical processes are incomplete without the flow of liquids due to continuous moving boundaries. For instance, sustenance stuff preparing, wire and fiber covering, expulsion process, polymer handling, substance preparing hardware, outline of the transfer of heat and so on. In this context, Crane [62] was initiated this phenomenon of flow of liquids due to linear stretched surface. His work has stretched out from various point of views together with physical prominence of the balance of mass and heat along flat plate, influence of injection/suction, magnetic field etc. Gupta and Gupta [63] have incorporated the physical impact of suction/injection on the flow of liquids due to stretching boundary. Ahmad and Asghar [64] utilized the importance of hyperbolic stretching boundary and modeled the flow equations along with transfer of heat and then discussed the numerical solution in detail. Turkyilmazoglu [65] continued the same flow problem while considering

the deforming bodies in 2D and 3D geometries with magnetic field and then examined the exact solutions. Deforming body convinced by the flow and transfer of heat through two-three dimensional surfaces was presented by Turkyilmazoglu [66]. Turkyilmazoglu [67] incorporated the significance of radiation and magnetic field while considering the flow of liquids due to moving boundary. In addition, Mat Yasin *et al.* [68] discussed the flow of two-phase dusty liquid with physical effect of MHD while incorporated the importance of modeler of heat on distorting isothermal surfaces. In a little while back, Turkyilmazoglu [69] examined the mathematical existence of the flow of micropolar liquid placed over a heated or cooled stretched surface in the presence of sink/source and magnetic field.

Reporting about the curvature effect is carried out to examine the flow behavior over a curved geometry rather than the planner surface is one of the major interest of many examiners today. In this regard, a very less attention has been made to explain the features of liquids flow over moving bended surfaces and the flow spirit inside the BL is not more insignificant as on account of moving sheet. Sajid *et al.* [70] considered the flow of viscous liquid over a bended moving surface and discovered that MBLT raises in case of bended moving surface as compared to flat surface. Rosca and Pop [71] inspected the BLF over time-dependent permeable shrinking/stretching sheet. Additionally, it is also intensely perceived that in case of curved surface as compared to flat boundary the drag force is minor. This phenomenon was then further elaborated by Sajid *et al.* [72]. Furthermore, Abbas *et al.* [73] demonstrated heat generation, slip effect and thermally radiated BLF on curved surface.

1.3 Numerical Methods

In this section, the methods that are followed for the solution of the entire flow, heat and mass problems in the thesis are presented with a brief explanation and basics procedures. All those methods that are considered in this thesis are illustrated as follows:

1.3.1 Runge-Kutta-Fehlberg Method

In mathematics, one of the algorithm through which a numerical solution of initial value problems (IVPs) is approximated is known as RK45-Fehlberg method (or Fehlberg method). This method was established by the German mathematician Erwin Fehlberg which is constructed as one of the large class of RK methods. However, RK45-Fehlberg is an mathematical approach of order $O(h^4)$ with an error estimator of order $O(h^5)$. By accomplishment of one additional calculation, the error in the result can be assessed and controlled by using the higher-order embedded method that permits for an adaptive step size to be determined inevitably. Naturally, the main drawback of RK4 and RK5 is the evaluation of the number of functions at each step and which is the most important step for this approach. For instance, by considering a common approach which uses both fourth and fifth order RK methods instead of separate evaluations of functions. Since to avoid such difficulties of computational burden the RK-Fehlberg method is utilized in RK5 method that uses the function evaluations provided by its associated RK4 method. This will decrease the number of function evaluations per step from 10 to 6.

Let an IVP be specified as follows

$$\frac{dy}{dx} = f_2(x, y), \quad y(x_0) = y_0. \quad (1.2)$$

To find an approximate continuous solution of Eq. (1.2), the function $f_2(x, y)$ and the values of x_0 and y_0 must be known to us. Thus the subsequent six functional values are defined as follows:

$$s_1^* = hf_2(t_{s^*}, u_{s^*}), \quad (1.3)$$

$$s_2^* = hf_2\left(t_{s^*} + \frac{1}{4}h, u_{s^*} + \frac{1}{4}s_1^*\right), \quad (1.4)$$

$$s_3^* = hf_2\left(t_{s^*} + \frac{3}{8}h, u_{s^*} + \frac{3}{32}s_1^* + \frac{9}{32}s_2^*\right), \quad (1.5)$$

$$s_4^* = hf_2 \left(t_s^* + \frac{12}{13}h, u_s^* + \frac{1932}{2197}s_1^* - \frac{7200}{2197}s_2^* + \frac{7296}{2197}s_3^* \right), \quad (1.6)$$

$$s_5^* = hf_2 \left(t_s^* + h, u_s^* + \frac{439}{216}s_1^* - 8s_2^* + \frac{3680}{513}s_3^* - \frac{845}{4104}s_4^* \right), \quad (1.7)$$

$$s_6^* = hf \left(t_s^* + \frac{1}{2}h, u_s^* - \frac{8}{27}s_1^* + 2s_2^* - \frac{3544}{2565}s_3^* + \frac{1819}{4104}s_4^* - \frac{11}{40}s_5^* \right). \quad (1.8)$$

Thus by using the above six functional values to approximate the solution we need to use Runge-Kutta fourth order method, i.e.,

$$u_{s^*+1} = u_s^* + \frac{25}{216}s_1^* + \frac{1408}{2565}s_3^* + \frac{2197}{4101}s_4^* - \frac{1}{5}s_5^*. \quad (1.9)$$

Furthermore, Runge-Kutta fifth order is implemented for a better value of the approximation to the solution. This relation is given as follows:

$$v_{s^*+1} = u_s^* + \frac{16}{135}s_1^* + \frac{6656}{256512825}s_3^* + \frac{28561}{56430}s_4^* - \frac{9}{50}s_5^* + \frac{2}{55}s_6^*. \quad (1.10)$$

The scalar m_1 can be multiplying with the original step size h to obtain the optimal step size m_1h . Where the scalar can be defined as:

$$m_1 = \left(\frac{tolh}{2|v_{s^*+1} - u_{s^*+1}|} \right)^{\frac{1}{4}} \approx 0.84 \left(\frac{tolh}{|v_{s^*+1} - u_{s^*+1}|} \right)^{\frac{1}{4}}. \quad (1.11)$$

Since, in order to compute the approximate solution of higher order ODEs we will reduce it into ODEs in first order. Main procedures regarding the approximate solution of higher order ODEs are as follows.

Let:

$$f_2 = x_1, \quad f_2' = x_1' = x_2, \quad f_2'' = x_2' = x_3, \quad f_2''' = x_3', \quad (1.12)$$

with associated transformed BCs are defined as:

$$f_2(0) = x_1(0), \quad f_2'(0) = x_2(0), \quad f_2'(\infty) = x_2(\infty). \quad (1.13)$$

1.3.2 Bvp4c Built in Solver

The `bvp4c` is a built in MATLAB function which comprises a finite difference technique that trappings the 3-stage Lobatto IIIa formula. This formula is usually known as the collocation formula where the collocation polynomial offers a C^1 continuous elucidation that is the fourth order accurate consistently in the interval of integration. The residual of the continuous solution guaranteed the mesh selection and error control. Of the division of the interval of integration into sub-intervals the collocation techniques use the mesh points. The numerical solution of a global system of algebraic equations determined by this solver with the conjunction of imposing BCs as well as the collocation conditions on all the subintervals. For solving such system of algebraic equations, Newton's method is applied, which needs the knowledge of the partial derivatives. In the package these derivatives are demarcated approximately, by using the finite difference scheme. Error estimation is carried out of the numerical solution on each sub-intervals. The solver will adapt the mesh in case when the numerical solution does not fulfill the tolerance criteria and the process will continue until the tolerance criteria is satisfied. The points of first mesh as well as a first approximation of the solution will be mostly provided by the user. In this regard, Kierzenka and Shampine [74] developed the core software for the solution of large class of two-point BVPs of the form.

$$\frac{dy}{dx} = f_2(x, y, p_1), a^* \leq x \leq b^*, \quad (1.14)$$

and a set of BCs

$$0 = g_2(y(a^*), y(b^*), p_1), \quad (1.15)$$

where f_2 is continuous and Lipschitz function in y and p_1 represents an unknown parameters which arise naturally during the modeling of the physical problem which may be introduce as part of the procedure of elucidating a BVP. So $S_2(x)$ is a piecewise-smooth function which represents the approximate solution of a BVP. This is a third degree polynomial over a respective sub-interval $[x_n, x_{n^*+1}]$ of a mesh $a^* = x_0 < x_1 \dots < x_n^* = b^*$ and

which also satisfies the corresponding BCs

$$0 = g_2(S_2(a^*), S_2(b^*), p_1). \quad (1.16)$$

At the end points and the midpoint of each subinterval, the same polynomial should have to satisfied the ODE's

$$S_2'(x_i) = f_2(x_i, S_2(x_i), p_1), \quad (1.17)$$

$$S_2'(x_{i+1}/2) = f_2(x_{i+1}/2, S_2(x_{i+1}/2), p_1), \quad (1.18)$$

$$S_2'(x_{i+1}) = f_2(x_{i+1}, S_2(x_{i+1}), p_1), \quad (1.19)$$

$$S_2'(x_{n+1}) = f_2(x_{n+1}, S_2(x_{n+1}), p_1). \quad (1.20)$$

As pointed out before, the collocation conditions at the end of the subinterval infer that $S_2(x) \in C^1[a, b]$. All together these conditions results in an arrangement of non-linear algebraic equations for the coefficients of the third degree polynomials that make up $S_2(x)$. At the point when the subtle elements are worked out, it is discovered that this function $S_2(x)$ is the normal consistent extension of the Simpson relation. In like manner, we can see this technique either as a collocation technique or as a finite difference technique with a perpetual augmentation. As $S_2(x)$ is declared a fourth order guess to a distinct solution $y(x)$, i.e., $\|y(x) - S_2(x)\| \leq C^*h^4$. Where h denotes the maximum of step sizes $h_i = x_{i+1} - x_n$ and C^* represents a constant. We can estimate $S_2(x)$ with the help of `bvp4c` routine at each x or set of x in $[a^*, b^*]$. The error estimation regarding this routine is based on the mesh selection and residual of $S_2(x)$ and defined as:

$$r^*(x) = S_2'(x) - f(x, S_2(x), p_1). \quad (1.21)$$

1.3.3 BVP Traprich Method (Richardson's Extrapolations)

Through various numerical schemes, the solution of BVP is one of the most attraction as related to all physical phenomenon. The sub methods with built in commands for methods, like BVP midrich, BVP traprich and RK4 methods etc., are very helpful techniques while using Maple software. BVP traprich is one of these methods which uses Richardson extrapolation for the solution of BVP. Be that as it may, numerous estimation systems in which one first picks h and after that creates a guess $E(h)$ to some coveted quantity E . Regularly the request of the error created by the system is known. As it were,

$$E = E(h) + K_1 h^l + K_1' h^{l+1} + K_1'' h^{l+2} + \dots, \quad (1.22)$$

with K_1, K_1', K_1'', \dots being some other (usually unknown) constants. For instance, E at some final time t_f , E might be the value of $y(t_f)$ for an IVP.

$$\frac{dy}{dx} = f_2(t, y), \quad y(t_0) = y_0. \quad (1.23)$$

Formerly $E(h)$ might be the approximation to $y(t_f)$ formed by Euler's method with h . In this case $l = 1$. If the upgraded Euler's method is utilized with $l = 2$. If Runge-Kutta is utilized with $l = 4$. The notation $O(h^{l+1})$ is predictably used to view for "a sum of terms of order h^{l+1} and greater". So the beyond equation might be written

$$E = E(h) + K_1 h^l + O(h^{l+1}), \quad (1.24)$$

If we somehow happened to drop the, ideally modest, term $O(h^{l+1})$ from this equation, we would have one linear equation, $E = E(h) + K_1 h^l$, in the two unknowns E and K_1 . Yet, this is extremely a different condition for each unique estimation of h . We can get a second such equation just by using an alternate advance size. At that point the two equations might be tackled, yielding estimated estimations of E and K_1 . This estimated approximation of E comprises another enhanced approximation, $E_1(h)$, for the correct E .

We do this now. Taking 2^l times

$$E = E\left(\frac{h}{2}\right) + K_1\left(\frac{h}{2}\right)^l + O(h^{l+1}), \quad (1.25)$$

(note that, in equations (1.22) and (1.24), the notation " $O(h^{l+1})$ " is incorporated to view for two dissimilar sums of terms of order h^{l+1} and greater) and subtracting equation (1.22) provides

$$(2^l - 1)E = 2^l E\left(\frac{h}{2}\right) - Eh + O(h^{l+1}), \quad (1.26)$$

$$E = \frac{2^l E\left(\frac{h}{2}\right) - Eh}{2^l - 1} + O(h^{l+1}). \quad (1.27)$$

Hence if we define

$$E_1(h) = \frac{2^l E\left(\frac{h}{2}\right) - Eh}{2^l - 1}, \quad (1.28)$$

then

$$E = E_1(h) + O(h^{l+1}), \quad (1.29)$$

what's more, we have delivered an approximation whose error is of order $l+1$ one superior to $E(h)$'s. One broadly utilized numerical reconciliation calculation, called Romberg integration, which relates this formula as often as possible to the trapezoidal rule.

1.4 Basic Physical Laws

The flow of fluid characteristics are generally anticipated without actually quantifying it while considering the theory of fluid mechanics. On the off chance that the underlying quantities of certain base number of amounts are known, at that point the qualities at some different areas can be obtained by utilizing certain principal connections. But, they are very considerably local in the sense that they cannot be used for different set of conditions. Such associations are called as exact laws/formulae and there are sure



connections which are for the most part suitable in a general flow distribution, falling under the class of 'fundamental laws'. Regarding to the idea of fluid mechanics, there are three most noteworthy fundamental laws in particular.

1.4.1 Conservation of Mass

Basic fluid mechanic laws direct that mass is preserved inside a control volume (CV) for constant density liquids. In this way, the total mass entering the CV must be equivalent to the total mass leaving the CV in addition to the mass gathering inside the control volume.

$$\left(\begin{array}{c} \text{mass of fluid} \\ \text{in volume } \Delta V \end{array} \right) = \left(\begin{array}{c} \text{flux of fluid} \\ \text{in/out of volume } \Delta V \end{array} \right) + \left(\begin{array}{c} \text{sources or} \\ \text{sinks in } \Delta V \end{array} \right).$$

The general form of conservation of any thing is given by the following equation

$$\frac{\partial \Phi}{\partial t} + \nabla \cdot (F + \Phi V) - r_1 = 0. \quad (1.30)$$

This general relation in continuum mechanics demonstrates all the physical conservation laws. For $\Phi = \rho v_i$, $F = 0$ and with no sink or source, i.e., $r_1 = 0$. The Eq. (1.30) can be converted in the subsequent form and is regularly known as continuity equation.

$$\frac{\partial \rho v_i}{\partial t} + \nabla \cdot \rho v_i = 0. \quad (1.31)$$

1.4.2 Conservation of Momentum

Momentum conservation or force balance can be inferred in the very similar way, however the momentum relation is a vector distribution. Accordingly, the total of momentum per unit volume is $\Phi = \rho v_i$. Other than advection momentum, the other approach to variance the momentum in our representative volume element (RVE) is to apply powers on it. These powers come in two characters. In the first place, there is the pressure that follows

up on the outward of the volume with neighborhood constrain $f_1 = \tau \cdot dS$. As stress is fundamentally force per unit area, the pressure can likewise be expected as a transition of force or $F = -\tau$ (the negative sign guarantees that if the net power on the volume focuses on, the momentum rises). The second force impacts the volume, are any body forces, for example, gravity. The body constrain acts a reason for force, in this way $r_1 = \rho g^*$ where g^* is the net speeding up. Exchanging into Eq. (1.30) characterized in past area which produces conservation of momentum. This is characterized as:

$$\begin{aligned} & \left(\begin{array}{c} \text{Total momentum} \\ \text{in the CV} \end{array} \right) + \left(\begin{array}{c} \text{Exchange of momentum} \\ \text{through the boundary of the CV} \end{array} \right) \\ & = \left(\begin{array}{c} \text{Forces acting on} \\ \text{the boundary} \end{array} \right) + \left(\begin{array}{c} \text{Body forces} \\ \text{on the CV} \end{array} \right), \\ & \frac{\partial \rho v_i}{\partial t} + \nabla \cdot (\rho v_i v_i) = \nabla \cdot \tau + \rho g^*. \end{aligned} \quad (1.32)$$

This equation can likewise be determined (maybe more basically) in view of the continuous type of Newton's Law $f_1 = ma^*$. The most straightforward approach to know Eq. (1.32) is to think regarding every one of the three Cartesian components of the linear which must be preserved exclusively. Utilizing index representation, Eq. (1.32) can be expressed for the i^{th} segment of the momentum as

$$\frac{\partial \rho v_i}{\partial t} + \frac{\partial}{\partial x_j} [\rho v_i v_j] + \frac{\partial \tau_{ij}}{\partial x_j} + \rho g_i^*, \quad (1.33)$$

where $i = 1, 2, 3$ and summation is supposed over $j = 1, 2, 3$. By considering mass balance relation, Eq. (1.32) can also be given as below:

$$\frac{\partial \mathbf{V}}{\partial t} + (\mathbf{V} \cdot \nabla) \mathbf{V} = \frac{1}{\rho} \nabla \cdot \tau + g^*. \quad (1.34)$$

Note that $(\mathbf{V} \cdot \nabla) \mathbf{V}$ is a non-linear advection momentum term and which clues to much of the considerable conduct in fluid mechanics.

1.4.3 Conservation of Energy

The principle of first law of thermodynamics is the energy conservation statement. As indicated by this physical statement that any rate of change of energy in the CV must be produced by the rates of energy flow into or out of the volume. The heat balance and the work are as of now included and the main other contribution must be related with the mass flow in and out, which conveys energy with it. The desired nature of the condition will be presented as follows:

$$\begin{aligned} \left(\begin{array}{c} \text{rate of change} \\ \text{of energy in } \Delta V \end{array} \right) &= \left(\begin{array}{c} \text{rate of heat} \\ \text{added to } \Delta V \end{array} \right) - \left(\begin{array}{c} \text{rate of} \\ \text{work done } \Delta V \end{array} \right) \\ &+ \left(\begin{array}{c} \text{rate of energy} \\ \text{flow into } \Delta V \end{array} \right) - \left(\begin{array}{c} \text{rate of energy flow} \\ \text{out of } \Delta V \end{array} \right). \end{aligned}$$

For a distinct phase material $\Phi = \rho c_p T$ is the quantity of heat per unit volume. The flux of heat has two components owing to conduction and transport. The heat flux $F = -k\nabla T$ is considered in the absence of transport. Moreover, ∇T and heat flows are opposite in direction, i.e., occurring of heat flow from hot cold. Where the transport flux is $\rho c_p T v$. At the end, dissimilar mass, heat can be produced in a region owing to expressions like viscous dissipation or radioactive decay or shear and viscous heating. We will simply lump all the source terms into r_1 . Accordingly the least difficult protection of heat equation is can be obtained by putting these terms and relations into Eq. (1.30)

$$\frac{\partial \rho c_p T}{\partial t} + \nabla \cdot (\rho c_p T v_i) = \nabla \cdot k \nabla \cdot T + r_1. \quad (1.35)$$

For the constant value of k and c_p , this equation can also be modified using Eq. (1.35) as:

$$\frac{\partial T}{\partial t} + v_i \cdot \nabla T = \alpha_1 \nabla^2 T + \frac{r_1}{\rho c_p}, \quad (1.36)$$

$$\frac{D_V T}{Dt} = \frac{\partial T}{\partial t} + \mathbf{V} \cdot \nabla T. \quad (1.37)$$

The left hand side is usually known as the material derivative while temperature is observed in with some velocity in a moving frame.

1.4.4 Conservation of Concentration

According to law of conservation of concentration, the rise in the total mass of species i in CV is equal to the net mass flow into CV plus the development rate of species in CV. However, we can have a diffusion component to the continuity equation, if we are considering different chemical species that can interact. For an arbitrary volume of some chemical species i , the mass-balance is:

$$\left(\begin{array}{c} \text{mass of species } i \\ \text{in volume } \Delta V \end{array} \right) = \left(\begin{array}{c} \text{flux of species } i \text{ in/out} \\ \text{volume } \Delta V \end{array} \right) + \left(\begin{array}{c} \text{mass produced} \\ \text{by reaction } \Delta V \end{array} \right),$$

which can be expressed as:

$$\frac{\partial c_i}{\partial t} + \nabla \cdot n_1 = r_1. \quad (1.38)$$

For a moving flow, however, the flux has a diffusion and a convection/advection component

$$n_1 = -D\nabla c_i + c_i v, \quad (1.39)$$

which would then allow Eq. (1.38) to be

$$\frac{\partial c_i}{\partial t} + \nabla \cdot c_i v = \nabla \cdot (D\nabla c_i) + r_1, \quad (1.40)$$

which is a convection-diffusion equation.

1.4.5 Curvilinear Coordinates

Let us suppose the rectangular Cartesian coordinates (z_1, z_2, z_3) of point P_2 in space and let (j_1, j_2, j_3) will be the three scalar point functions such that

$$j_1 = j_1(z_1, z_2, z_3), \quad j_2 = j_2(z_1, z_2, z_3), \quad j_3 = j_3(z_1, z_2, z_3). \quad (1.41)$$

If the functions and their partial derivatives as mentioned above are continuous, then for transformation the Jacobian \bar{J} can be defined as:

$$\bar{J} = \frac{\partial(j_1, j_2, j_3)}{\partial(z_1, z_2, z_3)} = \begin{vmatrix} \frac{\partial j_1}{\partial z_1} & \frac{\partial j_1}{\partial z_2} & \frac{\partial j_1}{\partial z_3} \\ \frac{\partial j_2}{\partial z_1} & \frac{\partial j_2}{\partial z_2} & \frac{\partial j_2}{\partial z_3} \\ \frac{\partial j_3}{\partial z_1} & \frac{\partial j_3}{\partial z_2} & \frac{\partial j_3}{\partial z_3} \end{vmatrix}. \quad (1.42)$$

If this jacobian is not equal to zero, then we can defined one-to-one correspondence between the pairs (z_1, z_2, z_3) and (j_1, j_2, j_3) . So for the point P_2 can be defined distinctively for the pairs (j_1, j_2, j_3) . Thus the curvilinear coordinates of a point P_2 are commonly written in the form of (j_1, j_2, j_3) . Let us consider j_1, j_2 and j_3 be the curvilinear orthogonal coordinates which can derived from the Cartesian coordinates z_1, z_2 and z_3 in the subsequent form:

$$\left. \begin{aligned} j_1 &= j_1((z_1, z_2, z_3)), \\ j_2 &= j_2((z_1, z_2, z_3)), \\ j_3 &= j_3((z_1, z_2, z_3)), \end{aligned} \right\} \quad (1.43a)$$

or

$$j_i = j_i(z_1, z_2, z_3). \quad (1.43b)$$

We assume that Eq. (1.43b) has a unique inverse

$$z_i = z_i(j_i). \quad (1.44)$$

If j_2 and j_3 are kept constant, the vector $z = z(j_1)$ represents the coordinate curve in space and a tangent vector to this curve is $j_1 \cdot \frac{\partial z}{\partial j_1}$. The growing of j_1 is a result of a unit vector in that direction is

$$e_1 = \frac{\partial z / \partial j_1}{|\partial z / \partial j_1|}. \quad (1.45)$$

Let $|\partial z / \partial j_1| = h_1$, then

$$\frac{\partial z}{\partial j_1} = e_1 h_1, \quad (1.46)$$

and in the same way

$$\frac{\partial z}{\partial j_2} = e_2 h_2, \quad (1.47)$$

$$\frac{\partial z}{\partial j_3} = e_3 h_3, \quad (1.48)$$

with $|\partial z / \partial j_2| = h_2$ and $|\partial z / \partial j_3| = h_3$, where these h_1 , h_2 and h_3 are known as scale factors.

Moreover,

$$dz = \frac{\partial z}{\partial j_1} dj_1 + \frac{\partial z}{\partial j_2} dj_2 + \frac{\partial z}{\partial j_3} dj_3 = h_1 dj_1 e_1 + h_2 dj_2 e_2 + h_3 dj_3 e_3. \quad (1.49)$$

If components v_1 , v_2 and v_3 of \mathbf{V} in the direction of rising j_1 , j_2 and j_3 , then $\nabla \cdot \mathbf{V}$, $\nabla \times \mathbf{V}$, ∇^2 and $\nabla \phi$ are specified curvilinear coordinates as:

$$\nabla \cdot \mathbf{V} = \frac{1}{h_1 h_2 h_3} \left[\frac{\partial}{\partial j_1} (h_2 h_3 v_1) + \frac{\partial}{\partial j_2} (h_3 h_1 v_2) + \frac{\partial}{\partial j_3} (h_1 h_2 v_3) \right], \quad (1.50)$$

$$\left. \begin{aligned} (\nabla \times \mathbf{V})_1 &= \frac{1}{h_2 h_3} \left[\frac{\partial}{\partial j_2} (h_3 v_3) - \frac{\partial}{\partial j_3} (h_2 v_2) \right], \\ (\nabla \times \mathbf{V})_2 &= \frac{1}{h_3 h_1} \left[\frac{\partial}{\partial j_3} (h_1 v_1) - \frac{\partial}{\partial j_1} (h_3 v_3) \right], \\ (\nabla \times \mathbf{V})_3 &= \frac{1}{h_1 h_2} \left[\frac{\partial}{\partial j_1} (h_2 v_2) - \frac{\partial}{\partial j_2} (h_1 v_1) \right], \end{aligned} \right\} \quad (1.51)$$

$$\nabla^2 = \frac{1}{h_1 h_2 h_3} \left[\frac{\partial}{\partial j_1} \left(\frac{h_2 h_3}{h_1} \frac{\partial}{\partial j_1} \right) + \frac{\partial}{\partial j_2} \left(\frac{h_3 h_1}{h_2} \frac{\partial}{\partial j_2} \right) + \frac{\partial}{\partial j_3} \left(\frac{h_1 h_2}{h_3} \frac{\partial}{\partial j_3} \right) \right], \quad (1.52)$$

$$\nabla\phi = \frac{1}{h_1} \frac{\partial\phi}{\partial j_1} e_1 + \frac{1}{h_2} \frac{\partial\phi}{\partial j_2} e_2 + \frac{1}{h_3} \frac{\partial\phi}{\partial j_3} e_3. \quad (1.53)$$

1.4.6 Continuity Equation for Curved Surface

From the general law of conservation as defined through Eq. (1.9) in section 1.3.1, the continuity equation with $r_1 = 0$ in curvilinear coordinates is defined as:

$$\frac{\partial\rho V}{\partial t} + \nabla \cdot \rho V = 0. \quad (1.54)$$

Using Eq. (1.50), we get

$$\frac{\partial\rho}{\partial t} + \frac{1}{h_1 h_2 h_3} \left[\frac{\partial}{\partial j_1} (h_2 h_3 \rho v_1) + \frac{\partial}{\partial j_2} (h_3 h_1 \rho v_2) + \frac{\partial}{\partial j_3} (h_1 h_2 \rho v_3) \right] = 0. \quad (1.55)$$

1.4.7 Momentum Equation for Curved Surface

The momentum equation in curvilinear coordinates can be defined through the following equation while using the general Eq. (1.30) in section 1.3.1. The new established momentum equation is

$$\rho \left[\frac{\partial \mathbf{V}}{\partial t} + \nabla \left(\frac{\mathbf{V}^2}{2} \right) - \mathbf{V} \times (\nabla \times \mathbf{V}) \right] = -\nabla p + \nabla \cdot \tau, \quad (1.56)$$

where the components of $\mathbf{V} \times (\nabla \times \mathbf{V})$ are defined below:

$$[\mathbf{V} \times (\nabla \times \mathbf{V})]_1 = \frac{v_2}{h_1 h_2} \left[\frac{\partial}{\partial j_1} (h_2 v_2) - \frac{\partial}{\partial j_2} (h_1 v_1) \right] - \frac{v_3}{h_3 h_1} \left[\frac{\partial}{\partial j_3} (h_1 v_1) - \frac{\partial}{\partial j_1} (h_3 v_3) \right], \quad (1.57)$$

$$[\mathbf{V} \times (\nabla \times \mathbf{V})]_2 = \frac{v_3}{h_2 h_3} \left[\frac{\partial}{\partial j_2} (h_3 v_3) - \frac{\partial}{\partial j_3} (h_2 v_2) \right] - \frac{v_1}{h_1 h_2} \left[\frac{\partial}{\partial j_1} (h_2 v_2) - \frac{\partial}{\partial j_2} (h_1 v_1) \right], \quad (1.58)$$

$$[\mathbf{V} \times (\nabla \times \mathbf{V})]_3 = \frac{v_1}{h_3 h_1} \left[\frac{\partial}{\partial j_3} (h_1 v_1) - \frac{\partial}{\partial j_1} (h_3 v_3) \right] - \frac{v_2}{h_2 h_3} \left[\frac{\partial}{\partial j_2} (h_3 v_3) - \frac{\partial}{\partial j_3} (h_2 v_2) \right]. \quad (1.59)$$

The stress tensor in the form of divergence components are:

$$\begin{aligned}
(\nabla \cdot \tau)_1 &= \frac{1}{h_1 h_2 h_3} \left[\frac{\partial}{\partial j_1} (h_2 h_3 \tau_{11}) + \frac{\partial}{\partial j_2} (h_3 h_1 \tau_{21}) + \frac{\partial}{\partial j_3} (h_1 h_2 \tau_{31}) \right] \\
&\quad + \frac{\tau_{21}}{h_1 h_2} \frac{\partial h_1}{\partial j_2} + \frac{\tau_{31}}{h_1 h_3} \frac{\partial h_1}{\partial j_3} - \frac{\tau_{22}}{h_1 h_2} \frac{\partial h_2}{\partial j_2} - \frac{\tau_{33}}{h_1 h_3} \frac{\partial h_3}{\partial j_1}, \tag{1.60}
\end{aligned}$$

$$\begin{aligned}
(\nabla \cdot \tau)_2 &= \frac{1}{h_1 h_2 h_3} \left[\frac{\partial}{\partial j_1} (h_2 h_3 \tau_{12}) + \frac{\partial}{\partial j_2} (h_3 h_1 \tau_{22}) + \frac{\partial}{\partial j_3} (h_1 h_2 \tau_{32}) \right] \\
&\quad + \frac{\tau_{32}}{h_2 h_3} \frac{\partial h_2}{\partial j_3} + \frac{\tau_{12}}{h_2 h_1} \frac{\partial h_2}{\partial j_1} - \frac{\tau_{33}}{h_2 h_3} \frac{\partial h_3}{\partial j_2} - \frac{\tau_{11}}{h_2 h_1} \frac{\partial h_1}{\partial j_2}, \tag{1.61}
\end{aligned}$$

$$\begin{aligned}
(\nabla \cdot \tau)_3 &= \frac{1}{h_1 h_2 h_3} \left[\frac{\partial}{\partial j_1} (h_2 h_3 \tau_{13}) + \frac{\partial}{\partial j_2} (h_3 h_1 \tau_{23}) + \frac{\partial}{\partial j_3} (h_1 h_2 \tau_{33}) \right] \\
&\quad + \frac{\tau_{13}}{h_3 h_1} \frac{\partial h_3}{\partial j_1} + \frac{\tau_{23}}{h_3 h_2} \frac{\partial h_3}{\partial j_2} - \frac{\tau_{11}}{h_3 h_1} \frac{\partial h_1}{\partial j_3} - \frac{\tau_{22}}{h_3 h_2} \frac{\partial h_2}{\partial j_3}. \tag{1.62}
\end{aligned}$$

The components of the stress of Cauchy-Poisson law in emblematic form is defined as follows:

$$e_{11} = \frac{1}{h_1} \frac{\partial v_1}{\partial j_1} + \frac{v_2}{h_1 h_2} \frac{\partial h_1}{\partial j_2} + \frac{v_3}{h_3 h_1} \frac{\partial h_1}{\partial j_3}, \tag{1.63}$$

$$e_{22} = \frac{1}{h_2} \frac{\partial v_2}{\partial j_2} + \frac{v_3}{h_2 h_3} \frac{\partial h_2}{\partial j_3} + \frac{v_1}{h_1 h_2} \frac{\partial h_2}{\partial j_1}, \tag{1.64}$$

$$e_{33} = \frac{1}{h_3} \frac{\partial v_3}{\partial j_3} + \frac{v_1}{h_3 h_1} \frac{\partial h_3}{\partial j_1} + \frac{v_2}{h_2 h_3} \frac{\partial h_3}{\partial j_2}, \tag{1.65}$$

$$2e_{32} = \frac{h_3}{h_2} \frac{\partial (v_3/h_3)}{\partial j_2} + \frac{h_2}{h_3} \frac{\partial (v_2/h_2)}{\partial j_3} = 2e_{23}, \tag{1.66}$$

$$2e_{13} = \frac{h_1}{h_3} \frac{\partial (v_1/h_1)}{\partial j_3} + \frac{h_3}{h_1} \frac{\partial (v_3/h_3)}{\partial j_1} = 2e_{31}, \tag{1.67}$$

$$2e_{21} = \frac{h_2}{h_1} \frac{\partial (v_2/h_2)}{\partial j_1} + \frac{h_1}{h_2} \frac{\partial (v_1/h_1)}{\partial j_2} = 2e_{12}. \tag{1.68}$$

Therefore, the components of momentum equation are given below:

$$\rho \left[\frac{\partial v_1}{\partial t} - \frac{v_2}{h_1 h_2} \left\{ \frac{\partial}{\partial j_1} (h_2 v_2) - \frac{\partial}{\partial j_2} (h_1 v_1) \right\} + \frac{v_3}{h_3 h_1} \left\{ \frac{\partial}{\partial j_3} (h_1 v_1) - \frac{\partial}{\partial j_1} (h_3 v_3) \right\} + \frac{1}{2} \frac{(v_1^2 + v_2^2 + v_3^2)}{\partial j_1} \right]$$

$$\begin{aligned}
&= -\frac{1}{h_1} \frac{\partial p}{\partial j_1} + \frac{1}{h_1 h_2 h_3} \left[\frac{\partial}{\partial j_1} (h_2 h_3 \tau_{11}) + \frac{\partial}{\partial j_2} (h_3 h_1 \tau_{21}) + \frac{\partial}{\partial j_3} (h_1 h_2 \tau_{31}) \right] \\
&\quad + \frac{\tau_{21}}{h_1 h_2} \frac{\partial h_1}{\partial j_2} + \frac{\tau_{31}}{h_1 h_3} \frac{\partial h_1}{\partial j_3} - \frac{\tau_{22}}{h_1 h_2} \frac{\partial h_2}{\partial j_2} - \frac{\tau_{33}}{h_1 h_3} \frac{\partial h_3}{\partial j_3}, \tag{1.69}
\end{aligned}$$

$$\begin{aligned}
\rho \left[\frac{\partial v_2}{\partial t} - \frac{v_3}{h_2 h_3} \left\{ \frac{\partial}{\partial j_2} (h_3 v_3) - \frac{\partial}{\partial j_3} (h_2 v_2) \right\} + \frac{v_1}{h_1 h_2} \left\{ \frac{\partial}{\partial j_1} (h_2 v_2) - \frac{\partial}{\partial j_2} (h_1 v_1) \right\} + \frac{1}{2} \frac{(v_1^2 + v_2^2 + v_3^2)}{\partial j_2} \right] \\
&= -\frac{1}{h_2} \frac{\partial p}{\partial j_2} + \frac{1}{h_1 h_2 h_3} \left[\frac{\partial}{\partial j_1} (h_2 h_3 \tau_{12}) + \frac{\partial}{\partial j_2} (h_3 h_1 \tau_{22}) + \frac{\partial}{\partial j_3} (h_1 h_2 \tau_{32}) \right] \\
&\quad + \frac{\tau_{32}}{h_2 h_3} \frac{\partial h_2}{\partial j_3} + \frac{\tau_{12}}{h_2 h_1} \frac{\partial h_2}{\partial j_1} - \frac{\tau_{33}}{h_2 h_3} \frac{\partial h_3}{\partial j_2} - \frac{\tau_{11}}{h_2 h_1} \frac{\partial h_1}{\partial j_2}, \tag{1.70}
\end{aligned}$$

$$\begin{aligned}
\rho \left[\frac{\partial v_3}{\partial t} - \frac{v_1}{h_3 h_1} \left\{ \frac{\partial}{\partial j_3} (h_1 v_1) - \frac{\partial}{\partial j_1} (h_3 v_3) \right\} + \frac{v_2}{h_2 h_3} \left\{ \frac{\partial}{\partial j_2} (h_3 v_3) - \frac{\partial}{\partial j_3} (h_2 v_2) \right\} + \frac{1}{2} \frac{(v_1^2 + v_2^2 + v_3^2)}{\partial j_3} \right] \\
&= -\frac{1}{h_3} \frac{\partial p}{\partial j_3} + \frac{1}{h_1 h_2 h_3} \left[\frac{\partial}{\partial j_1} (h_2 h_3 \tau_{13}) + \frac{\partial}{\partial j_2} (h_3 h_1 \tau_{23}) + \frac{\partial}{\partial j_3} (h_1 h_2 \tau_{33}) \right] \\
&\quad + \frac{\tau_{13}}{h_3 h_1} \frac{\partial h_3}{\partial j_1} + \frac{\tau_{23}}{h_3 h_2} \frac{\partial h_3}{\partial j_2} - \frac{\tau_{11}}{h_3 h_1} \frac{\partial h_1}{\partial j_3} - \frac{\tau_{22}}{h_3 h_2} \frac{\partial h_2}{\partial j_3}. \tag{1.71}
\end{aligned}$$

1.4.8 Boundary Layer Equations for Curved Surface

The equation for moving curved sheet will be derived in detail in chapter 9 while using the following coiled circle with radius R , then the vector

$$z = \left((r + R) \cos\left(\frac{s}{R}\right), (r + R) \sin\left(\frac{s}{R}\right), x \right), \tag{1.72}$$

Thus, the scale factors for the BLF equation can be defined as follows:

$$h_1 = 1, \quad h_2 = \left(\frac{R+r}{R} \right), \quad h_3 = 1. \tag{1.73}$$

1.4.9 Energy Equation for Curved Surface

The energy equation defined in section 1.3.3 in curvilinear coordinates in conjunction of viscous dissipation $r_1 = \tau \cdot L$ can be defined while using Eqs. (1.52) and (1.53) as:

$$\rho c_p \left[\frac{\partial T}{\partial t} + (\mathbf{V} \cdot \nabla) T \right] = k \nabla^2 T + r_1, \quad (1.74)$$

then

$$\begin{aligned} & \rho c_p \left[\frac{\partial T}{\partial t} + \frac{v_1}{h_1} \frac{\partial T}{\partial j_1} + \frac{v_2}{h_2} \frac{\partial T}{\partial j_2} + \frac{v_3}{h_3} \frac{\partial T}{\partial j_3} \right] \\ &= \frac{k}{h_1 h_2 h_3} \left\{ \frac{\partial}{\partial j_1} \left(\frac{h_2 h_3}{h_1} \frac{\partial T}{\partial j_1} \right) + \frac{\partial}{\partial j_2} \left(\frac{h_3 h_1}{h_2} \frac{\partial T}{\partial j_2} \right) + \frac{\partial}{\partial j_3} \left(\frac{h_1 h_2}{h_3} \frac{\partial T}{\partial j_3} \right) \right\} \\ &+ \eta \left[2(e_{11}^2 + e_{22}^2 + e_{33}^2) + e_{23}^2 + e_{13}^2 + e_{12}^2 \right]. \end{aligned} \quad (1.75)$$

1.4.10 Concentration Equation for Curved Surface

The concentration equation defined in section 1.3.4 in curvilinear coordinates with $r_1 = 0$ can be defined while using Eqs. (1.52) and (1.53) as

$$\begin{aligned} & \frac{\partial C}{\partial t} + \frac{v_1}{h_1} \frac{\partial C}{\partial j_1} + \frac{v_2}{h_2} \frac{\partial C}{\partial j_2} + \frac{v_3}{h_3} \frac{\partial C}{\partial j_3} \\ &= \frac{D}{h_1 h_2 h_3} \left\{ \frac{\partial}{\partial j_1} \left(\frac{h_2 h_3}{h_1} \frac{\partial C}{\partial j_1} \right) + \frac{\partial}{\partial j_2} \left(\frac{h_3 h_1}{h_2} \frac{\partial C}{\partial j_2} \right) + \frac{\partial}{\partial j_3} \left(\frac{h_1 h_2}{h_3} \frac{\partial C}{\partial j_3} \right) \right\}. \end{aligned} \quad (1.76)$$

1.5 The Sisko Rheological Model

In this dissertation we study the energy and mass balance problems with a simple three-parameters fluid model equation which was proposed by Sisko [2] in 1958 based on the concept of additive Newtonian and non-Newtonian stresses. The consideration of Sisko fluid is significant due to the shear-thinning /shear-thickening properties captured even in steady flows past rigid surfaces. Although it is the combination of viscous and power-law materials, but the properties of rate type fluids (relaxation/retardation times) cannot be

predicted. From the limitation point of view, this model is not explaining the suddenly increase phenomenon. However, the empirical relationship in Eq. (1.1) is modified for Sisko fluid model as and is given in the subsequent relation:

$$\tau = -\nabla p + \mathbf{S}, \quad (1.77)$$

where \mathbf{S} is denotes extra stress tensor, and is defined by the following equation

$$\mathbf{S} = [a + b|\dot{\gamma}|^{n-1}]\mathbf{A}_1, \quad (1.78)$$

where, b represents consistency, n is the Power-law index, which is a measure of non-Newtonian nature of the fluid, a shear rate and $\dot{\gamma}$ is the shear rate consistency. However, the shear rate $\dot{\gamma}$ is further defined as follows:

$$\dot{\gamma} = \sqrt{\frac{1}{2}tr(A_1^2)}, \quad (1.79)$$

where A_1 is given as follows:

$$\mathbf{A}_1 = (\mathit{grad}\mathbf{V}) + (\mathit{grad}\mathbf{V})^T. \quad (1.80)$$

This model, which joins low and intermediary shear (power-law) with high shear Newtonian restricting conduct, was found to give the best in the general portrayal of the flow bends for all shear-thinning slurries, at all strong loadings, over the whole estimated scope of shear rates. This outcome by Sisko is critical in the light of the fact that this model clearly works for most of non-Newtonian solid-fluid suspensions, and furthermore, it is pertinent over the scope of shear rate applications for pipeline transportation of the suspensions. Moreover, the pseudo-plasticity or shear-thinning behavior is illustrated as a reduction in the viscosity of the liquid with an enrichment in the shear rate. Some common materials that undergo the property of shear-thinning, for instance nail polish,

ketchup, silicone oil and whipped cream etc. The dilatant or shear-thickening trend is then demonstrated as being a reverse trend to shear-thinning. That means, an uplift in the liquid viscosity with a raise in the shear rate and are also called as thickening liquids. A common example of a thickening or dilatant liquid materials is the cornstarch solution in water.

1.6 Research Objectives

The research carried out in this dissertation is a contribution toward the recent development in science and technology while considering the generalized Newtonian Sisko liquid flow over moving boundaries. Therefore, due to such importance the mathematical modeling and numerical simulation of generalized Newtonian Sisko fluid flow over planar and curved stretching surfaces with heat and mass balances are the main target of this thesis. Thus, it could be a better way to demonstrate the outcomes of the proposed problem through different numerical schemes. However, the objective of this illustration provide important applications in the areas of science and technology. Thus this study embarks on the following objectives:

- Mathematical modeling of Sisko fluid flow over planar as well as curved stretching sheet is provided.
- The heat and mass transfer analysis is performed in the presence of different physical effects.
- Numerical illustrations are carried out to demonstrate different characteristics of flow, heat and mass transfer phenomena.

1.7 Contribution in Thesis

The work in this thesis will investigate the mathematical modeling and numerical computations with flow physics of Sisko fluid occurring in specific types of stretching geometries.

Indeed, before this initiation there had been no existing studies concerning the BLF of the Sisko rheological model with different physical aspects. For instance, this model did not discuss yet properly with 3D time dependent flow with many other physical effects, like the impacts of chemical reaction, nano-fluid, thermal radiation, double diffusion etc. However, main contributions in this thesis include the mathematical modeling and numerical simulations for the flow over stretching surfaces with different circumstances. The substantial contents of this thesis has already been published. The work in this thesis is organized as follows:

Chapter 1: This chapter is an introductory chapter containing the historical background, research motivation, scope and objective of the current research work.

Chapter 2: Regarding the aforementioned literature, the perseverance of this chapter is to deeply scrutinize the impact of generalized Fourier's and Fick's laws for the flow of Sisko fluid in the existence of thermal conductivity which depends upon temperature. The physical problem is modeled utilizing a system of highly partially coupled non-linear PDEs and are then reduced into highly coupled non-linear ODEs by means of proper transformations. These equations along with the corresponding BCs are solved with the implementation of built-in routine `bvp4c` while coded in MATLAB. The key outputs of this portion are published in "J. Mol. Liq., 224, (2016) 1016-1021".

Chapter 3: This chapter explores the characteristics of magneto nano-particles in the Sisko fluid flow over a bidirectional moving boundary accounting of non-linear radiation. Additionally, the convective surface and new mass flux constraints are imposed on the boundary. A tested suitable variables for conversion are employed to alter the PDEs into non-linear ODEs. These non-linear equations along with the appropriate BCs are then solved by utilizing the MATLAB function `bvp4c` and shooting technique with the RK Fehlberg method. The variation of pertinent flow appearing parameters on the profiles of velocities, temperature and concentration is demonstrated graphically and discussed in detail. Findings of this chapter are published in "J. Braz. Soc. Mech. Sci. Eng., 39(11), (2017) 4475-4487".

Chapter 4: The incentive for considering into description Sisko liquid flow in this chapter is that this model can precise much typical particularity of Newtonian and non-Newtonian liquids by selecting dissimilar physical parameters. In assessment of the argument in preceding works, the persistence of this chapter is to scrutinize the chemically-reactive flow of Sisko liquid. The problem is first modeled and then construction of non-dimensional foremost equations is accomplished. The time-independent 3D flow of Sisko liquid with non-Fouriers law (Cattaneo-Christove) heat flux is deliberated. The chemical reaction namely the heterogeneous-homogeneous is also employed to examine the recommended problem. The numerical approach is implemented to approximate the solution of the problem with relevant BCs. The results of this chapter are available in “*J. Mol. Liq.*, **238**, (2017) 19-26”.

Chapter 5: The leading objective of this chapter is to incorporate the unsteady 3D BLF of Sisko fluid and heat transfer by imposing convective conditions over a stretching surface. The transformed problem is obtained using newly modeled transformations. The results obtained are the output of the shooting method along with RK-45 Fehlberg method. Meanwhile the solutions are portrayed in the form of the velocity and temperature profiles. Furthermore, the validity of the method is verified through MATLAB built in function namely `bvp4c`. The results of this part are published in “*J. Braz. Soc. Mech. Sci. Eng.*, **40** (3), (2018) 166”.

Chapter 6: The work in this chapter is essentially inspired by the need to understand the heat transfer phenomenon involving the unsteady 3D flow of Sisko fluid by utilizing solid nanoparticles. The deliberation of Sisko fluid is substantial due to the shear-thinning /shear-thickening characteristics captured even in steady flows past rigid surfaces. Although it is the combination of viscous and power law materials, but the properties of rate type fluids (relaxation/retardation times) cannot be anticipated. Moreover, a rigorous analysis of accessible literature indicates that no effort has been made to the study of unsteady 3D flow of Sisko nanofluid. The governing mathematical system is complex and nonlinear in the frame of nonlinear forced convection effects and is inspected through the

implementation of the `bvp4c` function in MATLAB and shooting technique with Runge-Kutta Fehlberg and Newton-Raphson methods. The numerical solutions for nonlinear systems are calculated. The velocity, thermal and nano-particles concentration fields are demonstrated graphically in view of various appeared parameters. The findings of this part are published in “**Eur. Phys. J. Plus, 132, (2017) 373**”.

Chapter 7: This chapter illustrates the unsteady 3D Sisko nano-liquid flow in the presence of temperature-dependent thermal conductivity, magnetic field, heat source/sink and convective surfaces conditions. The transformed nonlinear ODE's are considered for the solution through a numerical technique MATLAB package `bvp4c`. All the findings are explained by a pictorial representation of liquid velocity, concentration and temperature. The rate of mass and heat balance is discussed in the form of Local-Nusselt and local-Sherwood number. Additionally, this illustration is validated in the limiting cases, where the comparison is performed with the earlier published figures. The subjects of this chapter are published in “**Res. Phys., 8, (2018) 1092-1103**”.

Chapter 8: The previous studies regarding Sisko fluid model with different impacts indicate that there is a huge gap which is not fill up until now. The perseverance of this chapter is to illustrate the 3D time-dependent flow of Sisko liquid due to bidirectional moving surface in the existence of a reaction known as heterogeneous-homogeneous, magnetic and nonlinear thermal radiation. The nonlinear coupled ODE's are then considered for the numerical solution while using `bvp4c` in MATLAB. The outcomes are displayed in the custom of velocity, temperature and concentration profile. Furthermore, all the physical quantities including skin-friction and local-Nusselt number are calculated in the tabular form. Moreover, present results are verified with the existing literature. The remarkable results of this portion are available through “**Pramana J. Phys., 91, (2018) 13**”.

Chapter 9: Prime objective of this chapter is to highlight 2D flow of Sisko fluid owing to a curved moving boundary. The flow equations are modeled while using the curvilinear coordinates system. The modeled momentum BL equations for Sisko fluid are then

transformed to non-linear ODEs. To the preeminent of our awareness, this formulation is an initial attempt towards the Sisko fluid model in curvilinear coordinates system. The numerical solutions are implemented by MATLAB package bvp4c is to approximate the flow of fluid and heat balance with help of the velocity and temperature profiles. The contents of this chapter are submitted in “**Physica Scripta.**”.

Chapter 10: In light of the existing literature, this chapter is a motivation towards the utilization and importance of practical effects like magnetic field and nano-particles incorporations in the BLF of Sisko liquid over bended surface along with mass and energy balance. The consideration of bended moving surface on which flow of Sisko liquid occurred required curvilinear coordinate’s geometry. However, this new formulated ODEs due introducing new geometry are prepared for approximate solution with the help of built-in routine based on collocation technique while taking help of MATLAB software. A number of novel outcomes in terms of flow pattern and velocity, temperature, pressure and concentration profiles are displayed. Important scenario about resistive forces and the rat of mass and heat are incorporated in tabular form. This new modeling is validated through a good correlation with previous published data. An alternate method namely Richardson extrapolation technique used to justify the findings of the employed method and shows very good correlation. The findings of this part are published in “**Microsystems Tech., 25(6), (2018) 2411-2428**”.

Chapter 11: Lastly, in this chapter the main conclusions of our research are summarized followed by several recommendations intended to identify future research directions.

Chapter 2

Numerical Computations of Generalized Fourier's and Fick's Laws for Sisko Fluid Flow

The principal highlighting of this chapter is to investigate the features of mass and heat flux models introduced by Cattaneo-Christov in combination with the time-independent flow of Sisko liquid over a non-linear stretching boundary. The generality of Fick's and Fourier's laws of mass and heat flux models is a novel modification by Cattaneo-Christov by introducing the time relaxation factors in both transfer of mass and heat, respectively. The heat transfer illustration is accomplished with thermal conductivity which varies with temperature. The non-linear ODEs are first established through the transformation procedure which are then elucidated numerically with a built in function command in MATLAB software and is usually known as the subclass of collocation methods. Every behavior of controlling parameter on the heat and mass balance is determined by the graphs. Results reveal that the temperature and the solute concentration profiles have converse relationship with the non-dimensional thermal and concentration relaxation time parameters. Moreover, it is also fascinating to note that the concentration profile is significantly influenced with the escalation in the power-law index when it escalates from

$n < 1$ to $n > 1$.

2.1 Flow Geometry

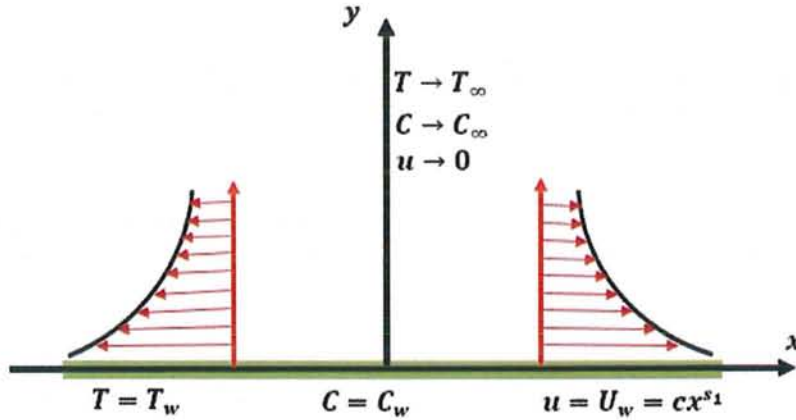


Fig. 2.1: Two dimensional flow geometry.

2.2 Constitutive Equations and Mathematical Formulation

We analyze the steady, 2D forced convective flow of Sisko fluid in the region $y > 0$ induced by a sheet stretching with the power-law velocity $U_w = cx^{s_1}$, where c is a positive constant and s_1 a non-linear stretching parameter as shown through Fig. 2.1. The modified Fourier's and Fick's laws are utilized to investigate the energy and mass balance analysis of the anticipated problem. Moreover, the energy balance is modeled in terms of a varying thermal conductivity with temperature. At boundary of the sheet, the temperature is T_w and concentration is C_w while far away from the sheet surface, the temperature is T_∞ and concentration is C_∞ . The constitutive equations and conservation laws for flow, heat and mass transfer for Sisko fluid are as follows:

$$\nabla \cdot \mathbf{V} = 0, \quad (2.1)$$

$$\rho_f (\mathbf{V} \cdot \nabla) \mathbf{V} = -\nabla p + \nabla \cdot \mathbf{S}, \quad (2.2)$$

$$(\rho c)_f (\mathbf{V} \cdot \nabla) T = -\nabla \cdot \mathbf{q}, \quad (2.3)$$

$$(\mathbf{V} \cdot \nabla) C = -\nabla \cdot \mathbf{J}, \quad (2.4)$$

$$\mathbf{S} = \left[a + b \left| \sqrt{\frac{1}{2} \text{tr}(\mathbf{A}_1)^2} \right|^{n-1} \right] \mathbf{A}_1, \quad (2.5)$$

$$\mathbf{q} + \delta_E \left(\frac{\partial \mathbf{q}}{\partial t} + \mathbf{V} \cdot \nabla \mathbf{q} + (\nabla \cdot \mathbf{V}) \mathbf{q} - \mathbf{q} \cdot \nabla \mathbf{V} \right) = -k(T) \nabla T, \quad (2.6)$$

$$\mathbf{J} + \delta_C \left(\frac{\partial \mathbf{J}}{\partial t} + \mathbf{V} \cdot \nabla \mathbf{J} + (\nabla \cdot \mathbf{V}) \mathbf{J} - \mathbf{J} \cdot \nabla \mathbf{V} \right) = -D \nabla C, \quad (2.7)$$

where \mathbf{V} represents the velocity vector, p the pressure, (a, b, n) the physical constants of the Sisko liquid, (T, C) illustrates the temperature and solute concentration of the liquid, ρ_f the fluid density, c_f the specific heat of fluid at constant temperature, \mathbf{S} the extra stress tensor, $\mathbf{A}_1 = (\nabla \mathbf{V}) + (\nabla \mathbf{V})^T$ the first Rivlin-Ericksen tensor, (\mathbf{J}, \mathbf{q}) normal mass and heat fluxes, respectively, (δ_C, δ_E) the relaxation times of mass and heat fluxes, respectively, D the molecular diffusivity of the concentration species and $k(T)$ the variable thermal conductivity given as

$$k(T) = k_\infty \left[1 + \varepsilon \left(\frac{T_\infty - T}{T_\infty - T_w} \right) \right], \quad (2.8)$$

where k_∞ is the thermal conductivity of the ambient liquid and ε a small scalar parameter. For the steady 2D flow in Cartesian coordinates, we pursue the velocity, temperature, concentration and stress fields is given as:

$$\mathbf{V} = [u(x, y), v(x, y), 0], \quad \mathbf{S} = \mathbf{S}(x, y), \quad T = T(x, y), \quad C = C(x, y). \quad (2.9)$$

Now plugging Eq. (2.9) in Eqs. (2.1) to (2.4), having in mind Eqs. (2.5), (2.6) and (2.7) a long way to formulate such a flow model but simple formulation toward the desired

and novel assumed problem and is illustrated as follows

$$\frac{\partial u}{\partial x} = -\frac{\partial v}{\partial y}, \quad (2.10)$$

$$u \frac{\partial u}{\partial x} + \frac{b}{\rho_f} \frac{\partial}{\partial y} \left(-\frac{\partial u}{\partial y} \right)^n = -v \frac{\partial u}{\partial y} + \frac{a}{\rho_f} \left(\frac{\partial^2 u}{\partial y^2} \right), \quad (2.11)$$

$$u \frac{\partial T}{\partial x} = \frac{1}{(\rho c)_f} \frac{\partial}{\partial y} \left(k(T) \frac{\partial T}{\partial y} \right) - v \frac{\partial T}{\partial y} - \delta_E \left[\begin{array}{l} 2uv \left(\frac{\partial^2 T}{\partial x \partial y} \right) + u^2 \left(\frac{\partial^2 T}{\partial x^2} \right) \\ + v^2 \left(\frac{\partial^2 T}{\partial y^2} \right) + \left(u \frac{\partial u}{\partial x} + v \frac{\partial u}{\partial y} \right) \frac{\partial T}{\partial x} \\ + \left(u \frac{\partial v}{\partial x} + v \frac{\partial v}{\partial y} \right) \frac{\partial T}{\partial y} \end{array} \right], \quad (2.12)$$

$$u \frac{\partial C}{\partial x} = D \left(\frac{\partial^2 C}{\partial y^2} \right) - v \frac{\partial C}{\partial y} - \delta_C \left[\begin{array}{l} 2uv \left(\frac{\partial^2 C}{\partial x \partial y} \right) + u^2 \left(\frac{\partial^2 C}{\partial x^2} \right) \\ + v^2 \left(\frac{\partial^2 C}{\partial y^2} \right) + \left(u \frac{\partial u}{\partial x} + v \frac{\partial u}{\partial y} \right) \frac{\partial C}{\partial x} \\ + \left(u \frac{\partial v}{\partial x} + v \frac{\partial v}{\partial y} \right) \frac{\partial C}{\partial y} \end{array} \right]. \quad (2.13)$$

The associated BCs for the present problem are:

$$\text{at } y = 0, \quad \begin{cases} U_w = cx^{s_1}, & v = 0, \\ T = T_w, & C = C_w, \end{cases} \quad (2.14)$$

$$\text{as } y \rightarrow \infty, \quad u \rightarrow 0, \quad T \rightarrow T_\infty \quad \text{and} \quad C \rightarrow C_\infty. \quad (2.15)$$

The above leading equations are simplified by presenting the suitable transformations (cf. Munir *et al.* [10]) as follows:

$$u = U_w f'(\eta), \quad v = -U_w Re_b^{-\frac{1}{n+1}} \frac{1}{n+1} [\{s_1(2n-1)+1\}f(\eta) + \{s_1(2-n)-1\}\eta f'(\eta)],$$

$$\theta(\eta) = \frac{T - T_\infty}{T_w - T_\infty}, \quad \phi(\eta) = \frac{C - C_\infty}{C_w - C_\infty}, \quad \eta = \frac{y}{x} Re_b^{\frac{1}{n+1}}. \quad (2.16)$$

In perspective of Eq. (2.16), we can obtain the following ODEs with respect to the

dimensionless variables η :

$$Af''' + n(-f'')^{n-1} f''' + \left(\frac{s_1(2n-1)+1}{n+1} \right) f' f'' - s_1 f'^2 = 0, \quad (2.17)$$

$$(1 + \varepsilon\theta) \theta'' + \varepsilon\theta'^2 + \text{Pr} \left(\frac{s_1(2n-1)+1}{n+1} \right) f\theta' - \text{Pr} \lambda_E \left(\frac{s_1(2n-1)+1}{(n+1)^2} \right) \\ \times [\{2+n+(n-2)s_1\} f f' \theta' + \{s_1(2n-1)+1\} f^2 \theta''] = 0, \quad (2.18)$$

$$\phi'' + Sc \left(\frac{s_1(2n-1)+1}{n+1} \right) f\phi' - Sc\lambda_C \left(\frac{s_1(2n-1)+1}{(n+1)^2} \right) \\ \times [\{2+n+(n-2)s_1\} f f' \phi' + \{s_1(2n-1)+1\} f^2 \phi''] = 0, \quad (2.19)$$

$$\text{at } \eta = 0, \quad \begin{cases} f = 0, & f' = 1, \\ \theta = 1, & \phi = 1, \end{cases} \quad (2.20)$$

$$\text{as } \eta \rightarrow \infty, \quad f' \rightarrow 0, \quad \theta \rightarrow 0, \quad \phi \rightarrow 0. \quad (2.21)$$

where $A \left(= \frac{Re_b^{\frac{2}{n+1}}}{Re_a} \right)$ is the physical Sisko fluid, $Re_a \left(= \frac{\rho x U_w}{a} \right)$ and $Re_b \left(= \frac{\rho x^n U_w^{2-n}}{b} \right)$ demonstrates the local Reynolds numbers, $\text{Pr} \left(= \frac{x U_w}{\alpha} Re_b^{-\frac{2}{n+1}} \right)$ the generalized Prandtl number, $\lambda_{E,C} \left(= \frac{U \delta_{E,C}}{x} \right)$ the relaxation times parameters of energy and mass balance, respectively and $Sc \left(= \frac{x U_w Re_b^{-\frac{2}{n+1}}}{D} \right)$ the generalized Schmidt number.

2.3 Numerical Method

The transformed problem defined through Eqs. (2.14), (6.19) and (2.24) along with the BCs (2.15), (2.20) and (2.25) are considered for the numerical solution. The bvp4c MATLAB package is implemented to find the computational results with the tolerance 10^{-6} . Rendering to the foremost requirements of this numerical technique, the key steps

of the method are given as follows: Let,

$$f = y_1, \quad f' = y'_1 = y_2, \quad f'' = y'_2 = y_3 \quad \text{and} \quad f''' = y'_3, \quad (2.22)$$

$$\theta = y_4, \quad \theta' = y'_4 = y_5 \quad \text{and} \quad \theta'' = y'_5, \quad (2.23)$$

$$\phi = y_6, \quad \phi' = y'_6 = y_7 \quad \text{and} \quad \phi'' = y'_7, \quad (2.24)$$

$$y'_3 = \frac{sy_2^2 - \left(\frac{s_1(2n-1)+1}{n+1}\right)y_1y_3}{A + n(-y_3)^{n-1}}, \quad (2.25)$$

$$y'_5 = \frac{Pr\lambda_E \left(\frac{s_1(2n-1)+1}{(n+1)^2}\right) \left[\{2 + n + (n-2)s_1\}y_1y_2y_5 \right] - Pr \left(\frac{s_1(2n-1)+1}{n+1}\right)y_1y_5 - \epsilon y_5^2}{1 + \epsilon y_4 - Pr\lambda_E \left(\frac{s_1(2n-1)+1}{(n+1)^2}\right) \{s_1(2n-1) + 1\}y_1^2}, \quad (2.26)$$

$$y'_7 = \frac{Sc\lambda_C \left(\frac{s_1(2n-1)+1}{(n+1)^2}\right) \left[\{2 + n + (n-2)s_1\}y_1y_2y_7 \right] - Sc \left(\frac{s_1(2n-1)+1}{n+1}\right)y_1y_7}{1 - Sc\lambda_C \left(\frac{s_1(2n-1)+1}{(n+1)^2}\right) \{s_1(2n-1) + 1\}y_1^2}, \quad (2.27)$$

while the relevant BCs, then becomes

$$y_1(0) = 0, \quad y_2(0) = 1, \quad y_4(0) = 1, \quad y_6(0) = 1, \quad (2.28)$$

$$y_2(\infty) \rightarrow 0, \quad y_4(\infty) \rightarrow 0, \quad y_6(\infty) \rightarrow 0. \quad (2.29)$$

2.4 Pictorial Interpretation and Discussion

In this specific portion the features of modified laws of Fourier's and Fick's for mass and heat balance phenomena are utilized on the flow of GNF where the surface of the flow is being considered non-linear. Although, the temperature in this case is finalized in terms of thermal conductivity function. The numerical analysis is performed to demonstrate the behavior of the controlling parameters of flow phenomena. Moreover, the main theme of this study to demonstrates the impacts of different parameters such as A , s_1 , Pr , $\lambda_{E,C}$

and Sc . The fluctuation in the temperature profiles corresponding to rise in the thermal conductivity parameter ϵ and stretching parameter s_1 is plotted through **Figs. 2.2(a,b)**. It is straightforward from these plots that the non-dimensional temperature field enhances with the increment in the variable thermal conductivity parameter while the opposite conduct is noticed for s_1 , i.e., stretching parameter. For $\epsilon = 0$, the temperature of the flow problem can be presented with constant thermal conductivity while for $\epsilon > 0$ we get the case of variable thermal conductivity and for which the temperature of the fluid is observed to demonstrate a growing conduct. **Figs. 2.3(a,b)** portray the behavior of temperature of liquid for both pseudo-plastic as well as dilatant liquids. The impact of n shows a reduction in the liquids temperature as well as TBLT. However, for shear-thinning liquid this behavior is more meaningful as compared to the shear-thickening liquid. **Fig. 2.4(a)** has been portrayed to show the impact of the Pr on the dimensionless temperature field. From this plot, it is seen that escalation in Pr results in a decay of the temperature distribution as well as associated TBLT. Physically, it is due to reason that an increase in Pr implies less rate of thermal diffusion. However, it can be noted from **Fig. 2.4(b)**, that with increase in heat relaxation parameter, the temperature distribution declines. This trend is because of the nature that more time shall be required to transfer the heat to the neighboring liquid particle. Likewise, the parameter of thermal relaxation enhancement guaranteed non-conductivity feature of the liquid particle and thus the upshots in the lessening of temperature profile.

Figs. 2.5(a,b) elucidate the non-constant behavior in the non-dimensional concentration distribution for distinct variation in the index of power-law. From these figures, it is anticipated that the concentration profile as well as corresponding CBLT decays decays with the enhancement in the power-law index for for both dilatant as well as pseudo plastic cases. **Figs. 2.6(a,b)** elucidate the non-constant in the non-dimensional concentration for various values s_1 , i.e.,the stretching parameter and A the material parameter of nonlinear materials, i.e., Sisko liquid. These figures show a declining conduct of concentration profile and associated CBLT for growing values of the stretching parameter as well

as the material parameter of the Sisko fluid. The variation of the Schmidt number Sc and concentration relaxation parameter λ_C on the concentration distribution is demonstrated through **Figs. 2.7(a,b)**. It can be noticed that the Schmidt number and the parameter of concentration relaxation results in decay of the concentration profile. Physically, Schmidt number is the function of molecular diffusivity and whenever this number raises, then molecular diffusivity diminished the concentration of non-linear materials.

Figs. 2.8(a,b) are plotted to test the behavior of flow pattern for non-linear stretching surfaces while keeping $n = 0.8$, $A = 0.5$, $Re_b = 10$ and $c = 1$. The speed of shear-thinning fluid plotted through **Figs. 2.8(b)** is noticed slightly high as compared to the plots as shown in **Fig. 2.8(a)**. This is why the flow pattern for higher values of stretching parameter is observed with uplifting conduct. For non-variant values of $n = 0.5$, $A = 0.5$, $s_1 = 1.2$, $\lambda_E = 0.2$ and $Pr = 2.0$, a comparison between the two plots of isotherms is developed through **Figs. 2.9(a,b)**. For **Fig. 2.9(a)** values of $\epsilon = 0$ and $T_\infty = 0.0$ are fixed. On the other hand, **Fig. 2.9(b)** is plotted for $T_\infty = 0.3$ and $\epsilon = 3.0$, respectively. The hotness and related TBLT observed through **Fig. 2.9(b)** are larger than the hotness and related TBLT of **Fig. 2.9(a)**. For non-variant values of $n = 0.5$, $A = 0.5$, $s_1 = 1.2$ and $\lambda_C = 0.2$, the mass fluxes are plotted through **Figs. 2.10(a,b)** with uplifting order variation in C_∞ and Sc . Thus, the mass flux and the associated BLT presented through **Fig. 2.10(a)** for $C_\infty = 0$ and $Sc = 1.0$ are lower as compare to **Fig. 2.10(b)** for $C_\infty = 0.3$ and $Sc = 3.0$.

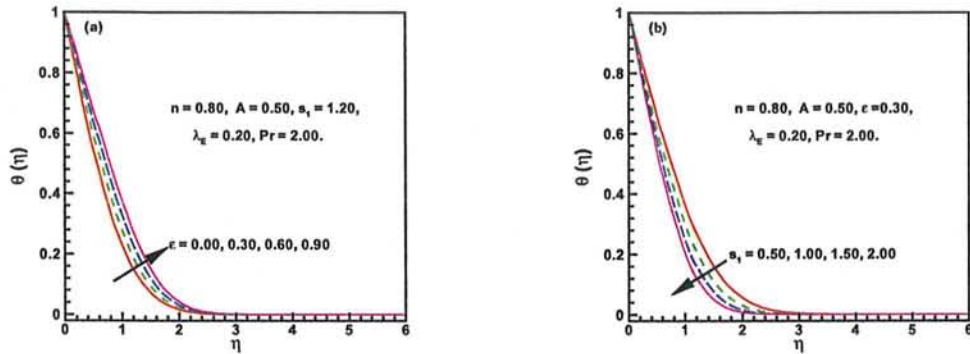


Fig. 2.2: Variation in temperature with ϵ and s_1 .

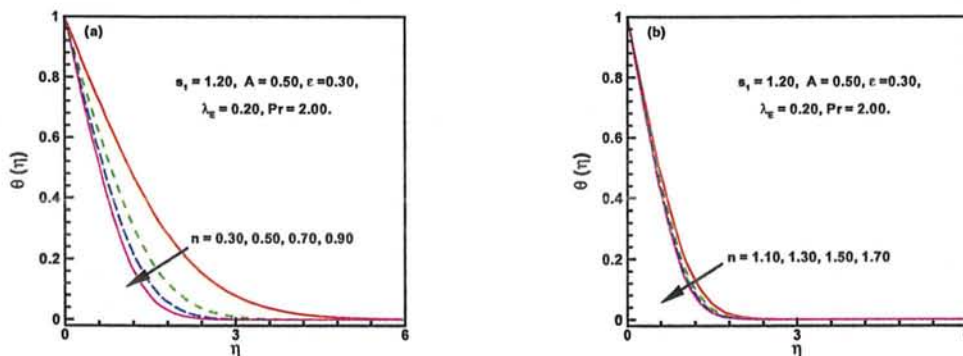


Fig. 2.3: Variation in temperature distribution with $0 < n < 1$ and $n > 1$.

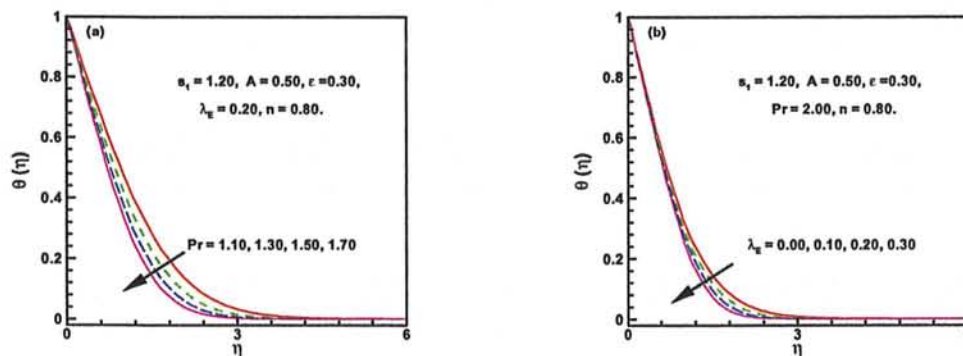


Fig. 2.4: Variation in temperature distribution with Pr and λ_E .

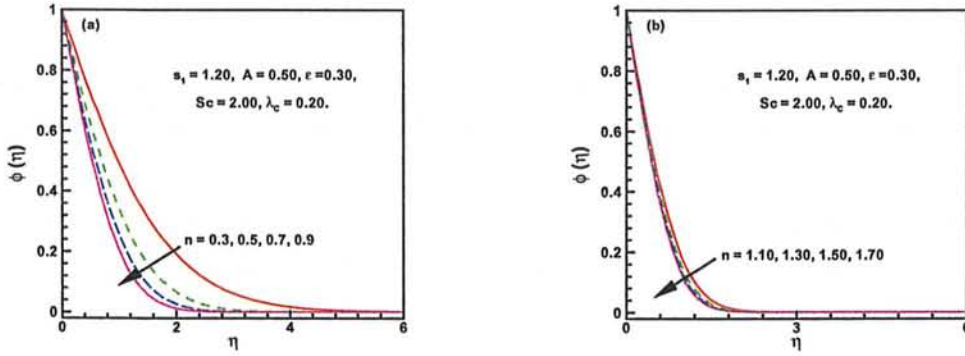


Fig. 2.5: Variation in temperature distribution with Pr and λ_E .

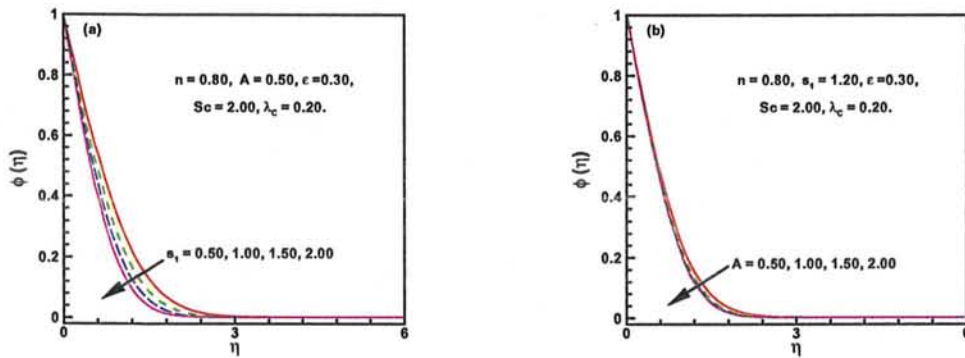


Fig. 2.6: Variation in concentration distribution with s_1 and A .

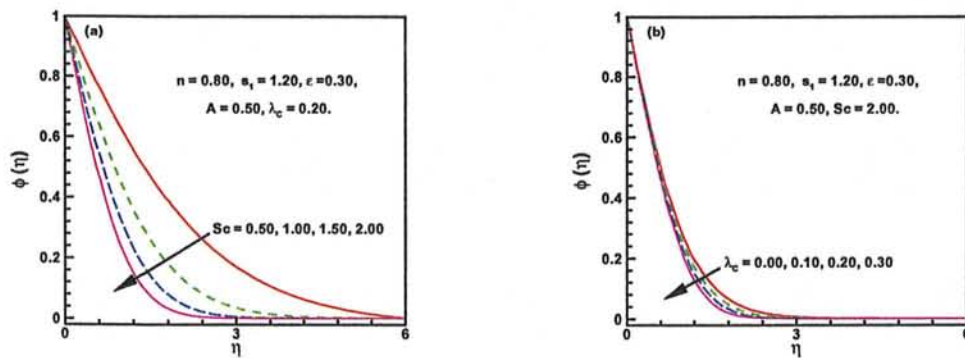


Fig. 2.7: Variation in concentration distribution with Sc and λ_C .

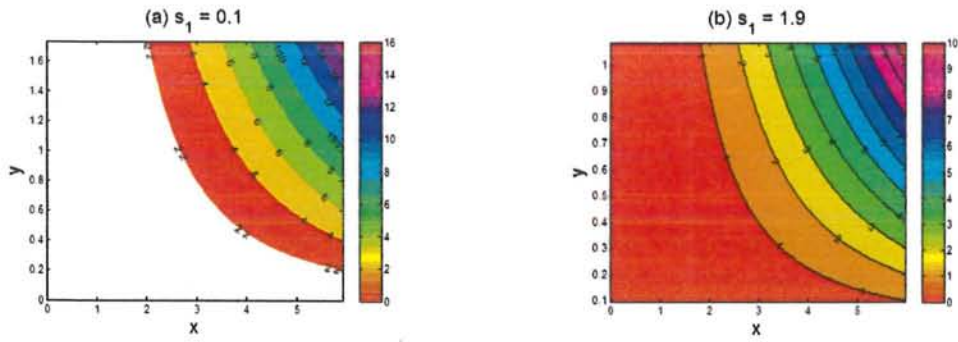


Fig. 2.8: Streamlines for s_1 .

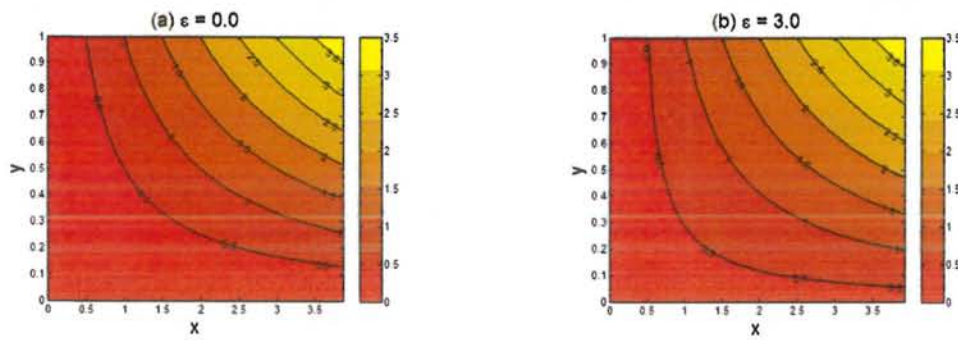


Fig. 2.9: Isotherms for ϵ .

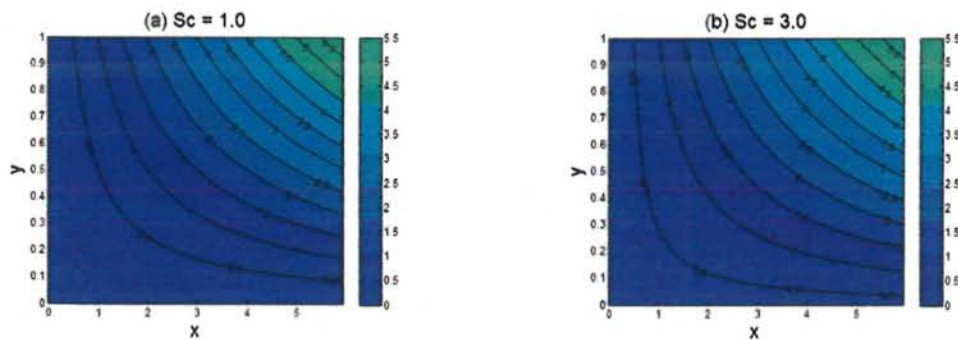


Fig. 2.10: Iso concentration for Sc .

Chapter 3

Numerical Study of Non-linear

Radiative Flow of Magneto

Nanoparticles for 3D Sisko Fluid

A numerical investigation is carried out in this chapter to study the three dimensional Sisko fluid flow by taking into account the non-linear thermal radiation and convective BCs over a bidirectional moving boundary. Additionally, the impact of newly proposed model for nanofluid is invoked that implies nanoparticles volume fraction at the boundary to be passively rather than strongly controlled. The numerical computations are performed by utilizing two different techniques namely the `bvp4c` function in MATLAB and shooting method with RKF and Newton Raphson methods. It is perceived that the temperature profile declines as the power-law index enhances. Furthermore, it is revealed that the liquid concentration is the decays function of parameter due to larger Brownian motion while a converse conduct is shown by the thermophoresis parameter. Additionally, these upshots are more noticeable for shear-thinning fluids when compared with shear-thickening fluids. To see the validity of the numerical computations, we compare the results of the shooting technique with the `bvp4c` and achieved an excellent correlation. The numerical results obtained in the limiting cases have shown an admirable agreement with the existing

literature.

3.1 Pictorial Interpretation of the Problem

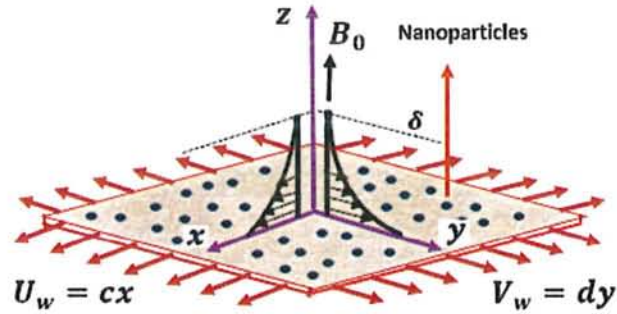


Fig. 3.1: Bidirectional stretching flow geometry.

3.2 Problem Formulation

Assuming an incompressible flow due to bidirectional moving surface of Sisko fluid with additional impacts in the form of Buongiorno's model and nonlinear thermal radiation. Further the flow configuration shows that a vertical magnetic field is employed having strength B_0 . The cause for bidirectional moving surface are the stretching velocity $U_w = cx$ in x -direction and $V_w = dy$ in y -direction. The flow deformation is detected in z -direction as shown in Fig. 3.1. Configuration regarding the transfer of convective heat during the flow of Sisko liquid takes the way, i.e., the heat transport coefficient h_f causes heat transfer from the boundary of the sheet and for which a hot liquid of temperature T_f is placed where underneath. However, the temperature away from the surface is presenting with T_∞ which can be treated as less temperature matching with liquid temperature. Another concern about the concentration is taking in the way, where C_w is the wall concentration and a constant concentration C_∞ is the concentration observed for away from the boundary. For the steady 3D flow, Eq. (2.9) is now extended for the velocity of liquid, extra stress tensor, thermal analysis in terms of temperature of liquid, and solute

concentration are expressed in the following form:

$$\mathbf{V} = [u(x, y, z), v(x, y, z), w(x, y, z)], \quad \mathbf{S} = \mathbf{S}(x, y, z), \quad T = T(x, y, z), \quad C = C(x, y, z). \quad (3.1)$$

The 3D flow of Sisko nanoliquid (cf. Munir *et al.* [12]) together with continuity equation are obtained while using the equations defined through Eqs. (2.1)-(2.5) and keeping in view Eq. (3.1). So the formulated main problem takes the subsequent form:

$$\frac{\partial u}{\partial x} = -\left(\frac{\partial v}{\partial y} + \frac{\partial w}{\partial z}\right), \quad (3.2)$$

$$u \frac{\partial u}{\partial x} + \frac{b}{\rho_f} \frac{\partial}{\partial z} \left(-\frac{\partial u}{\partial z}\right)^n + \left(\frac{\sigma B_0^2}{\rho_f}\right) u = -\left(v \frac{\partial u}{\partial y} + w \frac{\partial u}{\partial z}\right) + \frac{a}{\rho_f} \left(\frac{\partial^2 u}{\partial z^2}\right), \quad (3.3)$$

$$u \frac{\partial v}{\partial x} - \frac{b}{\rho_f} \frac{\partial}{\partial z} \left(-\frac{\partial u}{\partial z}\right)^{n-1} \frac{\partial v}{\partial z} + \left(\frac{\sigma B_0^2}{\rho_f}\right) v = -\left(w \frac{\partial v}{\partial z} + v \frac{\partial v}{\partial y}\right) + \frac{a}{\rho_f} \left(\frac{\partial^2 v}{\partial z^2}\right), \quad (3.4)$$

$$\begin{aligned} u \frac{\partial T}{\partial x} + \frac{1}{(\rho c)_f} \left(\frac{\partial q_r}{\partial z}\right) - \alpha_1 \left(\frac{\partial^2 T}{\partial z^2}\right) = & -\left(w \frac{\partial T}{\partial z} + v \frac{\partial T}{\partial y}\right) \\ & + \tau^* \left[D_B \left(\frac{\partial C}{\partial z}\right) \left(\frac{\partial T}{\partial z}\right) + \frac{D_T}{T_\infty} \left(\frac{\partial T}{\partial z}\right)^2 \right], \end{aligned} \quad (3.5)$$

$$u \frac{\partial C}{\partial x} - \frac{D_T}{T_\infty} \left(\frac{\partial^2 T}{\partial z^2}\right) = -\left(w \frac{\partial C}{\partial z} + v \frac{\partial C}{\partial y}\right) + D_B \left(\frac{\partial^2 C}{\partial z^2}\right), \quad (3.6)$$

with the associated BCs

$$\text{at } z = 0, \quad \begin{cases} U_w(x) = cx, \quad V_w(y) = dy, \quad w = 0, \quad -k \left(\frac{\partial T}{\partial z}\right) = -h_f (T_f - T), \\ C = C_w, \quad D_B \left(\frac{\partial C}{\partial z}\right) + \frac{D_T}{T_\infty} \left(\frac{\partial T}{\partial z}\right) = 0, \end{cases} \quad (3.7)$$

$$\text{as } z \rightarrow \infty, \quad u \rightarrow 0, \quad v \rightarrow 0, \quad T \rightarrow T_\infty \quad \text{and} \quad C \rightarrow C_\infty. \quad (3.8)$$

The Rosseland approximation leads to the following expression

$$q_r = -\frac{4\sigma^*}{3k^*} \left(\frac{\partial T^4}{\partial z} \right) = -\frac{16\sigma^*}{3k^*} T^3 \left(\frac{\partial T}{\partial z} \right). \quad (3.9)$$

The distinct classical case of non-linear thermal radiation is a well-known phenomenon and considered here. It is a simple rescaling of Prandtl number while having a radiation parameter and has usually appeared in the linearized form of Rosseland approximation and which leads to an important effect known as non-linear thermal radiation. This type of linearized approximation need not any further analytical and numerical struggles while considering the investigation of such problems. In view of strong non-linearity of energy balance equations, this physical effect making the energy equation more nonlinear with extra non-linear term appeared due to the ratio of wall and ambient temperature.

Using Eq. (3.9) in Eq. (3.5) we finally have

$$\begin{aligned} u \frac{\partial T}{\partial x} - \alpha_1 \left(\frac{\partial^2 T}{\partial z^2} \right) + \frac{16\sigma^*}{3k^* (\rho c)_f} \frac{\partial}{\partial z} \left(T^3 \frac{\partial T}{\partial z} \right) = - \left(v \frac{\partial T}{\partial y} + w \frac{\partial T}{\partial z} \right) \\ + \tau^* \left[D_B \left(\frac{\partial C}{\partial z} \right) \frac{\partial T}{\partial z} + \frac{D_T}{T_\infty} \left(\frac{\partial T}{\partial z} \right)^2 \right]. \end{aligned} \quad (3.10)$$

We are interested in finding the local similar solution of the above stated problem, so we use the transformations introduced (cf. Munir *et al.* [12]) and is given below:

$$u = cx f'(\eta), \quad v = cy g'(\eta), \quad w = -c \left(\frac{c^{n-2}}{\rho_f} \right)^{\frac{1}{n+1}} \left[\frac{2n}{n+1} f + \frac{1-n}{1+n} \eta f' + g \right] x^{\frac{n-1}{n+1}}, \quad (3.11a)$$

$$\theta(\eta) = \frac{T - T_\infty}{T_f - T_\infty}, \quad \phi(\eta) = \frac{C - C_\infty}{C_\infty}, \quad \eta = z \left(\frac{c^{2-n}}{b} \right)^{\frac{1}{n+1}} x^{\frac{1-n}{1+n}}. \quad (3.11b)$$

In view of transformations (3.11a) and (3.11b), Eq. (3.2) is equal to zero, i.e., identically contended and Eqs. (3.3-3.4), (3.6-3.8) and (3.10) take the following form:

$$A f''' + \left(\frac{2n}{n+1} \right) f f'' - (f')^2 + n (-f'')^{n-1} f''' + g f'' - M f' = 0, \quad (3.12)$$

$$Ag''' + \left(\frac{2n}{n+1}\right) fg'' + (-f'')^{n-1} g''' - (n-1)g''f''' (-f'')^{n-2} - (g')^2 + gg'' - Mg' = 0, \quad (3.13)$$

$$[\{1 + R_d(1 + \theta(\theta_w - 1))^3\} \theta']' + \text{Pr} \left[\left(\frac{2n}{n+1}\right) f\theta' + g\theta' + N_b(\phi'\theta') + N_t(\theta'^2) \right] = 0, \quad (3.14)$$

$$\phi'' + Le \text{Pr} \left[\left(\frac{2n}{n+1}\right) f\phi' + g\phi' \right] + \frac{N_t}{N_b} \theta'' = 0, \quad (3.15)$$

$$\text{at } \eta = 0, \quad \begin{cases} f = 0, & g = 0, & f' = 1, & g' = \alpha, \\ \theta' = -\gamma[1 - \theta], & N_b\phi' + N_t\theta' = 0, \end{cases} \quad (3.16)$$

$$\text{as } \eta \rightarrow \infty, \quad f' \rightarrow 0, \quad g' \rightarrow 0, \quad \theta \rightarrow 0, \quad \phi \rightarrow 0. \quad (3.17)$$

The governing flow parameters are formulated as:

$$M = \frac{\sigma B_0^2}{(\rho c)_f}, \quad \alpha = \frac{d}{c}, \quad R_d = \frac{16\sigma^* T_\infty^3}{3k^* k}, \quad \theta_w = \frac{T_f}{T_\infty}, \quad \gamma = \frac{h_f}{k} x Re_b^{-\frac{1}{n+1}},$$

$$N_b = \frac{\tau^* D_B C_\infty}{\nu}, \quad N_t = \frac{\tau^* D_B (T_f - T_\infty)}{T_\infty \nu}, \quad Le = \frac{\alpha_1}{D_B}. \quad (3.18)$$

The local Nusselt number, which of practical importance, is given by

$$Re_b^{-\frac{1}{n+1}} Nu_x = - [1 + R_d \theta_w^3] \theta'(0). \quad (3.19)$$

3.3 Graphical Results and Discussion

In this fragment, the graphical enlightenment about the results are displayed and elaborated. The non-linear ODE's defined through Eqs. (3.12) to (3.15) with imposed BCs (3.16) and (3.17) are presenting with non-exact solution approach in order to established the significance of parameters appeared in the flow consequences. However, these outcomes are demonstrated with graphical illustrations in the form of velocity, temperature and concentration profiles. Moreover, the flow phenomenon is also explained in the form

of resistive forces and rate of heat and mass balance. In order to show the importance of BLF modeled equation of Sisko fluid, we utilized the growing magnetic parameter M as an additional effect on the flow velocities, i.e., $f'(\eta)$ and $g'(\eta)$ of fluid as shown through **Figs. 3.2(a,b)** and **3.3(a,b)**, respectively, for pseudo-plastic as well as dilatant liquids. From these plots, it is noticed that the both velocities and the thickness of the BLF reduce due to increase in resistive forces with the enhancement of M . Another important flow parameter n is tested and the respective temperature fields are plotted through **Figs. 3.4(a,b)** for pseudo-plastic, i.e., ($0 < n < 1$) and dilatant, i.e., ($n > 1$) conditions of liquids. It is visualized that with the upshot in the values of n for both cases, i.e., ($0 < n < 1$) and $n > 1$, the fluid temperature and associated TBLT declined. But the result for the case ($0 < n < 1$) is more prominent. **Figs. 3.5(a,b)** demonstrate the depict of radiation parameter R_d on temperature profile for dilatant and pseudo-plastic liquids, respectively. It is manifested from the plots that the temperature distribution and associated TBLT enhance with the growth in the radiation parameter. This trend holds for both nonlinear and linearized radiation cases. Physically, with the enhancement in the radiation parameter results in penetration of more heat into the liquid and thus the TBLT is increased. Thus, the transfer rate of heat can be controlled by the radiation parameter. **Figs. 3.6(a,b)** delineate the depict of temperature ratio parameter θ_w on the temperature field. From these pictures it is perceived that the temperature distribution and associated TBLT enhance for the larger values of the temperature ratio parameter. In physical sense, whenever the values of θ_w , takes higher values, the upper temperature of the liquid enhances in comparison with temperature at surface of the liquid and thus this phenomenon results in the enhancement of the temperature and related TBLT.

Figs. 3.7(a,b) illustrate the significance of n on the liquid concentration for pseudo-plastic as well as dilatant liquids, respectively. It turns out from these plots that the concentration profile and related CBLT decline for both cases with an increase in n . **Figs. 3.8(a,b)** are plotted to visualize the behavior of the concentration BL for the Sisko fluid for growing values of the magnetic parameter M . It is observed that the

concentration distribution enriches, when magnetic parameter is enhanced. Physically, this is due to increase in the Lorentz force. Moreover, it is observed that these results are more prominent for pseudo-plastic as compared to dilatant fluids. **Figs. 3.9(a, b)** deliberated the importance of measure of growing Brownian motion N_b on the field of concentration during the flow of Sisko fluid. It can be seeming from the plots that the distribution of concentration and associated CBLT decline for the parameter arise owing to Brownian motion. Physically, with the increment in the total of the parameter of Brownian motion, the rate at which nano-particles move with not a same liquid velocities in altered/random direction also increases owing to the Brownian depict. The impact of the thermophoresis parameter N_t on concentration distribution is displayed through **Figs. 3.10(a,b)**. From these pictures, it is clear that the effect of thermophoresis parameter on the profile of concentration are quite the opposite to that of the Brownian motion parameter. **Figs. 3.11(a,b)** are prepared to envisaged the influence of the Lewis number Le on the profile of concentration. In fact the Lewis number is not with direct relation to the coefficient of Brownian diffusion. Here higher values of Lewis number parallel to small diffusivity and so liquid concentration declines.

To substantiate the authenticity of the present numerical computations, a appraisal between the `bvp4c` and shooting methods is presented through **Figs. 3.12(a,b)** and **3.13(a,b)**. A remarkable agreement between the two computational techniques is seen. This leads a confidence in our numerical computations.

The heat transfer rate at the moving boundary is presented through **table 3.1** for two cases of power-law fluids, i.e., shear-thinning as well as shear-thickening. Forthrightly, it seems from this table that the amount the heat transfer rate uplifted with uplifting values of Pr and γ whereas, it diminishes for escalating values of R_d , θ_w , N_t and Le . However, the effect of Brownian motion parameter are found constant while calculating the rate of heat transfer as shown in **table 3.1**. Additionally, it is seen from **table 3.2**, there is an outstanding correlation between the present work and the existing literature. Furthermore, from **Figs. 3.12(a, b)** and **3.13(a, b)**, it is flawless that the graphs plotted

of temperature and concentration distribution are in excellent agreement of the shooting technique with the MATLAB built-in function `bvp4c`.

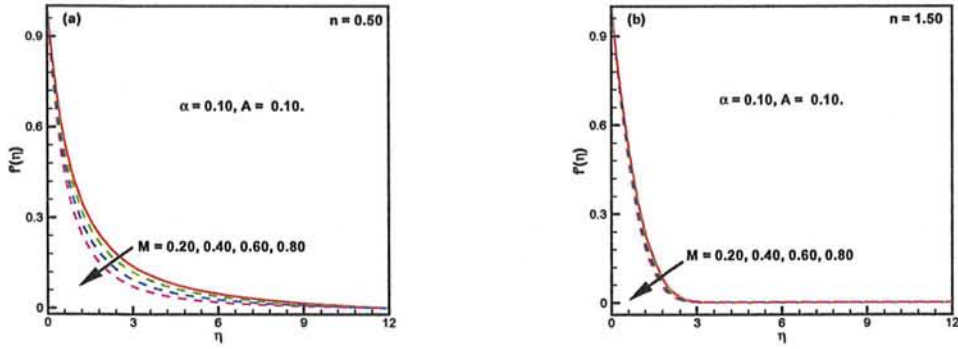


Fig. 3.2: Velocity field $f'(\eta)$ variation with M .

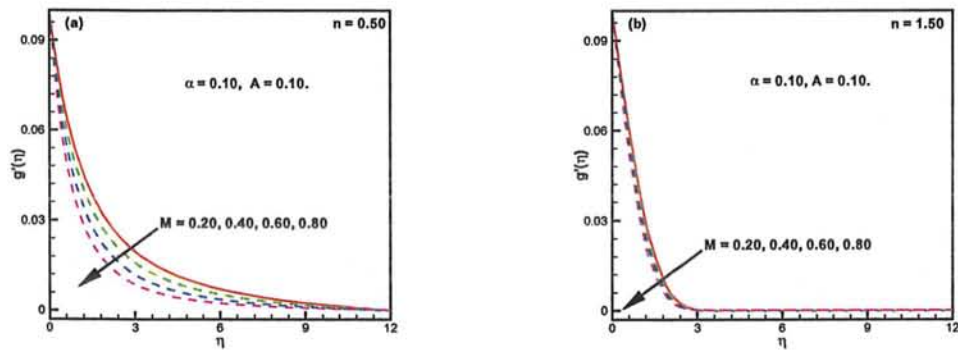


Fig. 3.3: Velocity distribution $g'(\eta)$ variation with M .

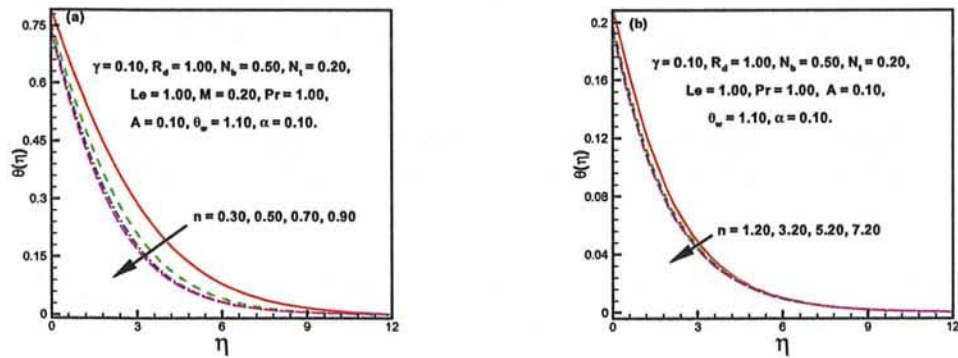


Fig. 3.4: Temperature field $\theta(\eta)$ variation with $0 < n < 1$ and $n > 1$.

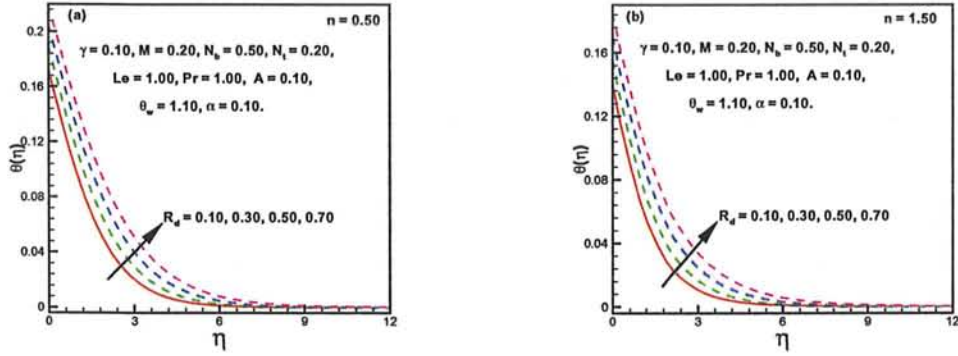


Fig. 3.5: Temperature field $\theta(\eta)$ variation with R_d .

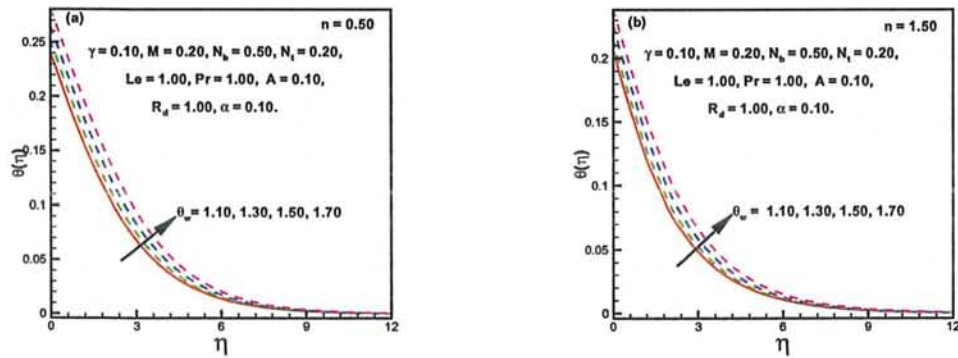


Fig. 3.6: Temperature field $\theta(\eta)$ variation with θ_w .

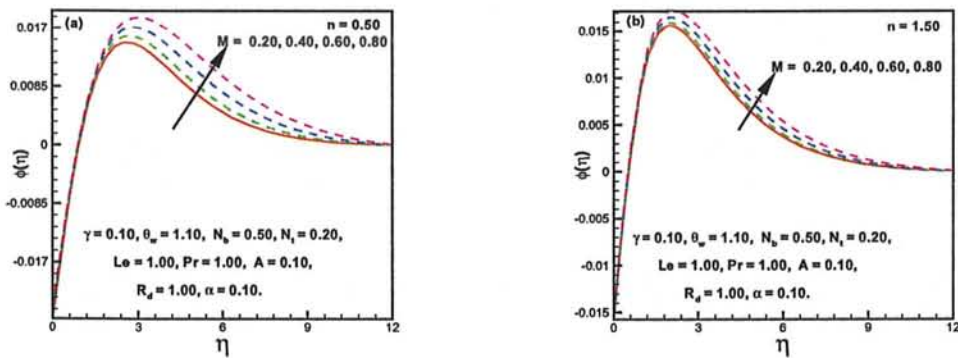


Fig. 3.7: Concentration field $\phi(\eta)$ variation with $0 < n < 1$ and $n > 1$.

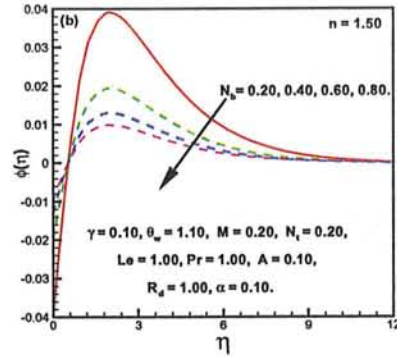
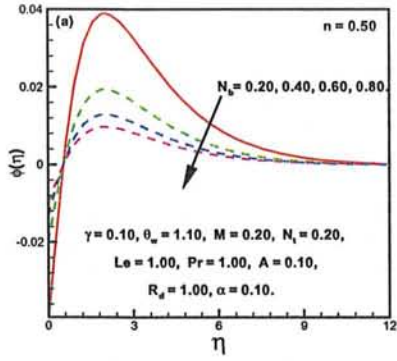


Fig. 3.8: Concentration field $\phi(\eta)$ variation with M .

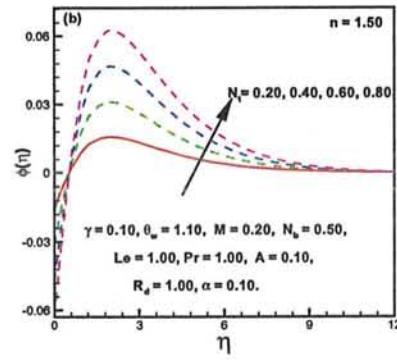
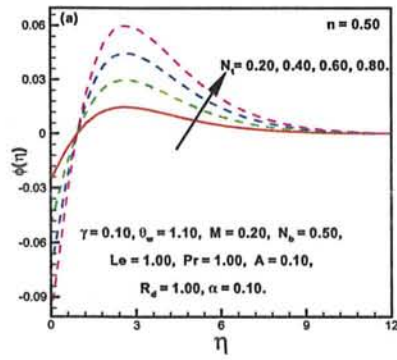


Fig. 3.9: Concentration field $\phi(\eta)$ variation with N_b .

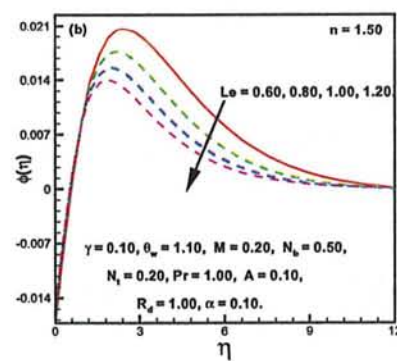
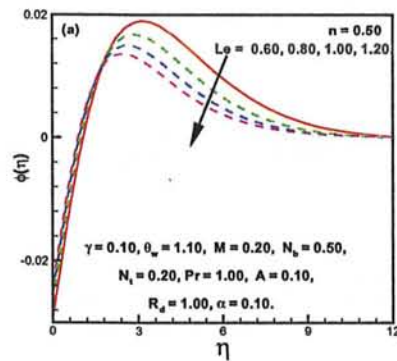


Fig. 3.10: Concentration field $\phi(\eta)$ variation with N_t .

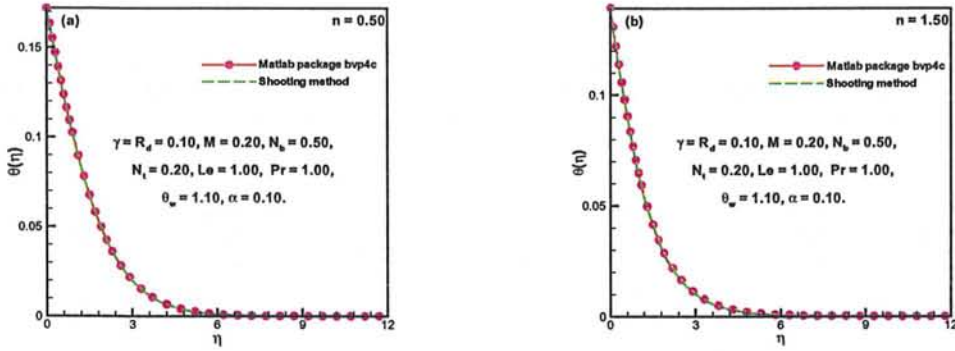


Fig. 3.11: Concentration field $\phi(\eta)$ variation with Le .

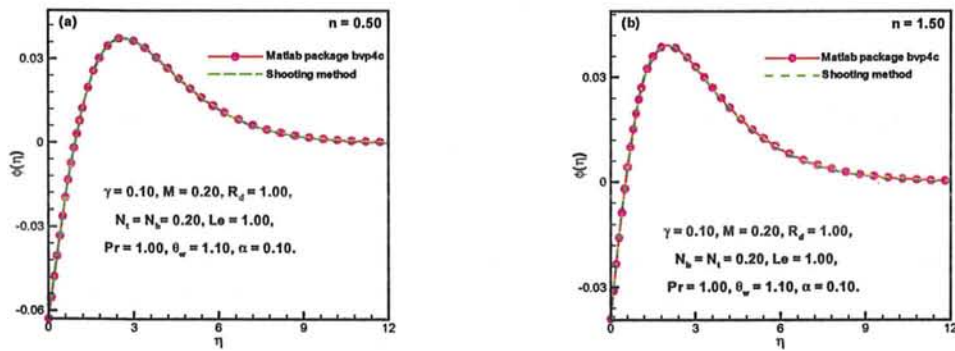


Fig. 3.12: A Comparison between bvp4c and shooting methods for $\theta(\eta)$.

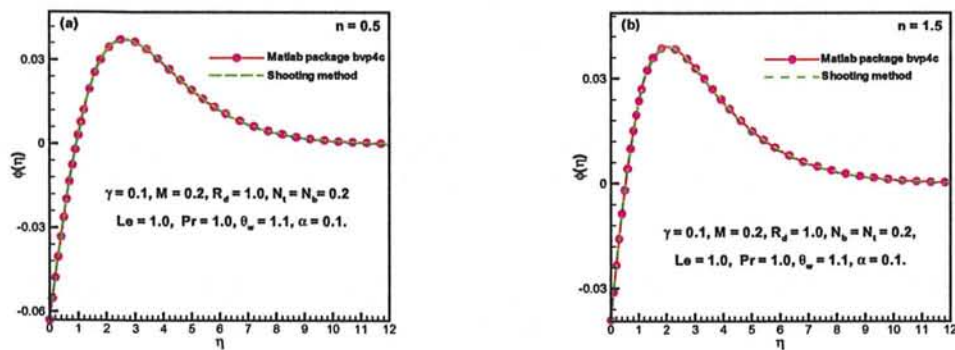


Fig. 3.13: A Comparison between bvp4c and shooting methods for $\phi(\eta)$.

Table 3.1: Influence of Le , Pr , N_b , N_t , R_d , θ_w , and γ on the Nusselt number when $M = 0.2$, $A = 0.1$ and $\alpha = 0.1$ are fixed.

Le	Pr	N_b	N_t	R_d	θ_w	γ	$\left(Re_b\right)^{-\frac{1}{n+1}} Nu_x$		
							$n = 0.50$	$n = 1.50$	
0.5	1.0	0.5	0.2	1.0	1.1	0.1	0.157595	0.163958	
							0.157546	0.163920	
							0.157517	0.163899	
1.0	0.5	0.5	0.2	1.0	1.1	0.1	0.139765	0.144926	
							0.157546	0.163920	
							0.166046	0.172306	
1.0	1.0	0.5	0.2	1.0	1.1	0.1	0.157546	0.163920	
							0.157546	0.163920	
							0.157546	0.163920	
1.0	1.0	0.5	0.0	1.0	1.1	0.1	0.157707	0.164059	
							0.157301	0.163709	
							0.156882	0.163349	
1.0	1.0	0.5	0.2	0.5	1.1	0.1	0.121762	0.126646	
							0.157546	0.163920	
							0.191406	0.199035	
1.0	1.0	0.5	0.2	0.5	1.1	0.1	0.157546	0.163920	
							0.167926	0.173244	
							0.180267	0.184176	
1.0	1.0	0.5	0.2	1.0	1.1	0.1	0.157546	0.163920	
							0.2	0.257884	0.275862
							0.3	0.326213	0.355923

Table 3.2: Comparison of Nusselt number with the previous existing results in limiting case when $Le = 0$, $\theta_w = 1.1$, $R_d = 0$, $M = 0$, $\gamma \rightarrow \infty$, $A = 1.5$ and $Pr = 1.0$ are fixed.

	Munir <i>et al.</i> [12]	Present outcomes	Munir <i>et al.</i> [12]	Present outcomes
α	n=0.50	n=0.50	n=1.50	n=1.50
0.2	-0.62074	-0.6209775	-0.78919	-0.7891393
0.4	-0.69468	-0.6948833	-0.84864	-0.8485694
0.6	-0.75957	-0.7597433	-0.90287	-0.9027951
0.8	-0.81827	-0.8184051	-0.95324	-0.9531557

Chapter 4

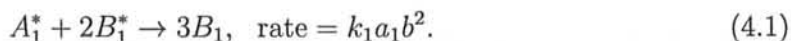
A 3D Study of Sisko Liquid Flow with non-Fourier's Heat Flux Model and Heterogeneous-Homogeneous Reactions

Considerations in this chapter are the correspondence between the two physical phenomena and Sisko liquid flow due to bidirectional moving surface. Such physical phenomena are presented in the form of Cattaneo-Christove heat flux model and heterogeneous-homogeneous reaction. The flow problem is modeled in the form of nonlinear PDEs and are then transformed into corresponding ODEs by incorporating suitable dimensionless transformations. A numerical investigation is taken into account for the analysis of proposed problem and a presentation of the significant outcomes is presented in the form of graphs which demonstrate the behavior of temperature and concentration with associated thickness of the BLs. According to the physical properties of this proposed model, the condition of pseudo plastic and dilatant fluids are tested to show both necessary properties while plotting the temperature and concentration fields. Temperature and relevant TBLT and temperature of the liquid observed an increasing function of time parameter

of relaxation.

4.1 Problem Formulation

Considering the influence of time relaxation of heat flux and heterogeneous-homogeneous chemical reactions in an incompressible 3D Sisko liquid flow due bidirectional moving surface. Moreover, an important physical property in the form of varying thermal conductivity with temperature is also a part of this formulation. The stretching velocities $U_w = cx$ and $V_w = dy$, are introduced to deform the fluid flow in the vertical z -direction, while x and y axes are taken perpendicular to z -axis. The surface temperature is replaced by the fluid temperature T_f and the fluid temperature at infinite distance is denoted by T_∞ . To incorporate the chemical reaction namely heterogeneous-homogeneous in the flow problem, Chaudhary and Merkin [37, 38] introduced a simple correspondence between heterogeneous (surface reaction) homogeneous (bulk) and reactions evolving the two chemical classes A_1^* and B_1^* . This interaction is further defined as follows, respectively:



Thus the first order isothermal reaction on the surface of the catalyst is as:



The chemical reaction will possess the constant temperature due to thermal equilibrium property of the heat flux (in and out of the transfer of heat). In the absence of auto catalyst B_1^* , the uniform concentration a_0 of A_1^* will take place instead of a_1 . All the flow equations of Sisko liquid [12] with the usual implementation of BL approximation are demonstrated as below:

$$\frac{\partial u}{\partial x} = -\left(\frac{\partial v}{\partial y} + \frac{\partial w}{\partial z}\right), \quad (4.3)$$

$$u \frac{\partial u}{\partial x} + \frac{b}{\rho_f} \frac{\partial}{\partial z} \left(-\frac{\partial u}{\partial z} \right)^n = - \left(v \frac{\partial u}{\partial y} + w \frac{\partial u}{\partial z} \right) + \frac{a}{\rho_f} \left(\frac{\partial^2 u}{\partial z^2} \right), \quad (4.4)$$

$$u \frac{\partial v}{\partial x} - \frac{b}{\rho_f} \frac{\partial}{\partial z} \left(-\frac{\partial u}{\partial z} \right)^{n-1} \frac{\partial v}{\partial z} = - \left(v \frac{\partial v}{\partial y} + w \frac{\partial v}{\partial z} \right) + \frac{a}{\rho_f} \left(\frac{\partial^2 v}{\partial z^2} \right), \quad (4.5)$$

$$\begin{aligned} \delta_E \left[2vw \left(\frac{\partial^2 T}{\partial y \partial z} \right) + u^2 \left(\frac{\partial^2 T}{\partial x^2} \right) + 2uw \left(\frac{\partial^2 T}{\partial x \partial z} \right) + v^2 \left(\frac{\partial^2 T}{\partial y^2} \right) + w^2 \left(\frac{\partial^2 T}{\partial z^2} \right) + 2uv \left(\frac{\partial^2 T}{\partial x \partial y} \right) \right. \\ \left. + \left(u \frac{\partial u}{\partial x} + v \frac{\partial u}{\partial y} + w \frac{\partial u}{\partial z} \right) \frac{\partial T}{\partial x} + \left(u \frac{\partial v}{\partial x} + v \frac{\partial v}{\partial y} + w \frac{\partial v}{\partial z} \right) \frac{\partial T}{\partial y} + \left(u \frac{\partial w}{\partial x} + v \frac{\partial w}{\partial y} + w \frac{\partial w}{\partial z} \right) \frac{\partial T}{\partial z} \right] \\ = - \left(u \frac{\partial T}{\partial x} + v \frac{\partial T}{\partial y} + w \frac{\partial T}{\partial z} \right) + \frac{1}{\rho c_p} \frac{\partial}{\partial z} \left(k(T) \frac{\partial T}{\partial z} \right), \quad (4.6) \end{aligned}$$

$$u \frac{\partial a_1}{\partial x} + k_1^* a_1 b_1^2 = - \left(v \frac{\partial a_1}{\partial y} + w \frac{\partial a_1}{\partial z} \right) + D_A \left(\frac{\partial^2 a_1}{\partial z^2} \right), \quad (4.7)$$

$$u \frac{\partial b_1}{\partial x} - k_1^* a_1 b_1^2 = - \left(v \frac{\partial b_1}{\partial y} + w \frac{\partial b_1}{\partial z} \right) + D_B \left(\frac{\partial^2 b_1}{\partial z^2} \right). \quad (4.8)$$

The BCs associated to the above governing equations are

$$\text{at } z = 0, \begin{cases} U_w = cx, & V_w = dy, & w = 0, & T = T_w, \\ D_A \left(\frac{\partial a_1}{\partial z} \right) = k_1^* a_1, & D_B \left(\frac{\partial b_1}{\partial z} \right) = -k_2^* a_1, \end{cases} \quad (4.9)$$

$$\text{as } z \rightarrow \infty, \quad u \rightarrow 0, \quad v \rightarrow 0, \quad T \rightarrow T_\infty, \quad a_1 \rightarrow a_0 \quad \text{and} \quad b_1 \rightarrow 0. \quad (4.10)$$

The emerging dimensionless variables are defined through the following equation:

$$a_1 = a_0 \phi(\eta), \quad b_1 = a_0 h(\eta). \quad (4.12)$$

Making use of transformations (3.11), (3.11) and (4.12), Eq. (4.3) is equal to zero, i.e., identically verified and Eqs. (4.4) to (4.10), having in mind Eq (2.8), lead to the following equations:

$$A f''' + \left(\frac{2n}{n+1} \right) f f'' + n (-f'')^{n-1} f''' - (f')^2 + g f'' = 0, \quad (4.13)$$



$$Ag''' + \left(\frac{2n}{n+1}\right) fg'' + (-f'')^{n-1} g''' - (n-1)g''f''' (-f'')^{n-2} - (g')^2 + gg'' = 0, \quad (4.14)$$

$$(1 + \varepsilon\theta)\theta'' - \text{Pr} \lambda_E \left[\begin{array}{c} \left(\frac{2n}{n+1}f + g\right) \left(\frac{2n}{n+1}f' + g'\right) \theta' \\ + \left(\frac{2n}{n+1}f + g\right)^2 \theta'' \end{array} \right] + \varepsilon(\theta')^2 + \text{Pr} \left(\frac{2n}{n+1}\right) f\theta' + \text{Pr} g\theta' = 0, \quad (4.15)$$

$$\phi'' + Sc \left(\frac{2n}{n+1}f + g\right) \phi' - Sck_1\phi(1-\phi)^2 = 0, \quad (4.16)$$

$$f = 0, \quad g = 0, \quad f' = 1, \quad g' = \alpha, \quad \theta = 1, \quad \phi' = k_2\phi \quad \text{at} \quad \eta = 0, \quad (4.17)$$

$$f' \rightarrow 0, \quad g' \rightarrow 0, \quad \theta \rightarrow 0, \quad \phi \rightarrow 1 \quad \text{as} \quad \eta \rightarrow \infty. \quad (4.18)$$

Here in Eq. (4.16) we assumed that the diffusion coefficients of the chemical species A_1^* and B_1^* are of comparable size such that

$$\phi(\eta) + h(\eta) = 1. \quad (4.19)$$

The governing flow parameters are stated as follows:

$$\lambda_E = \frac{U_w \delta_E}{x}, \quad k_1 = \frac{a_0^2 k_1^* x}{U_w}, \quad k_2 = \frac{k_2^* c x}{D_A z} Re_b^{-\frac{1}{n+1}}. \quad (4.20)$$

4.2 Numerical Results and Discussion

Numerical solutions to the non-linear DEs (4.13) to (4.16) with the BCs (4.17) to (4.18) are obtained by using the MATLAB routine `bvp4c` that uses collocation method. The profiles of temperature and concentration produced by the numerical illustration and which showing the important influence of physical parameters. These include the power-law index n , Sisko fluid parameter A , thermal conductivity parameter ε , relaxation time parameter λ_E , the parameters introduced by reaction namely, homogeneous-heterogeneous (k_1, k_2) , respectively.

Impact of n on the temperature is plotted through **Figs. 4.1(a)** and **4.1(b)** for dilatant ($n > 1$) as well as pseudo-plastic ($0 < n < 1$) liquids. The temperature and related

TBLT are diminishing functions of n as shown through these figures. But the temperature boost with the variation of n for pseudo plastic fluids is much remarkable as compared to the variation demonstrated for dilatant fluids. Meanwhile, with the enhancement of n , an increase is observed in the concentration field and the associated CBLT (see **Figs. 4.2(a,b)**). The outcome got for pseudo-plastic fluids is more conspicuous as contrast with dilatant liquids.

Figs. 4.3(a,b) are presented in pictorial for to show the features of A on the profile of temperature ($\theta(\eta)$). In these figures, the temperature field and TBLT exhibit a reducing behaviors for dilatant and pseudo-plastic properties of liquids. The results for pseudo plastic fluid displayed a prominent impact in comparison with dilatant property of the fluid. In physical sense, this conduct is due to the basic property of Sisko liquid parameter. The increase in this parameter causes reduction in viscosity of fluid while shear rate enhances and vise verse. This is why, the temperature field shows a reduction with the rising values of A . The impact of the parameter of Sisko liquid on the concentration profile is deliberated through **Figs. 4.4(a,b)**. This graphical illustration presents an uplifting behavior of concentration $\phi(\eta)$ and the associated CBLT for higher values of A . Both fundamental properties, i.e., dilatant and pseudo-plastic properties of liquids are described but a very noticeable outcome is found for pseudo-plastic fluid in comparison with the dilatant fluid.

Important growing behavior of temperature field $\theta(\eta)$ is noticed for the higher values of ε and is described through the graphs for both dilatant and pseudo-plastic liquids presented in **Figs. 4.5(a,b)**. This behavior of thermal conductivity on temperature field is a direct influence with a scalar parameter ε which arises by considering the variable thermal conductivity. In this regard, when the values of this parameter are higher then more temperature will be transferred from the wall of the sheet to the liquid. The impact of λ_E on the field of temperature $\theta(\eta)$ is plotted in **Figs. 4.6(a,b)**. These graphs illustrate the importance of relaxation time for the transfer of heat from the hot boundary to the cold boundary. Without the parameter of relaxation, i.e., $\lambda_E = 0$, an instantly greater

dispersion of temperature throughout the domain will take place which is practically impossible. So with the addition of this parameter in the form of modified Fourier's law stated that more time shall be required for the heat transfer from molecule to molecule of the fluid. Specifically, the temperature field $\theta(\eta)$ will be smaller for growing of λ_E . This trend is plotted for dilatant and pseudo-plastic liquids as well.

Impact of k_1 in **Figs. 4.7(a,b)** displayed in the form of reducing concentration $\phi(\eta)$ and the associated CBLT. This parameter may causes dissemination coefficients of reaction rates and as a result $\phi(\eta)$ reduces for $0 < n < 1$ as well as $n > 1$. However, the same behavior is depicted for higher values of k_2 in **Figs. 4.8(a,b)**, while considering both cases, i.e., $0 < n < 1$ as well as $n > 1$.

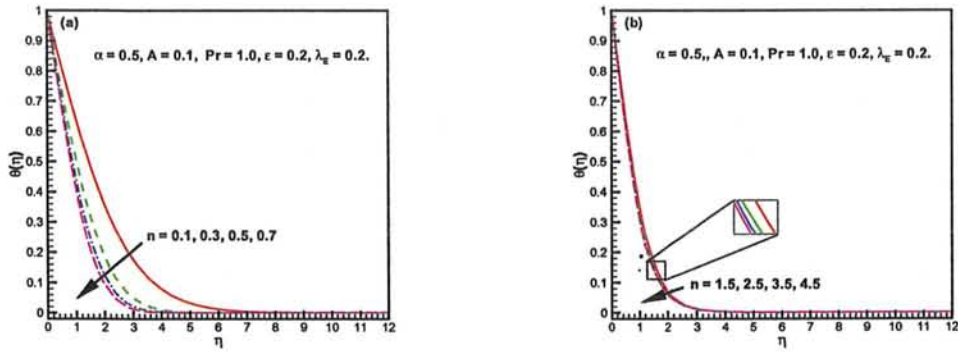


Fig. 4.1: Temperature profile $\theta(\eta)$ for n .

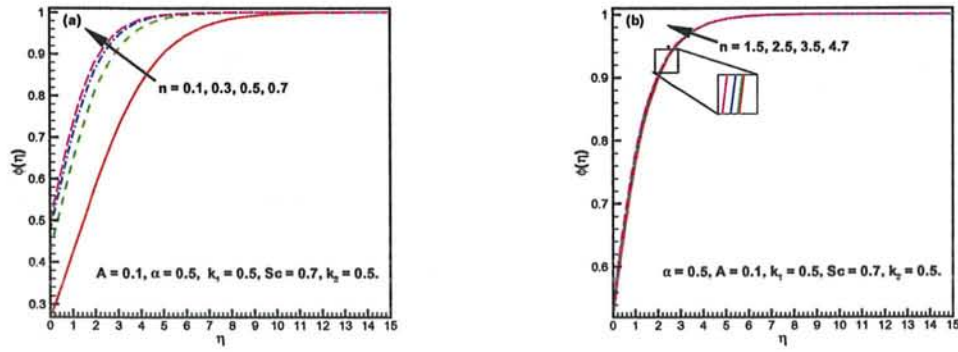


Fig. 4.2: Concentration profile $\phi(\eta)$ for n .

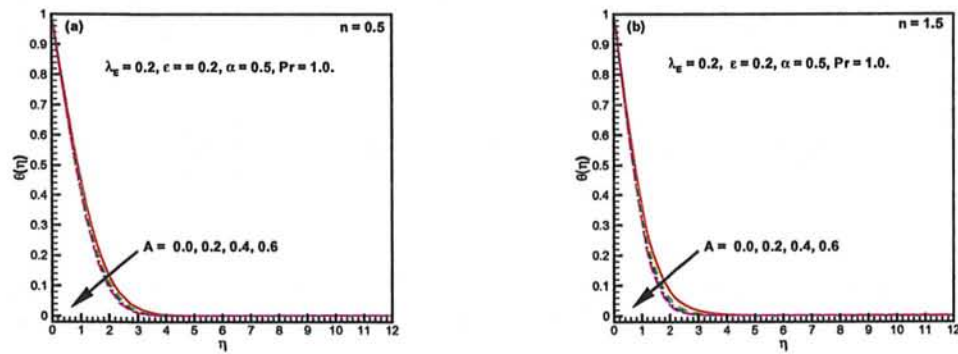


Fig. 4.3: Temperature profile $\theta(\eta)$ for A .

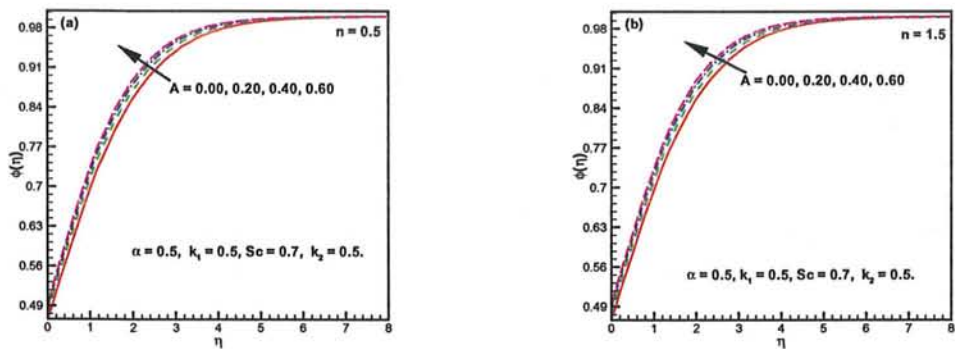


Fig. 4.4: Concentration profile $\phi(\eta)$ for A .

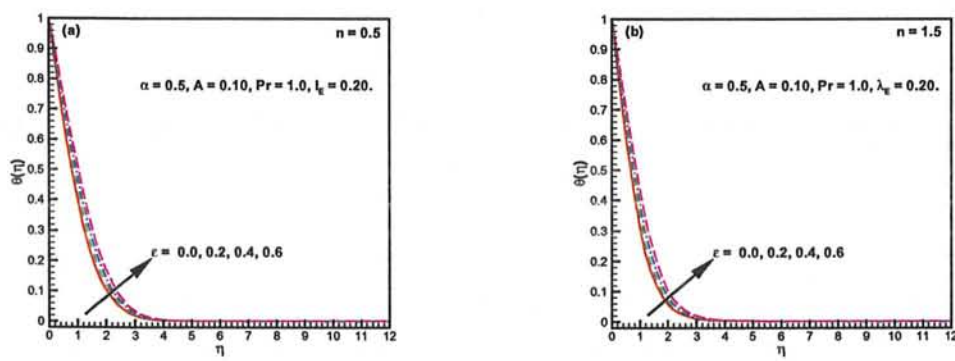


Fig. 4.5: Temperature profile $\theta(\eta)$ for ϵ .

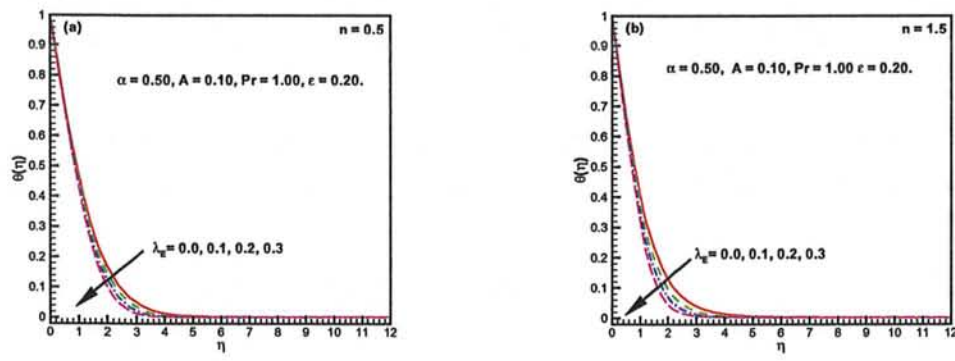


Fig. 4.6: Temperature profile $\theta(\eta)$ for λ_E .

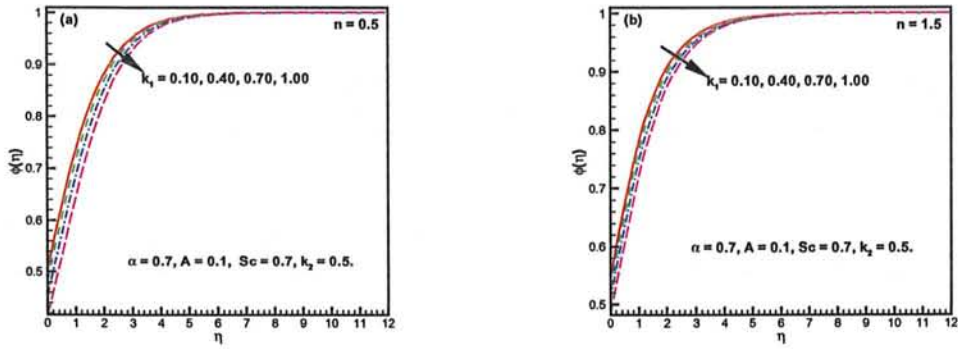


Fig. 4.7: Concentration profile $\phi(\eta)$ for k_1 .

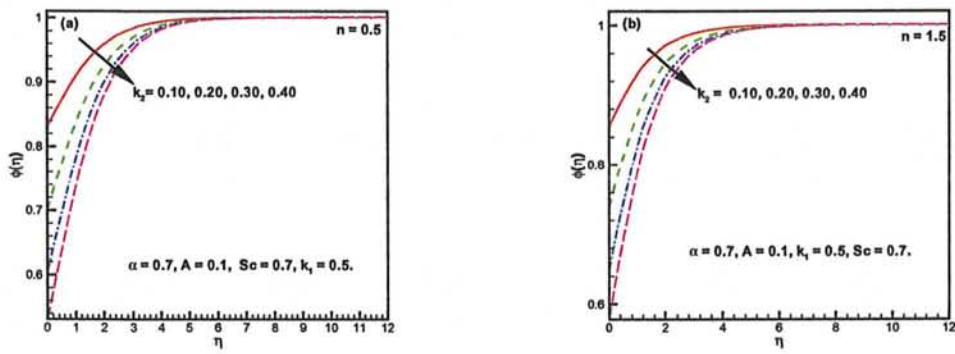


Fig. 4.8: Concentration profile $\phi(\eta)$ for k_2 .

Chapter 5

Numerical Computations of Unsteady Generalized Newtonian Fluid Flow with Convective Heat Transfer

In this chapter, the BLF and heat analysis are addressed for the unsteady 3D flow of Sisko liquid over a bidirectional time-dependent moving boundary. The governing PDEs involving momentum and temperature are transformed to non-linear ODEs by invoking suitable transformations. The modeled equations are then illustrated with numerical scheme viz shooting technique with RK-45 Fehlberg method. Additionally, in order to validate the exactness of the present results, we have provided a comparison between two different techniques namely the shooting technique and `bvp4c` in MATLAB. Moreover, a comparative study with previous published work is also presented and perceived an excellent agreement. Significant conclusions are drawn while portraying the profiles of velocity and temperature. The results are illustrated for both cases, i.e., shear-thinning ($0 < n < 1$) and shear-thickening ($n > 1$) liquids and it is perceived from the graphs that the velocity and temperature profiles raise with the augmentation of unsteady parameter for

the shear-thinning liquid while the opposite conduct is observed for the shear-thickening liquid. It is obvious from the graphs that the profile of temperature decreases for both cases including dilatant ($n > 1$) and pseudo-plastic ($0 < n < 1$) liquids, while the heat transfer rate raises for both cases.

5.1 Formulation of the Flow Problem

Assuming the time-dependent 3D forced convective BLF over a bidirectional moving surface of an inelastic non-Newtonian liquid that obeys the Sisko viscosity model. The stretching surface is located at $z = 0$ and stretched with velocity $U_w = \frac{cx}{1-\beta t}$ and $V_w = \frac{dy}{1-\beta t}$ along the x - and y - directions, respectively, where c , d and β are positive constants with dimension per. It is supposed that due to the convection by hot liquid, the lower surface of the moving sheet is heated to temperature T_f by convection from a hot liquid which results with a coefficient of heat transfer h_f . The ambient fluid temperature takes constant value T_∞ . Without body forces and the said restriction as mentioned above which leads the development of mass, momentum and energy balance equations as below:

$$\nabla \cdot \mathbf{V} = 0, \quad (5.1)$$

$$\rho_f \left(\frac{d\mathbf{V}}{dt} \right) = -\nabla p + \nabla \cdot \mathbf{S}, \quad (5.2)$$

$$(\rho c)_f \left(\frac{dT}{dt} \right) = -\nabla \cdot \mathbf{q}, \quad (5.3)$$

For a 3D unsteady flow in Cartesian system of coordinates, we can take the velocity, stress fields, temperature of the form

$$\mathbf{V} = [u(x, y, z, t), v(x, y, z, t), w(x, y, z, t)], \quad \mathbf{S} = \mathbf{S}(x, y, z, t), \quad T = T(x, y, z, t). \quad (5.4)$$

Plugging Eqs. (5.4) into Eqs. (5.1)-(5.3) and the use of BL approximation results in the following relations:

$$\frac{\partial u}{\partial x} = -\left(\frac{\partial v}{\partial y} + \frac{\partial w}{\partial z}\right), \quad (5.5)$$

$$\frac{\partial u}{\partial t} + u \frac{\partial u}{\partial x} + \frac{b}{\rho_f} \frac{\partial}{\partial z} \left(-\frac{\partial u}{\partial z}\right)^n = -\left(v \frac{\partial u}{\partial y} + w \frac{\partial u}{\partial z}\right) + \frac{a}{\rho_f} \left(\frac{\partial^2 u}{\partial z^2}\right), \quad (5.6)$$

$$\frac{\partial v}{\partial t} + u \frac{\partial v}{\partial x} - \frac{b}{\rho_f} \frac{\partial}{\partial z} \left(-\frac{\partial u}{\partial z}\right)^{n-1} \frac{\partial v}{\partial z} = -\left(v \frac{\partial v}{\partial y} + w \frac{\partial v}{\partial z}\right) + \frac{a}{\rho_f} \left(\frac{\partial^2 v}{\partial z^2}\right), \quad (5.7)$$

$$\frac{\partial T}{\partial t} + u \frac{\partial T}{\partial x} + \frac{k}{(\rho c)_f} \left(\frac{\partial^2 T}{\partial z^2}\right) = -\left(v \frac{\partial T}{\partial y} + w \frac{\partial T}{\partial z}\right). \quad (5.8)$$

Eqs. (5.6)-(5.9) are subjected to the following BCs:

$$\text{at } z = 0, \begin{cases} U_w = \frac{cx}{1-\beta t}, & V_w = \frac{dy}{1-\beta t}, \\ w = 0, & -k \left(\frac{\partial T}{\partial z}\right) = h_f(T - T_f), \end{cases} \quad (5.9)$$

$$\text{as } z \rightarrow \infty, \quad u \rightarrow 0, \quad v \rightarrow 0 \quad \text{and} \quad T \rightarrow T_\infty. \quad (5.10)$$

The governing Eqs. (5.5)-(5.8) subjected to BCs (5.9) and (5.10) can be stated with an easy way by presenting the subsequent transform variables:

$$u = \frac{cx}{1-\beta t} f'(\eta), \quad v = \frac{cy}{1-\beta t} g'(\eta), \quad (5.11)$$

$$w = -c \left(\frac{c^{n-2}}{\frac{\rho_f}{b}}\right)^{\frac{1}{n+1}} \left[\frac{2n}{n+1} f + \frac{1-n}{1+n} \eta f' + g \right] x^{\frac{n-1}{n+1}} (1-\beta t)^{\frac{1-2n}{n+1}}, \quad (5.12)$$

$$\theta(\eta) = \frac{T - T_\infty}{T_f - T_\infty}, \quad \eta = z \left(\frac{c^{2-n}}{\frac{b}{\rho_f}}\right)^{\frac{1}{n+1}} x^{\frac{n-1}{n+1}} (1-\beta t)^{\frac{n-2}{n+1}}. \quad (5.13)$$

In view of Eqs. (5.11)-(5.13), we get the following set of non-linear ODEs:

$$A f''' - S \left[f' + \frac{2-n}{1+n} \eta f'' \right] + \left(\frac{2n}{n+1} \right) f f'' + n (-f'')^{n-1} f''' - (f')^2 + g f'' = 0, \quad (5.14)$$

$$\begin{aligned}
Ag''' - S \left[g' + \frac{2-n}{1+n} \eta g'' \right] + \left(\frac{2n}{n+1} \right) fg'' + (-f'')^{n-1} g''' \\
-(n-1)g''f'''(-f'')^{n-2} - (g')^2 + gg'' = 0,
\end{aligned} \tag{5.15}$$

$$\theta'' + \text{Pr} \left(\frac{2n}{n+1} f + g \right) \theta' - \text{Pr} S \left[\frac{2-n}{1+n} \eta \theta' \right] = 0, \tag{5.16}$$

where all the primes represent derivative of the function with independent variable η . The imposed BCs are

$$\text{at } \eta = 0, \quad \begin{cases} f = 0, & g = 0, & f' = 1, \\ g' = \alpha, & \theta' = -\gamma[1 - \theta], \end{cases} \tag{5.17}$$

$$\text{as } \eta \rightarrow \infty, \quad f' \rightarrow 0, \quad g' \rightarrow 0, \quad \theta \rightarrow 0. \tag{5.18}$$

The non-dimensional controlling parameters that leading the problem are stated through Eqs. (5.14)-(5.18) are stated below

$$\begin{aligned}
A = \frac{Re_b^{\frac{2}{n+1}}}{Re_a}, \quad Re_a = \frac{U_w x \rho_f}{a}, \quad Re_b = \frac{U_w^{2-n} x^n \rho_f}{b}, \quad \alpha_1 = \frac{k}{(\rho c)_f}, \\
\alpha = \frac{d}{c}, \quad \text{Pr} = \frac{x U_w}{\alpha_1} Re_b^{-\frac{2}{n+1}}, \quad S = \frac{\beta}{c}, \quad \gamma = \frac{h_f}{k} x Re_b^{-\frac{1}{n+1}}.
\end{aligned} \tag{5.19}$$

The drag force and Nusselt number coefficients that declared the engineering extents are C_{fx} , C_{fy} and transfer rate of heat Nu_x and are stated as

$$Re_b^{\frac{1}{n+1}} C_{fx} = Af''(0) - (-f''(0))^n, \tag{5.20}$$

$$Re_b^{\frac{1}{n+1}} C_{fy} = \frac{V_w}{U_w} [(-f''(0))^{(n-1)} g''(0) + Ag''(0)], \tag{5.21}$$

$$Re_b^{-\frac{1}{n+1}} Nu_x = -\theta'(0). \tag{5.22}$$

5.2 Numerical Scheme

The coupled ODEs (5.14)-(5.16) with boundary constraints (5.17) and (5.18) are abridged to a system of eight first order ODEs and six flow parameters along with boundary constraints. In order to compute the solution of simultaneous system of first order equations, we need two initial conditions for f'' and g'' , while one for θ . Once the initial guess is fixed with finite value of η_∞ , then we can solve it by implementing RK-45 Fehlberg method. RK-45 Fehlberg method is a numerical technique to find the results while providing an appropriate step size h . At each step two altered approximations for the solutions are finished and matched. If two results have close agreement, then the computations are acceptable. If two answers are not agree with the desired accuracy, then the step size shall be reduced. If the approximation is strongly agree up to more significant digit, the step size shall be increased. Thus it will need the six functional values and other basics equations as defined through Eqs. (1.3)-(1.11).

Since, for this specific anticipated problem, the values of f' , g' and θ at infinity are known and the values of f'' , g'' and θ at the surface can be guessed. However, the general procedures followed to compute the numerical solution is shooting technique for which we have adopted the following procedures.

Let

$$f = x_1, \quad f' = x'_1 = x_2, \quad f'' = x'_2 = x_3, \quad f''' = x'_3, \quad (5.32)$$

$$g = x_4, \quad g' = x'_4 = x_5, \quad g'' = x'_5 = x_6, \quad g''' = x'_6, \quad (5.33)$$

$$\theta = x_7, \quad \theta' = x'_7 = x_8, \quad \theta'' = x'_8, \quad (5.34)$$

$$x'_3 = \frac{S(x_2 + \frac{2-n}{n+1}\eta x_3) - \frac{2n}{n+1}x_1x_3 - x_4x_3 + x_2^2}{[A + n(-x_3)^{n-1}]}, \quad (5.35)$$

$$x'_6 = \frac{S(x_5 + \frac{2-n}{n+1}\eta x_6) - \frac{2n}{n+1}x_1x_6 - x_4x_6 + x_5^2 + (n-1)x_6x'_3(-x_3)^{n-2}}{[A + (-x_3)^{n-1}]}, \quad (5.36)$$

$$x'_8 = \text{Pr} S\left(\frac{2-n}{n+1}\eta x_8\right) - \text{Pr}\left(\frac{2n}{n+1}x_1 + x_4\right)x_8, \quad (5.37)$$

with the dimensionless BCs

$$x_1(0) = 0, x_4(0) = 0, x_2'(0) = 1, x_5'(0) = \alpha, x_8'(0) = -\gamma [1 - x_7(0)], \quad (5.38)$$

$$x_2 \rightarrow 0, x_5 \rightarrow 0, x_7 \rightarrow 0 \text{ as } \eta \rightarrow \infty. \quad (5.39)$$

The guessing conditions are given as follows:

$$x_3(0) = r_1^*, x_6(0) = r_2^*, x_7(0) = r_3^*. \quad (5.40)$$

5.3 Testing of Method

To perceive the verification of the current numerical results evaluated with the help of shooting technique and another numerical scheme viz bvp4c built-in routine is used to justify the present scenario. An exceptional correlation is reported between two numerical techniques while plotting the liquid velocity and temperature through **Figs. 5.1(a-d)** and **5.2(a,b)**, respectively. The variation of the skin-friction in the restraining cases is shown in the **table 5.1** which shows an excellent correlation with the existing literature as provided by Ariel [75]. The tabular values of the Nusselt number through **table 5.2** shows an exceptional treaty with the upshots reported by Ishak *et al.* [76] and Elbashbeshy [77].

5.4 Computational Results and Discussion

The numerical computations of highly non-linear ODEs (5.14)-(5.16) subject to BCs (5.17) and (5.18) are performed. The graphical illustrations are provided to analyze the influence of the main parameters of flow which lead the anticipated problem namely the unsteadiness parameter (S), power-law parameter (n), Sisko fluid parameter (A), Biot number (γ) and stretching parameter (α) on the velocity and temperature distributions. A comparison

of two adopted numerical approaches namely the shooting technique along with RK-45 Fehlberg method and bvp4c package has been done to check the accuracy of the numerical results.

The computational results plotted through **Figs. 5.3(a-d)** present a significant trend of n on the fluid velocity components. These plots are representing a reduction in velocity components for both cases that is dilatant ($n > 1$) liquid and pseudo plastic ($0 < n < 1$) liquid. Further it is depicted that the associated MBLT attained in this flow, is also reduced. However, from these pictures, it can be found that the MBLT is much higher in situation of pseudo-plastic liquid, when compared with dilatant fluid. Through **Figs. 5.4(a,b)**, the field of temperature shows a diminishing behavior while increasing the power law index with both pseudo-plastic and dilatant cases. Additionally, it is seen that the liquid temperature are more significant in situation of shear-thinning liquid in comparison with shear-thickening property.

The velocity profiles as shown in **Figs. 5.5(a-d)** exhibit an escalating behavior by increasing the Sisko fluid parameter. In the aforementioned figures, for both dilatant and pseudo-plastic cases, the TBLT is enhanced. A decline in the temperature distribution is noticed for increasing Sisko fluid parameter and is portrayed through **Figs. 5.6(a,b)**. Again, it is seen that the momentum as well as TBLT are greater in case of ($0 < n < 1$) fluid in comparison with ($n > 1$) liquid. The effects of the unsteadiness parameter on the velocity and temperature distributions are shown in **Figs. 5.7(a-d)** and **5.8(a,b)**, respectively. From these figures, it is noticed that the increasing values of S result in a slight decline in the velocity and temperature of the liquid and the corresponding TBLT in the case of shear-thickening fluid. However, a relatively reverse trend is revealed for the case of shear-thinning liquid.

Fig. 5.9(a,b) exhibit a declining conduct while plotting of velocity component $f'(\eta)$ while keeping the stretching parameter in increasing order. It is revealed that the velocity field and the associated BL structure decay for increasing values of α for the cases, i.e., pseudo-plastic and dilatant liquids. The opposite behaviors are noticed during

the intrigues of other velocity component $g'(\eta)$ as portrayed in **Figs. 5.9(c,d)**. **Figs. 5.10(a,b)** describe the impact of the increasing values of the Biot number on the temperature distribution and the associated TBLT. Temperature and associated TBLT liquid show and uplifting conduct by the higher values of Biot number. This is owing of the enhancement in transfer of heat.

The results presented in **table 5.3** indicate that as the unsteadiness parameter increases from $S = 0.0$ to 0.4 , the skin-friction reveal an enhancing trend for pseudo-plastic liquids and the same trend is detected for dilatant liquids. It is further noted that the drag force is stronger in case of pseudo-plastic liquid for smaller values of the unsteadiness parameter. We further observed from the **table 5.4** that the effect of unsteadiness parameter on Nusselt number shows an increasing conduct for dilatant and pseudo-plastic liquids as well. Additionally, the effect of Biot number on the Nusselt number is tested which increases from $\gamma = 1.1$ to 1.3 and which exhibit an uplifting behavior for two cases, i.e., pseudo-plastic and dilatant liquids, respectively. It is concluded from the approximate values that the rate of heat transfer is more prominent in shear-thinning fluids.

Table 5.1: A matching with earlier results for growing values of α when $A = 0, S = 0, n = 1, Pr = 1.2$ and $\gamma \rightarrow \infty$.

α	$-f''(0)$			$-g''(0)$		
	Ariel [75]		Present results	Ariel [75]		Present results
	Exact	Approx	Approx	Exact	Approx	Approx
0.0	1.00000000	1.00000000	1.000008	0.00000000	0.00000000	0.00000000
0.1	1.02025978	1.01952736	1.020264	0.06684715	0.06796849	0.06684863
0.2	1.03949519	1.03827716	1.039498	0.14873691	0.15018484	0.14873840

Table 5.2: A matching with earlier results for growing values of Pr when $A = 0, S = 0, n = 1$ and $\gamma \rightarrow \infty$.

$-\theta'(0)$			
Pr	Ishak <i>et al.</i> [76]	Elbashbeshy [77]	Present results
0.72	0.8086	0.8161	0.8088342
1.0	1.0000	1.0000	1.0000080
10	3.7202	3.7202	3.7206700

Table 5.3: Influence of flow parameters on skin-friction, when $Pr = 1.2$ and $\gamma = 1.2$ are fixed.

Parameters			$-\frac{1}{2} \left(Re_b^{\frac{1}{n+1}} \right) C_{fx}$		$-\frac{1}{2} \left(Re_b^{\frac{1}{n+1}} C_{fy} \right)$	
A	S	α	$n = 0.50$	$n = 1.50$	$n = 0.50$	$n = 1.50$
0.3	0.2	1.5	1.492243	1.493997	2.449393	2.444652
0.6			1.671741	1.642484	2.749315	2.686316
0.9			1.827711	1.78218	3.009472	2.913729
0.3	0.0	1.5	1.454925	1.419253	2.397469	2.338542
	0.2		1.492243	1.493997	2.449393	2.444652
	0.4		1.531868	1.567131	2.503422	2.548762
0.3	0.2	1.3	1.468945	1.457906	2.024574	2.004631
		1.5	1.492243	1.493997	2.449393	2.444652
		1.7	1.51497	1.529287	2.89628	2.913510

Table 5.4: Effect of various flow parameters on Nusselt number.

Parameters					$-\left(\text{Re}_b^{-\frac{1}{n+1}}\right)Nu_x$	
A	S	α	Pr	γ	$n = 0.50$	$n = 1.50$
0.3	0.2	1.5	1.2	1.2	0.6449692	0.6752807
0.6					0.6523803	0.680455
0.9					0.6574618	0.6843759
0.3	0.0	1.5	1.2	1.2	0.6400963	0.6622351
	0.2				0.6449692	0.6752807
	0.4				0.6501400	0.6873459
0.3	0.2	1.3	1.2	1.2	0.6378863	0.6688928
		1.5			0.6449692	0.6752807
		1.7			0.6516804	0.6813764
0.3	0.2	1.5	1.0	1.2	0.6122373	0.6422419
			1.2		0.6449692	0.6752807
			1.4		0.6720866	0.7023523
0.3	0.2	1.5	1.2	1.1	0.6149232	0.6424162
				1.2	0.6449692	0.6752807
				1.3	0.6727849	0.7058343

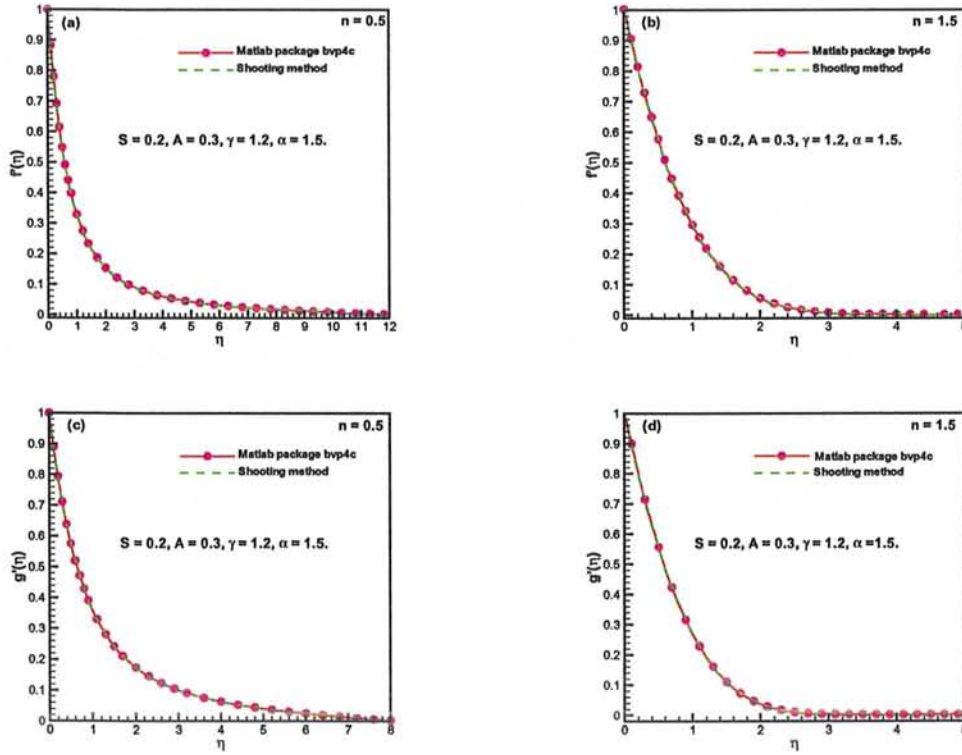


Fig. 5.1: Comparison of the shooting and bvp4c solutions for velocity components.

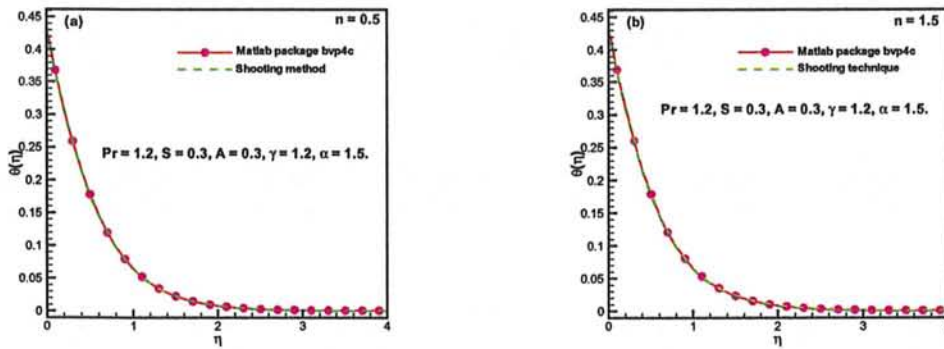


Fig. 5.2: Comparison of the shooting and bvp4c solutions for temperature.

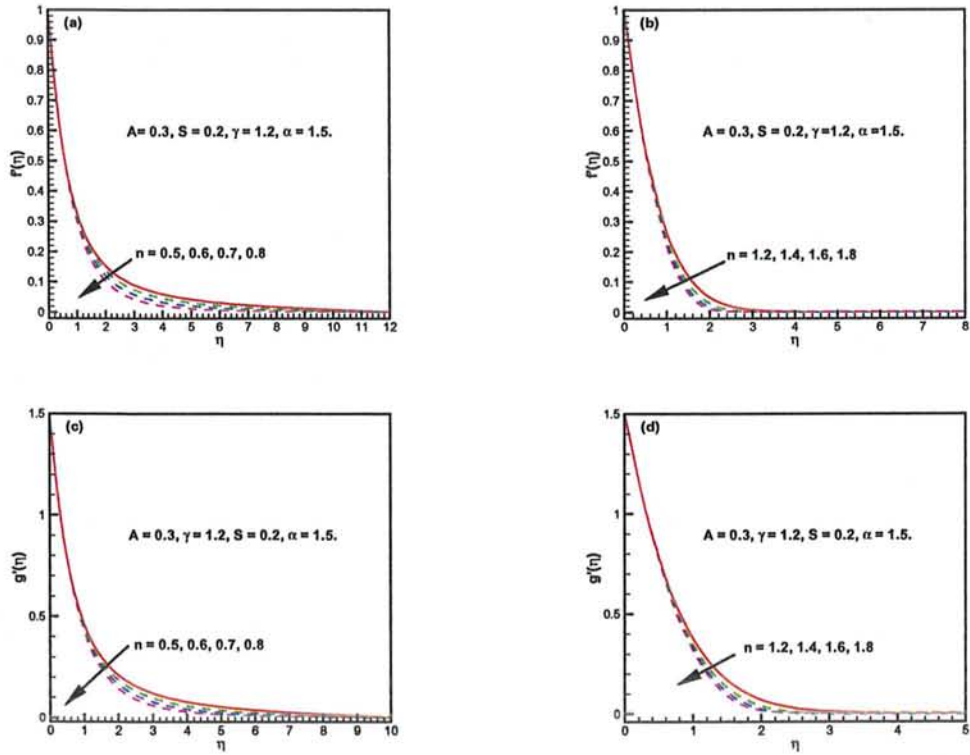


Fig. 5.3: Influence of n on the velocity components.

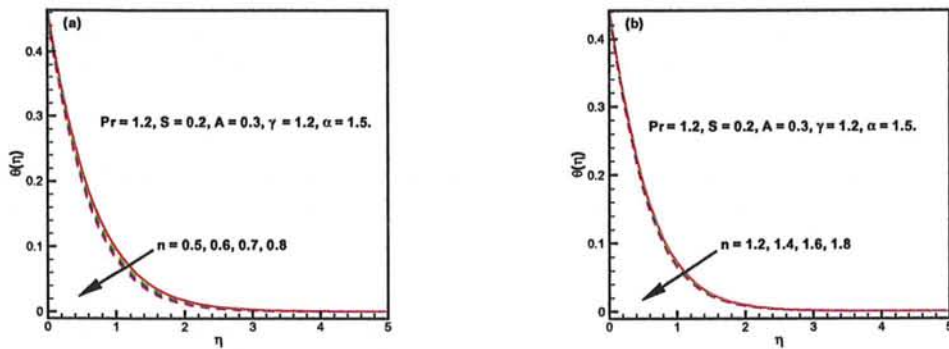


Fig. 5.4: Influence of n on the temperature.

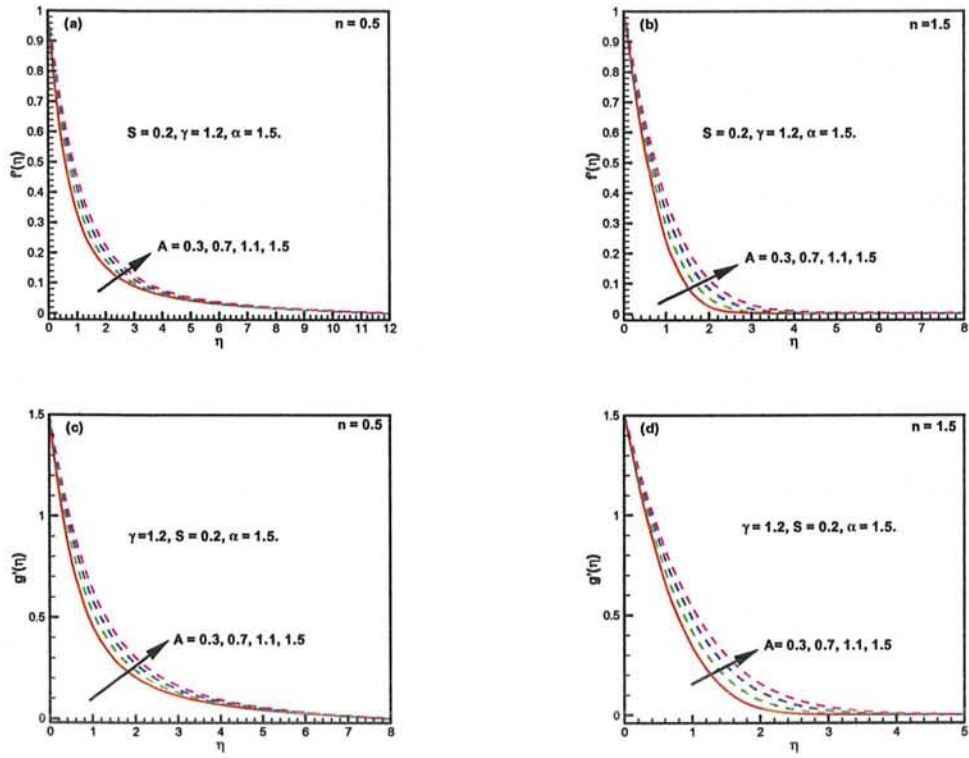


Fig. 5.5: Influence of A on velocity components.

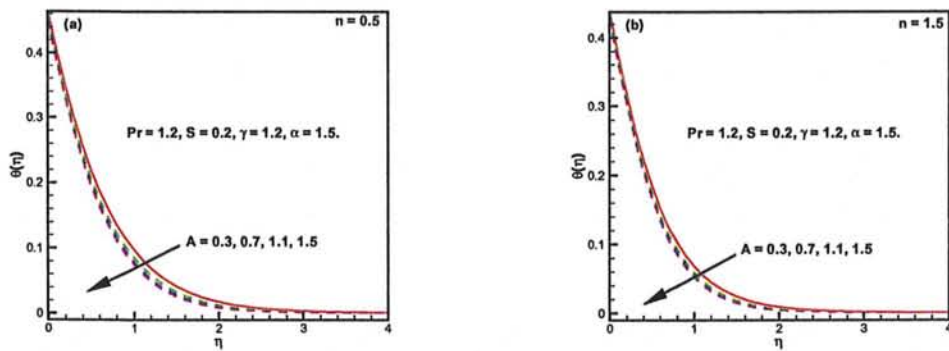


Fig. 5.6: Influence of A on temperature.

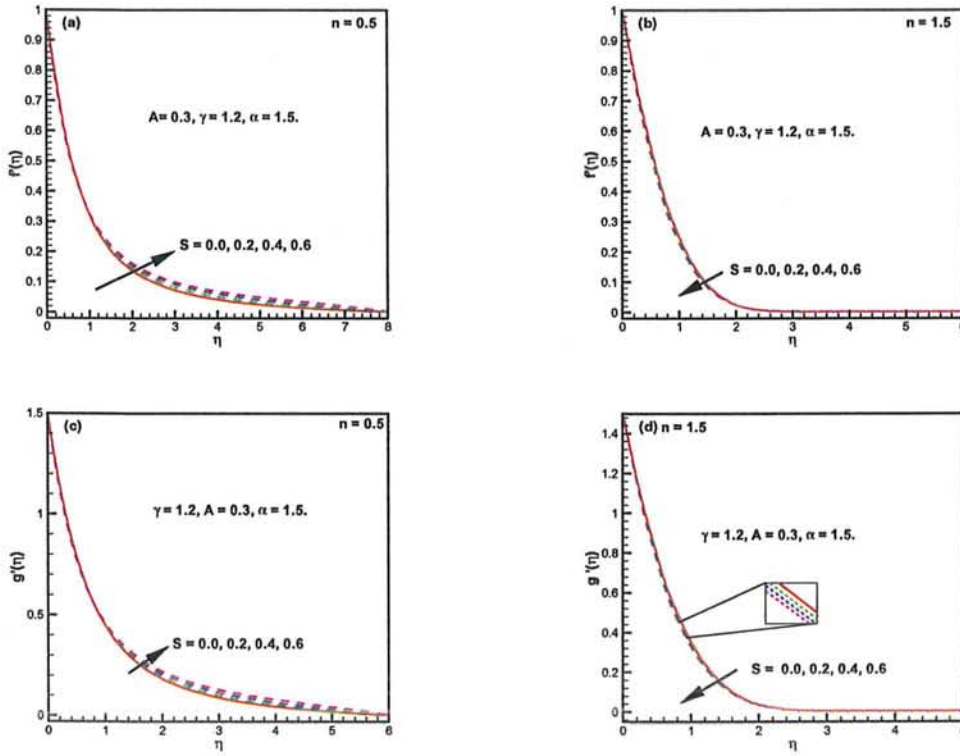


Fig. 5.7: Influence of S on velocity components.

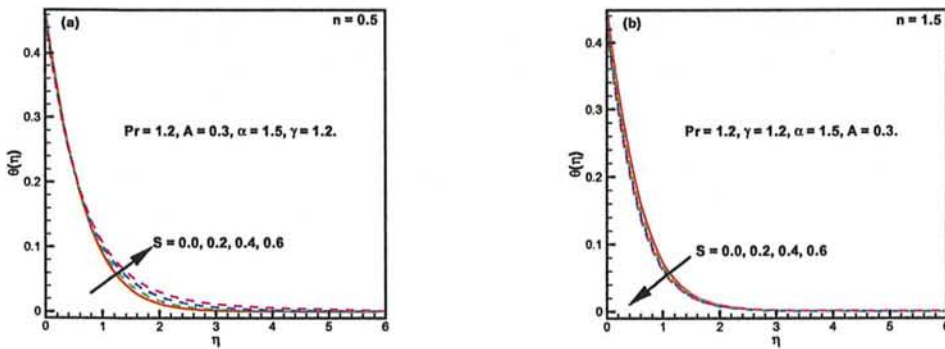


Fig. 5.8: Influence of S on temperature.

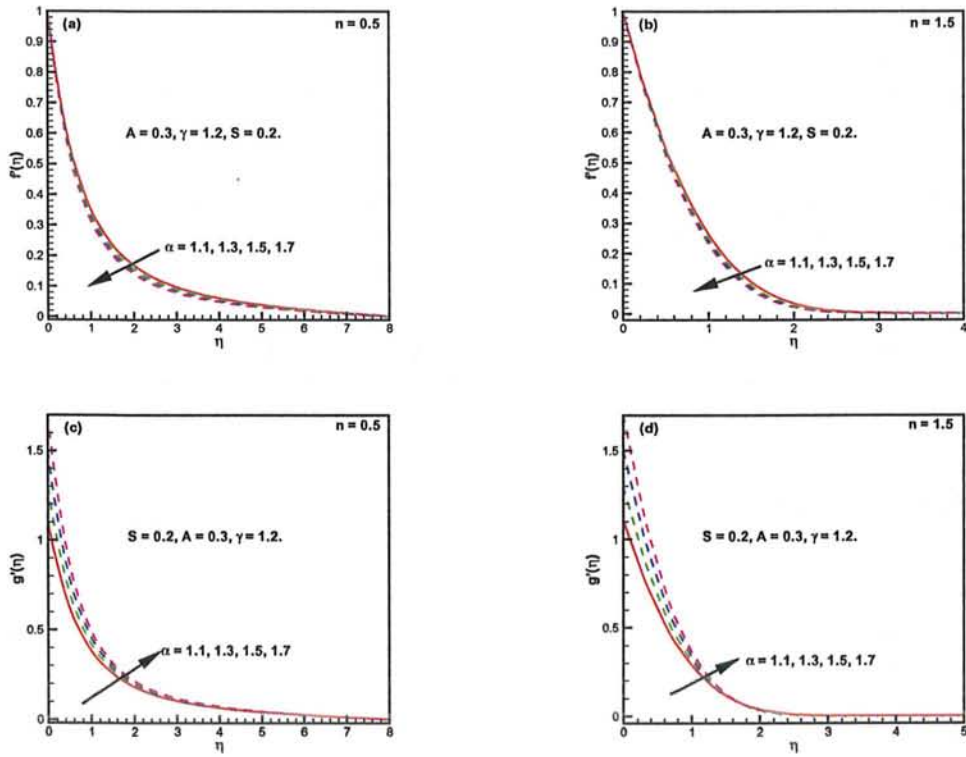


Fig. 5.9: Influence of α on velocity components.

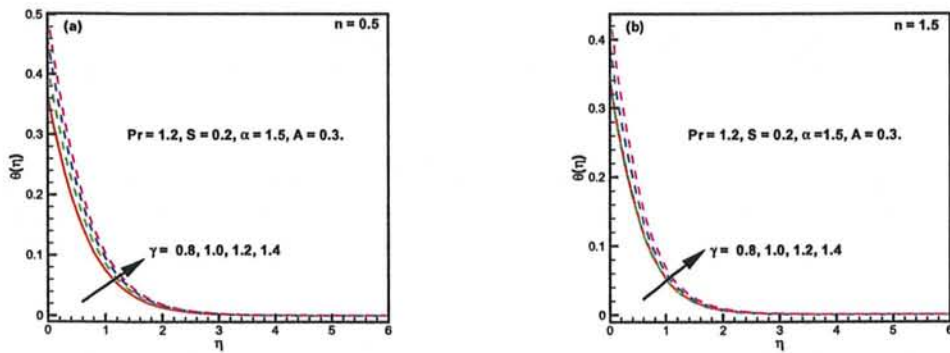


Fig. 5.10: Influence of γ on temperature.

Chapter 6

Thermophoresis and Brownian Motion Applications to the Flow of Unsteady 3D Magneto-Sisko Liquid: A Numerical Study

In this chapter, the impact of Buongiorno's model in 3D flow of unsteady Sisko liquid is discussed in the occurrence of zero nanoparticles mass flux constraint. The 3D time-dependent Sisko liquid equations are first formulated through classical BL approximations and then non-dimensionalized by incorporating the suitable variables. The approximate illustration for ensuing flow, and transfer of heat and mass are computed by utilizing the two different numerical techniques namely `bvp4c` built-in code in MATLAB and shooting technique with RK45 Fehlberg and Newton-Raphson methods. Numerical results are demonstrated by presenting a pictorial view of the liquid temperature and concentration. The distinct behaviors of the nano-liquid distributions of velocity, temperature and concentration for shear-thinning ($0 < n < 1$) and shear-thickening ($n > 1$) cases are reported. In the revised nature condition, the change in temperature owing by Brownian motion is detected in a very minor behavior and has been ignored. To see the authentication of the

numerical computations, we compare the finding of the numerical techniques bvp4c with an efficient numerical method namely the shooting technique and RK45 Fehlberg method and an excellent correlation between these methods is seen.

6.1 Mathematical Construction of the Model

Consider the 3D unsteady flow with constant density of Sisko nano-fluid past a bidirectional stretched surface. The uniform transverse nature of a magnetic field $B = [0, 0, B_0]$ is imposed in the main problem and due a very less impact of the magnetic Reynolds number which is ignorable in this proposed physical problem. The moving surface, which physically characterizes a nano-polymer is prompted by applying four equal and opposed forces simultaneously along the x - and y - axes with velocities $U_w = \frac{cx}{1-\beta t}$ and $V_w = \frac{dy}{1-\beta t}$, respectively, with both $(c, d) > 0$ are the moving rates. The x - and y - axes are fixed along the continuous moving sheet and the z axis is dignified normal to the x - and y - axes. The boundary temperature (T_w) is anticipated to be higher than that of the temperature of the of the nanoliquid at T_∞ which are far-off from the moving boundary. Furthermore, transfer of heat and mass phenomena are carried out by employing Buongiorno's relation. The aforementioned assumptions goes to formulate the said problem in the subsequent way of relations

$$\frac{\partial u}{\partial x} = -\left(\frac{\partial v}{\partial y} + \frac{\partial w}{\partial z}\right), \quad (6.1)$$

$$\frac{\partial u}{\partial t} + u\frac{\partial u}{\partial x} + \frac{b}{\rho_f}\frac{\partial}{\partial z}\left(-\frac{\partial u}{\partial z}\right)^n + \left(\frac{\sigma B_0^2}{\rho_f}\right)u = -\left(v\frac{\partial u}{\partial y} + w\frac{\partial u}{\partial z}\right) + \frac{a}{\rho_f}\left(\frac{\partial^2 u}{\partial z^2}\right), \quad (6.2)$$

$$\frac{\partial v}{\partial t} + u\frac{\partial v}{\partial x} - \frac{b}{\rho_f}\frac{\partial}{\partial z}\left(-\frac{\partial u}{\partial z}\right)^{n-1}\frac{\partial v}{\partial z} + \left(\frac{\sigma B_0^2}{\rho_f}\right)v = -\left(v\frac{\partial v}{\partial y} + w\frac{\partial v}{\partial z}\right) + \frac{a}{\rho_f}\left(\frac{\partial^2 v}{\partial z^2}\right), \quad (6.3)$$

$$\frac{\partial T}{\partial t} + u\frac{\partial T}{\partial x} - \alpha_1\left(\frac{\partial^2 T}{\partial z^2}\right) = -\left(v\frac{\partial T}{\partial y} + w\frac{\partial T}{\partial z}\right) + \tau^*\left[D_B\left(\frac{\partial C}{\partial z}\right)\left(\frac{\partial T}{\partial z}\right) + \frac{D_T}{T_\infty}\left(\frac{\partial T}{\partial z}\right)^2\right], \quad (6.4)$$

$$\frac{\partial C}{\partial t} + u \frac{\partial C}{\partial x} - \frac{D_T}{T_\infty} \left(\frac{\partial^2 T}{\partial z^2} \right) = - \left(v \frac{\partial C}{\partial y} + w \frac{\partial C}{\partial z} \right) + D_B \left(\frac{\partial^2 C}{\partial z^2} \right). \quad (6.5)$$

The subsequent appropriate BCs are imposed at the moving surface and in the free stream

$$\text{at } z = 0, \begin{cases} U_w = \frac{cx}{1-\beta t}, & V_w = \frac{dy}{1-\beta t}, & W_w = 0, \\ T = T_w, & \frac{D_T}{T_\infty} \left(\frac{\partial T}{\partial z} \right) + D_B \left(\frac{\partial C}{\partial z} \right) = 0, \end{cases} \quad (6.6)$$

$$\text{as } z \rightarrow \infty, \quad u \rightarrow 0, \quad v \rightarrow 0, \quad T \rightarrow T_\infty \quad \text{and} \quad C \rightarrow C_\infty. \quad (6.7)$$

The analysis is further proceed by presenting the following suitable transformation:

$$\phi(\eta) = \frac{C - C_\infty}{C_\infty}, \quad (6.8)$$

where $T_w = T_\infty + \frac{e^* x}{1-\beta t}$. In perspective of Eqs. (5.11), (5.12), (5.13) and (6.8), we can obtain the subsequent ODEs with respect to the dimensionless variable η :

$$A f''' - S \left[f' + \left(\frac{2n}{n+1} \right) f f'' + \frac{2-n}{1+n} \eta f'' \right] + n (-f'')^{n-1} f''' - f'^2 + g f'' - M f' = 0, \quad (6.9)$$

$$\begin{aligned} A g''' - S \left[g' + \left(\frac{2n}{n+1} \right) f g'' + \frac{2-n}{1+n} \eta g'' \right] + (-f'')^{n-1} g''' \\ - (n-1) g'' f''' (-f'')^{n-2} - g'^2 + g g'' - M g' = 0, \end{aligned} \quad (6.10)$$

$$\theta'' + \text{Pr} \left(\frac{2n}{n+1} f + g \right) \theta' - \text{Pr} S \left[\theta + \frac{2-n}{1+n} \eta \theta' \right] - \text{Pr} f' \theta + \text{Pr} (N_b \theta' \phi' + N_t \theta'^2) = 0, \quad (6.11)$$

$$\phi'' + \text{Le Pr} \left(\frac{2n}{n+1} f + g \right) \phi' - \text{Le Pr} S \left[\frac{2-n}{1+n} \eta \phi' \right] + \left(\frac{N_t}{N_b} \right) \theta'' = 0, \quad (6.12)$$

$$\text{at } \eta = 0, \begin{cases} f = 0, & g = 0, & f' = 1, & g' = \alpha, \\ \theta = 1, & N_b \phi' + N_t \theta' = 0, \end{cases} \quad (6.13)$$

$$\text{as } \eta \rightarrow \infty, \quad f' \rightarrow 0, \quad g' \rightarrow 0, \quad \theta \rightarrow 0, \quad \phi \rightarrow 0. \quad (6.14)$$



The flow parameters are stated below:

$$N_b = \frac{\tau^* D_B C_\infty}{\nu}, \quad N_t = \frac{\tau^* D_T (T_w - T_\infty)}{T_\infty \nu},$$

$$\alpha = \frac{d}{c}, \quad S = \frac{\beta}{c}, \quad Le = \frac{\alpha_1}{D_B}. \quad (6.15)$$

6.2 Engineering Quantities

From the physical opinion, the interest in leading extents are the local skin-friction and Nusselt number. Physically skin-friction represents the resistive force oppose to the flow of liquids and local Nusselt number specifies the heat transfer rate of nanoliquid. These extents of physical curiosity can be deliberated by the consequent expressions as:

$$C_{fx} = \frac{\tau_{xz}}{\frac{1}{2}\rho U_w^2}, \quad C_{fy} = \frac{\tau_{yz}}{\frac{1}{2}\rho U_w^2}, \quad (6.16)$$

$$Nu_x = \frac{x}{(T_\infty - T_f)} \left(\frac{\partial T}{\partial z} \right) \Big|_{z=0}. \quad (6.17)$$

The above expressions in dimensionless variables take the form:

$$\frac{1}{2} Re_b^{\frac{1}{n+1}} C_{fx} = A f''(0) - (-f''(0))^n, \quad (6.18)$$

$$\frac{1}{2} Re_b^{\frac{1}{n+1}} C_{fy} = \frac{V_w}{U_w} [A g''(0) + g''(0)(-f''(0))^{(n-1)}], \quad (6.19)$$

$$Re^{-\frac{1}{n+1}} Nu_x = -\theta'(0). \quad (6.20)$$

6.3 Authentication of Numerical Outcomes

To authenticate the correctness of the numerical outcomes achieved through the `bvp4c` function in MATLAB scheme, an assessment of the transfer rate of heat is made with results obtained through the shooting method along with RKF and Newton-Raphson meth-

ods. A comparison between the two numerical approaches namely the shooting technique and built-in package `bvp4c` in MATLAB are illustrated through **Figs. 6.1(a,b), 6.2(a,b) and 6.3(a,b)** for the velocity, temperature and nanoparticle concentration distributions, respectively. From these plots, one can find an outstanding agreement between these two methods. It is important to mention that in the nonexistence of unsteadiness parameter, magnetic parameter, Lewis number, Brownian motion and thermophoresis parameter, the results are matching with the recent illustrated work [12] (see **tables 6.3 and 6.4**). Furthermore, in the nonexistence of Sisko liquid parameter, magnetic parameter, Lewis number, Brownian motion and thermophoresis parameter, then the reduced problem for this investigation reduces to the problem which was analyzed by Ishak *et al.* [76] and Elbashbeshy *et al.* [77]. The comparison is listed in **table 6.5** presenting a good correlation regarded this work with those presented by the previously cited authors.

6.4 Description of the Results

To inspect the significance of newly proposed more realistic relation for the Sisko nano-liquid over a moving surface is the main theme and to be presented here. Important numerical scrutiny have been exemplified to explore the features and parameters diverse depicts of the flow of Sisko nano-liquid.

The tabular values of drag forces are illustrated in **table 6.1**. Here an enhancement is noticed by increasing the unsteadiness parameter S for $(0 < n < 1)$ as well as $(n > 1)$. The effect is more noticeable for the case of shear-thickening liquid. In the aforementioned table, a significance increment is reported by taking the values in increasing order of parameter M . It is because due to strong resistance with the existence of the magnetic field. The numerical values of the local-Nusselt number is presented in **table 6.2**, while different flow parameters are taken in an increasing order. An escalation in transfer rate of heat is reported with the uplifting values of the unsteadiness parameter S for dilatant as well as pseudo-plastic liquids. Moreover, in the tabular values, for the incrementation

in the Brownian motion parameter N_b , no effect is seen on the heat transfer rate. On the other hand, a decrease in the heat transfer rate is observed by varying the thermophoresis parameter N_t .

The features of nano-liquid component of velocity $g'(\eta)$ for raising values of magnetic parameter M is illustrated through **Figs. 6.4(a,b)**. Here a reduction determination about nano-liquid velocity and relatable MBLT is noticed in the preceding pictorial presentation by larger values of magnetic parameter. Physically, this arises owing to the fact that an escalation in Lorentz force yields much opposition to the nanoliquid flow and thus the nanoliquid velocity declines. Consequently, collision between the nano-particles enhances and this mechanism declines the associated MBLT. Parameter of stretching rates α influenced remarkably the nano-liquid velocity and related MBLT and is noticed such velocity with enrichment conduct for fixed values of pseudo-plastic and dilatant liquids conditions. These plots are presented through **Figs. 6.5(a,b)**. It is estimated by these sketches that the velocity of the nano-liquid and associated MBLT enriches as the ratio of stretching rates parameter rises. In physical sense, it is owing to the fact that whenever stretching rates are increased, then velocity of nano-liquid becomes dominant in y -direction in matching with the velocity in x -direction. Consequently, the velocity of the nano-liquid boosts.

Figs. 6.6(a-d) are figured to exemplified the behavior of temperature and solute concentration of nano-liquid and the relevant TBLT and CBLT. It can be professed from these sketches that the temperature and concentration distributions decay for an escalation in the power law index n . However, the characteristics of the power-law index on the temperature and concentration fields are more outstanding for $(0 < n < 1)$ as compared to the case $(n > 1)$. **Figs. 6.7(a-d)** are designed to envisage the development of the nanofluid temperature field as well as concentration distribution for increasing values of Sisko liquid parameter A . It can be perceived from these graphs that for escalating values of the Sisko liquid parameter a deterioration in the nano-fluid temperature and concentration profiles is found. Furthermore, it can be visualize from these graphs that

the relevant TBLT and CBLT are diminishing functions of A . The flow results of this plotting for $(0 < n < 1)$ is more significant in comparison with $(n > 1)$ property. This is due to the fact that whenever, A is taken into higher order values, the said viscosity of the fluid reduces due to increase in shear rates and this causes a decline in nano-liquid temperature field as well as concentration profile. Thus, the same trend is noticed for the associated TBLT and CBLT. Another important effect in the form of higher temperature as well as concentration fields for the intensifying values of S are detected through **Figs. 6.8(a-d)**. In these graphs more prominent outcome for $(0 < n < 1)$ is detected in comparison with $(n > 1)$ property. **Figs. 6.9(a-d)** are devoted to present the fluctuations in the fields of temperature and solute concentration for altered values of the ratio of stretching rates parameter α . We detected a deterioration in the nano-liquid profiles of temperature and concentration for rising values of the ratio of stretching rates parameter. **Figs. 6.10(a-d)** disclose the disparity of the temperature and concentration disseminations in reply to a change in the Prandtl Pr. As the values of Pr increases the temperature and concentration distributions along with the TBLT reduce. When the values of the Pr are taken in growing order, the rate of thermal diffusion slows down. Moreover, if the Prandtl number increases the concentration profile inclines at the surface. Additionally, for the greater values of Prandtl number, the liquid reduce more slowly as compared to the fluids with higher values of Prandtl number. **Figs. 6.11(a-d)** are sketched to investigate the features of the thermophoresis parameter N_t on the nanoliquid temperature as well as concentration distributions. Physically, escalating the values of N_t implies that the small nanomaterials are taken away from the warm boundary to the cold boundary and thus the liquid temperature raises due to the reason that greater number of nanoparticles are dragged away from the surface. **Figs. 6.12 (a, b)** are captured to measure the changes in the distribution of nanoliquid concentration with the impact of Lewis number Le . In fact, Lewis number is indirectly proportional to the coefficient of Brownian diffusion. Here uplifting values of Lewis number correspond to small diffusivity and so concentration distribution declines. Through **Figs. 6.13(a,b)**, a reduction is observed in

the concentration of the nanoparticles and relatable CBLT due to the enhancing values of the Brownian motion parameter N_b .

Table 6.1: Local skin-friction for several values of the flow parameters.

A	S	M	α	$-\frac{1}{2} \left(Re_b \right)^{\frac{1}{n+1}} C_{fx}$		$-\frac{1}{2} \left(Re_b \right)^{\frac{1}{n+1}} C_{fy}$	
				$n = 0.50$	$n = 1.50$	$n = 0.50$	$n = 1.50$
0.0	0.2	0.2	1.5	1.439957	1.351255	2.093931	2.209080
0.3				1.508605	1.511288	2.470231	2.469150
0.6				1.690839	1.661289	2.774023	2.712863
0.9				1.849082	1.802409	3.037372	2.942205
0.3	0.0	0.2	1.5	1.471667	1.436997	2.418817	2.363599
	0.1			1.489841	1.474345	2.444239	2.416626
	0.2			1.508605	1.511288	2.470231	2.469150
	0.3			1.527902	1.547834	2.496714	2.521178
0.3	0.2	0.0	1.5	1.492240	1.493998	2.449389	2.444653
		0.2		1.508605	1.511288	2.470231	2.469150
		0.4		1.555917	1.562471	2.531117	2.541787
		0.6		1.629652	1.645604	2.627655	2.660135
0.3	0.2	0.2	1.3	1.485668	1.475515	2.044150	2.026689
			1.5	1.508605	1.511288	2.470231	2.469150
			1.7	1.530987	1.546284	2.918229	2.940334
			1.9	1.552862	1.580573	3.386686	3.438981

Table 6.2: Local-Nusselt number for the incremented values of the flow parameters.

A	S	M	N _b	N _t	α	$-\left(Re_b\right)^{-\frac{1}{n+1}}Nu_x$	
						n = 0.50	n = 1.50
0.0	0.2	0.2	0.5	0.2	1.5	1.312273	1.478652
0.3						1.370060	1.516477
0.6						1.405775	1.544084
0.3	0.0	0.2	0.5	0.2	1.5	1.344122	1.447659
	0.2					1.356920	1.482358
	0.4					1.370060	1.516477
0.3	0.2	0.0	0.5	0.2	1.5	1.374596	1.518531
		0.2				1.370060	1.516477
		0.4				1.356849	1.510416
0.3	0.2	0.2	0.3	0.2	1.5	1.370060	1.516477
			0.5			1.370060	1.516477
			0.7			1.370060	1.516477
0.3	0.2	0.2	0.5	0.2	1.5	1.370060	1.516477
				0.4		1.350504	1.490996
				0.6		1.331269	1.465869
0.3	0.2	0.2	0.5	0.2	1.3	1.338812	1.484755
					1.5	1.370060	1.516477
					1.7	1.400434	1.547492

Table 6.3: A comparison of the local skin-friction for various values of α , when $S = 0$, $A = 1.5$, $M = 0.0$, $Pr = 1.0$, $Le = 0.0$, $N_b = 0.000002$ and $N_t = 0.0$ are fixed.

α	$\frac{1}{2} \left(Re_b \right)^{\frac{1}{n+1}} C_{fx} \left(\frac{U_w}{V_w} \right)$ $n = 0.50$		$\frac{1}{2} \left(Re_b \right)^{\frac{1}{n+1}} C_{fy} \left(\frac{U_w}{V_w} \right)$ $n = 0.50$	
	Current results Munir <i>et al.</i> [12]		Current results Munir <i>et al.</i> [12]	
0.2	-1.745057	-1.74610	-0.2447305	-0.24536
0.4	-1.797203	-1.79819	-0.5776021	-0.57842
0.6	-1.846428	-1.84739	-0.9776739	-0.97856

Table 6.4: A comparison of the local skin-friction for various values of α , when $S = 0$, $A = 1.5$, $M = 0.0$, $Pr = 1.0$, $Le = 0.0$, $N_b = 0.000002$ and $N_t = 0.0$ are fixed.

α	$\frac{1}{2} \left(Re_b \right)^{\frac{1}{n+1}} C_{fx} \left(\frac{U_w}{V_w} \right)$ $n = 1.50$		$\frac{1}{2} \left(Re_b \right)^{\frac{1}{n+1}} C_{fy} \left(\frac{U_w}{V_w} \right)$ $n = 1.50$	
	Current results Munir <i>et al.</i> [12]		Current results Munir <i>et al.</i> [12]	
0.2	-1.602168	-1.60218	-0.2354871	-0.23549
0.4	-1.660495	-1.66050	-0.5462859	-0.55234
0.6	-1.715682	-1.71569	-0.918764	-0.93386

Table 6.5: A comparison of the Nusselt number for various values of Pr, when $S = 0$, $A = 0.0$, $M = 0.0$, $n = 1$, $\alpha = 0$, $Le = 0.0$, $N_b = 0.000001$ and $N_t = 0.0$ are fixed.

$Re_b^{-\frac{1}{2}}Nu_x$			
Pr	Ishak <i>et al.</i> [76]	Elbashbeshy <i>et al.</i> [77]	Present result
0.72	0.8086	0.8086	0.8088342
1.0	1.0000	1.0000	1.0000080
10.0	3.7202	3.7204	3.7206360

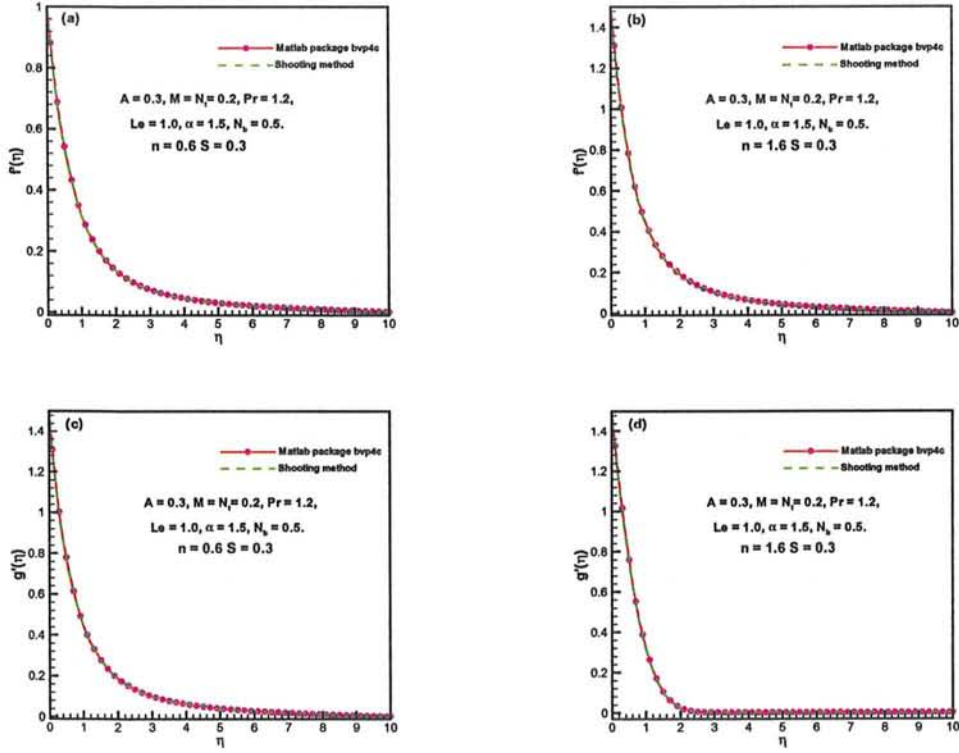


Fig. 6.1: Bvp4c and shooting methods comparison for velocity components.

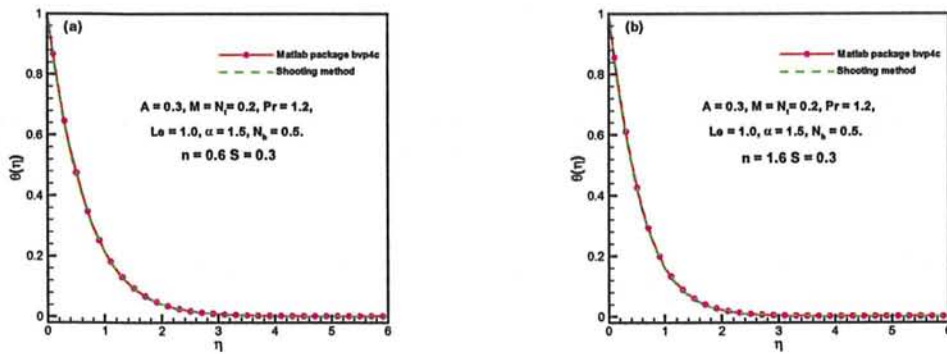


Fig. 6.2: Bvp4c and shooting method comparison for temperature distributions.

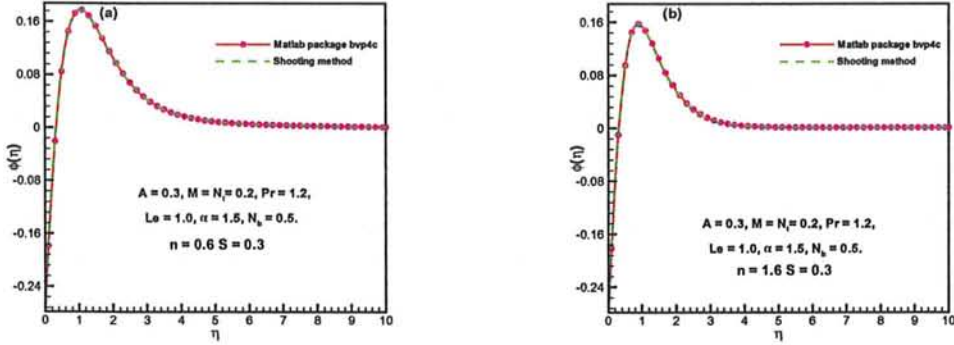


Fig. 6.3: Bvp4c and shooting method for comparison for concentration distribution.

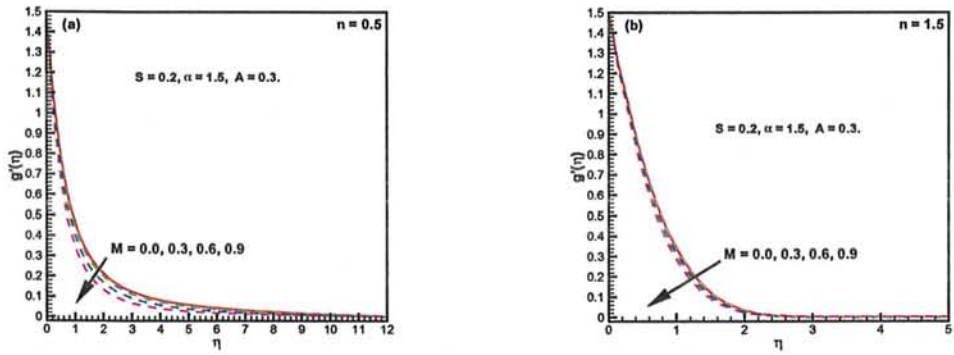


Fig. 6.4: Velocity behavior with M .

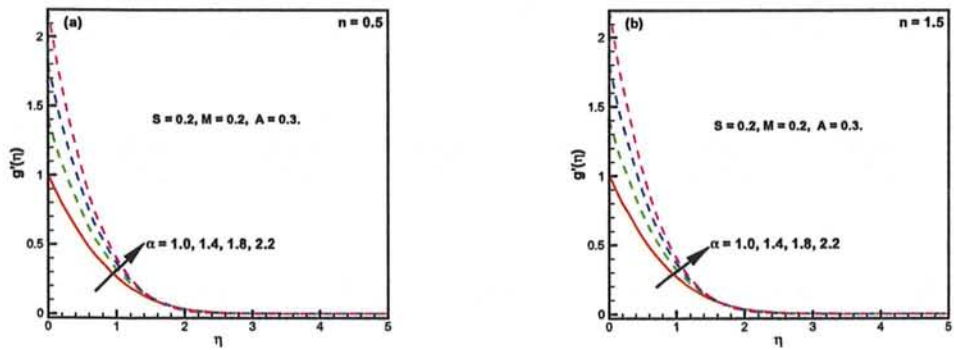


Fig. 6.5: Velocity behavior with α .

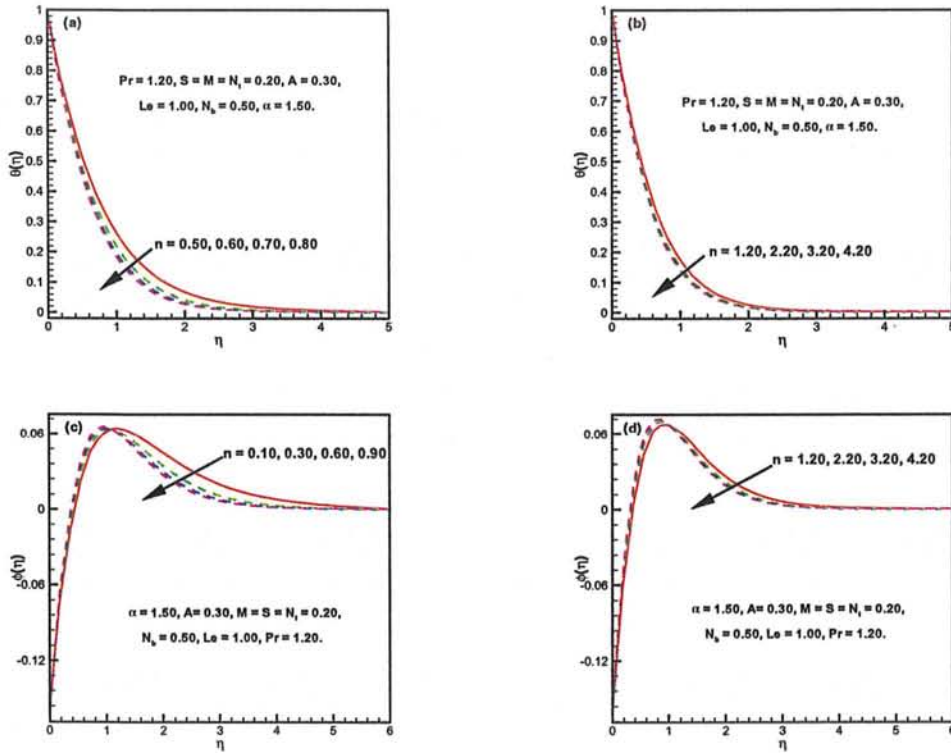


Fig. 6.6: Temperature and concentration behavior with n .

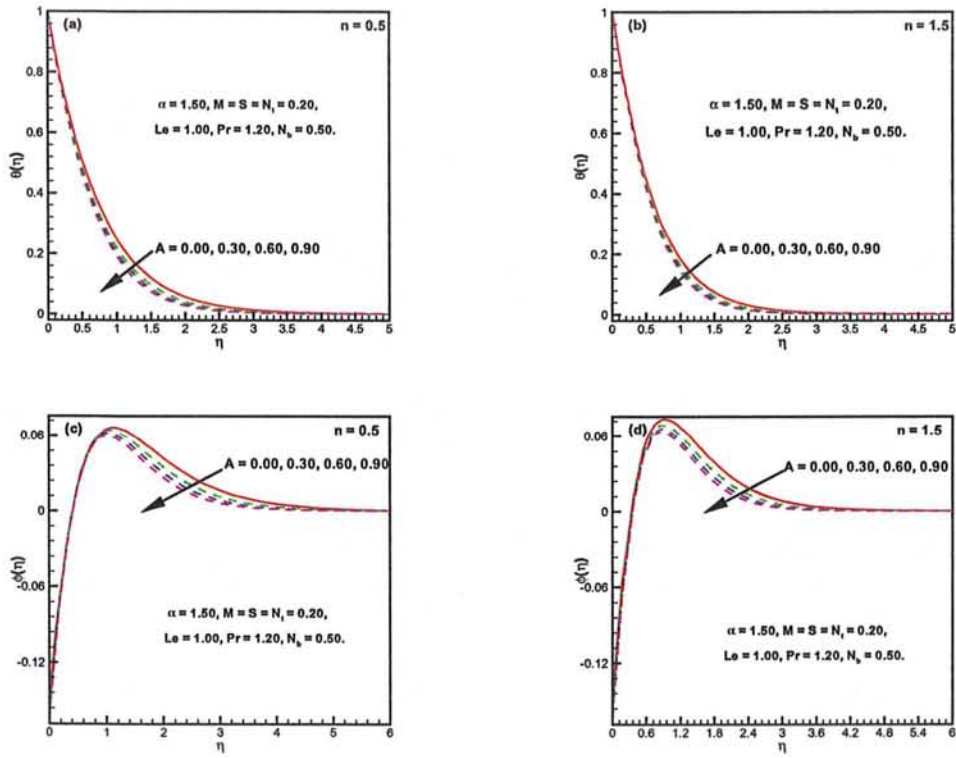


Fig. 6.7: Temperature and concentration behavior with A .

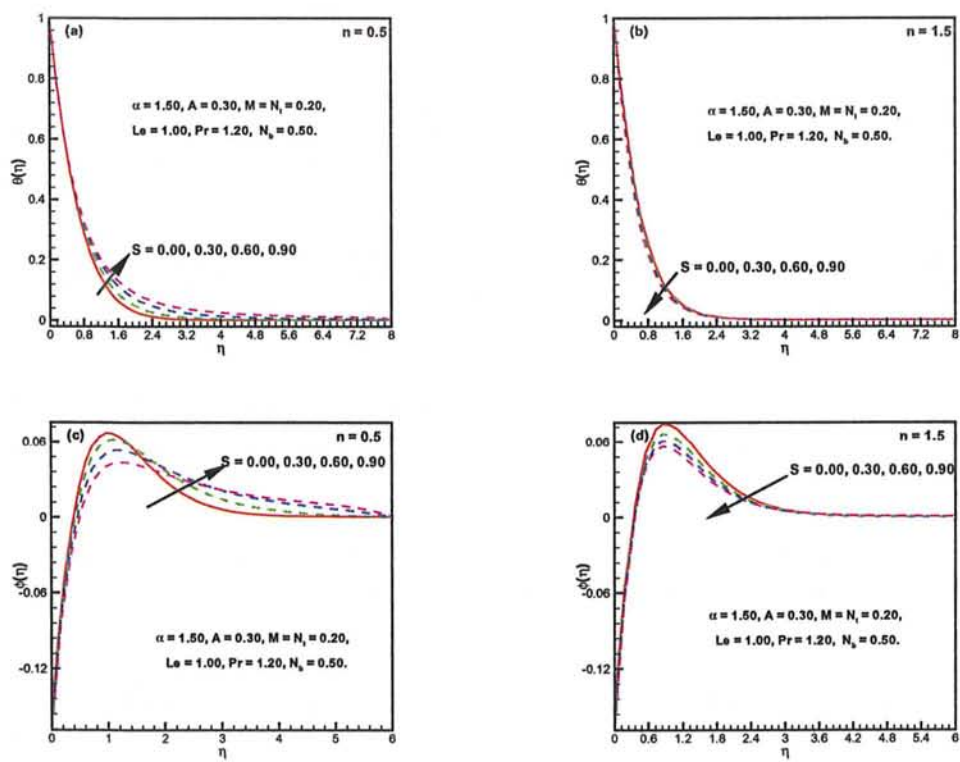


Fig. 6.8: Temperature and concentration behavior with S .

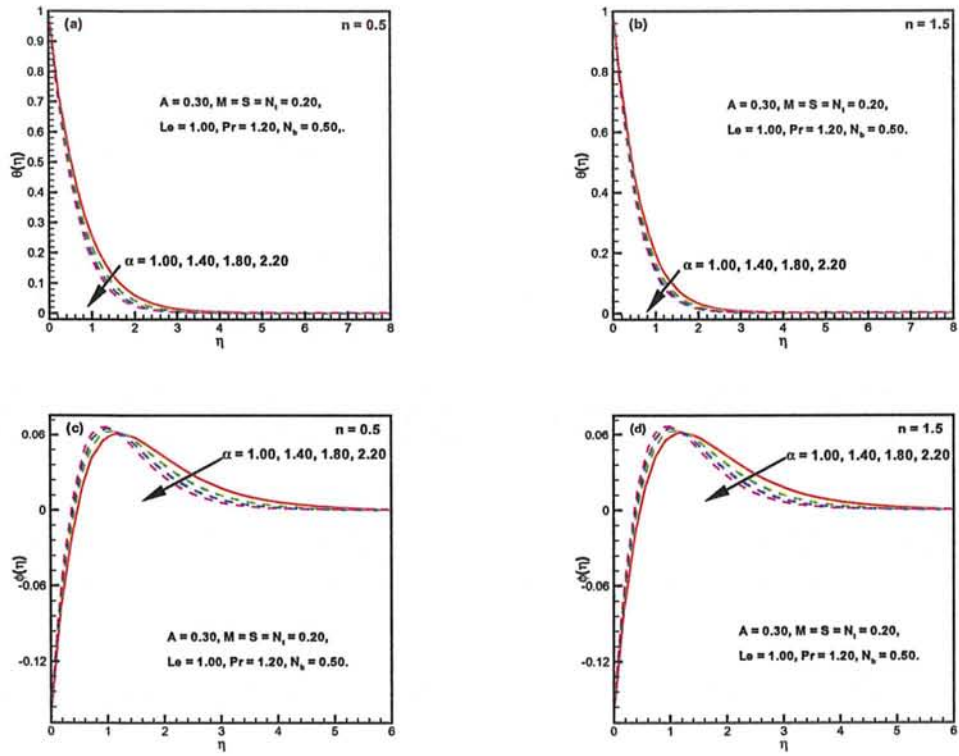


Fig. 6.9: Temperature and concentration behavior with α .

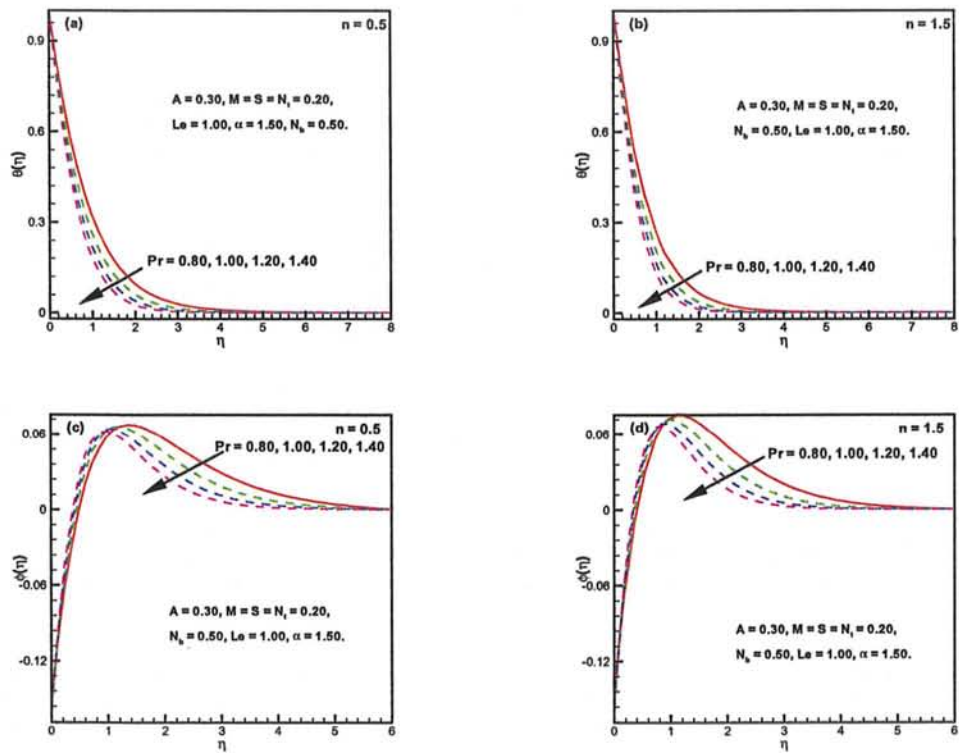


Fig. 6.10: Temperature and concentration behavior with Pr.

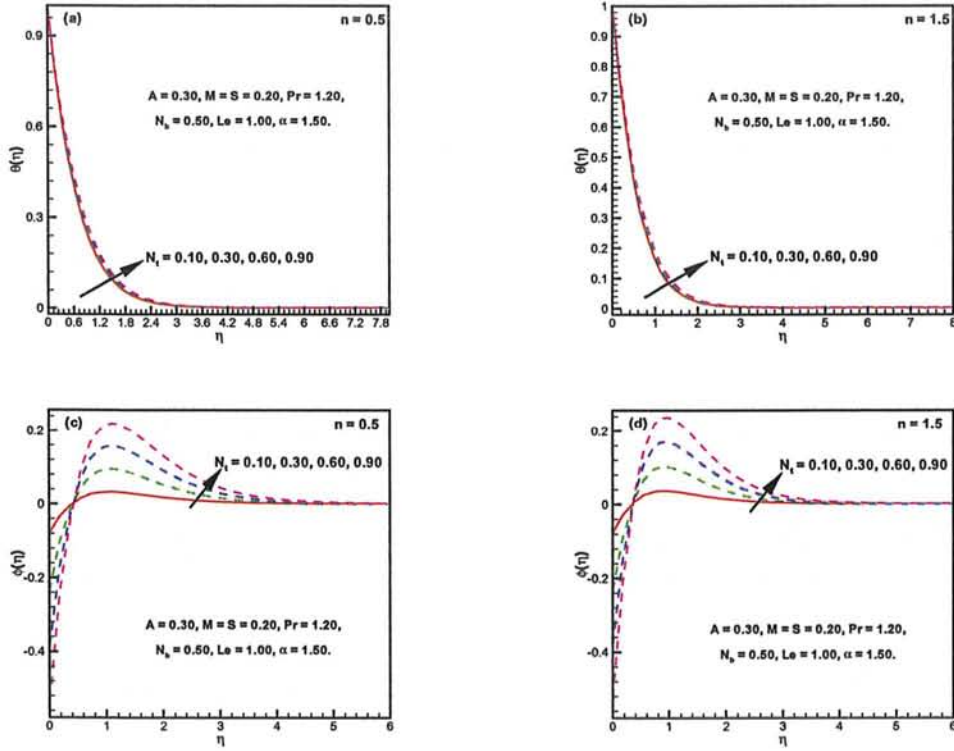


Fig. 6.11: Temperature and concentration behavior with N_t .

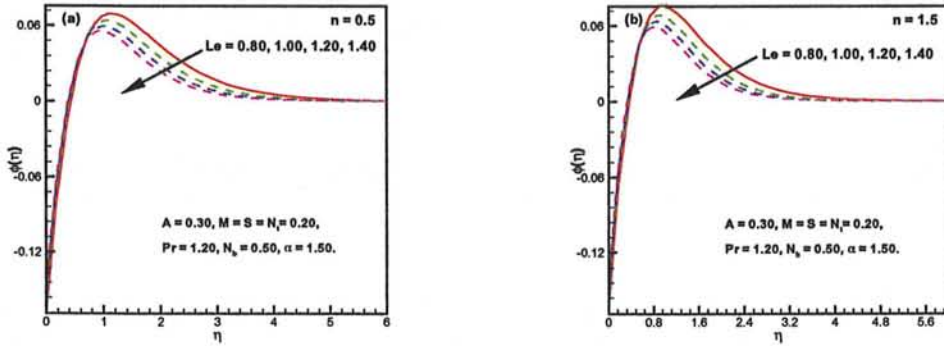


Fig. 6.12: Concentration behavior with Le .

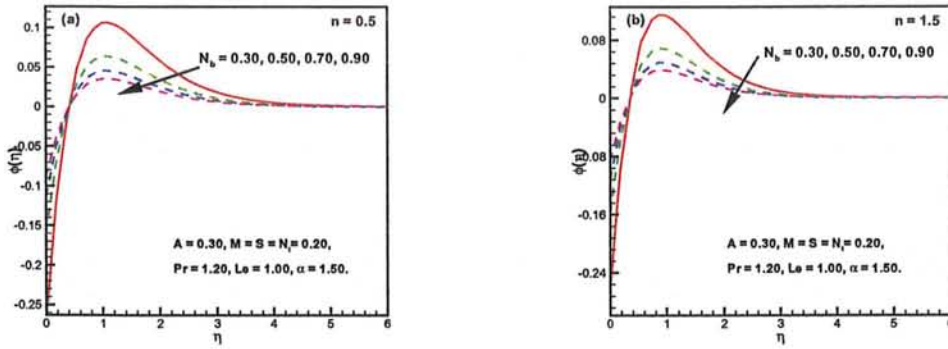


Fig. 6.13: Concentration behavior with N_b .

Chapter 7

Unsteady 3D Sisko Nano-magnetic Liquid Flow with Heat Absorption and Temperature Dependent Thermal Conductivity

The influence of temperature functional thermal conductivity and time-dependent flow of 3D Sisko liquid with convective surface constraints is incorporate. In addition, nano-materials are used in conjunction with magnetic and heat source/sink depicts. However, a theoretical and mathematical scenario has been presented to show the features of the novel parameters that are seemed in the flow problem. Moreover, the Biot number and heat source/sink parameter introduce a phenomenal prominence in the liquid flow temperature and concentration by presenting the pictorial characteristics. These parameters are showing guarantee for the enhancement of temperature and concentration of liquid while testing pseudo-plastic and dilatant cases of liquids. Meanwhile, the Biot number γ_1 illustrated a very novel significance during the rate transfer of mass and heat, where the rate transfer of heat uplifted and rate transfer of mass is found in reduction for pseudo-plastic and dilatant liquids. The second Biot number γ_2 demonstrated a reverse scenario

for the same physical features. In order to certify the entire novel work, we presented matching phenomenon and reached at the point once again that the results are matching in limiting conditions.

7.1 Flow Analysis

We assume an electrically conducted and incompressible 3D Sisko nanofluid flow over a bidirectional moving boundary with time and space dependent stretching velocities $U_w = \frac{cx}{1-\beta t}$ and $V_w = \frac{dy}{1-\beta t}$. Where the velocity U_w is along x -axis with stretching rate $c > 0$ and the velocity V_w is along y -axis with stretching rate $d > 0$. The disturbance in the fluid is restrained in the z -axis which vertical to the boundary of moving surface. It is also considered that the temperature and nano-particle fraction of the fluid adjacent to the wall of the sheet is larger than the temperature and nano-particle fraction at infinite distance. No slip between suspended nano-particles and base fluid is assumed due to the thermal equilibrium. Some more detail about the temperature differences which arises between the wall and away from the wall can be characterized with the help of heat generation/absorption and temperature dependent thermal conductivity. Specifically, surface conditions for transfer of heat and mass are imposed to elaborate the flow phenomenon. Foremost equations of the current unsteady flow under these aforesaid assumptions deliberated above are given by

$$\frac{\partial u}{\partial x} = -\left(\frac{\partial v}{\partial y} + \frac{\partial w}{\partial z}\right), \quad (7.1)$$

$$\frac{\partial u}{\partial t} + u \frac{\partial u}{\partial x} + \frac{b}{\rho_f} \frac{\partial}{\partial z} \left(-\frac{\partial u}{\partial z}\right)^n + \left(\frac{\sigma B_0^2}{\rho_f}\right) u = -\left(v \frac{\partial u}{\partial y} + w \frac{\partial u}{\partial z}\right) + \frac{a}{\rho_f} \left(\frac{\partial^2 u}{\partial z^2}\right), \quad (7.2)$$

$$\frac{\partial v}{\partial t} + u \frac{\partial v}{\partial x} - \frac{b}{\rho_f} \frac{\partial}{\partial z} \left(-\frac{\partial u}{\partial z}\right)^{n-1} \frac{\partial v}{\partial z} + \left(\frac{\sigma B_0^2}{\rho_f}\right) v = -\left(v \frac{\partial v}{\partial y} + w \frac{\partial v}{\partial z}\right) + \frac{a}{\rho_f} \left(\frac{\partial^2 v}{\partial z^2}\right), \quad (7.3)$$

$$\frac{\partial T}{\partial t} + u \frac{\partial T}{\partial x} - \frac{\partial}{\partial z} \left(k(T) \frac{\partial T}{\partial z}\right) = -\left(v \frac{\partial T}{\partial y} + w \frac{\partial T}{\partial z}\right) + \alpha_1 \left(\frac{\partial^2 T}{\partial z^2}\right)$$

$$\frac{Q_0}{(\rho c_p)_f} (T - T_f) + \tau^* \left[D_B \frac{\partial C}{\partial z} \left(\frac{\partial T}{\partial z} \right) + \frac{D_T}{T_\infty} \left(\frac{\partial T}{\partial z} \right)^2 \right], \quad (7.4)$$

$$\frac{\partial C}{\partial t} + u \frac{\partial C}{\partial x} - \frac{D_T}{T_\infty} \left(\frac{\partial^2 T}{\partial z^2} \right) = - \left(v \frac{\partial C}{\partial y} + w \frac{\partial C}{\partial z} \right) + D_B \left(\frac{\partial^2 C}{\partial z^2} \right). \quad (7.5)$$

The imposed boundary constraints are employed as follows:

$$\text{at } z = 0, \begin{cases} U_w = \frac{cx}{1-\beta t}, & V_w = \frac{dy}{1-\beta t}, & w = 0, \\ k \left(\frac{\partial T}{\partial z} \right) = h_f (T - T_f), & D_B \left(\frac{\partial C}{\partial z} \right) = k_m (C - C_f), \end{cases} \quad (7.6)$$

$$\text{as } z \rightarrow \infty, \quad u \rightarrow 0, \quad v \rightarrow 0, \quad T \rightarrow T_\infty \quad \text{and} \quad C \rightarrow C_\infty. \quad (7.7)$$

By plugging these set of (5.11), (5.12), (5.13) and (6.8) and the variable thermal conductivity defined through Eq. (2.8), the above model can then be transformed into non-linear ODEs as below:

$$\begin{aligned} Af''' - S \left[f' + \frac{2-n}{1+n} \eta f'' \right] + n (-f'')^{n-1} f''' \\ + \left(\frac{2n}{n+1} \right) f f'' - f'^2 + g f'' - M f' = 0, \end{aligned} \quad (7.8)$$

$$\begin{aligned} Ag''' - S \left[g' + \frac{2-n}{1+n} \eta g'' \right] + \left(\frac{2n}{n+1} \right) f g'' + (-f'')^{n-1} g''' \\ - (n-1) g'' f''' (-f'')^{n-2} - g'^2 + g g'' - M g' = 0, \end{aligned} \quad (7.9)$$

$$\begin{aligned} (1 + \varepsilon \theta) \theta'' + \text{Pr} \left(\frac{2n}{n+1} f + g \right) \theta' + \text{Pr} \lambda \theta - \text{Pr} S \left[\frac{2-n}{1+n} \eta \theta' \right] + \varepsilon (\theta')^2 \\ + \text{Pr} (N_b \theta' \phi' + N_t \theta'^2) = 0, \end{aligned} \quad (7.10)$$

$$\phi'' + \text{Le Pr} \left(\frac{2n}{n+1} f + g \right) \phi' - \text{Le Pr} S \left(\frac{2-n}{1+n} \right) \eta \phi' + \left(\frac{N_t}{N_b} \right) \theta'' = 0, \quad (7.11)$$

$$\text{at } \eta = 0, \quad \begin{cases} f = 0, & g = 0, & f' = 1, & g' = \alpha, \\ \theta' = -\gamma_1 \left[\frac{1-\theta}{1+\varepsilon\theta} \right], & \phi' = -\gamma_2 [1 - \phi], \end{cases} \quad (7.12)$$

$$\text{as } \eta \rightarrow \infty, \quad f' \rightarrow 0, \quad g' \rightarrow 0, \quad \theta \rightarrow 0, \quad \phi \rightarrow 0. \quad (7.13)$$

where the non-dimensional governing parameters are defined:

$$\lambda = \frac{Q_0 T_\infty}{(\rho c)_f (1 - \beta t)}, \quad \gamma_1 = \frac{h_f}{k} x Re_b^{-\frac{2}{n+1}}, \quad \gamma_2 = \frac{k_m}{D_B} x Re_b^{-\frac{2}{n+1}}. \quad (7.14)$$

7.2 Physical Quantities

Physical perspective of the Sisko nano-fluid flow shows the importance of many physical quantities namely skin-friction which represents resistance to the flow, local-Nusselt denotes the transfer rate of heat and the transfer of mass declared as Sherwood number. Representation of drag forces and transfer rate of mass and heat are the physical quantities to show a very significant role on the surface where the flow occurred. Such quantities of interest can be formulated in the subsequent form:

$$C_{fx} = \frac{\tau_{xz}}{\frac{1}{2}\rho U_w^2}, \quad C_{fy} = \frac{\tau_{yz}}{\frac{1}{2}\rho U_w^2}, \quad (7.15)$$

$$Nu_x = -\frac{x}{(T_f - T_\infty)} \left(\frac{\partial T}{\partial z} \right) \Big|_{z=0}, \quad (7.16)$$

$$Sh_x = -\frac{x}{(C_f - C_\infty)} \left(\frac{\partial C}{\partial z} \right) \Big|_{z=0}. \quad (7.17)$$

The aforementioned relations in the form of non-dimensional variables are

$$\frac{1}{2} Re_b^{\frac{1}{n+1}} C_{fx} = A f''(0) - (-f''(0))^n, \quad (7.18)$$

$$\frac{1}{2} Re_b^{\frac{1}{n+1}} C_{fy} = \frac{V_w}{U_w} [A g''(0) + (-f''(0))^{(n-1)} g''(0)], \quad (7.19)$$

$$\text{Re}^{-\frac{1}{n+1}} Nu_x = -\theta'(0), \quad (7.20)$$

$$\text{Re}^{-\frac{1}{n+1}} Sh_x = -\phi'(0). \quad (7.21)$$

7.3 Validation of Code

A comparison for verifications of the contemporary numerical solution with the exiting literature is accomplished by presenting the approximate values of skin-friction, local Nusselt number and local Sherwood number as shown in **table 7.4**. These computations are carried out in the absence of unsteadiness parameter, magnetic parameter, Lewis number, parameters of Brownian motion and thermophoresis parameter, respectively, and variable thermal conductivity. The generalized Biot numbers are taken very large as approaches to infinity. The other parameters are being considered as fixed. All the values in tables listed are near equal to the tabular values listed by Khan *et al.* [78].

7.4 Results Description

The unsteady numerical simulations of MHD 3D Sisko nano-fluid flow with temperature dependent thermal conductivity, convective BCs and heat source/sink are illustrated. The transformed nonlinear Eqs. (7.8) to (7.11) subject to the constraints (7.12) and (7.13) are considered to analyze the flow characteristics of the fluid. All the numerical consequences are revealed in the form of flow velocity, temperature and nano-particle volume fraction plots. The effect of all physical parameters are thoroughly examined which govern the flow namely the Sisko fluid parameter (A), index of power-law (n), stretching ratio parameter (α), Lewis number (Le), unsteadiness parameter (S), thermophoresis parameter (N_t), Brownian motion parameter (N_b), Prandtl number (Pr), magnetic parameter (M), variable thermal conductivity (ε), heat generation/absorption parameter (λ) and generalized Biot numbers (γ_1, γ_2).

The tabular outcomes of the skin-friction, local Nusselt and Sherwood numbers for

both cases, i.e., ($0 < n < 1$) and ($n > 1$) characteristics of fluids are determined to visualize the resistive forces, heat and mass transfer rates respectively, and presented in tables 7.1, 7.2 and 7.3. The resistive forces to the flow of the fluid are noticed in the increasing order when the unsteadiness parameter is increased as shown in table 7.1. In table 7.2, the diminishing behavior is observed whenever testing the impact of the heat sink/source parameter on the transfer rate. Effect of the parameter owing to Brownian motion and Biot numbers γ_1 on the transfer rate of heat is found in the decreasing and enhancing conduct, respectively. The transfer rate of mass is growing by Brownian motion parameter and Biot number γ_2 varying in an increasing order as shown in table 7.3.

7.5 Velocity Profiles

The impact of M on the profile of the fluid velocity is shown in Figs. 7.1(a,b). An uplifting in M resulted in a decay of velocity field while taking both cases of dilatant ($n < 1$) and pseudo-plastic ($0 < n < 1$) liquids. The the Lorentz forces are increasing by taking the strong magnetic field effect and this is why the velocity of the fluid is decreased. This trend is more remarkable in the case of shear-thinning fluids.

7.6 Temperature Profiles

The temperature of the fluid is portrayed in Figs. 7.2(a,b), where the increasing values of both the Sisko fluid and unsteadiness parameter are tested. In the preceding plots the profiles of the fluid temperature is described for increasing values of A is growing and a reverse conduct is depicted when the values of S are increasing. Both the situations of ($0 < n < 1$) and ($n > 1$) properties of fluids are considered, where the results are very clear in the shear-thinning fluid. Physically, the dependency of the fluid flow for the higher values of S shows that the rate of cooling is much slower and will take minimum time during the steady flows as illustrated in Fig. 7.2(b).

The decreases in $\theta(\eta)$ through **Fig. 7.3(a)** due to increasing of stretching ratio parameter and this reduction can be indorsed to the increased evaporation in the liquid. The enhancement in the stretching ratio parameter attains the evaporation of ambient liquid and increased toward the isothermal stretched surface. As a result the local fluid temperature decreases. In **Fig. 7.3(b)**, the effect of the growing values of Pr is presented and the temperature of the fluid flow reducing along with the TBLT reduces while considering both cases of pseudo-plastic and dilatant liquids. In both figures the results are very much appropriate in case of pseudo plastic as compared to dilatant fluids. In physical sense, the higher values of Pr causes a reduction in conduction due to low thermal conductivity the related TBLT. Moreover, an increase in Pr at the surface of the nanofluids which causes a rise in heat transfer rate and due to enhancement of the temperature gradient.

Fig. 7.4(a) shows the temperature profiles for growing values of Lewis number Le where the noticeable diminishing behavior is observed by temperature fields. The depict of Biot number γ_1 on the field of temperature and is presented in **Fig. 7.4(b)**, in which a critical enhancement is reported for both cases of $(0 < n < 1)$ and $(n > 1)$ and the related TBLT is also augmented. Physically, it is because of the measure of the ratio of conduction resistance to convection resistance inside of the body. Whenever γ_1 increases, the plate thermal resistance decreases and the non-dimensional surface temperature rises in both cases. In the restrictive case, when γ_1 declared a very large quantity, the dimensionless surface temperature reaches at its maximum value (isothermal condition).

A minor declining effect of Biot number γ_2 in plots of $\theta(\eta)$ is demonstrated in **Fig. 7.5(a)**, where the relevant TBLT is also reduced with the applications of both conditions of pseudo-plastic and dilatant liquids. A very significant behavior is observed in pseudo-plastic fluid as compared to dilatant fluid. On the other hand the effect of λ on $\theta(\eta)$ is shown in **Fig. 7.5(b)** and an increasing trend adjacent to the sheet is noticed for $(0 < n < 1)$ and $(n > 1)$ along with the allied TBLT. In physical view, the attribution of the fact that whenever the values of λ increases, the production of a hot layer of fluid is appeared near the surface and therefore the temperature is increases and this is while

reductions occurs in the transfer rate of heat from the boundary.

Fig. 7.6(a) depicts the influence of thermal conductivity on $\theta(\eta)$ for pseudo-plastic fluid and dilatant liquid. In case of pseudo-plastic fluid the outcomes are more manifest. The temperature field as well as the related TBLT are also increased. The impact of N_t on $\theta(\eta)$ and the associated TBLT is noticed in the escalating order as shown in **Fig. 7.6(b)**. Basically, this is due to the reason that by rising N_t , the dissimilarity between the surface temperature and location temperature increases which causes growth in $\theta(\eta)$. Through **Fig. 7.7(a)** an enhancement conduct is noticed when the values of N_b are increased and the TBLT is reported to boost for both cases ($0 < n < 1$) and ($n > 1$). Examining the physical aspects of N_b on $\theta(\eta)$, we detect that when the parameter N_b enhances, the random motion of the nano-particles escalating. This is why the temperature profile of the nanoparticles is enhanced. The magnetic effect on $\theta(\eta)$ and associated TBLT is observed in the escalating behavior where both cases ($0 < n < 1$) and ($n > 1$) are tested as depicted in **Fig. 7.7(b)**. Meanwhile the influence of magnetic parameter on an electrically conducting liquid upshots in a resistive sort of forces called as Lorentz force, which has propensity to rise the temperature profile. Because of this, the magnetic field impact has numerous probable control-based uses like the resembling electromagnetic forming of metals in MHD power generation, MHD ion population etc.

7.7 Concentration Profiles

Fig. 7.8(a) demonstrates the impact of A on the nano-materials concentration $\phi(\eta)$ and related CBLT, very small decrement is found in concentration profiles. The pseudo-plastic ($0 < n < 1$) liquid and dilatant ($n > 1$) liquid conditions are applied. Influence of S is illustrated through **Fig. 7.8(b)** and the graphical results and the relevant CBLT shows boosting conduct. It is owing to the situation that S is inversely proportional to the stretching coefficient c . Therefore a rise in S reduces the stretching rate. As the velocity declines significantly which enhances $\phi(\eta)$ as well as the associated CBLT.

The growing trends is noticeable by the concentration profiles $\phi(\eta)$ in Fig. 7.9(a) while testing different values of α and this effect also escalates the associated CBLT. Fig. 7.9(b) is indication towards the effect of Pr on $\phi(\eta)$ and associated CBLT, respectively, increases. Physically, inverse relation between thermal conductivity and Pr demonstrates heat diffusion rate from the surface. The higher the values of Pr implies to low heat diffusion rate from the sheet.

Figs. 7.10(a) and 7.10(b) exhibit the impact of Le and γ_1 on $\phi(\eta)$ and found in significant conduct. For a base fluid of assured kinematic viscosity ν , a higher Le implies an inferior Brownian diffusion coefficient D_B which leads to shorter penetration deepness for CBLT as we perceived in the plot. If the convective heat of the sheet is growing alternatively, the thermal penetration deepness rises. Therefore, the concentration is obsessed by the temperature field, one expects that a higher γ_1 would stimulate a more depth penetration of the concentration. This eagerness is actually realized in the preceding figure and which implies higher concentrations at increasing values of γ_1 .

Through Fig. 7.11(a) the enhancing effect is displayed by $\phi(\eta)$ for growing values of γ_2 . The CBLT of concentration profile rises with the increase of Biot number. Physical significance of this effect is explained above in detail. Furthermore, the influence of λ is shown in Fig. 7.11(b). To interpret the physical aspects of the concentration of the fluid flow, a growing situation is perceived while plotting $\phi(\eta)$ and its relevant CBLT is also raised.

The impacts of N_t and N_b on $\phi(\eta)$ are tested through graphs plotted in Figs. 7.12(a) and 7.12(b). The behavior of $\phi(\eta)$ is higher, when we varying the values of N_t in increasing order and a same trend is observed while using the increasing values of N_b during the portraying of $\phi(\eta)$ as shown in Fig. 7.12(b). Physically, the random motion of the nanofluid increases with the increase in N_b , whereas N_b is kept in enrichment order. The influence tested causes decrease in $\phi(\eta)$.

Table 7.1: Testing of resistive forces with variation of controlling parameters.

A	S	M	α	$-\frac{1}{2} \left(\text{Re}_b \right)^{\frac{1}{n+1}} C_{fx}$		$-\frac{1}{2} \left(\text{Re}_b \right)^{\frac{1}{n+1}} C_{fy} \left(\frac{U_w}{V_w} \right)$	
				$n = 0.5$	$n = 1.5$	$n = 0.5$	$n = 1.5$
1.0	0.2	0.2	1.5	1.871886	1.611681	3.068527	3.489146
1.3				2.009747	1.061501	3.294339	3.770665
1.6				2.138669	1.929547	3.505221	3.977659
1.9				2.260406	2.134144	3.704064	5.064756
1.2	0.0	0.2	1.5	1.900203	1.674699	3.130234	3.934534
	0.2			1.964892	1.899536	3.220902	3.074173
	0.4			2.029973	2.065704	3.311985	3.277913
	0.6			2.095227	2.207032	3.403229	3.492805
1.2	0.2	0.0	1.5	1.942754	1.864645	3.190721	3.025719
		0.3		1.992238	1.941608	3.258258	3.127344
		0.6		2.134084	2.167892	3.453254	3.425954
		0.9		2.351597	2.313938	3.75588	3.746374
1.2	0.2	0.2	1.2	1.907677	1.842199	2.382011	2.218939
			1.4	1.946051	1.880279	2.93258	2.778990
			1.6	1.983515	1.918143	3.517553	3.376522
			1.8	2.020143	1.95661	4.134894	4.011131

Table 7.2: Heat transfer rate for distinct leading parameter.

S	N_b	N_t	ε	λ	γ_1	γ_2	$-\left(Re_b\right)^{-\frac{1}{n+1}} Nu_x$	
							$n = 0.8$	$n = 1.8$
0.0	0.5	0.2	0.2	0.2	0.8	0.8	0.419915	0.4056838
0.2							0.4040555	0.4506852
0.4							0.3833639	0.4451075
0.2	0.2	0.2	0.2	0.2	0.8	0.8	0.4209792	0.4643934
	0.4						0.409745	0.4552936
	0.6						0.398321	0.4460394
0.2	0.5	0.1	0.2	0.2	0.8	0.8	0.4100231	0.4555609
		0.3					0.3980188	0.4457605
		0.5					0.3857454	0.4357718
0.2	0.5	0.2	0.0	0.2	0.8	0.8	0.3974259	0.4441975
			0.2				0.4040555	0.4506852
			0.4				0.4112208	0.4575416
0.2	0.5	0.2	0.2	0.0	0.8	0.8	0.4313932	0.4671937
				0.2			0.4040555	0.4506852
				0.4			0.3673692	0.4312704
0.2	0.5	0.2	0.2	0.2	0.4	0.8	0.2692334	0.2890302
					0.6		0.3463764	0.3799939
					0.8		0.4040555	0.4506852
0.2	0.5	0.2	0.2	0.2	0.8	0.4	0.413592	0.4588244
						0.6	0.4082851	0.4543484
						0.8	0.4040555	0.4506852

Table 7.3: Mass transfer rate for distinct leading parameters.

S	N_b	N_t	Le	ε	γ_1	γ_2	$-\left(Re_b\right)^{-\frac{1}{n+1}} Sh_x$	
							$n = 0.8$	$n = 1.8$
0.0	0.5	0.2	1.0	0.2	0.8	0.8	0.437383	0.4220338
0.2							0.4257258	0.4572825
0.4							0.4112959	0.4524949
0.2	0.2	0.2	1.0	0.2	0.8	0.8	0.3648144	0.3985029
	0.4						0.4155686	0.4474801
	0.6						0.4325002	0.4638209
0.2	0.5	0.1	1.0	0.2	0.8	0.8	0.4427412	0.4741172
		0.3					0.4097782	0.4413584
		0.5					0.3810772	0.412242
0.2	0.5	0.2	1.0	0.2	0.8	0.8	0.4257258	0.4572825
			1.3				0.4622709	0.4915485
			1.6				0.4892774	0.5167112
0.2	0.5	0.2	1.0	0.0	0.8	0.8	0.4251665	0.4566129
				0.2			0.4257258	0.4572825
				0.4			0.4263165	0.4579819
0.2	0.5	0.2	1.0	0.2	0.4	0.8	0.4369348	0.4693267
					0.6		0.430457	0.4625035
					0.8		0.4257258	0.4572825
0.2	0.5	0.2	1.0	0.2	0.8	0.4	0.2689472	0.2822936
						0.6	0.3564601	0.3790033
						0.8	0.4257258	0.4572825

Table 7.4: A comparison of the transfer rate of heat and mass for various values of n , when $S = M = \lambda = \varepsilon = \alpha = 0$, $Le = 1.5$, $N_b = 0.1$, $Pr = 1.0$, $A = 0.5$ and $N_t = 0.1$ are fixed.

n	$-Re_b^{-\frac{1}{n+1}} Nu_x$		$-Re_b^{-\frac{1}{n+1}} Sh_x$	
	Khan <i>et al.</i> [78]	Present results	Khan <i>et al.</i> [78]	Present results
1	0.085352	0.08537674	0.752096	0.7515991
2	0.086843	0.08689009	0.864615	0.8657731

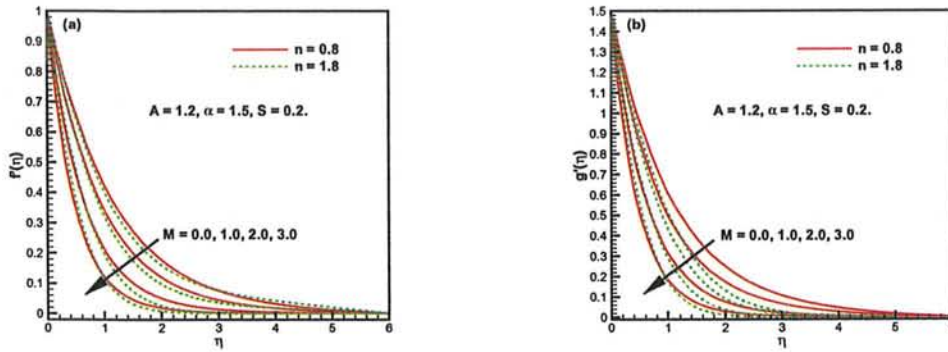


Fig. 7.1: Behavior of the components of velocity for M .

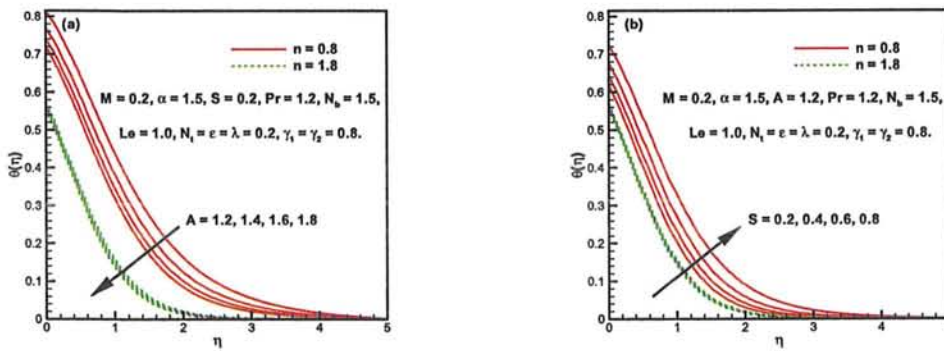


Fig. 7.2: Effect of A and S on $\theta(\eta)$.

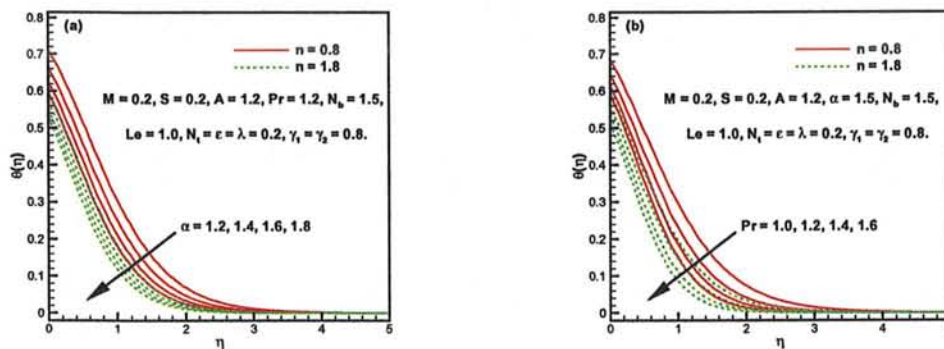


Fig. 7.3: Effect of α and Pr on $\theta(\eta)$.

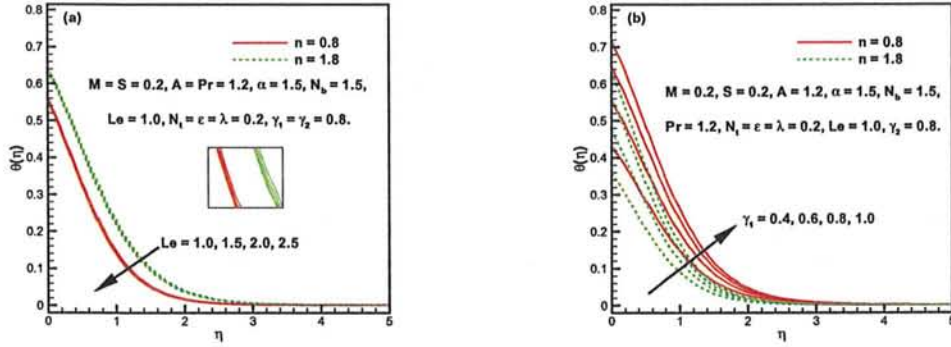


Fig. 7.4: Effect of Le and γ_1 on $\theta(\eta)$.

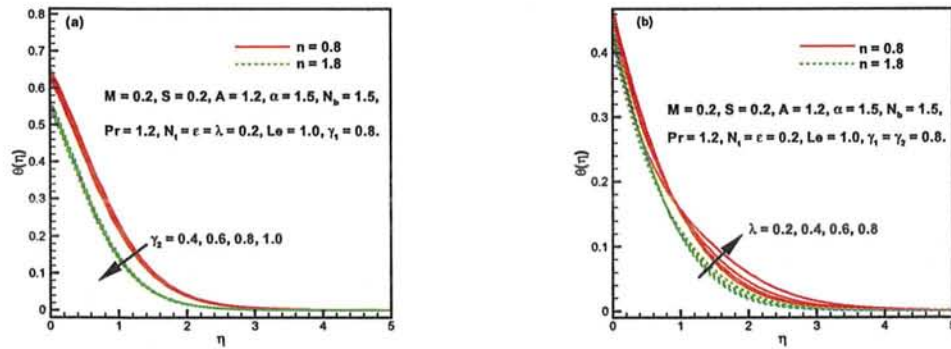


Fig. 7.5: Effect of γ_2 and λ on $\theta(\eta)$.

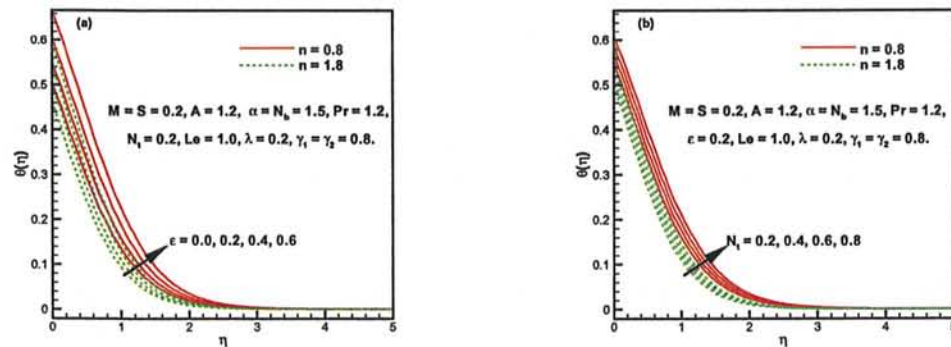


Fig. 7.6: Effect of ϵ and N_t on $\theta(\eta)$.



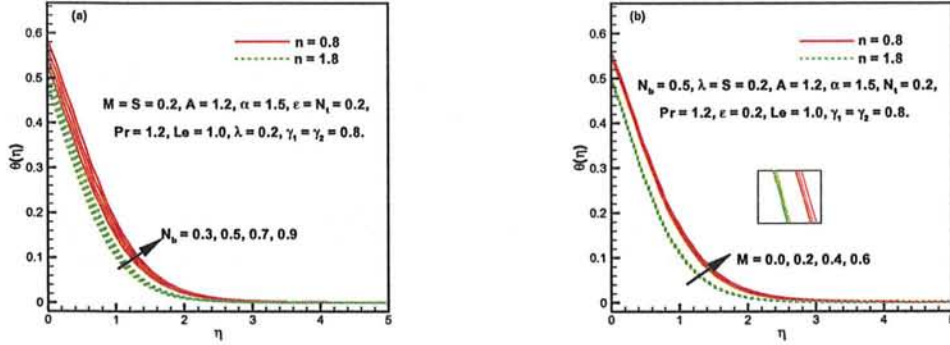


Fig. 7.7: Effect of N_b and M on $\theta(\eta)$.

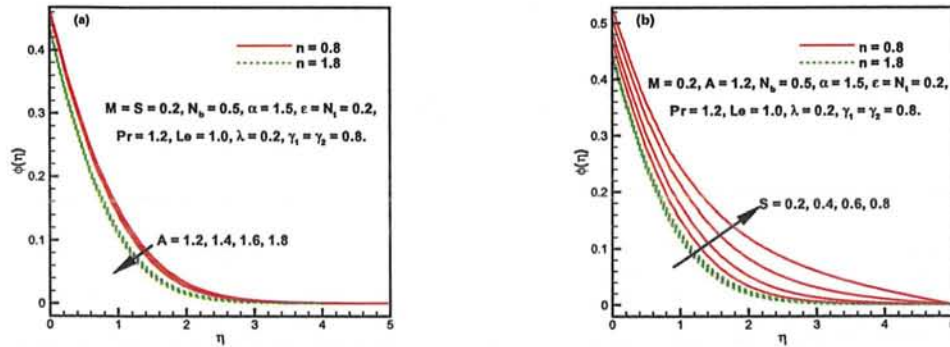


Fig. 7.8: Effect of A and S on $\phi(\eta)$.

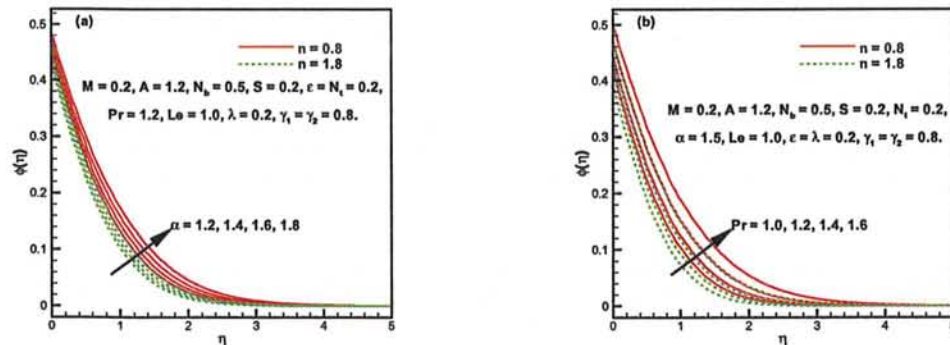


Fig. 7.9: Effect of α and Pr on $\phi(\eta)$.

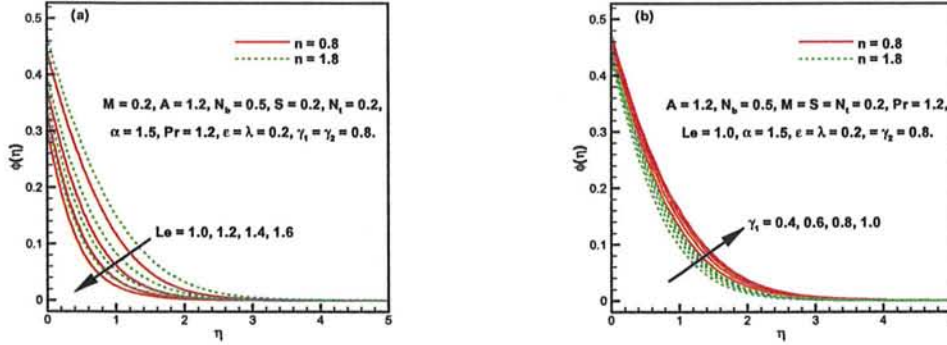


Fig. 7.10: Effect of Le and γ_1 on $\phi(\eta)$.

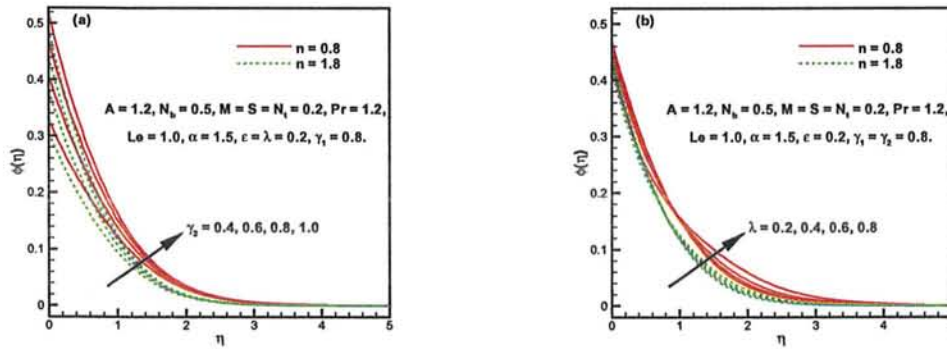


Fig. 7.11: Effect of γ_2 and λ on $\phi(\eta)$.

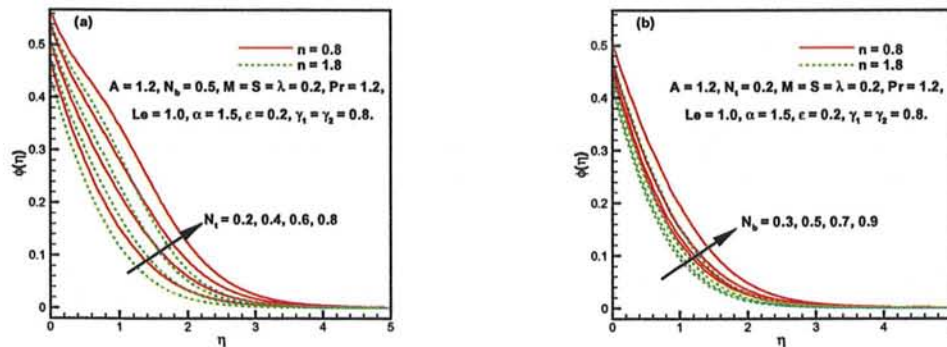


Fig. 7.12: Effect of N_t and N_b on $\phi(\eta)$.

Chapter 8

Chemically reactive Flow of MHD Transient 3D Sisko Liquid with Thermal Radiation

In this chapter, significant considerations are given to the 3D flow of Sisko liquid in view of chemical reaction in the form of homogeneous-heterogeneous and nonlinear thermal radiation effects. Here the flow is considered time-dependent with an external applied magnetic field. This flow is initiated by an external agents namely the bidirectional stretching velocities. The anticipated problem is initially formulated in the form of PDEs and then converted to ODEs by utilizing some dimensionless variables. These resulting ODEs are highly nonlinear in nature and are tackled with numerical scheme. It is noted from the field of temperature which raise by taking the higher values of R_d and θ_w with both constraints of power-law liquids, i.e., dilatant ($n > 1$) and pseudo-plastic ($0 < n < 1$). In the same way, the concentration profile is detected in the diminishing trend for the growing values of homogeneous-heterogeneous parameters (k_1, k_2). Additionally, the problem further expressed by examining in custom of resistive forces and transfer rate of heat. This phenomenon will explore the flow resistance and transfer rate of heat. The tabular values of resistive forces demonstrate a declining conduct for the uplifting values

of α and similarly the local-Nusselt number exhibits an uplifting trend with the variation in R_d and θ_w . These trends are confirmed by using a comparison between two methods namely, bvp4c and shooting with RKF. Moreover, a comparison with the previous data presents more validation of the proposed problem.

8.1 Problem Description

Consider the unsteady 3D generalized Newtonian fluid flow with thermally radiative heat and chemically reacting mass transfer with the application of magnetic field. The liquid flow is owing to the time-dependent stretching velocities at $z = 0$ as $U_w = \frac{cx}{1-\beta t}$ and $V_w = \frac{dy}{1-\beta t}$, having same magnitude but in opposed direction. The magnetic field applied in a parallel direction, i.e., along z -axis and is considered with uniform magnitude. The moving boundary temperature is $T_w = T_\infty + \frac{e^*x}{1-\beta t}$ and the concentration of the liquid at the stretching boundary kept constant. The liquid temperature and solute concentration of material away from the boundary are taken as T_∞ and C_∞ , respectively. Chaudhary and Merkin [37, 38] introduced a simple interaction of chemical reaction namely heterogeneous-homogeneous in this flow problem as discussed in earlier chapter (cf. chapter 4). By using the approximation of BLF and the aforementioned assumption the mass, force, energy and concentration balance equations are reduced in the following relations:(cf. chapter 6)

$$\frac{\partial u}{\partial x} = -\left(\frac{\partial v}{\partial y} + \frac{\partial w}{\partial z}\right), \quad (8.1)$$

$$\frac{\partial u}{\partial t} + u \frac{\partial u}{\partial x} + \frac{b}{\rho_f} \frac{\partial}{\partial z} \left(-\frac{\partial u}{\partial z}\right)^n + \left(\frac{\sigma B_0^2}{\rho_f}\right)u = -\left(v \frac{\partial u}{\partial y} + w \frac{\partial u}{\partial z}\right) + \frac{a}{\rho_f} \left(\frac{\partial^2 u}{\partial z^2}\right), \quad (8.2)$$

$$\frac{\partial v}{\partial t} + u \frac{\partial v}{\partial x} - \frac{b}{\rho_f} \frac{\partial}{\partial z} \left(-\frac{\partial u}{\partial z}\right)^{n-1} \frac{\partial v}{\partial z} + \left(\frac{\sigma B_0^2}{\rho_f}\right)v = -\left(v \frac{\partial v}{\partial y} + w \frac{\partial v}{\partial z}\right) + \frac{a}{\rho_f} \left(\frac{\partial^2 v}{\partial z^2}\right), \quad (8.3)$$

$$\frac{\partial T}{\partial t} + u \frac{\partial T}{\partial x} + \frac{1}{(\rho c)_f} \left(\frac{\partial q_r}{\partial z}\right) = -\left(v \frac{\partial T}{\partial y} + w \frac{\partial T}{\partial z}\right) + \alpha_1 \left(\frac{\partial^2 T}{\partial z^2}\right), \quad (8.4)$$

$$\frac{\partial a_1}{\partial t} + u \frac{\partial a_1}{\partial x} + k_1^* a_1 b_1^2 = - \left(v \frac{\partial a_1}{\partial y} + w \frac{\partial a_1}{\partial z} \right) + D_A \left(\frac{\partial^2 a_1}{\partial z^2} \right), \quad (8.5)$$

$$\frac{\partial b_1}{\partial t} + u \frac{\partial b_1}{\partial x} - k_1^* a_1 b_1^2 = - \left(v \frac{\partial b_1}{\partial y} + w \frac{\partial b_1}{\partial z} \right) + D_B \left(\frac{\partial^2 b_1}{\partial z^2} \right). \quad (8.6)$$

Eqs. (8.2)-(8.6) are subjected to the subsequent BCs:

$$\text{at } z = 0, \begin{cases} U_w = \frac{cx}{1-\beta t}, & V_w = \frac{dy}{1-\beta t}, & w = 0, & T = T_w, \\ D_A \left(\frac{\partial a_1}{\partial z} \right) = k_1^* a_1, & D_B \left(\frac{\partial b_1}{\partial z} \right) = -k_2^* a_1, \end{cases} \quad (8.7)$$

$$\text{as } z \rightarrow \infty, \quad u \rightarrow 0, \quad v \rightarrow 0, \quad T \rightarrow T_\infty, \quad a_1 \rightarrow a_0 \quad \text{and} \quad b_1 \rightarrow 0. \quad (8.8)$$

Again, by making use of the set of non-dimensional variables (4.12) and (5.11-5.13), in view of Eq. (3.9), the above Eqs. (8.2)-(8.6) and the BCs (8.7) and (8.8) reduce in the following way:

$$A f''' - S \left[f' + \frac{2-n}{1+n} \eta f'' \right] + \left(\frac{2n}{n+1} \right) f f'' - (f')^2 - M f' + n (-f'')^{n-1} f''' + g f'' = 0, \quad (8.9)$$

$$\begin{aligned} A g''' - S \left[g' + \frac{2-n}{1+n} \eta g'' \right] + \left(\frac{2n}{n+1} \right) f g'' + (-f'')^{n-1} g''' \\ - M g' - (n-1) g'' f''' (-f'')^{n-2} - (g')^2 + g g'' = 0, \end{aligned} \quad (8.10)$$

$$\begin{aligned} [\{1 + (1 + \theta(\theta_w - 1))^3 R_d\} \theta']' + \text{Pr} \left(\frac{2n}{n+1} f + g \right) \theta' \\ - \text{Pr} S \left[\theta + \frac{2-n}{1+n} \eta \theta' \right] - \text{Pr} f' \theta = 0, \end{aligned} \quad (8.11)$$

$$\phi'' + Sc \left(\frac{2n}{n+1} f + g \right) \phi' - Sc S \left(\frac{2-n}{1+n} \eta \phi' \right) - Sck_1 (1-\phi)^2 \phi = 0, \quad (8.12)$$

$$\text{at } \eta = 0, \quad \begin{cases} f = 0, & g = 0, & f' = 1, \\ g' = \alpha, & \theta = 1, & \phi' = k_2\phi, \end{cases} \quad (8.13)$$

$$\text{as } \eta \rightarrow \infty, \quad f' \rightarrow 0, \quad g' \rightarrow 0, \quad \theta \rightarrow 0, \quad \phi \rightarrow 1. \quad (8.14)$$

In the overhead equations, prime designates the differentiation with admiration to η . The A_1^* and B_1^* are assumed to be analogous in size, then the subsequent relation will be obtained as follows:

$$\phi(\eta) + h(\eta) = 1. \quad (8.15)$$

The above relation is further a necessary condition to get Eq. (8.12).

The dimensionless flow parameters are illustrated as below:

$$k_1 = \frac{a_0^2 k_1^* x}{U_w}, \quad k_2 = \frac{k_2^* c x}{D_A} Re_b^{-\frac{1}{n+1}}, \quad R_d = \frac{16\sigma^* T_\infty^3}{3k^* k}, \quad \theta_w = \frac{T_w}{T_\infty}.$$

8.2 Physical Quantities

Physical quantities appearing in the chemically reactive and nonlinear thermally radiative 3D flow of magneto-Sisko fluid are the resistive forces namely skin-friction(resistive forces) and transfer rate of heat (local-Nusselt number). These physical quantities are computed in the tabular form for both ($0 < n < 1$) and ($n > 1$).

The aforesaid dimensionless relations are defined as:

$$\frac{1}{2} Re_b^{-\frac{1}{n+1}} C_{fx} = Af''(0) - (-f''(0))^n, \quad (8.18)$$

$$\frac{1}{2} Re_b^{-\frac{1}{n+1}} C_{fy} = \frac{V_w}{U_w} [(-f''(0))^{(n-1)} g''(0) + Ag''(0)], \quad (8.19)$$

$$Re_b^{-\frac{1}{n+1}} Nu_x = - [1 + R_d \theta_w^3] \theta'(0). \quad (8.20)$$

8.3 Validation of Scheme

The computations presented in this study are validated viz tabular values of the resistive forces and transfer rate of heat as shown through tables 8.1 and 8.2. This comparison incorporates the effect of α on the resistive forces by keeping the other parameters fixed. These tabular values show an excellent agreement between bvp4c routine and shooting technique with RK-45 Fehlberg method. Another comparison of the current analysis is performed with the earlier published work by Malik *et al.* [11] and reveals a very good correlation with each other and is presented in table 8.3.

8.4 Computational Results and Discussion

A numerical technique is employed to solve the governing equations (8.9) to (8.12) with associated BCs (8.13) and (8.14). The present investigation is about the effect of heterogeneous-homogeneous reaction together with nonlinear thermal radiation on the 3D unsteady magneto-Sisko fluid flow. Various dimensionless quantities are tested and their effects on the profiles of velocity, temperature and concentration and is graphically presented and the approximated values of drag forces and transfer rate of heat are also computed. These governing parameters are: the material parameter (A), unsteadiness parameter (S), magnetic parameter (M), power law-index (n), Prandtl number (Pr), stretching ratio parameter (α), thermal radiation parameter (R_d), temperature ratio parameter (θ_w), Schmidt number (Sc), homogeneous parameter (k_1) and heterogeneous parameter (k_2).

8.4.1 Drag Forces and Heat Transfer Rate

Impact of M and S on drag force

The drag force coefficients are illustrated in tables 8.4 and 8.5. The local skin-friction in both cases of power-law fluids with the properties of pseudo-plastic fluid and dilatant fluid is found to be in increasing order with the enrichment values of M and S . The

physical perspective in this regard indicates that the flow resistance is due to Lorentz forces created by magnetic field.

Impact of R_d and θ_w on heat transfer rate

The depict of R_d and θ_w on the Nusselt number in case of pseudo-plastic fluid and dilatant fluid is presented in the form of tabular values and is displayed through **table 8.6**. The transfer rate of heat enhances in favor of these parameters. Physical significance concerning this effect shows that when the radiation is applied, the liquid temperature escalates. Impact of temperature ratio parameter on the transfer rate of heat is because of the higher fluid temperature as compared to ambient temperature.

8.4.2 Velocity Profiles

Influence of M on $f'(\eta)$ and $g'(\eta)$

Influence of enhancing values of M on velocity components $f'(\eta)$ and $g'(\eta)$ for both pseudo-plastic fluid and dilatant liquid causes a decay in velocity field as presented in **Figs. 8.1(a,b)**. Associated MBLT is also reduced. Physically, growth in Lorentz forces is due to the larger values of M and this is why the velocity of the fluid is declined.

8.4.3 Temperature Profiles

Influence of A and θ_w on $\theta(\eta)$

Through **Fig. 8.2(a)**, a declining conduct in profile of temperature is reported for the rising values of A for dilatant liquid and pseudo-plastic liquid as well. fluid. The TBLT is also found in the reducing order. Results obtained while portraying this figure are more noticeable in the pseudo plastic fluid condition. From physical point of view the diminishing effect in the consistency index, i.e., viscosity of fluid is due to the higher values of A . Another very effective plot in **Fig. 8.2(b)** is illustrated to show the impact of the increasing values of θ_w on $\theta(\eta)$ showing enhancement conduct. The associated TBLT is

found in the escalating order. Both cases of this fluid model, i.e., shear-thickening and shear-thinning are tested but a remarkable result is noticed in the shear-thinning case. The enhancement in temperature of such type of fluid model is due to the temperature ratio parameter and it is because of the larger value of the fluid temperature.

Influence of Pr and R_d on $\theta(\eta)$

By utilizing both restrictions of dilatant and pseudo-plastic, temperature and the associated TBLT are continuously decreasing inside the BL for the growing values of Pr and is demonstrated in **Fig. 8.3(a)**. This is identified that with the higher values of Pr and which causes fast rate of cooling, while diminishing of temperature occurs during this variation. The significance growing effect of the augmented values of R_d on $\theta(\eta)$ is sketched in **Fig. 8.3(b)**. Physically, this effect indicates that radiation supplied to the fluid flow will enhance the transfer rate of heat and as a result the fluid temperature increases.

Influence of M and α on $\theta(\eta)$

Fig. 8.4(a) elucidates the impact of M on $\theta(\eta)$ for both pseudo-plastic and dilatant liquids as well and a remarkable enhancement in the temperature of fluid is seen. The relevant TBLT is also enhanced for rising values function of M . This increasing agent of the fluid temperature is accountable for the enrichment of Lorentz forces. Other important behavior of the growing values of α on $\theta(\eta)$ is portrayed in **Fig. 8.4(b)**, where the temperature of the fluid is increasing. This effect is because of the distance increasing amongst the fluid particles and as a result the heat transfer rate shall be slowly down.

8.4.4 Concentration Profiles

Influence of α and Sc on $\phi(\eta)$

In **Figs. 8.5(a,b)**, the concentration $\phi(\eta)$ of the fluid flow is recorded in escalating conduct while testing both the conditions, i.e., pseudo plastic fluid and dilatant fluid with variation of α and Sc . This effect is observed with in the BL and the associated CBLT is also increased. **Fig. 8.6(a)** displays the increasing conduct in the concentration species of the fluid and this is because of the higher values of stretching ratio parameter. More stretching of the surface will increase mass transfer rate. **Fig. 8.6(b)** shows the impact of Sc on $\phi(\eta)$ and therefore this effect is because of the ratio of viscous diffusion rate and molecular diffusion rate. Thus more amount of Sc will enhance concentration species.

Influence of S and M on $\phi(\eta)$

Impact of S on $\phi(\eta)$ is demonstrated through **Fig. 8.7(a)**, an uplift in $\phi(\eta)$ is visualized for increasing values of S . This effect is observed for both cases, i.e., pseudo-plastic and dilatant liquids. In both cases the concentration and corresponding CBLT increases. Effect of M on $\phi(\eta)$ is illustrated in **Fig. 8.7(b)**. The concentration of the species and the associated CBLT diminishes for increasing values of M . The Lorentz forces introduced with the help of M while plotting the concentration distribution causing a resistive drag force and as a result less mass will be transfer.

Influence of k_1 and k_2 on $\phi(\eta)$

The impact of k_1 and k_2 on $\phi(\eta)$ is shown through **Figs. 8.8(a,b)**. From these figures, a declining behavior is observed. The graphs displayed are further tested for both constraints, i.e., ($0 < n < 1$) and ($n > 1$) properties of fluids. Whereas the associated CBLT of reactants is reported in the increasing order as the concentration of the liquid is carried away from the wall. Depreciation of $\phi(\eta)$ in case of both reactant parameters k_1 and k_2 is because of the fact that the reaction rates dominate diffusion coefficients.

Table 8.1: Comparison of bvp4c and shooting technique, while fixing $A = 0.2, S = 0.2, M = 0.2, R_d = 1.0, Pr = 1.2, \theta_w = 1.2, k_1 = 0.2, k_2 = 0.6$ and $Sc = 1.0$.

$-\frac{1}{2} \left(Re_b \right)^{\frac{1}{n+1}} C_{fx}$				
Parameter	bvp4c		shooting method	
α	$n = 0.8$	$n = 1.8$	$n = 0.8$	$n = 1.8$
0.2	1.245485	1.210381	1.245485	1.21038
0.4	1.27748	1.254568	1.27748	1.254567
0.6	1.308056	1.29697	1.308056	1.29697
$-\frac{1}{2} \left(Re_b \right)^{\frac{1}{n+1}} C_{fy} \left(\frac{U_w}{V_w} \right)$				
Parameter	bvp4c		shooting method	
α	$n = 0.8$	$n = 1.8$	$n = 0.8$	$n = 1.8$
0.2	0.1874347	0.1885341	0.1874348	0.1885339
0.4	0.4257742	0.4257988	0.4257743	0.4257985
0.6	0.7052276	0.7056185	0.7052277	0.7056181

Table 8.2: Comparison of bvp4c and shooting technique, while fixing $A = 0.2, S = 0.2, M = 0.2, \alpha = 0.5, Pr = 1.2, \theta_w = 1.2, k_1 = 0.2, k_2 = 0.6$ and $Sc = 1.0$.

$-\left(Re_b \right)^{-\frac{1}{n+1}} Nu_x$				
Parameter	bvp4c		shooting method	
R_d	$n = 0.8$	$n = 1.8$	$n = 0.8$	$n = 1.8$
1.0	1.815448	1.919434	1.815448	1.919434
1.2	1.891554	1.992434	1.891554	1.992434
1.4	1.961893	2.059251	1.961893	2.059251

Table 8.3: Comparison of present work with previous results, while fixing $S = \alpha = 0.0$.

$-\frac{1}{2}Re_b^{\frac{1}{n+1}}C_f$		
n	Present results	Malik <i>et al.</i> [11]
1.0	2.000008	2.00000
2.0	1.914495	1.914495
3.0	1.875080	1.875081

Table 8.4: The local-skin-friction Coefficient variation with A , S , M and α , when $Pr = 1.2$, $R_d = 1.0$, $\theta_w = 1.2$, $k_1 = 0.2$, $k_2 = 0.6$ and $Sc = 1.0$.

A	S	M	α	$-\frac{1}{2}\left(Re_b\right)^{\frac{1}{n+1}}C_{fx}$	
				$n = 0.8$	$n = 1.8$
0.1	0.2	0.2	0.5	1.235467	1.229421
0.3				1.34679	1.321894
0.5				1.448259	1.411706
0.1	0.0	0.2	0.5	1.180555	1.142934
	0.1			1.20795	1.186503
	0.2			1.235467	1.229421
0.1	0.2	0.0	0.5	1.217823	1.211355
		0.2		1.235467	1.229421
		0.4		1.286565	1.282907
0.1	0.2	0.2	0.2	1.190714	1.164741
			0.4	1.220898	1.208323
			0.6	1.249739	1.250132

Table 8.5: The local-skin-friction Coefficient variation with A , S , M and α , when $Pr = 1.2$, $R_d = 1.0$, $\theta_w = 1.2$, $k_1 = 0.2$, $k_2 = 0.6$ and $Sc = 1.0$.

A	S	M	α	$-\frac{1}{2} \left(Re_b \right)^{\frac{1}{n+1}} C_{fy} \left(\frac{U_w}{V_w} \right)$	
				$n = 0.8$	$n = 1.8$
0.1	0.2	0.2	0.5	0.5362644	0.5399272
0.3				0.5841034	0.5811563
0.5				0.6277770	0.6211994
0.1	0.0	0.2	0.5	0.5257358	0.4933554
	0.1			0.5283926	0.5168608
	0.2			0.5362644	0.5399272
0.1	0.2	0.0	0.5	0.5257358	0.5302135
		0.2		0.5362644	0.5399272
		0.4		0.5663981	0.5603459
0.1	0.2	0.2	0.2	0.1794329	0.1812007
			0.4	0.4072864	0.4098021
			0.6	0.6741979	0.6798624

Table 8.6: The local-Nusselt number variation with A , S , M , α , Pr , R_d and θ_w , when $k_1 = 0.2$, $k_2 = 0.6$ and $Sc = 1.0$.

A	S	M	α	Pr	R_d	θ_w	$-\left(Re_b\right)^{-\frac{1}{n+1}}Nu_x$	
							$n = 0.8$	$n = 1.8$
0.1	0.2	0.2	0.5	1.2	1.0	1.2	1.791724	1.823125
0.3							1.835962	1.868718
0.5							1.871799	1.906778
0.1	0.0	0.2	0.5	1.2	1.0	1.2	1.690877	1.638012
	0.1						1.740617	1.735306
	0.2						1.791724	1.823125
0.1	0.2	0.0	0.5	1.2	1.0	1.2	1.80152	1.827276
		0.2					1.791724	1.823125
		0.4					1.763769	1.811025
0.1	0.2	0.2	0.2	1.2	1.0	1.2	1.720181	1.751024
			0.4				1.768489	1.799538
			0.6				1.814445	1.846328
0.1	0.2	0.2	0.5	0.8	1.0	1.2	1.376801	1.38432
				1.0			1.592817	1.612378
				1.2			1.791724	1.823125
0.1	0.2	0.2	0.5	1.2	1.0	1.2	1.791724	1.823125
					1.2		1.865334	1.886941
					1.4		1.933073	1.945582
0.1	0.2	0.2	0.5	1.2	1.0	1.2	1.791724	1.892808
						1.4	1.943122	2.038512
						1.6	2.102364	2.187498



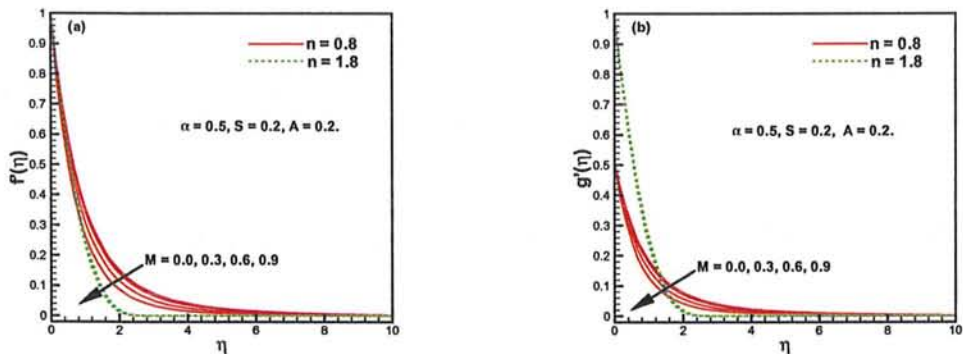


Fig. 8.1: Influence M on velocity components $f'(\eta)$ and $g'(\eta)$.

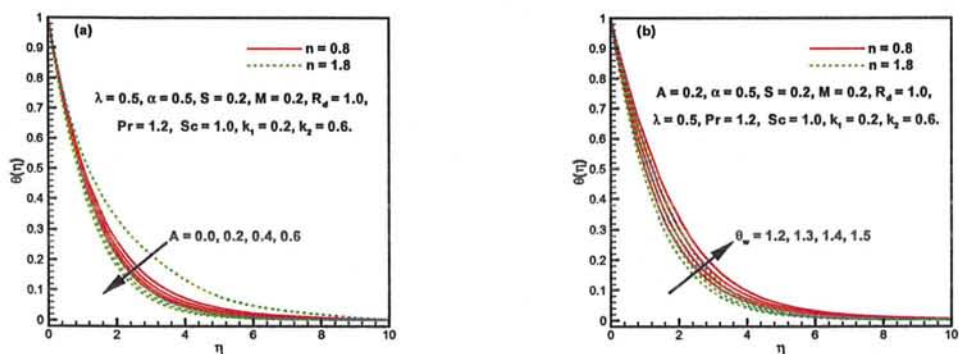


Fig. 8.2: Influence A and θ_w on temperature.

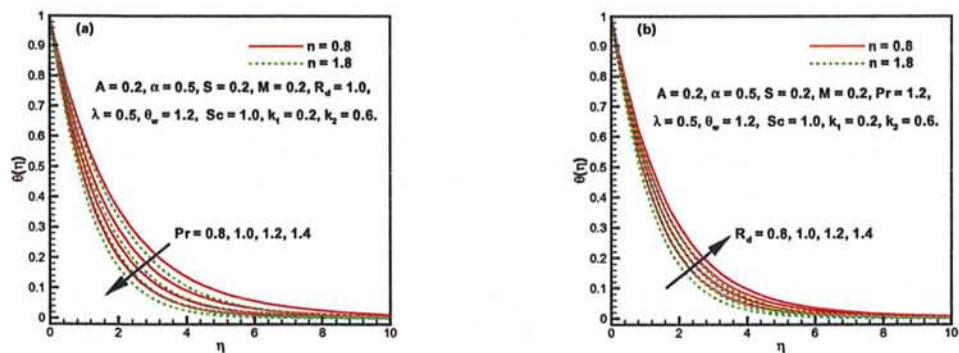


Fig. 8.3: Influence of Pr and R_d on temperature.

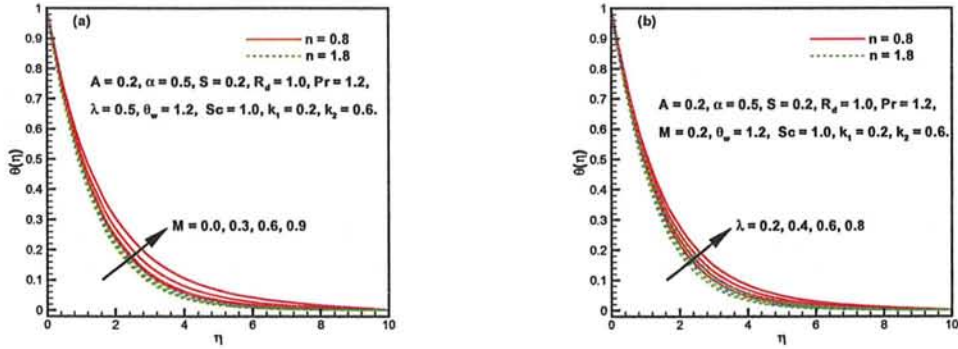


Fig. 8.4: Influence of M and α on temperature.

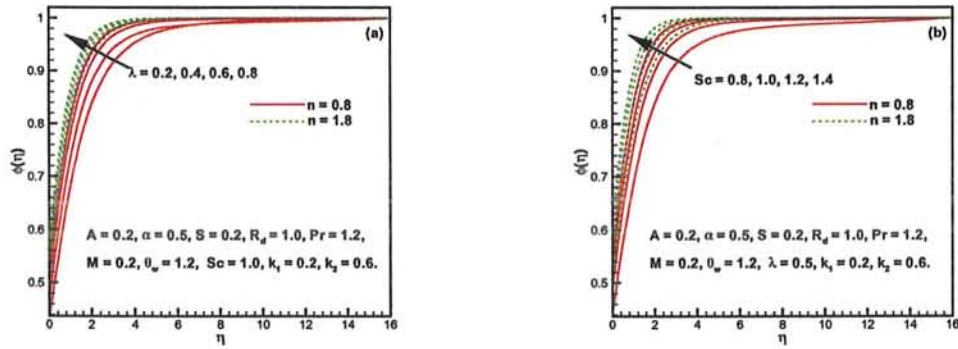


Fig. 8.5: Influence of α and Sc on concentration.

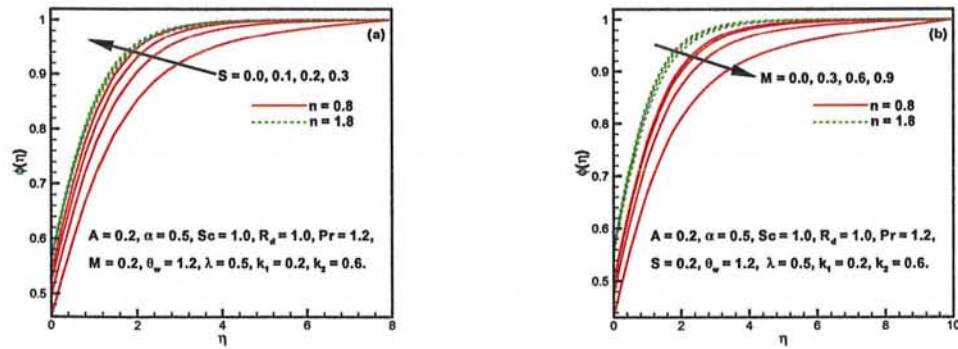


Fig. 8.6: Influence of S and M on concentration.

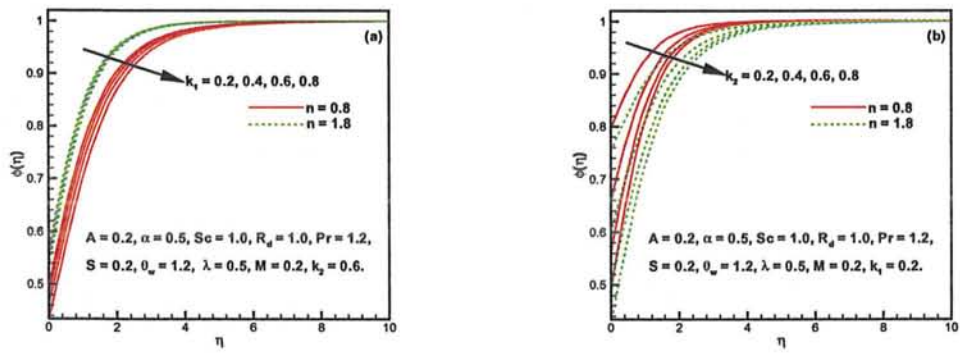


Fig. 8.7: Influence of k_1 and k_2 on concentration.

Chapter 9

Modeling and Computations of Sisko Liquid Flow with Transfer of Heat over a Curved Boundary

This chapter focuses on newly modeled flow of 2D Sisko liquid and transfer of heat mechanism over a curved moving boundary. The flow equations of Sisko fluid are formulated in the curvilinear coordinates system. By utilizing the curved system coordinates, the modeled PDEs are customized to non-linear ODEs while incorporating dimensionless variables. The numerical solutions of flow and transfer of heat balances are obtained through coding in MATLAB built in function `bvp4c`. An impact of increasing values of parameters due curved nature on the velocity causes an uprise for pseudo-plastic liquids. The diminishing trend of temperature field is the effective outcome of important radius of curvature parameter with enhancing values. Magnitude of the pressure inside the BL is observed in the form of reduction for pseudo-plastic liquids. Curvature parameter shows dominance trends in terms of the reducing depict while calculating transfer rate of heat and resistive forces. The current study is validated in case of infinite curvature parameter value for planner sheet case and tabular values demonstrate an excellent agreement with the existing literature.

9.1 Governing Equations

Keeping in mind the BL mathematical assumptions, the force balance equation is a constraining type of equation under the high Reynolds number (Re) due zero kinematic viscosity ν . An answer of these restricting conditions may consequently sensibly be required to depict approximately the laminar BLF for which Reynolds number is higher but not exactly infinite. For fluid flow with incompressible fluid condition, the conservation of mass, linear momentum as well as energy without body forces, are expressed in the vector notations as follows:

$$\text{div}\mathbf{V}=0, \quad (9.1)$$

$$\rho \left[-\mathbf{V} \times (\nabla \times \mathbf{V}) + \nabla \left(\frac{V^2}{2} \right) \right] = \text{div}\tau, \quad (9.2)$$

$$\rho c_p [(\mathbf{V} \cdot \nabla) T] = k \nabla^2 T. \quad (9.3)$$

For an incompressible 2D flow in curvilinear coordinates, we pursue the velocity and temperature fields as:

$$\mathbf{V} = [v(r, s), u(r, s), 0], \quad T = T(r, s), \quad (9.4)$$

where v and u are the velocity names responsible for the moments along r - and s - axes, respectively. By substituting Eq. (9.4) having in mind Eqs. (1.78) to (1.80)(cf. Chapter 1) and reference [70], the shear rate of Sisko fluid is given by

$$\left| \sqrt{\frac{1}{2} \text{tr}(\mathbf{A}_1^2)} \right|^{n-1} = \left[2 \left(\frac{\partial v}{\partial r} \right)^2 + \left(\frac{\partial u}{\partial r} + \frac{R}{r+R} \frac{\partial v}{\partial s} - \frac{u}{r+R} \right)^2 + 2 \left(\frac{R}{r+R} \frac{\partial u}{\partial s} + \frac{v}{r+R} \right)^2 \right]^{\frac{n-1}{2}}. \quad (9.5)$$

By plugging Eq. (9.5) into Eq. (1.78), we obtained the momentum equation. Thus

the governing equations for balance of mass and linear momentum as follows:

$$R \frac{\partial u}{\partial s} + \frac{\partial}{\partial r} \{(R+r)v\} = 0, \quad (9.6)$$

$$\begin{aligned} \rho \left[v \frac{\partial v}{\partial r} + \frac{Ru}{R+r} \frac{\partial v}{\partial s} - \frac{u^2}{R+r} \right] &= -\frac{\partial p}{\partial r} + \frac{2a}{R+r} \frac{\partial}{\partial r} \left[(R+r) \left(\frac{\partial v}{\partial r} \right) \right] \\ &+ \frac{2b}{R+r} \frac{\partial}{\partial r} \left[(R+r) \left\{ 2 \left(\frac{\partial v}{\partial r} \right)^2 + \left(\frac{\partial u}{\partial r} + \frac{R}{R+r} \frac{\partial v}{\partial s} - \frac{u}{R+r} \right)^2 \right\}^{\frac{n-1}{2}} \frac{\partial v}{\partial r} \right] \\ &+ \frac{Ra}{R+r} \frac{\partial}{\partial s} \left[\left(\frac{\partial u}{\partial r} + \frac{R}{R+r} \frac{\partial v}{\partial s} - \frac{u}{R+r} \right) \right] - \frac{2a}{R+r} \left(\frac{R}{R+r} \frac{\partial u}{\partial r} + \frac{v}{R+r} \right) \\ &+ \frac{Rb}{R+r} \frac{\partial}{\partial s} \left[\left\{ 2 \left(\frac{\partial v}{\partial r} \right)^2 + \left(\frac{\partial u}{\partial r} + \frac{R}{R+r} \frac{\partial v}{\partial s} - \frac{u}{R+r} \right)^2 \right\}^{\frac{n-1}{2}} \left(\frac{\partial u}{\partial r} + \frac{R}{R+r} \frac{\partial v}{\partial s} - \frac{u}{R+r} \right) \right] \\ &- \frac{2b}{R+r} \left[2 \left(\frac{\partial v}{\partial r} \right)^2 + \left(\frac{\partial u}{\partial r} + \frac{R}{R+r} \frac{\partial v}{\partial s} - \frac{u}{R+r} \right)^2 \right]^{\frac{n-1}{2}} \left(\frac{R}{R+r} \frac{\partial u}{\partial r} + \frac{v}{R+r} \right), \quad (9.7) \end{aligned}$$

$$\begin{aligned} \rho \left[v \frac{\partial u}{\partial r} + \frac{Ru}{r+R} \frac{\partial u}{\partial s} + \frac{uv}{r+R} \right] &= -\frac{R}{r+R} \frac{\partial p}{\partial s} \\ &+ \frac{a}{(r+R)^2} \frac{\partial}{\partial r} \left[(r+R)^2 \left(\frac{\partial u}{\partial r} + \frac{R}{r+R} \frac{\partial v}{\partial s} - \frac{u}{r+R} \right) \right] + \frac{2Ra}{r+R} \frac{\partial}{\partial s} \left[\left(\frac{R}{r+R} \frac{\partial u}{\partial s} + \frac{v}{r+R} \right) \right] \\ &+ \frac{b}{(r+R)^2} \frac{\partial}{\partial r} \left[(r+R)^2 \left\{ 2 \left(\frac{\partial v}{\partial r} + \frac{R}{r+R} \frac{\partial u}{\partial s} + \frac{v}{r+R} \right)^2 \right\}^{\frac{n-1}{2}} \left(\frac{\partial u}{\partial r} + \frac{R}{r+R} \frac{\partial v}{\partial s} - \frac{u}{r+R} \right) \right] \\ &+ \frac{2Rb}{r+R} \frac{\partial}{\partial s} \left[\left\{ 2 \left(\frac{\partial v}{\partial r} \right)^2 + \left(\frac{\partial u}{\partial r} + \frac{R}{r+R} \frac{\partial v}{\partial s} - \frac{u}{r+R} \right)^2 \right\}^{\frac{n-1}{2}} \left(\frac{R}{r+R} \frac{\partial u}{\partial s} + \frac{v}{r+R} \right) \right]. \quad (9.8) \end{aligned}$$

To make the above equations non-dimensional while using the standard approach, we take L as the typical length, U the reference speed and δ the BLT. Thus, we present the

subsequent dimensionless variables:

$$s^* = \frac{s}{L}, \quad r^* = \frac{r}{\delta}, \quad u^* = \frac{u}{U}, \quad v^* = \frac{v}{U} \frac{L}{\delta}, \quad p^* = \frac{p}{\rho U^2}. \quad (9.9)$$

In view of the above variables, we observe that balance Eqs. (9.7) and (9.8) go over in the non-dimensional form

$$\begin{aligned} & \frac{1}{Re} \left[+ \frac{Ru}{R+r} \frac{\partial v}{\partial s} + v \frac{\partial v}{\partial r} \right] - \epsilon \frac{u^2}{R+r} = -\epsilon \frac{\partial p}{\partial r} + \frac{1}{Re} \left[\frac{2}{R+r} \frac{\partial}{\partial r} \left\{ (R+r) \left(\frac{\partial v}{\partial r} \right) \right\} \right] \\ & + \frac{2}{R+r} \frac{1}{Re} \frac{\partial}{\partial r} \left[(R+r) \left\{ \begin{aligned} & 2 \left(\frac{\partial v}{\partial r} \right)^2 + \left(\frac{\partial u}{\partial r} + \frac{R}{R+r} \frac{\partial v}{\partial s} - \frac{u}{R+r} \right)^2 \\ & + 2 \left(\frac{R}{R+r} \frac{\partial u}{\partial s} + \frac{v}{R+r} \right)^2 \end{aligned} \right\}^{\frac{n-1}{2}} \frac{\partial v}{\partial r} \right] \\ & + \frac{R}{R+r} \frac{1}{Re} \frac{\partial}{\partial s} \left[\left(\frac{\partial u}{\partial r} + \frac{R}{R+r} \frac{\partial v}{\partial s} - \frac{u}{R+r} \right) \right] - \frac{1}{Re} \frac{2}{R+r} \left(\frac{R}{R+r} \frac{\partial u}{\partial r} + \frac{v}{R+r} \right) \\ & + \frac{R}{R+r} \frac{1}{Re} \frac{\partial}{\partial s} \left[\left\{ \begin{aligned} & 2 \left(\frac{\partial v}{\partial r} \right)^2 + \left(\frac{\partial u}{\partial r} + \frac{R}{R+r} \frac{\partial v}{\partial s} - \frac{u}{R+r} \right)^2 \\ & + 2 \left(\frac{R}{R+r} \frac{\partial u}{\partial s} + \frac{v}{R+r} \right)^2 \end{aligned} \right\}^{\frac{n-1}{2}} \left(\frac{\partial u}{\partial r} + \frac{R}{R+r} \frac{\partial v}{\partial s} - \frac{u}{R+r} \right) \right] \\ & - \frac{1}{Re} \frac{2}{R+r} \left[\begin{aligned} & 2 \left(\frac{\partial v}{\partial r} \right)^2 + \left(\frac{\partial u}{\partial r} + \frac{R}{R+r} \frac{\partial v}{\partial s} - \frac{u}{R+r} \right)^2 \\ & + 2 \left(\frac{R}{R+r} \frac{\partial u}{\partial s} + \frac{v}{R+r} \right)^2 \end{aligned} \right]^{\frac{n-1}{2}} \left(\frac{R}{R+r} \frac{\partial u}{\partial r} + \frac{v}{R+r} \right), \quad (9.10) \\ & \left[v \frac{\partial u}{\partial r} + \frac{Ru}{R+r} \frac{\partial u}{\partial s} + \frac{uv}{R+r} \right] = -\frac{1}{\rho} \frac{R}{R+r} \frac{\partial p}{\partial s} \\ & + \frac{2R}{R+r} \frac{1}{Re} \frac{\partial}{\partial s} \left[\left(\frac{R}{R+r} \frac{\partial u}{\partial s} + \frac{v}{R+r} \right) \right] \\ & + \frac{1}{(R+r)^2} \frac{\partial}{\partial r} \left[\begin{aligned} & \nu (R+r)^2 \left(\frac{\partial u}{\partial r} \right) \\ & + (R+r)^2 \frac{1}{Re} \frac{R}{R+r} \frac{\partial v}{\partial s} - \nu (R+r)^2 \frac{u}{R+r} \end{aligned} \right] \end{aligned}$$

$$\begin{aligned}
& + \frac{1}{(R+r)^2} \frac{\partial}{\partial r} \left[\begin{aligned} & \nu(R+r)^2 \left\{ 2 \left(\frac{\partial v}{\partial r} \right)^2 + \left(\frac{\partial u}{\partial r} + \frac{R}{R+r} \frac{\partial v}{\partial s} - \frac{u}{R+r} \right)^2 \right\}^{\frac{n-1}{2}} \frac{\partial u}{\partial r} \\ & + (R+r)^2 \frac{1}{Re} \frac{R}{R+r} \left\{ 2 \left(\frac{\partial v}{\partial r} \right)^2 + \left(\frac{\partial u}{\partial r} + \frac{R}{R+r} \frac{\partial v}{\partial s} - \frac{u}{R+r} \right)^2 \right\}^{\frac{n-1}{2}} \frac{\partial v}{\partial s} \\ & - \nu(R+r)^2 \left\{ 2 \left(\frac{\partial v}{\partial r} \right)^2 + \left(\frac{\partial u}{\partial r} + \frac{R}{R+r} \frac{\partial v}{\partial s} - \frac{u}{R+r} \right)^2 \right\}^{\frac{n-1}{2}} \frac{u}{R+r} \end{aligned} \right] \\
& + \frac{2R}{R+r} \frac{1}{Re} \frac{\partial}{\partial s} \left[\left(\frac{R}{R+r} \frac{\partial u}{\partial s} + \frac{v}{R+r} \right) \left\{ \begin{aligned} & \left(\frac{\partial u}{\partial r} + \frac{R}{R+r} \frac{\partial v}{\partial s} - \frac{u}{R+r} \right)^2 \\ & + 2 \left(\frac{\partial v}{\partial r} + \frac{R}{R+r} \frac{\partial u}{\partial s} + \frac{v}{R+r} \right)^2 \end{aligned} \right\}^{\frac{n-1}{2}} \right], \quad (9.11)
\end{aligned}$$

where asterisks have been omitted for simplicity. As in the usual boundary layer assumption, s , u and p having order 1 while r and v having order δ . Additionally, the parameter ϵ is also of order 1 and is defined as:

$$\epsilon = \frac{\nu}{uL} \left(\frac{L}{\delta} \right)^2. \quad (9.12)$$

With the above assumptions and keeping terms of order 1 or higher, we finally obtain the governing BLF equations in the form

$$\frac{\partial}{\partial r} \{(R+r)v\} = -R \frac{\partial u}{\partial s}, \quad (9.13)$$

$$\frac{u^2}{R+r} - \frac{1}{\rho} \frac{\partial p}{\partial r} = 0, \quad (9.14)$$

$$\begin{aligned}
& v \frac{\partial u}{\partial r} + \frac{Ru}{R+r} \left(\frac{\partial u}{\partial s} \right) + \frac{uv}{R+r} = -\frac{1}{\rho} \frac{R}{R+r} \frac{\partial p}{\partial s} \\
& + \frac{a/\rho}{(R+r)^2} \frac{\partial}{\partial r} \left[(R+r)^2 \left(\frac{\partial u}{\partial r} - \frac{u}{R+r} \right) \right] + \frac{b/\rho}{(R+r)^2} \frac{\partial}{\partial r} \left[(R+r)^2 \left(\frac{\partial u}{\partial r} - \frac{u}{R+r} \right)^n \right]. \quad (9.15)
\end{aligned}$$

Additionally, in view of the conventional BLF approach, we obtain the energy equation in the form

$$\rho c_p \left[v \frac{\partial T}{\partial r} + \frac{uR}{R+r} \left(\frac{\partial T}{\partial s} \right) \right] = k \left[\frac{\partial^2 T}{\partial r^2} + \frac{1}{R+r} \frac{\partial T}{\partial r} \right]. \quad (9.16)$$

9.2 Model Development

An incompressible steady flow of Sisko liquid over a moving curved boundary is considered. The flow geometry is sketched for this fluid while using curvilinear coordinate system. The flow structure is further shown through **Fig. 9.1**. The assumption related to the flow of liquid over this boundary allow to define the stretching velocity $U_w = cs$ along s - axis with stretching rate $c > 0$ and as a result the flow takes place in domain $r > 0$. The distance of the curved boundary from origin R concludes the shape of the bended boundary. Additionally, the analysis of transfer of heat is carried out with T_w as the temperature of the moving surface. The mass, force and energy balance governing equations of steady 2D Sisko liquid flow over the curved moving surface are expressed below:

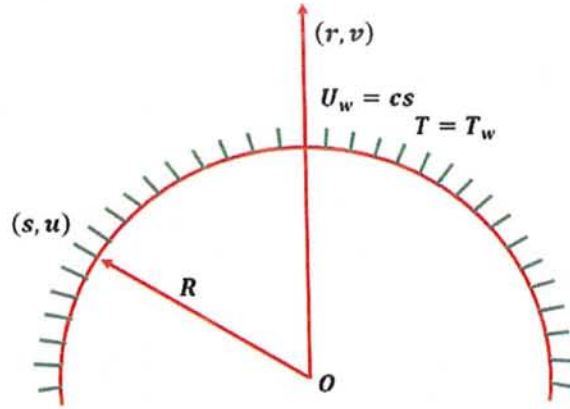


Fig. 9.1: Problem schematic representation

$$R \frac{\partial u}{\partial s} + \frac{\partial}{\partial r} \{ (R+r)v \} = 0, \quad (9.17)$$

$$\frac{u^2}{R+r} - \frac{1}{\rho} \frac{\partial p}{\partial r} = 0, \quad (9.18)$$

$$v \frac{\partial u}{\partial r} + \frac{uR}{R+r} \left(\frac{\partial u}{\partial s} \right) + \frac{uv}{R+r} = -\frac{1}{\rho} \frac{R}{R+r} \frac{\partial p}{\partial s} + \frac{a}{\rho(R+r)^2} \frac{\partial}{\partial r} \left[(R+r)^2 \left(\frac{\partial u}{\partial r} - \frac{u}{R+r} \right) \right] + \frac{b}{\rho(R+r)^2} \frac{\partial}{\partial r} \left[(R+r)^2 \left(\frac{\partial u}{\partial r} - \frac{u}{R+r} \right)^n \right], \quad (9.19)$$

$$v \frac{\partial T}{\partial r} + \frac{Ru}{R+r} \frac{\partial T}{\partial s} = \alpha_1 \left[\frac{\partial^2 T}{\partial r^2} + \frac{1}{R+r} \frac{\partial T}{\partial r} \right], \quad (9.20)$$

where $\alpha_1 (= \frac{k}{\rho c_p})$ is declared as thermal diffusivity regarding this liquid with ρ as the density of the base liquid, the specific heat and thermal conductivity of liquid are (c_p, k) , respectively. The associated BCs are of the form:

$$\text{at } r = 0, \begin{cases} U_w(s) = cs, v = 0, \\ T = T_w, \end{cases} \quad (9.21)$$

$$\text{as } r \rightarrow \infty, \quad u \rightarrow 0, \quad \frac{\partial u}{\partial r} \rightarrow 0 \quad \text{and} \quad T \rightarrow T_\infty. \quad (9.22)$$

The force and energy balance equations can be reduced into the coupled non-linear ODEs by using the subsequent suitable variables

$$u = U_w f'(\eta), \quad v = \frac{-U_w R}{R+r} Re_b^{-\frac{1}{n+1}} \left[\frac{2n}{n+1} f(\eta) + \frac{1-n}{1+n} \eta f'(\eta) \right],$$

$$\theta(\eta) = \frac{T - T_\infty}{T_w - T_\infty}, \quad p = \rho a^2 s^2 P(\eta), \quad \eta = \frac{r}{s} Re_b^{\frac{1}{n+1}}. \quad (9.23)$$

By substituting the dimensionless variables (9.23), Eq. (9.17) is verified identically and Eqs. (9.18) to (9.22) render into the form

$$\frac{\partial P}{\partial \eta} = \frac{f'^2}{K + \eta}, \quad (9.24)$$

$$\frac{2K}{K + \eta} P = \frac{K}{K + \eta} \left(\frac{2n}{n+1} \right) \left(f f'' + \frac{1}{K + \eta} f f' \right) + \frac{2}{K + \eta} \left(f'' - \frac{1}{K + \eta} f' \right)^n$$

$$\begin{aligned}
& -\frac{K}{K+\eta}f'^2 + A \left[f''' + \frac{1}{K+\eta}f'' - \frac{1}{(K+\eta)^2}f' \right] \\
& + n \left(f'' - \frac{1}{K+\eta}f' \right)^{n-1} \left(f''' - \frac{1}{K+\eta}f'' + \frac{1}{(K+\eta)^2}f' \right). \quad (9.25)
\end{aligned}$$

Eliminating the pressure term between Eqs. (9.24) and (9.25), we get the subsequent governing problem

$$\begin{aligned}
& A \left[f'''' + \frac{2}{K+\eta}f''' - \frac{1}{(K+\eta)^2}f'' + \frac{1}{(K+\eta)^3}f' \right] - \frac{2K}{K+\eta}f'f'' - \frac{2K}{(K+\eta)^2}f'^2 \\
& + \left(\frac{2n}{n+1} \right) \left[\frac{\frac{K}{K+\eta}(ff''' + f'f'')}{\frac{K}{(K+\eta)^2}(ff'' + f'^2)} - \frac{\frac{K}{(K+\eta)^3}ff'}{\frac{K}{(K+\eta)^3}ff'} \right] \\
& + n \left(f'' - \frac{1}{K+\eta}f' \right)^{n-1} \left(f'''' + \frac{2}{K+\eta}f''' - \frac{1}{(K+\eta)^2}f'' + \frac{1}{(K+\eta)^3}f' \right) \\
& + n(n-1) \left(f'' - \frac{1}{K+\eta}f' \right)^{n-2} \left(f''' - \frac{1}{K+\eta}f'' + \frac{1}{(K+\eta)^2}f' \right)^2 \\
& + 2n \left(f'' - \frac{1}{K+\eta}f' \right)^{n-1} \left(\frac{1}{K+\eta}f'''' - \frac{1}{(K+\eta)^2}f'' + \frac{1}{(K+\eta)^3}f' \right) = 0, \quad (9.26)
\end{aligned}$$

$$\theta'' + \frac{\text{Pr}K}{K+\eta} \left(\frac{2n}{n+1} \right) f\theta' + \frac{1}{K+\eta}\theta' = 0, \quad (9.27)$$

$$\text{at } \eta = 0, \quad \begin{cases} f = 0, & f' = 1, \\ \theta = 1, \end{cases} \quad (9.28)$$

$$\text{as } \eta \rightarrow \infty, \quad f' \rightarrow 0, \quad f'' \rightarrow 0, \quad \theta \rightarrow 0. \quad (9.28)$$

The leading quantities arising in modeling of the anticipated problem are given as:

$$\begin{aligned}
A &= \frac{Re_b^{\frac{2}{n+1}}}{Re_a}, \quad Re_a = \frac{U_w s \rho}{a}, \quad Re_b = \frac{U_w^{2-n} s^n \rho}{b}, \\
K &= \frac{R}{s} Re_b^{\frac{1}{n+1}}, \quad Pr = \frac{s U_w}{\alpha_1} Re_b^{-\frac{2}{n+1}}. \quad (9.30)
\end{aligned}$$

The drag forces in the form of local skin-friction and the transfer rate of heat in the form of local-Nusselt number are defined as follows:

$$C_f = \frac{\tau_{rs}}{1/2\rho U_w^2}, \text{ and } Nu_s = \frac{sq_w}{k(T_w - T_\infty)}, \quad (9.31)$$

where

$$\tau_{rs} = \left[\left(a + b \left| \frac{\partial u}{\partial r} - \frac{u}{R+r} \right|^{n-1} \right) \left(\frac{\partial u}{\partial r} - \frac{u}{R+r} \right) \right]_{r=0} \text{ and } q_w = -k \left[\frac{\partial T}{\partial r} \right]_{r=0}. \quad (9.32)$$

With the help of Eq. (9.32) in Eq. (9.31), we obtained the following relations for local skin-friction and local Nusselt number

$$\frac{1}{2} Re_b^{-\frac{1}{n+1}} C_f = A \left(f''(0) - \frac{1}{K} f'(0) \right) + \left(f''(0) - \frac{1}{K} f'(0) \right)^n, \quad (9.33)$$

$$Re_b^{-\frac{1}{n+1}} Nu_s = -\theta'(0). \quad (9.34)$$

9.3 Testing of Code

The relation for pressure in Eq. (9.25) and DE's (9.26) and (9.27) along with the BCs (9.28) and (9.29) are considered for the numerical computations with the help of MATLAB function `bvp4c`. The major outcomes are validated in the form of resistive forces as shown in **table 9.3**. Meanwhile, these results are matched with the existing literature as presented by Abbas *et al.* [79] and Sanni *et al.* [80]. The present outcomes are originated in excellent settlement with these published work.

9.4 Numerical Outcomes and Discussion

A numerical technique is applied to demonstrate the problem through Eqs. (9.25) to (9.27) along with BCs (9.28) and (9.29). A well-known function `bvp4c` in MATLAB is utilized to approximate the numerical solution. This built in function is based on collocation three steps Lobatto IIIA formula. Generally, Lobatto IIIA methods of fourth order accuracy have been utilized for BVPs and another positive property in terms of stability in the whole interval is also the main theme of this approach. In this methodology the higher order ODEs are first converted to first order system of ODEs with BCs viz some new variables. The accuracy in the foremost method is kept up to the tolerance level 10^{-6} . Furthermore, depict of the different parameters of flow like the material parameter (A), Prandtl number (Pr), curvature parameter (K) is demonstrated through the velocity, temperature and pressure graphs.

Fig. 9.2(a) is portrayed to present the effect of material parameter A on the distribution of the liquid velocity. It is noted that the liquid velocity is enhancing with the increment in material parameter. This increase in the velocity and the MBLT is because of the higher viscosities occur at less rate of shear and higher rate of shear causes low viscosity. The graphical behavior of the velocity and associated MBLT with the variation in the dimensionless radius of curvature is shown through Fig. 9.2(b). Again, this figure reveals an enhancing trend for $0 < n < 1$. Physically, this exposes that the velocity and MBLT enhance with the diminishing values of the curvature radius and the flow sheet turns out to be more bended (arch increments). It can be elucidated on the foundation that curvature of the boundary provides upsurge to a tributary flow owing to the curvilinear trend of the liquid flow under the accomplishment of centrifugal force as liquid particles traverse the curved path along the boundary of the flat. The auxiliary flow is subsequently overlaid on the essential flow to upgrade the speed field. The effect of the arch is little along the surface (s -direction) and is larger in the r -direction because of the centrifugal force on the direction to origin.

A decreasing impact on the temperature distribution for rising values of material

parameter is presented in Fig. 9.3(a). The relevant TBLT is also reduced for shear-thinning fluids. Fig. 9.3(b) shows a reducing behavior of the temperature for increasing radius of curvature for shear-thinning fluids.

Fig. 9.4(a) displays the discrepancy in the pressure for altered values of curvature parameter. It is found that a decrease in radius of curvature causes a rise in the magnitude of the pressure profile inside the BL. Moreover, the magnitude of the pressure away from the wall goes to zero whenever the dimensionless radius of curvature extends to infinity. This is because of the flat surface, where the pressure is negligible. An enhancement trend of the magnitude of pressure is noticed during plotting of the pressure profile corresponding to material parameter A as shown in Fig. 9.4(b). The magnitude of the pressure uplifts due to the reduction in values of the material parameter. The enhancement in the magnitude of the pressure is due to the higher viscosities causing low shear rate and higher shear rate causing low viscosity.

Flow pattern plotted through Figs. 9.5(a,b) for fixed values of $n = 0.8$, $A = 2.0$, $Re_b = 10$ and $c = 1$ while taking two increasing values of K . Fig. 9.5(a) is noticed with low speed of the liquid for $K = 1$ as compared to the speed of the Sisko liquid and related MBLT presented through Fig. 9.5(b) for $K = 10$. Similar output is noticed through Figs. 9.6(a,b) for the case of Newtonian liquid, i.e., for $n = 1$ and $A = 0$. For fixed values of $n = 0.8$, $A = 2.0$ and $Pr = 1.2$, the isotherms are plotted through Figs. 9.7(a,b) for two different values of K and T_∞ . Thus the hotness of Sisko fluid for $K = 1$ and $T_\infty = 0$ is slightly less than the isotherms plotted for $K = 10$ and $T_\infty = 0.3$ and is shown through Figs. 9.7(a,b).

The effect of material parameter on the local skin-friction through table 9.1 is found in the enhancement for both constraints of pseudo-plastic and dilatant liquids. The results are tabulated for simple power-law fluid as well as Sisko fluid and the effect of the radius of curvature caused a decline in skin-friction coefficient. In the absence of material parameter ($n = 1$) the variation with respect to curvature parameter for Newtonian fluid shows a decreasing local skin-friction. The depict of Pr , K and A on the transfer rate of heat

is illustrated through **table 9.2**. Here the transfer rate of heat exhibited an increasing behavior for rise in A and Pr . Additionally, in the same table, a reverse trend is noted for larger values of curved nature parameter for both restriction, i.e., pseudo-plastic and dilatant liquids. A similar behavior is observed while computing the local-Nusselt number.

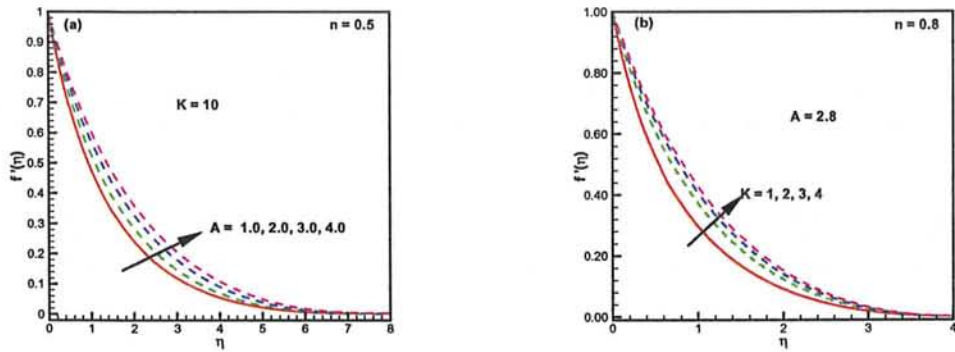


Fig. 9.2: Effect of A and K on velocity $f'(\eta)$.

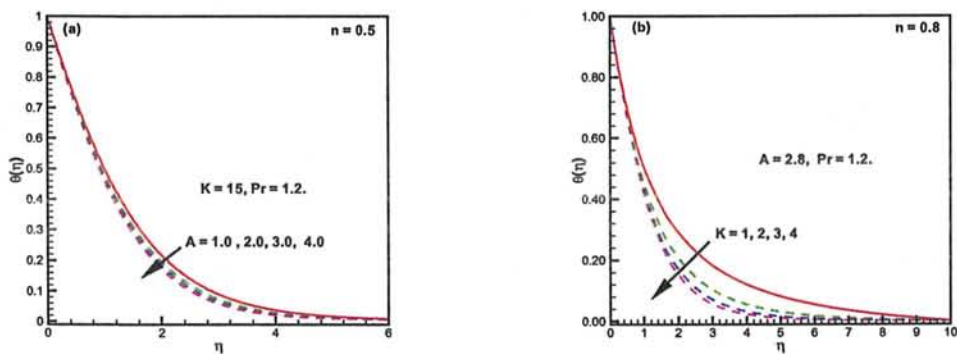


Fig. 9.3: Effect of A and K on temperature $\theta(\eta)$.

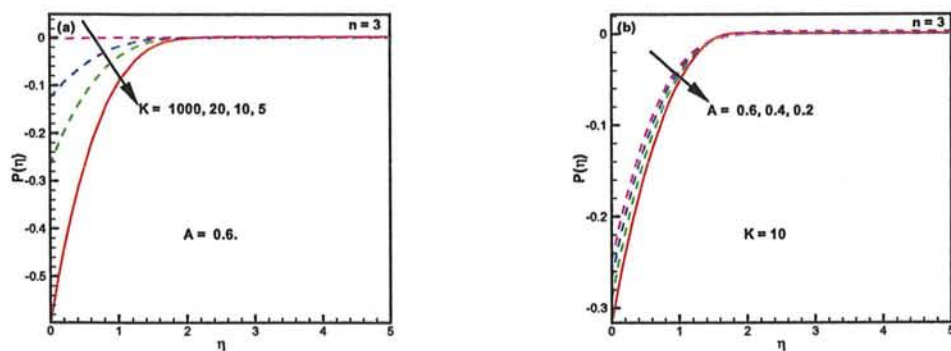


Fig. 9.4: Effect of K and A on pressure $P(\eta)$.

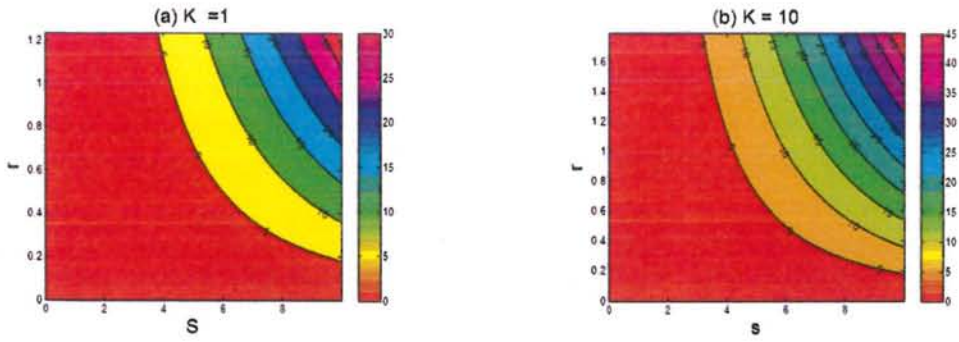


Fig. 9.5: Streamlines for (a) $K = 1$ and (b) $K = 10$.

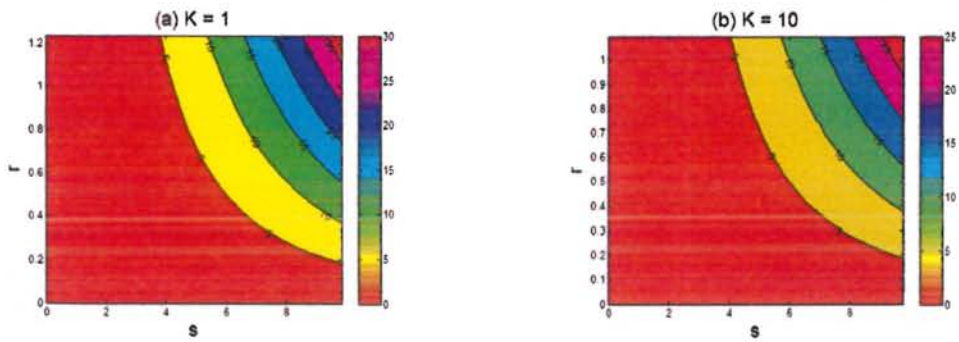


Fig. 9.6: Streamlines for Newtonian fluid (a) $K = 1$ and (b) $K = 10$.

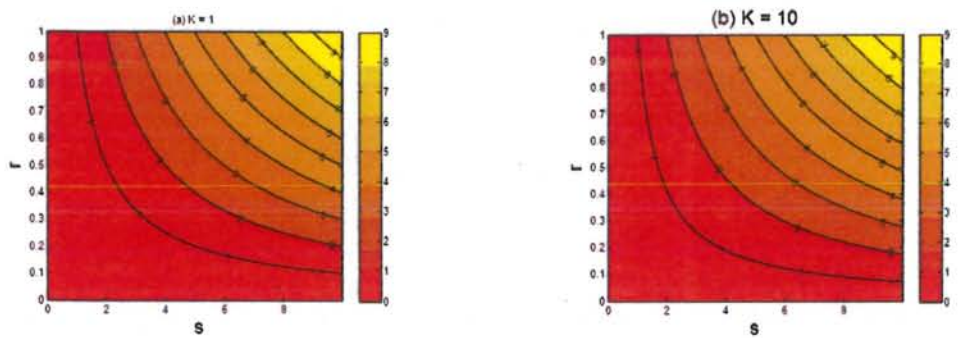


Fig. 9.7: Isotherms for (a) $K = 1$ and (b) $K = 10$.

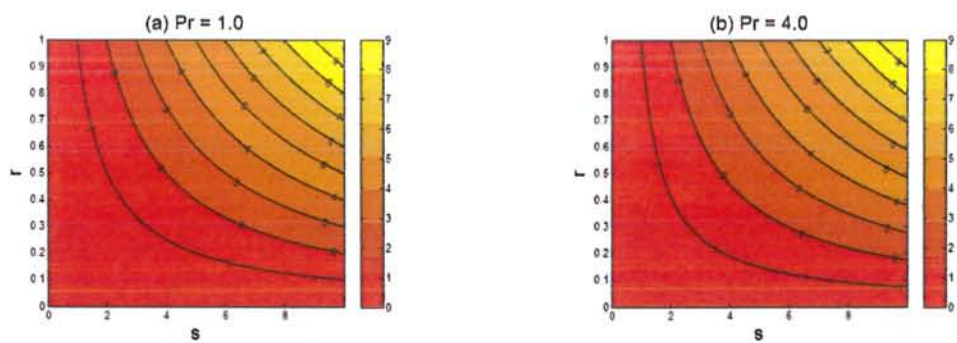


Fig. 9.8: Isotherms for (a) $Pr = 1$ and (b) $Pr = 4$.

Table 9.1: The variations in the drag forces for different values of A and K .

A	K	$-\frac{1}{2} \left(Re_b \right)^{\frac{1}{n+1}} C_f$		
		$n = 0.6$	$n = 1.2$	$n = 1$
2.0	5	2.015136	2.174674	2.348902
3.0		2.619319	2.72183	2.905463
4.0		3.202379	3.288387	3.457279
0.0	5	0.242255	0.8584477	1.157641
	10	0.2111138	0.7927129	1.073495
	15	0.1937494	0.7623595	1.047958
2.0	5	2.015136	2.174674	2.348902
	10	1.678795	1.870389	2.010173
	15	1.573729	1.789958	1.912810

Table 9.2: The variations in the transfer rate of heat for distinct growing values of A , Pr and K .

A	Pr	K	$\left(Re_b\right)^{-\frac{1}{n+1}} Nu_s$		
			$n = 0.6$	$n = 1.2$	$n = 1$
1.0	1.2	5	0.6139801	0.7981227	0.7552627
2.0			0.6464552	0.8168537	0.7765525
3.0			0.6632442	0.8287568	0.7877522
2.0	1.2	5	0.6464552	0.8168537	0.7765525
		1.4	0.7063354	0.890762	0.8474486
		1.6	0.7625116	0.959461	0.9133882
2.0	1.2	5	0.6464552	0.8168537	0.7765525
		10	0.6358174	0.7999638	0.763569
		15	0.6333700	0.793773	0.7581987

Table 9.3: A matching with the previous data for distinct growing values of K when $A = 0$ and $n = 1$.

Parameter	$-\frac{1}{2} \left(Re_b \right)^{\frac{1}{n+1}} C_f$		
K	Present results	Abbas <i>et al.</i> [79]	Sanni <i>et al.</i> [80]
5	1.157641	1.1576	1.1576
10	1.073495	1.0735	1.0734
20	1.035613	1.0356	1.0355
30	1.023533	1.0235	1.0235
40	1.017588	1.0176	1.0176
50	1.014050	1.0141	1.0140
100	1.007039	1.0070	1.0070
200	1.003564	1.0036	1.0036
1000	1.000799	1.0008	1.0008
∞	1.000000	1.0000	1.0000

Chapter 10

Numerical Computations for MHD Flow of Sisko-nanoliquid over a Moving Curved Boundary

In this chapter, an analysis regarding diverse features of Sisko liquid flow over a curved moving boundary by taking into account magneto-nanoparticles is presented. Parameter of curvature with higher values for which the curved surface is going to be reduced into the planner sheet. The governing equations are modeled in curvilinear coordinate system and transformed into system of non-linear ODEs. The obtained equations are solved numerically by employing the built in solver (bvp4c) in MATLAB as well as BVP traprich in Maple. From the obtained results, we observed a decline in the magnitude of velocity field as well as pressure inside the BL for increasing values of magnetic parameter. On the other hand, the temperature of liquid exhibited an enhancing trend with growing values of Brownian motion as well as thermophoresis parameters. Moreover, concentration is also found to be growing with augmented values of the Schmidt number. A comparison for validation of the present outputs is displayed between one of the collocated coding in MATLAB and the extrapolation method introduced by Richardson while using Maple software and the findings are matched with previous data in restrictive condition.

10.1 Configuration of the Problem

The parameters of Brownian motion along with thermophoresity introduced in the incompressible steady flow of Sisko liquid due to curved moving sheet with the use of magnetic field is considered. Flow configuration presented is modeled in curvilinear coordinated and is shown in **Fig. 9.1** (cf. Chapter 9). The curved boundary coiled in a circle with radius R and formulated while using curvilinear coordinates (r, s) and is stretched kinematically along the axial direction s with velocity $U_w = cs$. The structured of the problem indicates that the bended boundary formed by determining the distance between the origin and the surface. So that larger values of R goes to slightly curved sheet. The liquid temperature T_w and concentration C_w at boundary are defined, while the ambient liquid temperature T_∞ and concentration C_∞ denotes for away temperature and solute concentration from boundary. Under the aforementioned assumptions, the basic equations for the Sisko nanofluid flow in the form of continuity, momentum along with Boussinesq approximation, heat and concentration are developed as follows (cf. Chapter 9):

$$R \frac{\partial u}{\partial s} + \frac{\partial}{\partial r} \{(R+r)v\} = 0, \quad (10.1)$$

$$\frac{u^2}{R+r} - \frac{1}{\rho} \frac{\partial p}{\partial r} = 0, \quad (10.2)$$

$$v \frac{\partial u}{\partial r} + \frac{uR}{R+r} \left(\frac{\partial u}{\partial s} \right) + \frac{uv}{R+r} = -\frac{1}{\rho} \frac{R}{R+r} \frac{\partial p}{\partial s} + \frac{a}{\rho(R+r)^2} \frac{\partial}{\partial r} \left[(R+r)^2 \left(\frac{\partial u}{\partial r} - \frac{u}{R+r} \right) \right] + \frac{b}{\rho(R+r)^2} \frac{\partial}{\partial r} \left[(R+r)^2 \left(\frac{\partial u}{\partial r} - \frac{u}{R+r} \right)^n \right] - \frac{\sigma B_0^2}{\rho} u, \quad (10.3)$$

$$v \frac{\partial T}{\partial r} + \frac{uR}{R+r} \left(\frac{\partial T}{\partial s} \right) = \alpha_1 \left(\frac{\partial^2 T}{\partial r^2} + \frac{1}{R+r} \frac{\partial T}{\partial r} \right) + \tau^* \left[D_B \left(\frac{\partial T}{\partial r} \frac{\partial C}{\partial r} \right) + \frac{D_T}{T_\infty} \left(\frac{\partial T}{\partial r} \right)^2 \right], \quad (10.4)$$

$$v \frac{\partial C}{\partial r} + \frac{uR}{R+r} \left(\frac{\partial C}{\partial s} \right) = D_B \left(\frac{\partial^2 C}{\partial r^2} + \frac{1}{R+r} \frac{\partial C}{\partial r} \right) + \frac{D_T}{T_\infty} \left(\frac{\partial^2 T}{\partial r^2} + \frac{1}{R+r} \frac{\partial T}{\partial r} \right). \quad (10.5)$$

The associated BCs are as follows:

$$\text{at } r = 0, \begin{cases} U_w(s) = cs, & v = 0, \\ T = T_w, & C = C_w, \end{cases} \quad (10.6)$$

$$\text{as } r \rightarrow \infty, \quad u \rightarrow 0, \quad \frac{\partial u}{\partial r} \rightarrow 0, \quad T \rightarrow T_\infty \quad \text{and} \quad C \rightarrow C_\infty. \quad (10.7)$$

The subsequent dimensionless variables are incorporated to convert the balance equations of force, energy and concentration in terms of non-linear ODE's.

$$u = U_w f'(\eta), \quad v = \frac{-U_w R}{R+r} Re_b^{-\frac{1}{n+1}} \left[\frac{2n}{n+1} f(\eta) + \frac{1-n}{1+n} \eta f'(\eta) \right], \quad \psi = s U_w Re_b^{-\frac{1}{n+1}} f(\eta),$$

$$\theta(\eta) = \frac{T_\infty - T}{T_\infty - T_w}, \quad \phi(\eta) = \frac{C_\infty - C}{C_\infty - C_w}, \quad p = \rho a^2 s^2 P(\eta), \quad \eta = \frac{r}{s} Re_b^{\frac{1}{n+1}}. \quad (10.8)$$

Inserting transformations (10.8), Eq. (10.1) is becoming zero, i.e., identically contended and Eqs. (10.2) and (10.3) are reduced in the subsequent form

$$\frac{\partial P}{\partial \eta} = \frac{f'^2}{K + \eta}, \quad (10.9)$$

$$\begin{aligned} \frac{2K}{K + \eta} P &= \frac{K}{K + \eta} \left(\frac{2n}{n+1} \right) \left(f f'' + \frac{1}{K + \eta} f f' \right) - \frac{K}{K + \eta} f'^2 \\ + A \left[f''' + \frac{1}{K + \eta} f'' - \frac{1}{(K + \eta)^2} f' \right] &+ \frac{2}{K + \eta} \left(f'' - \frac{1}{K + \eta} f' \right)^n - M f' \\ + n \left(f'' - \frac{1}{K + \eta} f' \right)^{n-1} &\left(f''' - \frac{1}{K + \eta} f'' + \frac{1}{(K + \eta)^2} f' \right) \end{aligned} \quad (10.10)$$

Abolishing the pressure relation between Eqs. (10.9) and (10.10) in combination with Eq. (10.8), Eqs. (10.4) to (10.7) results in

$$\begin{aligned}
& A \left[f'''' + \frac{2}{K+\eta} f''' - \frac{1}{(K+\eta)^2} f'' + \frac{1}{(K+\eta)^3} f' \right] - \frac{2K}{(K+\eta)^2} f'^2 - \frac{2K}{K+\eta} f' f'' \\
& + \left(\frac{2n}{n+1} \right) \left[\frac{K}{K+\eta} (f f''' + f' f'') + \frac{K}{(K+\eta)^2} (f f'' + f'^2) - \frac{K}{(K+\eta)^3} f f' \right] \\
& + n \left(f'' - \frac{1}{K+\eta} f' \right)^{n-1} \left(f'''' + \frac{2}{K+\eta} f''' - \frac{1}{(K+\eta)^2} f'' + \frac{1}{(K+\eta)^3} f' \right) \\
& + n(n-1) \left(f'' - \frac{1}{K+\eta} f' \right)^{n-2} \left(f''' - \frac{1}{K+\eta} f'' + \frac{1}{(K+\eta)^2} f' \right)^2 - M \left(f'' - \frac{1}{K+\eta} f' \right) \\
& + 2n \left(f'' - \frac{1}{K+\eta} f' \right)^{n-1} \left(\frac{1}{K+\eta} f'''' - \frac{1}{(K+\eta)^2} f'' + \frac{1}{(K+\eta)^3} f' \right) = 0, \quad (10.11)
\end{aligned}$$

$$\theta'' + \frac{\text{Pr} K}{K+\eta} \left(\frac{2n}{n+1} \right) f \theta' + \frac{1}{K+\eta} \theta' + \text{Pr} \left(N_b \theta' \phi' + N_t (\theta')^2 \right) = 0, \quad (10.12)$$

$$\phi'' + \frac{\text{Sc} K}{K+\eta} \left(\frac{2n}{n+1} \right) f \phi' + \frac{1}{K+\eta} \phi' + \frac{N_t}{N_b} \left(\theta'' + \frac{1}{K+\eta} \phi' \right) = 0, \quad (10.13)$$

$$\text{at } \eta = 0, \quad \begin{cases} f = 0, & f' = 1, \\ \theta = 1, & \phi = 1, \end{cases} \quad (10.14)$$

$$\text{as } \eta \rightarrow \infty, \quad f' \rightarrow 0, \quad g' \rightarrow 0, \quad \theta \rightarrow 0, \quad \phi \rightarrow 0. \quad (10.15)$$

where all the physical parameters which govern the flow are listed below:

$$\begin{aligned}
\alpha_1 &= \frac{k}{\rho c_p}, \quad \text{Sc} = \frac{s U_w}{D_B} \text{Re}_b^{-\frac{2}{n+1}}, \quad M = \frac{\sigma B_0^2}{\rho c}, \\
N_b &= -\frac{\tau^* D_B (C_\infty - C_w)}{\alpha_1}, \quad N_t = -\frac{\tau^* D_T (T_\infty - T_w)}{\alpha_1 T_\infty}. \quad (10.16)
\end{aligned}$$

The substantial physical extents of interest specifically the drag force coefficient, Nus-

selt and Sherwood numbers are illustrated by

$$C_f = \frac{\tau_{rs}}{\frac{1}{2}\rho U_w^2}, \quad Nu_s = \frac{-q_w s}{k(T_\infty - T_w)}, \quad Sh_s = \frac{-q_m s}{D_B(C_\infty - C_w)}, \quad (10.17)$$

where

$$\tau_{rs} = \left[\left\{ a + b \left| \left(\frac{\partial u}{\partial r} - \frac{u}{R+r} \right) \right|^{n-1} \right\} \left(\frac{\partial u}{\partial r} - \frac{u}{R+r} \right) \right]_{r=0}, \quad (10.18)$$

$$q_w = -k \left(\frac{\partial T}{\partial r} \right)_{r=0} \quad \text{and} \quad q_m = -D_B \left(\frac{\partial C}{\partial r} \right)_{r=0}. \quad (10.19)$$

Using the transformations defined through Eq. (10.8), significant physical quantities are in terms of drag force(skin-friction), transfer rate of heat and mass (Nusselt and Sherwood numbers), respectively, formulated for further physical interpretation regarding this analysis and is illustrated as below.

$$\frac{1}{2} Re_b^{-\frac{1}{n+1}} C_f = A \left(f''(0) - \frac{1}{K} f'(0) \right) + \left(f''(0) - \frac{1}{K} f'(0) \right)^n, \quad (10.20)$$

$$Re_b^{-\frac{1}{n+1}} Nu_s = -\theta'(0), \quad (10.21)$$

$$Re_b^{-\frac{1}{n+1}} Sh_s = -\phi'(0). \quad (10.22)$$

10.2 Results Validation

The governing nonlinear ODEs (10.11)-(10.13) subjected to BCs (10.14)-(10.15) are considered for the numerical solution. The results obtained with the implementation of bvp4c method are given through **table 10.1** and are compared with BVP traprich in Maple which uses Richardson extrapolation method. A tremendous agreement is established between these two numerical methods. Numerical outcomes produced in the limiting cases are also compared with published works by Mabood and Das [81] and Imtiaz *et al.* [82]. The results found in present study are in excellent correlation with the earlier works (see **table 10.2**).

10.3 Physical Interpretation of Results

The numerical computation of the Sisko magneto-nanofluid flow due to curved stretching surface is performed. The Buongiorno nano-liquid model is incorporated to study transfer of heat and mass phenomena in flow of Sisko liquid. Highly nonlinear Eqs.(10.11) to (10.13) with the BCs (10.14) and (10.15) are modeled in curvilinear coordinates. All governing parameters like material parameter (A), magnetic parameter (M), power-law parameter (n), radius of curvature (K), Brownian motion (N_b), thermophoresis (N_t), Prandtl number (Pr), and Schmidt number (Sc) are used to demonstrate the flow, transfer of heat and mass characteristics of Sisko nanofluid.

10.3.1 Flow Pattern

To visualize the flow pattern for fixed values of $Re_b = 1000$, $c = 1$ and $M = 2.0$, the streamlines are plotted for distinct values of material parameter A and power-law parameter n . **Fig. 10.1(a)** are plotted for the Newtonian fluid, ($n = 1$ and $A = 0$). The flow pattern subject to this case exhibits a non-symmetric reduction behavior near the curved surface, while on the other hand (see **Fig. 10.1(b)**), the behavior of the flow near the stretching surface is prominent for shear-thinning fluid and the flow in this case reduces symmetrically about the horizontal axis. In both figures, the effects of A and n cause the flow being drag into the center and this is due to the equal forces of buoyant flow. The flow pattern of Sisko fluid plotted through **Fig. 10.2(a)**, where the fluid flow is stretched toward the curved surface is symmetrically about the horizontal axis and flow of Sisko fluid is reduced near the curved stretching surface for $n > 1$. Another flow pattern is plotted through **Fig. 10.2(b)** for $A = 2.5$ and $n = 1$. A symmetric conduct about the horizontal axis away from the curved stretching surface is observed and fluid flow is reduced near the stretching curved surface, where the fluid flow is found in non-uniform pattern. The flow pattern produced for shear-thinning and shear-thickening fluids in **Figs. 10.3(a,b)**, where the fluid flow is stretched near the curved stretching surface for both

restrictions, i.e., ($0 < n < 1$) and ($n > 1$).

10.3.2 Velocity Profiles

A considerable growing effect is displayed by the velocity profile and related MBLT of Sisko liquid flow over a bended moving boundary for uplifting values of A as shown in **Figs. 10.4(a,b)**. The result for the case ($0 < n < 1$) is more effective as compared to the case ($n > 1$). This physical enhancement conduct with the variation of material parameter causes low shear rate with higher viscosity and high shear rate for low viscosity regarding Sisko nanoliquid flow. The influence of uplifting values of K on velocity profile for pseudo-plastic as well as dilatant liquids is found in uplifting order along with associated MBLT as demonstrated through **Figs. 10.5(a,b)**. Here the result is more acceptable in the case of pseudo-plastic liquid. It has been examined that the radius of curved surface increases for augmented values of curvature parameter K due to which motion of the fluid rises. A very significant reduction behavior is observed through **Figs. 10.6(a,b)** for growing values of M , for both ($0 < n < 1$) and ($n > 1$) and relevant MBLT is perceived in reduction conduct. The physical reason concerning this conduct is owing to the enrichment in Lorentz forces which declines the velocity of the liquid.

10.3.3 Pressure Profiles

Fig. 10.7(a) establishes an escalating trend in the magnitude of the pressure for decreasing order values of n . On other hand, the effect of reducing values of material parameter on the pressure magnitude inside BL is observed in the form of uplifting behavior and is shown through **Fig. 10.7(b)**. In both cases the associated pressure BLT is detected in enrichment demeanor. Furthermore, the decreasing values of curvature parameter cause an escalating behavior in the magnitude of pressure profile within the BL and is shown in **Fig. 10.8(a)**. Wherein a curved surface is reduced in the planner surface for higher value of K and the pressure profile becomes zero. For smaller values of K , the curved surface will be more curved. It can be enlightened on the basis that the curvature of the

surface give rises to a secondary flow due to the curved nature of the liquid flow under the accomplishment of centrifugal force as the liquid particles navigate the bended track along the boundary of the sheet. The secondary flow is therefore dominant on the primary flow due to augmentation the velocity of liquid. Though, in the situation of a curved surface the variation of pressure is significant inside the BL and therefore the pressure discrepancy cannot be neglected as is frequently done for a flat stretching sheet. **Fig. 10.8(b)** exhibits a growing trend in the pressure magnitude profile inside the boundary and associated pressure BLT for the reducing values of magnetic parameter.

10.3.4 Temperature Profiles

Figs. 10.9(a,b) demonstrate a diminishing trend from the profile of temperature with increasing values of A . Whereas the relevant TBLT also reduces for $(0 < n < 1)$ and $(n > 1)$ fluids. Physically, the reality behind this scene demonstrates the uplifting nature of shear rate is the result by incorporating higher values of A and this trend goes to reduces the viscosity in the said configuration of transfer of heat. The impact of the several uplifting values of K reduces the liquid temperature and the TBLT in both cases, i.e., $(0 < n < 1)$ and $(n > 1)$ and this behavior is presented in **Figs. 10.10(a,b)**. Through **Figs. 10.11(a,b)**, an enhancement behavior is perceived while plotting the temperature profile of the liquid flow corresponding to growing values of M . **Figs. 10.12(a,b)** are showing a diminishing conduct of temperature profiles with increasing values of Pr for $(0 < n < 1)$ as well as $(n > 1)$ of power-law liquids. The associated TBLT is also reduced in this case. Enhancement of Brownian motion parameter results in growing the temperature field and related TBLT for $(0 < n < 1)$ and $(n > 1)$ restrictions of liquids as shown through **Figs. 10.13(a,b)**. From **Fig. 10.14(a,b)**, it is concluded that whenever the thermophoresis parameter is considered in the increasing order the temperature profile and the associated TBLT will be enhanced while testing both restrictions, i.e., $(0 < n < 1)$ and $(n > 1)$ properties of liquids.

10.3.5 Concentration Profiles

In **Figs. 10.15(a,b)** we have investigated the variation of A while plotting the nanoparticles concentration profile. Wherein a reduction is found for both pseudo-plastic and dilatant liquids. The associated CBLT is also diminished. A remarkable increasing nanoparticle concentration with the several values of M is plotted through **Figs. 10.16(a,b)**, where both cases are considered namely pseudo-plastic and dilatant liquids. The result is very significant in case of pseudo-plastic. **Figs. 10.17(a,b)** illustrate the influence of K on the nanoparticle concentration. It is noticed that for the growing values of K the concentration profile and the associated CBLT are diminishing for both situations, i.e., ($0 < n < 1$) as well as ($n > 1$) properties of liquids. From **Figs. 10.18(a,b)** it is seen that by varying N_b , a deteriorating behavior is demonstrated while plotting the nanoparticles concentration for dilatant as well as pseudo-plastic liquids cases. In this regard the CBLT is also reduced. In **Figs. 10.19(a,b)** the increasing values of N_t cause a reduction in the profile of nanoparticles concentration and associated CBLT. Shear-thinning and shear-thickening liquids properties are also utilized but the result are more acceptable in case of shear-thinning liquids. **Figs. 10.20(a,b)** depict a diminishing behavior of nanoparticles concentration for growing values of Sc and related CBLT is also reduced in both pseudo-plastic as well as dilatant liquids.

10.3.6 Drag Forces, Heat and Mass Transfer Rates

Influence of A on the local-skin-friction is observed in the uplifting for both ($0 < n < 1$) and ($n > 1$) and is shown in **Figs. 10.21(a,b)**. Diminishing behavior is illustrated during plotting of local-Nusselt number in both situations of power-law fluids and is presented in **Figs. 10.22(a,b)**. Through **Figs. 10.23(a,b)**, the impact of rising values of Sc on the local-Sherwood number is found in the augmented conduct for pseudo-plastic and dilatant liquids. The effect of A , M and K are utilized to demonstrate the impact of resistive forces. In this regard the tabular values as shown in **table 10.3** are computed to

depict the effect of frictional forces during fluid flow. The local skin-friction is depicted with increasing trend for higher values for the parameter arises due to magnetic field and on the other hand enhancing values of curvature parameter causes a reduction. In preceding table three constraints are imposed on the power-law index n , i.e., for $n = 1$ (Newtonian fluid), $n = 0.5$ (shear-thinning fluid) and $n = 1.5$ (shear-thickening fluid). The impacts of different governing flow parameters on the transfer rate of heat is depicted in **table 10.4**. Larger parameter M introduced owing to magnetic field is incorporated while calculating the transfer rate of heat and found in decreasing manner. However, the behavior of the same phenomenon detected in terms of intensifying function of curvature K for all conditions. A decreasing behavior is noticed for the transfer rate of heat when the parameters of Brownian motion and thermophoresity are tested for various uplifting values. **table 10.5** is presented to show the transfer rate of mass with the influence of different flow parameters like A , M , K , Pr , N_b , N_t and Sc . The mass transfer rate is diminishing whenever the curvature parameter K increases for the same restrictions on the power-law index n as presented in the previous table. Enhancement in transfer rate of mass is perceived for numerous values of the parameter of N_b (Brownian motion) and reverse trend is depicted for different growing values of thermophoresis parameter N_t . Rate of mass transfer also increases when the Schmidt number rises for all three restrictions on the power-law index n .

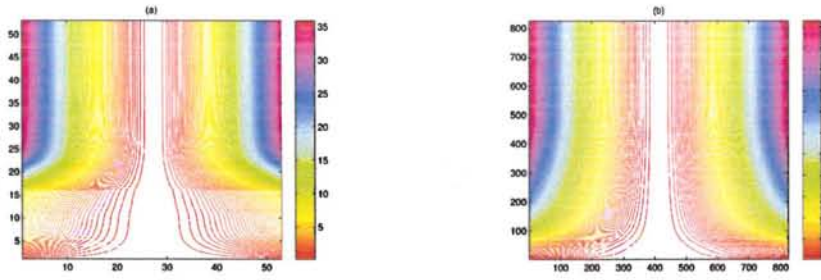


Fig. 10.1: Streamlines pattern for $A=0$, (a) $n=1.0$ and (b) $n=0.5$.

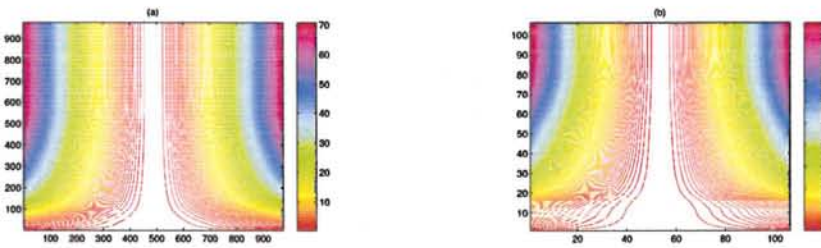


Fig. 10.2: Streamlines pattern for $A=2.5$, (a) $n=1.5$ and (b) $n=1.0$.

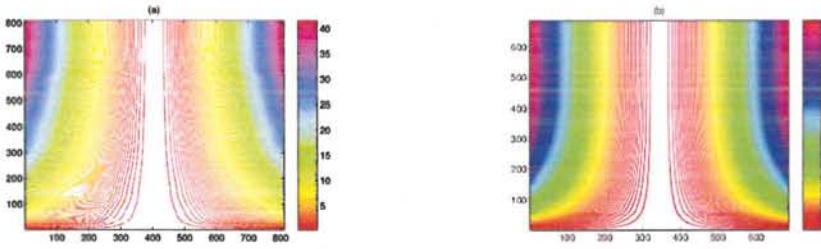


Fig. 10.3: Streamlines pattern for $A=0$, (a) $n=0.5$ and (b) $n=1.5$.

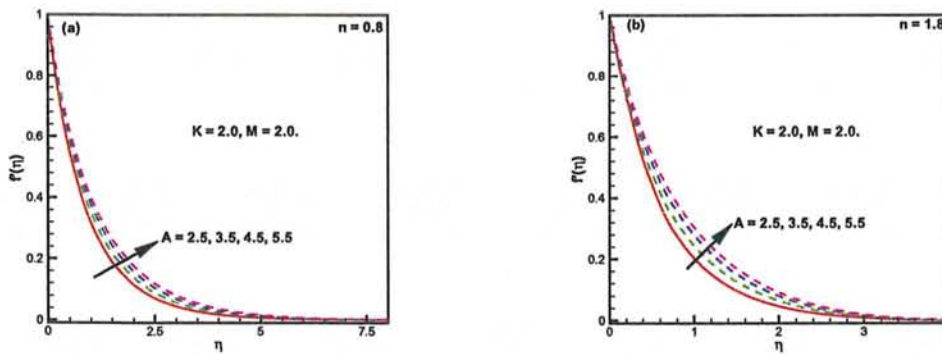


Fig. 10.4: Effect of A on velocity $f'(\eta)$.

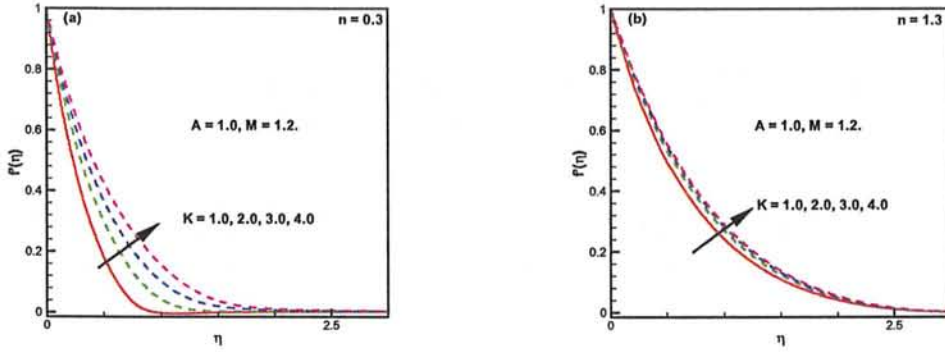


Fig. 10.5: Effect of K on velocity $f'(\eta)$

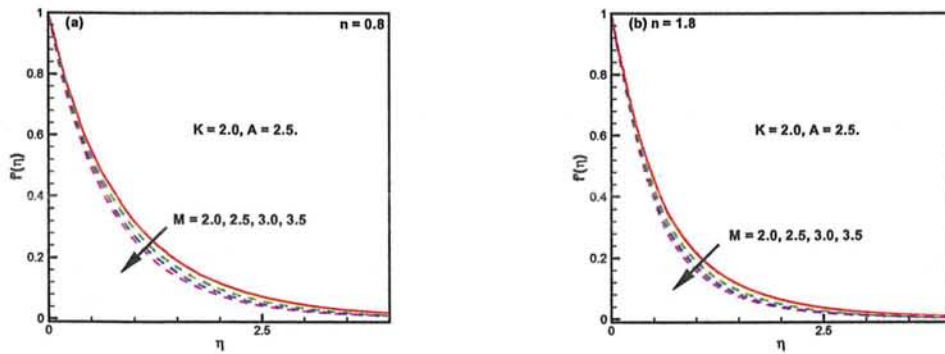


Fig. 10.6: Effect of M on velocity $f'(\eta)$.

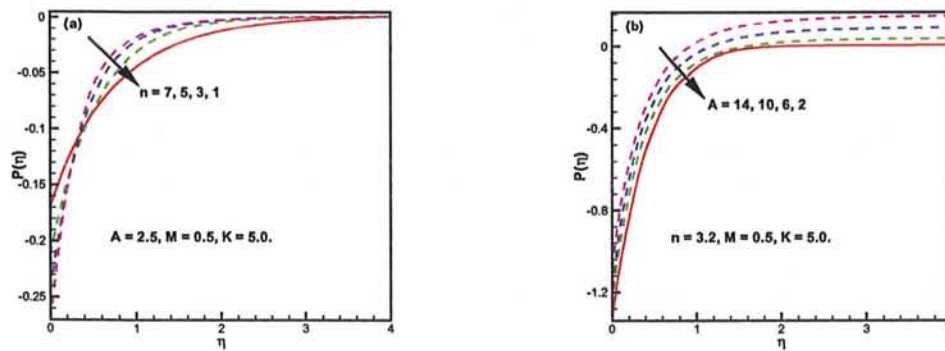


Fig. 10.7: Effect of n and A on pressure $P(\eta)$.

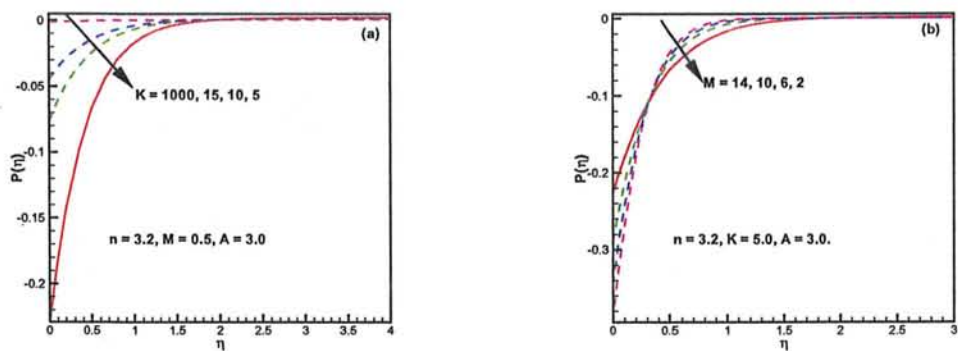


Fig. 10.8: Effect of K and M on pressure $P(\eta)$.

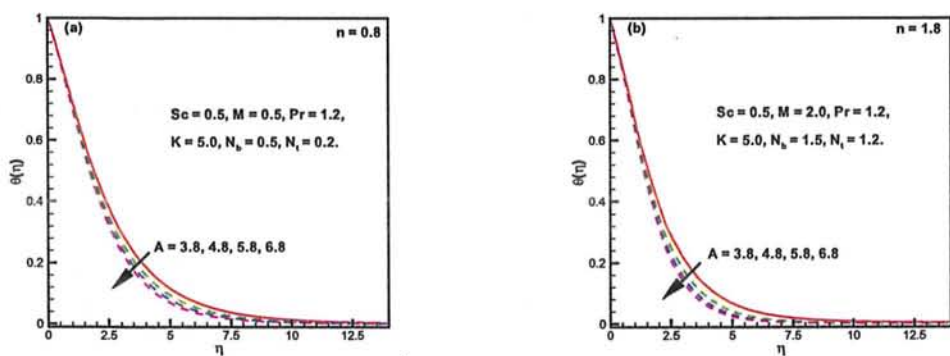


Fig. 10.9: Effect of A on temperature $\theta(\eta)$.

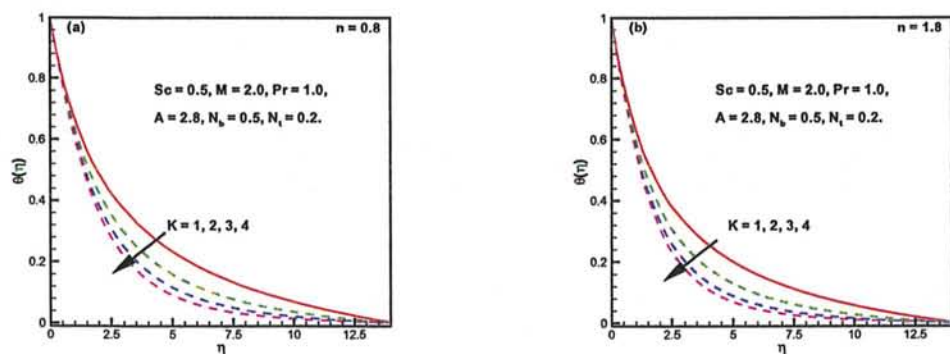


Fig. 10.10: Effect of K on temperature $\theta(\eta)$.

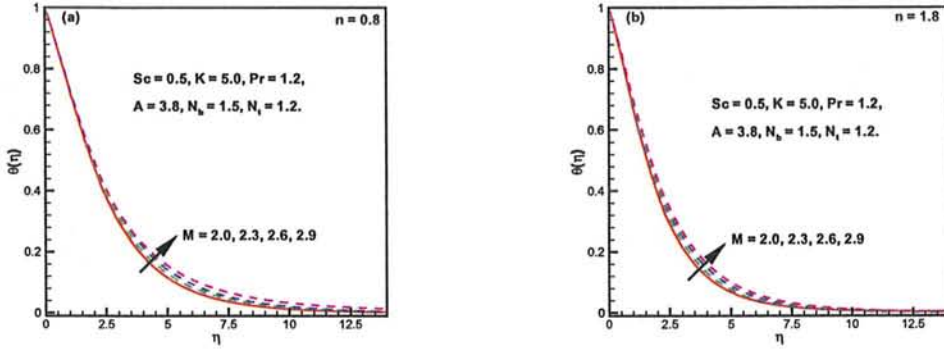


Fig. 10.11: Effect of M on temperature $\theta(\eta)$.

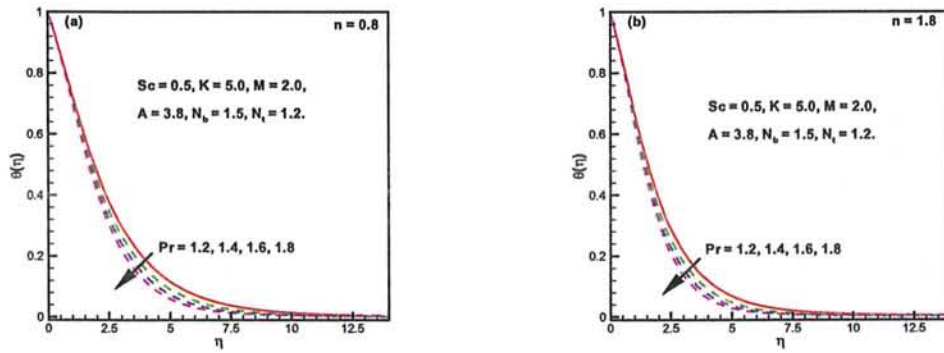


Fig. 10.12: Effect of Pr on temperature $\theta(\eta)$.

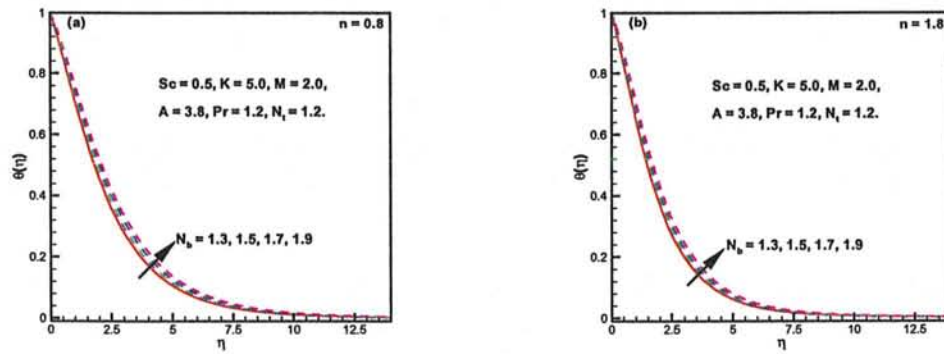


Fig. 10.13: Effect of N_b on temperature $\theta(\eta)$.

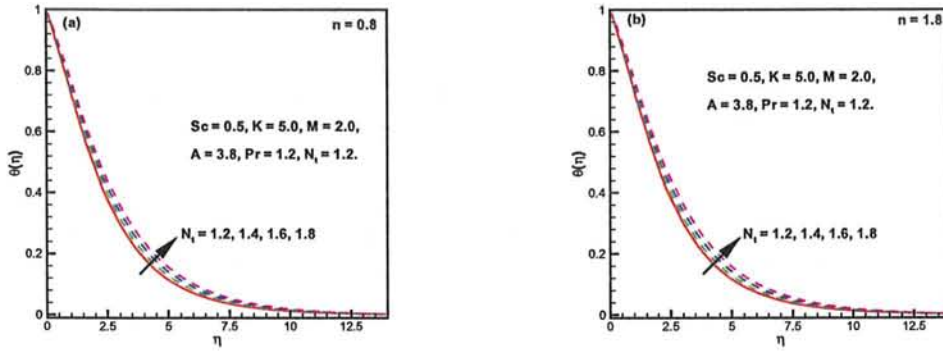


Fig. 10.14: Effect of N_t on temperature $\theta(\eta)$.

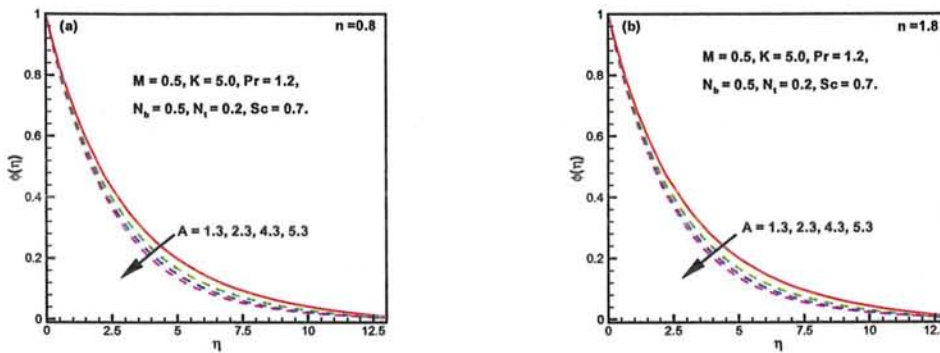


Fig. 10.15: Effect of A on concentration $\phi(\eta)$.

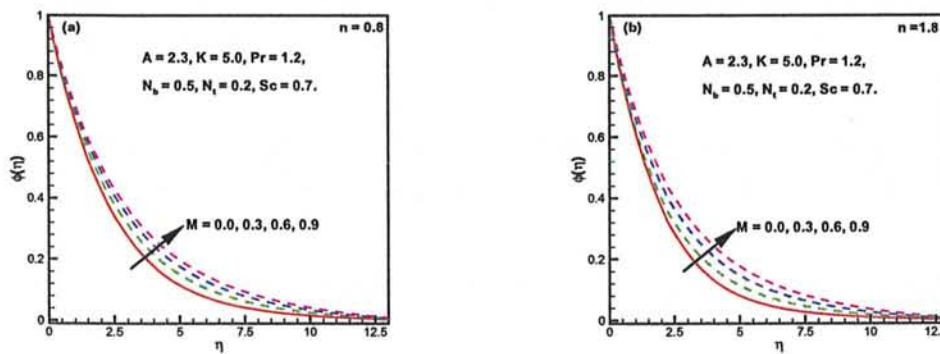


Fig. 10.16: Effect of M on concentration $\phi(\eta)$.

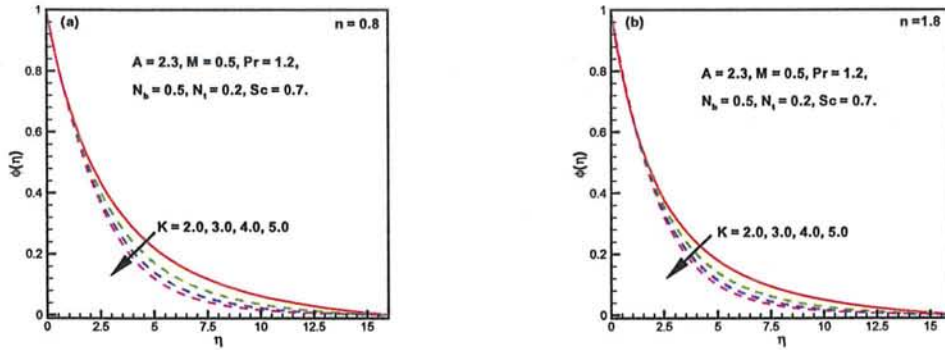


Fig. 10.17: Effect of K on concentration $\phi(\eta)$.

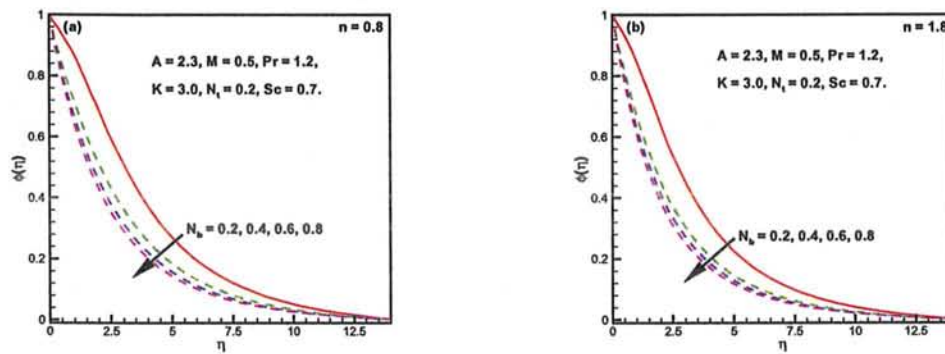


Fig. 10.18: Effect of N_b on concentration $\phi(\eta)$.

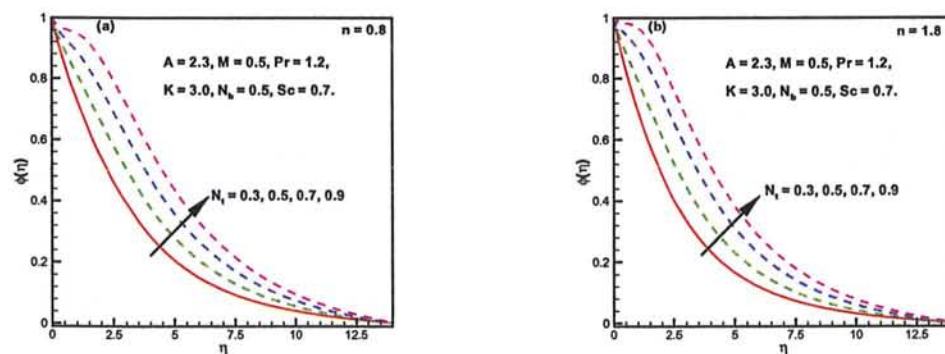


Fig. 10.19: Effect of N_t on concentration $\phi(\eta)$.

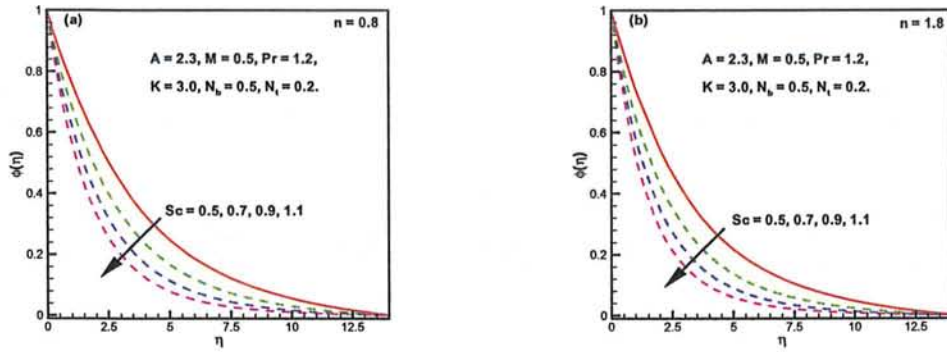


Fig. 10.20: Effect of Sc on concentration $\phi(\eta)$.

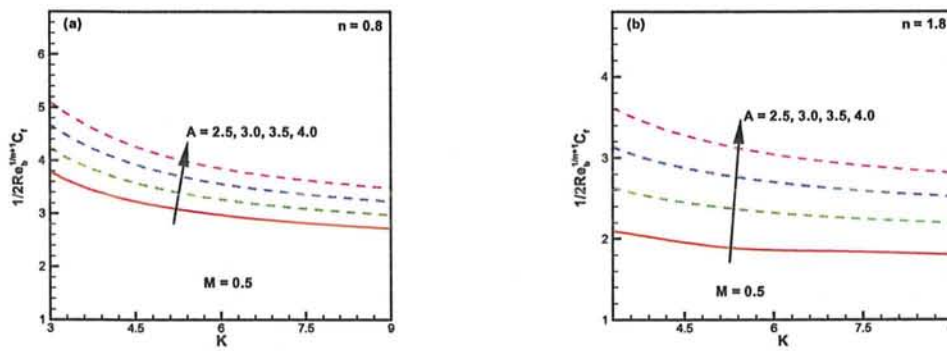


Fig. 10.21: Local skin friction via K for different values of A .

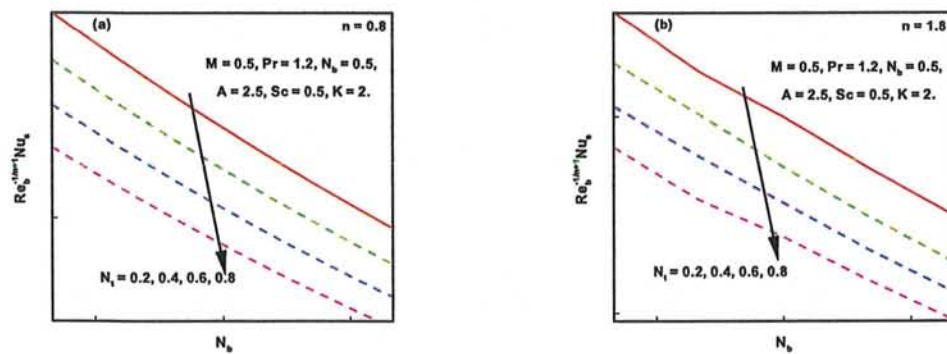


Fig. 10.22: Local Nusselt number via N_b for different values of N_t .

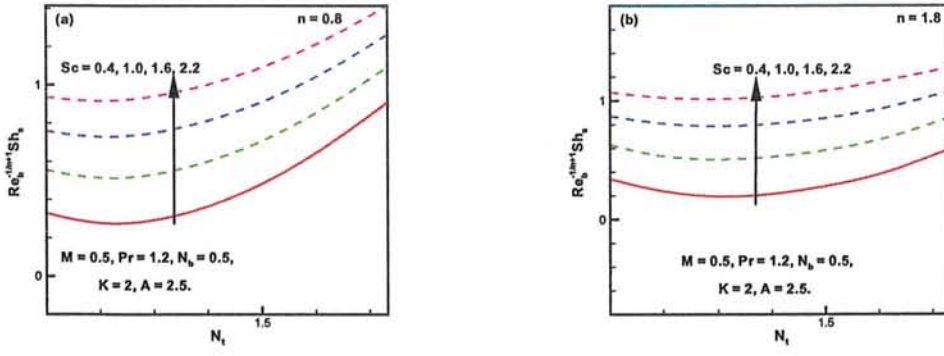


Fig. 10.23: Local Sherwood number via N_t for different values of Sc .

Table 10.1: A comparison of bvp4c with Richardson extrapolation method, when $n = 3$, $A = 3.5$ and $K = 1$.

Parameter	$-\frac{1}{2} \left(Re_b \right)^{\frac{1}{n+1}} C_f$	
M	bvp4c outcomes	Richardson extrapolation outcomes
1	12.25384	12.25449348
2	13.4114	13.47354718
3	14.56970	14.52145277
4	15.41951	15.43107230

Table 10.2: Comparison of the present work with previous results when $n = 1$, $A = 0$ and $K \rightarrow \infty$.

Parameter	$-\frac{1}{2} \left(Re_b \right)^{\frac{1}{n+1}} C_f$		
M	Present results	Mabood and Das [81]	Imtiaz <i>et al.</i> [82]
1	1.414323	1.4142135	1.4142
5	2.449627	2.4494897	2.4494
10	3.316768	3.3166200	3.3166
50	7.141577	7.1414284	7.1414

Table 10.3: The variation in the local-skin-friction for varying values of A , M and K .

Parameters			$-\frac{1}{2} \left(Re_b \right)^{\frac{1}{n+1}} C_f$		
A	M	K	$n = 1$	$n = 0.5$	$n = 1.5$
1.0	0.5	5.00	2.184967	1.271161	1.092852
2.0			2.824880	2.091291	2.033590
3.0			3.418372	2.771860	2.762832
4.0			3.986743	3.392510	3.396965
2.5	0.0	5.00	2.572119	2.090984	1.998892
	0.3		2.927944	2.293858	2.261481
	0.6		3.216605	2.509374	2.475155
	0.9		3.465605	2.706815	2.662586
2.5	0.5	1.00	7.859173	6.723026	5.365357
		5.00	3.125707	2.440097	2.404286
		10.0	2.676065	2.075501	2.142240
		10000	2.293271	1.762268	1.888027

Table 10.4: The variation in the transfer rate of heat for varying values of A , M , K , Pr , N_b and N_t .

Parameters						$(Re_b)^{-\frac{1}{n+1}} Nu_s$		
A	M	K	Pr	N_b	N_t	$n = 1$	$n = 0.5$	$n = 1.5$
1.0	0.5	5.00	1.2	0.5	0.2	0.5428404	0.3904329	0.6062883
2.0						0.5680547	0.4250426	0.6180089
3.0						0.5819859	0.4482958	0.6344736
2.5	0.0	5.00	1.2	0.5	0.2	0.6010958	0.4906416	0.6535533
	0.3					0.5851487	0.4512341	0.6367576
	0.6					0.5715394	0.4314192	0.6229344
2.5	0.5	1.00	1.2	0.5	0.2	0.5681793	0.392331	0.6446413
		2.00				0.5762132	0.4604958	0.6451662
		3.00				0.5783584	0.4443001	0.6348335
2.5	0.5	5	1.0	0.5	0.2	0.5318680	0.4011869	0.5780918
			1.2			0.5758907	0.4368973	0.6273031
			1.4			0.6136945	0.4691347	0.6696514
2.5	0.5	5	1.2	0.2	0.2	0.6583165	0.5010048	0.7155884
				0.4		0.6026236	0.4579071	0.6559572
				0.6		0.5498898	0.417402	0.5994468
2.5	0.5	5	1.2	0.5	0.2	0.5758907	0.4368973	0.6273031
					0.5	0.5271755	0.3974202	0.5760875
					0.8	0.4826844	0.3601035	0.5293191

Table 10.5: The variation in transfer rate of mass for varying values of A , M , K , Pr , N_b , N_t and Sc .

Parameters							$(Re_b)^{-\frac{1}{n+1}} Sh_s$		
A	M	K	Pr	N_b	N_t	Sc	$n = 1$	$n = 0.5$	$n = 1.5$
1.0	0.5	5.00	1.2	0.5	0.2	0.5	0.2639435	0.2136013	0.2869661
2.0							0.2901100	0.2277653	0.3013438
3.0							0.3080178	0.2419765	0.3261540
2.5	0.0	5.00	1.2	0.5	0.2	0.5	0.3387689	0.2801454	0.358471
	0.3						0.3130858	0.2444946	0.3293312
	0.6						0.2940983	0.2308953	0.3089076
2.5	0.5	1.00	1.2	0.5	0.2	0.5	0.4844747	0.4653732	0.5061337
		2.00					0.3574861	0.3518147	0.3864713
		3.00					0.3224309	0.2833551	0.340895
2.5	0.5	5	1.0	0.5	0.2	0.5	0.3138149	0.2471073	0.3305256
			1.2				0.2998606	0.2341961	0.3149727
			1.4				0.2878966	0.2236126	0.3015996
2.5	0.5	5	1.2	0.2	0.2	0.5	0.00468151	0.01129199	-0.0111103
				0.4			0.2510269	0.1975569	0.2610270
				0.6			0.3321572	0.2591847	0.3506789
2.5	0.5	5	1.2	0.5	0.2	0.5	0.2998606	0.2341961	0.3149727
					0.4		0.1749665	0.144632	0.1739438
					0.6		0.0706546	0.07289905	0.05445231
2.5	0.5	5	1.2	0.5	0.2	0.5	0.2998606	0.2341961	0.3149727
						0.9	0.5259361	0.3936558	0.5648702
						1.3	0.7033079	0.531955	0.7598461

Chapter 11

Conclusions and Further Research

The ambition of the research work illustrated in this thesis is to provide the mathematical modeling and numerical computations of the Sisko fluid flow under various flow conditions and geometries. The research emphasizes on the study of flow, transfer of heat and mass of a generalized Newtonian fluid. For the purpose of this study, the Sisko rheological model is investigated to incorporate the planar and curved stretching geometries under various flow circumstances. Thus, major purpose of the current research work is to rally the current understanding of the mathematical modeling and numerical computations of the Sisko fluid. Thus, this chapter summarizes all the remarkable outcomes of the research work presented in this thesis. Moreover, this chapter indicates about the future research directions. Section 11.1 provides an overview of the research that has been followed. In section 11.2 conclusions captured from the previous chapters are summarized. In last section 11.3, possible direction for future research are listed.

11.1 General Overview

This study is a step toward the exploration of the Sisko liquid flows which is a subclass of non-Newtonian liquids. Such fluids are characterized by shear dependent viscosity. Mathematical modeling of this model is presented in the form of PDEs. The numerical

computations captures the various characteristics of the generalized Sisko fluid flow over planner and curved stretching surfaces. The obtained upshots are displayed in the form of velocity, pressure, temperature and concentration profiles. To that end, the numerical procedures of RK45-Fehlberg scheme was adopted to achieve this goal. Moreover, the built in function `bvp4c` which implement a finite difference three stages IIIA Lobato formula was incorporated for the numerical computations.

11.2 Conclusions

In this thesis, an important rheological study of generalized Newtonian Sisko fluid flows with different physical aspects was performed. The approximation of BL was considered for the modeling of proposed problem in terms of PDEs and was then converted into ODEs by using some suitable transformations. The acquiring system of ODEs was then solved with numerical approach by using RK45-Fehlberg along with shooting technique and `bvp4c` built in solver in MATLAB. Important obtained results are presented in the pictorial and numerical forms for the fluid distribution of velocity, pressure, temperature and concentration.

The leading conclusions of the research are listed as follows:

11.3 Flow Analysis

- The effect of material parameter and power-law index on the liquid velocity and the related MBLT were noticed in an increasing conduct.
- The reduction was observed in both components of velocity and related MBLT for the increasing variation in magnetic parameter.
- With uplifting values of the transient parameter, increase in velocity and MBLT were noticed for shear-thinning liquid and a decreasing behavior is observed for shear-thickening liquid.

- The velocity and related MBLT were noticed in higher trend for higher values of radius of curvature K .
- A reduction in the local-skin friction was observed for increasing values of curvature parameter for three cases, i.e., shear-thinning liquid, shear-thickening fluids and Newtonian liquid.

11.4 Heat Transfer Analysis

- A diminishing trend of temperature and associated TBLT were noted for growing values of material parameter and power-law index while considering pseudo-plastic as well as dilatant liquids.
- An uprise in the parameter of thermal relaxation displayed a decline in the liquid temperature and associated TBLT. However, an opposite trend was detected with enrichment values of thermal conductivity parameter.
- Effect of the generalized Biot number γ_1 on temperature distribution was noticed in escalating behavior while decreasing trend was seen in temperature distribution for various values of generalized Biot number γ_2 for both cases, i.e., shear-thinning and shear-thinning liquids, respectively.
- It was affirmed from the above analysis that the nonlinear thermal radiative parameter R_d enhanced the temperature of the fluid.
- The impact of the radius of curvature on the temperature and related TBLT was noted in reducing character for dilatant as well as pseudo-plastic liquids.
- From the tabular values of the local-Nusselt number, an enhancement and reduction, respectively, were confirmed for higher values of radiation and curvature parameters.

11.5 Mass Transfer Analysis

- The concentration and associated CBLT were declined for the augmented values of the relative parameter of Sisko liquid and relaxation parameter of concentration as well.
- The profile of concentration was declined with heightening of the homogeneous/heterogeneous reactions strength parameters by using of both shear-thinning and shear-thickening fluids cases.
- The higher values of Brownian motion parameter resulted in reduction nanoparticles concentration while the concentration was uplifted by boosting the thermophoresis parameter.
- The concentration and CBLT were reduced with various enrichment values of curvature parameter for pseudo-plastic and dilatant liquids.
- The escalation in unsteadiness parameter was reduced the transfer rate of mass for pseudo plastic liquids and enhanced for dilatant liquids.

11.6 Pressure Analysis

- The magnitude of the pressure inside the BL was observed in declined order while the radius of curvature and material parameter were incremented.
- With diminishing values of the curved nature parameter, the magnitude of pressure profile exhibited an increasing order inside BL. However, outside BL it became zero.
- The magnitude of the pressure inside the BL was presented an increasing function of reducing values of magnetic parameter.

11.7 Future Research

With this study, the development of mathematical formulation and numerical computations of Sisko fluid flow, transfer of heat and mass over planar and curved moving surfaces were established. The characteristics and advantages of the current analysis have been evidently exemplified by its applications to altered practical circumstances. Moreover, this numerical study of generalized Newtonian Sisko fluid flows explored the prominence of many physical phenomena in the form of graphical representations. However, a lot of improvements can be made to the Sisko fluid flow to extend its applications and make it further useful. In this regard, further work in this direction can be suggested as follows:

- The present mathematical model can be extended to thin film Sisko liquid flow over a bidirectional moving boundary.
- Mathematical modeling for Sisko liquid flow over a rotating cone could be one of the important consideration in future.
- The stagnation point flow over a curved moving boundary is an open problem for future.
- The time dependent mathematical modeling of flows over curved surface may also be considered in future work.
- Thin film flow over curved surface can also be one of the main consideration for future research work.

Bibliography

- [1] R.B. Bird, C.F. Curtiss, R.C. Armstrong and O. Hassager, Dynamics of polymeric liquids, John Wiley and Sons Inc., New York, USA, 1987.
- [2] A.W. Sisko, The flow of lubricating greases, *Ind. Eng. Chem.*, **50** (1958) 1789-1792.
- [3] A.M. Siddiqui, M. Ahmed and Q.K. Ghori, Thin film flow of non-Newtonian fluids on a moving belt, *Chaos Solitons Fractals*, **33** (2007) 1006–1016.
- [4] S. Asghar, T. Hayat and A.H. Kara, Exact solutions of thin film flows, *Nonlinear Dyn.*, **50** (2007) 229-233.
- [5] Y. Wang, T. Hayat, N. Ali and M. Oberlack, Magnetohydrodynamic peristaltic motion of a Sisko fluid in a symmetric or asymmetric channel, *Physica A*, **387** (2008) 347-362.
- [6] S. Abelman, T. Hayat and E. Momoniat, On the Rayleigh problem for a Sisko fluid in a rotating frame, *Appl. Math. Comput.*, **215** (2009) 2515-2520.
- [7] M. Molati, T. Hayat and F. Mahomed, Rayleigh problem for a MHD Sisko fluid, *Nonlinear Anal: Real World Appl.*, **10** (2009) 3428-3434.
- [8] T. Hayat, R.J. Moitsheki and S. Abelman, Stokes first problem for Sisko fluid over a porous wall, *Appl. Math. Comput.*, **217** (2010) 622-628.
- [9] M. Khan and A. Shahzad, On boundary layer flow of a Sisko fluid over a stretching sheet, *Quaestiones Mathematicae*, **36(1)** (2013) 137-151.

- [10] A. Munir, A. Shahzad and M. Khan, Forced convective heat transfer in boundary layer flow of Sisko fluid over a nonlinear stretching sheet, *PLOS ONE*, **9(6)** (2014): e100056.
- [11] R. Malik, M. Khan, A. Munir and W.A. Khan, Flow and heat transfer in Sisko fluid with convective boundary condition, *PLOS ONE*, **9(10)** (2014): e107989.
- [12] A. Munir, A. Shahzad and M. Khan, Convective flow of Sisko fluid over a bidirectional stretching surface, *PLOS ONE*, **10** (2015): e0130342.
- [13] J.B.J. Fourier, *Théorie Analytique De La Chaleur*, Paris, (1822).
- [14] M. Chester, Second sound in solids, Lattice thermal conductivity of disordered semiconductor alloys at high temperatures, *Phys. Rev.*, **131(5)** (1963) 2013-2015.
- [15] D.D. Joseph and L. Preziosi, Heat waves, *Rev. Mod. Phys.*, **61(1)** (1989) 41-73.
- [16] C.L. Tien and G. Chen, Challenges in microscale conductive and radiative heat transfer, *J. Heat Transf.*, **116** (1994) 799-807.
- [17] C. Cattaneo, Sulla conduzionedelcalore, *AttiSemin. Mat. Fis. Univ. Modena Reggio Emilia*, **3** (1948) 83-101.
- [18] C.I. Christov, On frame indifferent formulation of the Maxwell-Cattaneo model of finite speed heat conduction, *Mech. Res. Commun.*, **36** (2009) 481-486.
- [19] M. Ciarletta and B. Straughan, Uniqueness and structural stability for the Cattaneo-Christov equations, *Mech. Res. Commun.*, **37** (2010) 445-447.
- [20] T. Hayat, M. Imtiaz, A. Alsaedi and S. Almezal, On Cattaneo-Christov heat flux in MHD flow of Oldroyd-B fluid with homogeneous-heterogeneous reactions, *J. Mol. Liq.*, **401** (2016) 296-303.
- [21] M. Khan and W.A. Khan, Three-dimensional flow and heat transfer to Burgers fluid using Cattaneo-Christov heat flux model, *J. Mol. Liq.*, **221** (2016) 651-657.

- [22] M. Waqas, T. Hayat, M. Farooq, S.A. Shehzad and A. Alsaedi, Cattaneo-Christov heat flux model for flow of variable thermal conductivity generalized Burgers fluid, *J. Mol. Liq.*, **220** (2016) 642-648.
- [23] J. Sui, L. Zheng and X. Zhang, Boundary layer heat and mass transfer with Cattaneo-Christov double-diffusion in upper-convected Maxwell nanofluid past a stretching sheet with slip velocity, *Int. J. Therm. Sci.*, **104** (2016) 461-468.
- [24] L. Liu, L. Zheng, F. Liu and X. Zhang, Anomalous convection diffusion and wave coupling transport of cells on comb frame with fractional Cattaneo-Christov flux, *Commun. Nonlinear Sci. Numer. Simulat.*, **38** (2016) 45-58.
- [25] W.A. Khan, M. Khan and A. S. Alshomrani, Impact of chemical processes on 3D Burgers fluid utilizing Cattaneo-Christov double-diffusion: Applications of non-Fourier's heat and non-Fick's mass flux models, *J. Mol. Liq.*, **223** (2016) 1039-1047.
- [26] S.U.S. Choi, Enhancing thermal conductivity of fluids with nanoparticles, *Proc. ASME Int. Mech. Eng. Cong. Exp.*, **66** (1995) 99-105.
- [27] J. Buongiorno, Convective transport in nanofluids, *J. Heat Transf.*, **128(3)** (2006) 240-250.
- [28] A.V. Kuznetsov and D.A. Nield, Natural convective boundary-layer flow of a nanofluid past a vertical plate, *Int. J. Therm. Sci.*, **49** (2010) 243-247.
- [29] M. Turkyilmazoglu, Exact analytical solutions for heat and mass transfer of MHD slip flow in nanofluids, *Chem. Eng. Sci.*, **84** (2012) 182-187.
- [30] S. Nadeem, R.U. Haq, N.S. Akbar, C. Lee and Z.H. Khan, Numerical study of boundary layer flow and heat transfer of Oldroyd-B nanofluid towards a stretching sheet, *PLOS ONE*, **8(8)** (2013): e0069811.

- [31] A.V. Kuznetsou and D.A. Nield, Natural convective boundary-layer flow of a nanofluid past a vertical plate: A revised model, *Int. J. Therm. Sci.*, **77** (2014) 126-129.
- [32] W.A. Khan, M. Khan and R. Malik, Three-dimensional flow of an Oldroyd-B nanofluid towards stretching surface with heat generation/absorption, *PLOS ONE*, **9(8)** (2014): e105107.
- [33] S.U. Rahman, R. Ellahi, S. Nadeem and Q.M. Zaigham Zia, Simultaneous effects of nanoparticles and slip on Jeffrey fluid through tapered artery with mild stenosis, *J. Mol. Liq.*, **218** (2016) 484-493.
- [34] M. Akbarzadeh, S. Rashidi, M. Bovand and R. Ellahi, A sensitivity analysis on thermal and pumping power for the flow of nanofluid inside a wavy channel, *J. Mol. Liq.*, **220** (2016) 1-13.
- [35] S. Rehman, R. Ul Haq, Z.H. Khan and C. Lee, Entropy generation analysis of non-Newtonian nanofluid with zero normal flux of nanoparticles at the stretching surface, *J. Taiwan Inst. Chem. Eng.*, **63** (2016) 226-235.
- [36] T. Hayat, M. Waqas, S.A. Shehzad and A. Alsaedi, On model of Burgers fluid subject to magneto nanoparticles and convective conditions, *J. Mol. Liq.*, **222** (2016) 181-187.
- [37] M.A. Chaudhary and J.H. Merkin, A simple isothermal model for homogeneous-heterogeneous reactions in boundary-layer flow. I Equal diffusivities , *Fluid Dyn. Res.*, **16(6)** (1995) 311-333.
- [38] M.A. Chaudhary and J.H. Merkin, A simple isothermal model for homogeneous-heterogeneous reactions in boundary-layer flow. II Different diffusivities for reactant and autocatalyst, *Fluid Dyn. Res.*, **16(6)** (1995) 335-359.

- [39] G. Pizza, J. Mantzaras and C.E. Frouzakis, Suppression of combustion instabilities of premixed hydrogen/air flames in microchannels using heterogeneous reactions, *Proc. Combust. Inst.*, **32(2)** (2009) 3051-3058.
- [40] G. Pizza, J. Mantzaras and C.E. Frouzakis, Flame dynamics in catalytic and non-catalytic mesoscale microreactors, *Catal. Today*, **155** (2010) 123-130.
- [41] Y. Wang, Z. Zhou and W. Yang, Combustion of hydrogen-air in micro combustors with catalytic Pt layer, *Energ. Convers. Manage.*, **51(6)** (2010) 1127-1133.
- [42] Y.H. Li, G.B. Chen and F.H. Wu, Effects of catalyst segmentation with cavities on combustion enhancement of blended fuels in a micro channel, *Combust. Flame*, **159(4)** (2012) 1644-1651.
- [43] R. Nandkeolyar, S.S. Mosta and P. Sibanda, Viscous and joule heating in the stagnation point nanofluid flow through a stretching sheet with homogenous-heterogeneous reactions and nonlinear convection, *J. Nanotechnol. Eng. Med.*, **4** (2014): 041001.
- [44] M. Ramzan, M. Bilal and J.D. Chung, MHD stagnation point Cattaneo-Christov heat flux in Williamson fluid flow with homogeneous-heterogeneous reactions and convective boundary condition: A numerical approach, *J. Mol. Liq.*, **225** (2017) 856-862.
- [45] S. Qayyum, R. Khan and H. Habib, Simultaneous effects of melting heat transfer and inclined magnetic field flow of tangent hyperbolic fluid over a nonlinear stretching surface with homogeneous-heterogeneous reactions, *Int. J. Mech. Sci.*, **133** (2017) 1-10.
- [46] M. Rahman, M. Manzur and M. Khan, Mixed convection heat transfer to modified second grade fluid in the presence of thermal radiation, *J. Mol. Liq.*, **223** (2016) 217-223.

- [47] M. Kothandapani and J. Prakash, Effects of thermal radiation parameter and magnetic field on the peristaltic motion of Williamson nanofluids in a tapered asymmetric channel, *Int. J. Heat Mass Transf.*, **81** (2015) 234-245.
- [48] M.A. Seddeek and A.M. Abdel, Effects of radiation and thermal diffusivity on heat transfer over a stretching surface with variable heat flux, *Phys. Lett. A*, **348** (2006) 172-179 .
- [49] M. Khan, M. Irfan and W.A. Khan, Impact of nonlinear thermal radiation and gyrotactic microorganisms on the magneto-Burgers nanofluid, *Int. J. Mech. Sci.*, **130** (2017) 375-382.
- [50] M. Khan, M. Irfan, W.A. Khan and L. Ahmad, Modeling and simulation for 3D magneto Eyring-Powell nanomaterial subject to nonlinear thermal radiation and convective heating, *Results Phys.*, **7** (2017) 1899-1906.
- [51] A. Aziz, A similarity solution for laminar thermal boundary layer over a flat plate with a convective surface boundary condition, *Commun. Nonlinear Sci. Numer. Simulat.*, **14** (2009) 1064-1068.
- [52] A. Aziz and W.A. Khan, Natural convective boundary layer flow of a nanofluid past a convectively heated vertical plate, *Int. J. Therm. Sci.*, **52** (2012) 83-90.
- [53] T. Hayat, Z. Iqbal, M. Mustafa and A. Alsaedi, Momentum and heat transfer of an upper-convected Maxwell fluid over a moving surface with convective boundary conditions, *Nucl. Eng. Des.*, **252** ((2012) 242-247.
- [54] M. Imtiaz, T. Hayat and A. Alsaedi, Mixed convection flow of Casson nanofluid over a stretching cylinder with convective boundary conditions, *Adv. Pow. Tech.*, **27(5)** (2016) 2245-2256.

- [55] M. Khan, M. Azam and A.S. Alshomrani, On unsteady heat and mass transfer in Carreau nanofluid flow over expanding or contracting cylinder with convective surface conditions, *J. Mol. Liq.*, **231** (2017) 474-484.
- [56] M. Waqas, M. Farooq, M. I. Khan, A. Alsaedi, T. Hayat and T. Yasmeen, Magneto-hydrodynamic (MHD) mixed convection flow of micropolar liquid due to nonlinear stretched sheet with convective condition, *Int. J. Heat Mass Transf.*, **102** (2016) 766-772.
- [57] L. Todd, A family of laminar boundary layers along a semi-infinite flat plate, *Fluid Dyn. Res.*, **19** (1997) 235-249.
- [58] A. Ishak, R. Nazar and I. Pop, Heat transfer over an unsteady stretching permeable surface with prescribed wall temperature, *Nonlinear Anal.: Real World Appl.*, **10** (2009) 2909-2913.
- [59] Y. Zhang, M. Zhang and Y. Bai, Flow and heat transfer of an Oldroyd-B nanofluid thin film over an unsteady stretching sheet, *J. Mol. Liq.*, **220** (2016) 665-670.
- [60] J. Ahmed, T. Mahmood, Z. Iqbal, A. Shahzad and R. Ali, Axisymmetric flow and heat transfer over an unsteady stretching sheet in power law fluid, *J. Mol. Liq.*, **221(44)** (2016) 386-393.
- [61] Y. Zhang, M. Zhang and Y. Bai, Unsteady flow and heat transfer of power-law nanofluid thin film over a stretching sheet with variable magnetic field and power-law velocity slip effect, *J. Taiwan Inst. Chem. Eng.*, **70** (2017) 104-110.
- [62] L.J. Crane, Flow past a stretching plate, *ZAMM - J. Appl. Math. Phys.*, **21** (1970) 645-647.
- [63] P. Gupta and A. Gupta, Heat and mass transfer on a stretching sheet with suction or blowing, *Can. J. Chem. Eng.*, **55** (1977) 744-746.

- [64] A. Ahmad and S. Asghar, Flow and heat transfer over hyperbolic stretching sheets, *Appl. Math. Mech.*, **33** (2012) 445-54.
- [65] M. Turkyilmazoglu, An analytical treatment for the exact solutions of MHD flow and heat over two–three dimensional deforming bodies, *Int. J. Heat Mass Transf.*, **90** (2015) 781-789.
- [66] M. Turkyilmazoglu, Equivalences and correspondences between the deforming body induced flow and heat in two-three dimensions, *Phys. Fluids*, **28** (2016): 043102.
- [67] M. Turkyilmazoglu, Magnetohydrodynamic two-phase dusty fluid flow and heat model over deforming isothermal surfaces, *Phys. Fluids*, **29** (2017): 013302.
- [68] M.H. Mat Yasin, A. Ishak and I. Pop, MHD heat and mass transfer flow over a permeable stretching/shrinking sheet with radiation effect, *J. Mag. Mag. Mat.*, **407** (2016) 235-240.
- [69] M. Turkyilmazoglu, Mixed convection flow of magnetohydrodynamic micropolar fluid due to a porous heated/cooled deformable plate: Exact solutions, *Int. J. Heat Mass Transf.*, **106** (2017) 127-134.
- [70] M. Sajid, N. Ali, T. Javed and Z. Abbas, Stretching a curved surface in a viscous fluid, *Chin. Phys. Lett.*, **27(2)** (2010): 024703.
- [71] N.C. Rosca and I. Pop, Unsteady boundary layer flow over a permeable curved stretching/shrinking surface, *Eur. J. Mech. B/Fluids*, **51** (2015) 61-67.
- [72] M. Sajid, N. Ali, Z. Abbas, and T. Javed, Flow of a micropolar fluid over a curved stretching surface, *J. Engi. Phys. Termophys.*, **4(84)** (2011) 864-871.
- [73] Z. Abbas, M. Naveed and M. Sajid, Hydromagnetic slip flow of nanofluid over a curved stretching surface with heat generation and thermal radiation, *J. Mol. Liq.*, **215** (2016) 756-762.

- [74] J. Kierzenka and F.L. Shampine, A BVP Solver Based on Residual Control and the MATLAB PSE, *ACM TOMS*, **27(3)** (2001) 299-316.
- [75] P.D. Ariel, Generalized three-dimensional flow due to a stretching sheet, *ZAMM – J. App. Math. Mech.*, **83(12)** (2003) 844-852.
- [76] A. Ishak, R. Nazar and I. Pop, Heat transfer over an unsteady stretching surface with prescribed heat flux, *Can. J. Phys.*, **86** (2008) 853-855.
- [77] E.M.A. Elbashbeshy, Heat transfer over a stretching surface with variable heat flux, *J. Phys. D: Appl. Phys.*, **31** (1998) 1951-1955.
- [78] M. Khan, R. Malik, A. Munir and W.A. Khan, Flow and heat transfer to Sisko nanofluid over a nonlinear stretching sheet, *PLOS ONE*, **10(5)** (2015): e0125683.
- [79] Z. Abbas, M. Naveed and M. Sajid, Heat transfer analysis for stretching flow over a curved surface with magnetic field, *J. Eng. Thermophys.*, **22(4)** (2013) 337.
- [80] K.M. Sanni, S. Asghar, M. Jalil and N.F. Okechi, Flow of viscous fluid along a nonlinearly stretching curved surface, *Results Phys.*, **7(1)** (2017) 1-4.
- [81] F. Mabood and K. Das, Melting heat transfer on hydromagnetic flow of a nanofluid over a stretching sheet with radiation and second-order slip, *Europ. Phys. J. Plus*, **131** (2016) 3.
- [82] M. Imtiaz, T. Hayat and A. Alsaedi, MHD Convective flow of Jeffrey fluid due to a curved stretching surface with homogeneous-heterogeneous reactions, *PLOS ONE*, **11(9)** (2016): e0161641.

Turnitin Originality Report

Mathematical Modeling and Numerical Simulation of Sisko Fluid Flow over a Stretching Surface by Latif Ahmad .



From DRSM (DRSML)

- Processed on 22-Aug-2019 09:09 PKT
- ID: 1162229176
- Word Count: 52163

Similarity Index

16%

Similarity by Source

Internet Sources:

10%

Publications:

4%

Student Papers:

10%

Focal Person (Turnitin)
Quairat-Azhar University
Islamabad

sources:

- 1 1% match (student papers from 05-Jan-2017)
[Submitted to Higher Education Commission Pakistan on 2017-01-05](#)
 - 2 < 1% match (student papers from 07-Nov-2017)
[Submitted to Higher Education Commission Pakistan on 2017-11-07](#)
 - 3 < 1% match (Internet from 01-Nov-2014)
<http://80.64.99.26/icudt40l.dat>
 - 4 < 1% match (student papers from 06-Jun-2018)
[Submitted to Higher Education Commission Pakistan on 2018-06-06](#)
 - 5 < 1% match (student papers from 25-Apr-2017)
[Submitted to Higher Education Commission Pakistan on 2017-04-25](#)
 - 6 < 1% match (Internet from 12-Jul-2017)
<http://thermalscience.vinca.rs/pdfs/papers-2017/TSCI160807132K.pdf>
 - 7 < 1% match (Internet from 18-Oct-2017)
<http://eprints.hec.gov.pk/6443/1/16014S.pdf>
 - 8 < 1% match (student papers from 02-Jan-2015)
[Submitted to Higher Education Commission Pakistan on 2015-01-02](#)
 - 9 < 1% match (Internet from 12-Dec-2018)
http://server.thermallfluidscentral.com/journals/index.php/Heat_Mass_Transfer/article/view/561/484
 - 10 < 1% match (Internet from 06-May-2015)
<http://www.slideshare.net/meylismamedov/calculus-solutions>
 - 11 < 1% match (publications)
[Khan, Waqar Azeem, Masood Khan, and Ali Saleh Alshomrani. "Impact of chemical processes on 3D Burgers fluid utilizing Cattaneo-Christov double-diffusion: Applications of non-Fourier's heat and non-Fick's mass flux models". Journal of Molecular Liquids, 2016.](#)
 - 12 < 1% match (Internet from 28-Nov-2017)
<https://link.springer.com/content/pdf/10.1134%2FS0965542517060021.pdf>
 - 13 < 1% match (publications)
[Latif Ahmad, Asif Munir, Masood Khan. "Locally non-similar and thermally radiative Sisko fluid flow with magnetic and Joule heating effects". Journal of Magnetism and Magnetic Materials, 2019](#)
- < 1% match (student papers from 21-Sep-2017)